JSCSEN 75(5)595–732(2010)

Journal of the Serbian Chemical Society

VOLUME 75

No 5

BELGRADE 2010

Available on line at

www.shd.org.rs/JSCS/

Journal of the Serbian Chemical Society
JSCS@tmf.bg.ac.rs • www.shd.org.rs/JSCS

J. Serb. Chem. Soc. Vol. 75, No. 5 (2010)

CONTENTS

Published by the Serbian Chemical Society
Karnegijeva 4/III, 11000 Belgrade, Serbia
Printed by the Faculty of Technology and Metallurgy
Karnegijeva 4, P.O. Box 35-03, 11120 Belgrade, Serbia

J. Serb. Chem. Soc. 75 (5) 595–603 (2010)
JSCS–3990

Journal of the Serbian Chemical Society
JSCS@tmf.bg.ac.rs • www.shd.org.rs/JSCS

UDC 547.295.2+547.288.2+542.913+
547:616.032:611.778
Original scientific paper

Esters and amides of hexanoic acid substituted with tertiary amino group in terminal position and their activity as transdermal permeation enhancers

OLDŘICH FARSA[1]*, PAVEL DOLEŽAL[2] and ALEXANDR HRABÁLEK[3]

[1]*Institute of Chemical Drugs, Faculty of Pharmacy, University of Veterinary and Pharmaceutical Sciences Brno, Palackého 1/3, 612 42 Brno,* [2]*Department of Pharmaceutical Technology, Faculty of Pharmacy, Charles University, Hradec Králové and* [3]*Department of Inorganic and Organic Chemistry, Faculty of Pharmacy, Charles University, Hradec Králové, Czech Republic*

(Received 27 May 2009, revised 4 January 2010)

Abstract: Series of alkyl esters of 6-(diethylamino)-, 6-(pyrrolidin-1-yl)-, 6-(piperidin-1-yl) and 6-(morpholin-4-yl)hexanoic acids and alkylamides of 6-(dimethylamino)-, 6-(piperidin-1-yl) and 6-(morpholin-4-yl)hexanoic acids, containing 8–12 carbon atoms in the alkyl chain, were prepared by methods of classical organic synthesis. The appropriate secondary amine was alkylated with ethyl 6-bromohexanoate to give ester of ω-substituted hexanoic acid, except of ethyl 6-(dimethylamino)hexanoate (**1**), which was prepared by Eschweiler–Clarke methylation of 6-aminohexanoic acid followed by direct esterification with ethanol. The resulted esters of ω-substituted hexanoic acids underwent direct transesterification with long chain alkanols to yield the desired amino esters, or they were treated with long-chain alkylamines to prepare secondary amides of the appropriate heterocyclic hexanoic acids. These products were *in vitro* tested on their activity as transdermal permeation enhancers on the strips of the excised human skin with theophylline as the model permeant. The activity was evaluated using parameter enhancement ratio (*ER*), defined as the ratio between the overall amount of the permeant passing through the skin with the tested enhancer and that without tested substance. Decyl 6-(pyrrolidin-1-yl)hexanoate (**9**) with *ER* = 30 showed the highest activity. The enhancing effects of the esters were generally better than those of the amides.

Keywords: transdermal permeation enhancers; ω-amino acid derivatives.

INTRODUCTION

Transdermal permeation enhancers (TPEs) are special pharmaceutical excipients, which enable or facilitate the passage of various drugs through the skin

* Corresponding author. E-mail: farsao@vfu.cz
doi: 10.2298/JSC090303031T

barrier to the blood circulation, thereby enabling their systemic effect. Together with antimicrobial preservatives and antioxidants, they belong to a narrow group of excipients which can be characterized by their own enumerable activities. Only a few drugs with high lipophilicity, such as steroids, nitrates, some opioid analgesics (fentanyl) and several alkaloids (*e.g.*, nicotine or scopolamine), are capable of penetrating through the skin by themselves. For this reason TPEs constitute important ingredients of transdermal application systems, which are popular because of their benefits and used not only in human, but more recently also in veterinary therapy.[1] They can provide steady-state plasma concentrations of drugs and long-term therapy from a single dose, avoid the hepatic first-pass metabolism associated with oral administration and allow easy termination of drug input. The role of chemical TPEs is to reversibly alter the barrier properties of the *stratum corneum* (SC), which is the outermost layer of skin, by disruption of the membrane structures or by maximizing drug solubility within the skin.[2]

Compounds used or tested as TPEs constitute a very diverse group of structures. Various derivatives of amino acids occupy among them a comparatively important position. Previously, a series of long chain alkyl esters of 6-(dimethylamino)hexanoic acid with a linear alkyl chain having 8 to 12 carbon atoms were prepared.[3] The distance of 5 carbon atoms between the terminal amino group and the carboxyl as well as the range of lengths of alkyl chains were selected based on previous experiences. The older results demonstrated that alkyl esters of ω-amino acids have their optimum transdermal permeation enhancing effect for linear octyl to dodecyl groups, that branching of an alkyl chain essentially lowers the activity,[4] and that derivatives of 6-aminohexanoic acid are significantly more potent than those with another number of carbon atoms in the acyl chain.[5] It was found that these compounds showed high enhancement activity of transdermal permeation of theophylline as a model permeant of "moderate lipophilicity". The highest effect was obtained with dodecyl 6-(dimethylamino)hexanoate (DDAK) with an enhancement ratio (*ER*) of nearly 80. Such a significant activity was rationalized based on the higher basicity of the tertiary amino group of this compound.[3] It is also supposed this increase of activity must be connected with an essentially higher toxicity due to high stability against enzymatic hydrolysis. For this reason, this type of structural modification temporarily became of marginal interest. More recently, the above-mentioned DDAK was shown to be an effective enhancer of percutaneous permeation of adefovir[6] and hydrocortisone. Surprisingly, DDAK was demonstrated to be rapidly metabolized by porcine esterase with $t_{1/2}$ = 17.2 min and displayed low acute toxicity. It also showed reversibility of action on treated skin expressed as electrical resistance (impedance) at 120 kHz, which during 3 h after treatment with DDAK dropped to 20 % of its initial value and after removal of the enhancer slowly increased.[7] These results returned our interest to the field of enhancers with a tertiary amino group. The

aim of this preliminary pilot study was to determine the influence of expansion of the dimethylamino group into either an open diethylamino group or a closed saturated heterocyclic ring, *i.e.*, pyrrolidine, piperidine or morpholine, on permeation enhancement activity. Simultaneously, the effect of substitution of the ester group with an amide moiety could also be evaluated.

RESULTS

Synthesis of compounds and determination of their activity

Long-chain alkyl esters of 6-aminohexanoic acids with a tertiary amino group. Ethyl esters of 6-(diethylamino)hexanoic, 6-(pyrrolidin-1-yl)hexanoic, 6-(piperidin-1-yl)hexanoic and 6-(morpholin-4-yl)hexanoic acids were prepared by direct alkylation of the appropriate secondary amine with ethyl 6-bromohexanoate. Their transesterification with an appropriate long-chain alkanol catalyzed with *in situ* prepared sodium alcoholate under the simultaneous distilling off of the arising ethanol according to Franke *et al.*[8] led to octyl to dodecyl esters of these ω-amino acids (Scheme 1).

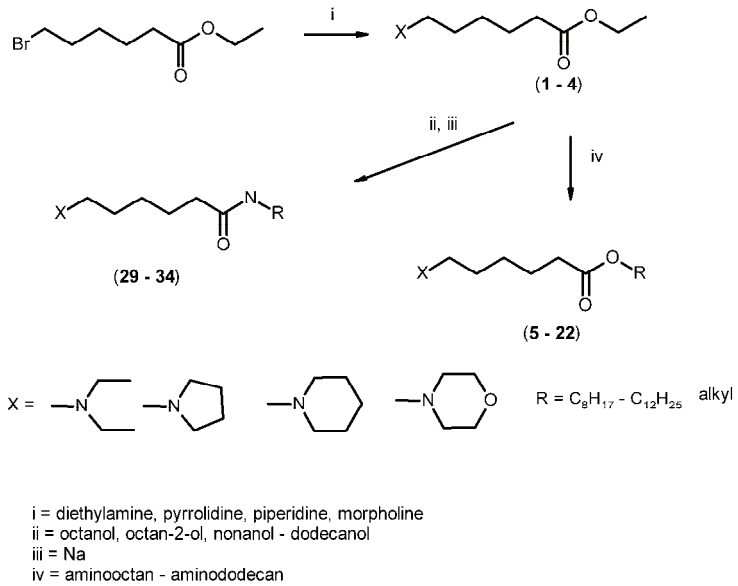

Scheme 1. Procedure of the synthesis of alkyl esters and *N*-alkylamides of 6-(diethylamino)hexanoic, 6-(pyrrolidin-1-yl)hexanoic, 6-(piperidin-1-yl)hexanoic and 6-(morpholin-4-yl)hexanoic acids.

Long chain alkyl amides of 6-(dimethylamino)hexanoic acid. Eschweiler–Clarke methylation of 6-aminohexanoic acid with formaldehyde and formic acid according to Fusco *et al.*[9] (the detailed description of the reaction procedure is given in the literature[3]) gave 6-(dimethylamino)hexanoic acid, which was di-

rectly esterified with ethanol. The resulting ethyl-6-(dimethylamino)hexanoate was heated with an appropriate aminoalkane to yield the corresponding alkylamide of 6-(dimethylamino)hexanoic acid (Scheme 2).

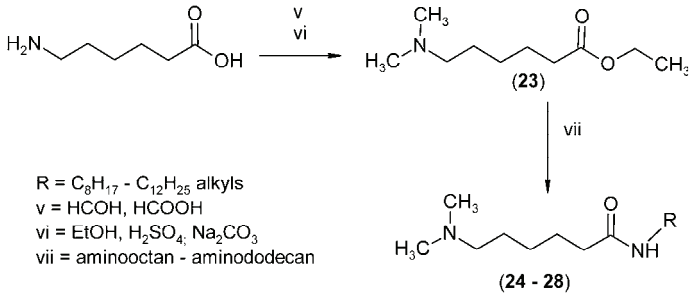

Scheme 2. Procedure of the synthesis of *N*-alkyl-6-dimethylaminohexanamides (**24**–**28**).

Long chain alkyl amides of N,N-*disubstituted 6-aminohexanoic acids.* Octyl to dodecyl amides of 6-(diethylamino)hexanoic, 6-(pyrrolidin-1-yl)hexanoic, 6-(piperidin-1-yl)hexanoic and 6-(morpholin-4-yl)hexanoic acids were synthesized similarly by heating of the appropriate aminoalkane with an ω-substituted ethyl hexanoate under the simultaneous distilling off of the arising ethanol (Scheme 1).

All products were isolated and purified either by distillation under reduced pressure or by crystallization from a suitable system of solvents, or only by sorption filtration through an alumina column. The identities of all the compounds were confirmed by their IR, ^{1}H- and ^{13}C-NMR-spectra and by elemental analysis.

Analytical and spectral data of the synthesized compounds

The complete analytical and spectral data of the synthesized compounds can be found in the electronic version of the paper as Supplementary material (http://www.shd.org.rs/JSCS/), from the office of the Serbian Chemical Society upon request (JSCS@shd.org.rs) or from the corresponding author upon request.

Evaluation of the activity of the synthesized compounds and their results

Testing of the transdermal permeation enhancing activity was performed *in vitro* on strips of excised human skin with theophylline, thought to be a drug of "middle lipophilicity", as a model penetrant in the system of liberation cells according to Franz[10] from a propylene glycol medium. Due to capacity utilization of the testing workplace, only one or several members of each homologous series underwent the evaluation procedure. The final results of the testing are presented as values of the enhancement ratio (*ER*), defined simply as the ratio between the overall amount of the permeant which passed through the skin with tested enhancer and that without the tested substance. These values are given in Table I.

TABLE I. Values of the enhancement ratio (*ER*) of the prepared and related compounds (X-$(CH_2)_5$CO-Y-R)

Compd.	X	Y	R	*ER*	Compd.	X	Y	R	*ER*
DDAK	$_3)_2$N–	–O–	C_8H_{17}	82.4±19.0[a]	**17**		–O–	$C_{12}H_{25}$	2.0±0.4
	$(CH_3)_2$N–	–O–	2-C_8H_{17}	–	**18**		–O–	C_8H_{17}	–
	$(CH_3)_2$N–	–O–	C_9H_{19}	89.3±11.0[a]	**19**		–O–	C_9H_{19}	–
	$(CH_3)_2$N–	–O–	$C_{10}H_{21}$	104.5±11.0[a]	**20**		–O–	$C_{10}H_{21}$	15.0±2.9
	$(CH_3)_2$N–	–O–	$C_{11}H_{23}$	118.3±19.0[a]	**21**		–O–	$C_{11}H_{23}$	–
	$(CH_3)_2$N–	–O–	$C_{12}H_{25}$	79.7±19.0[a]	**22**		–O–	$C_{12}H_{25}$	–
5	$(C_2H_5)_2$N–	–O–	C_8H_{17}	–	**24**	$(CH_3)_2$N–	–NH–	C_8H_{17}	11.2±2.2
6	$(C_2H_5)_2$N–	–O–	$C_{10}H_{21}$	10.0±2.3	**25**	$(CH_3)_2$N–	–NH–	2-C_8H_{17}	–
7	$(C_2H_5)_2$N–	–O–	$C_{12}H_{25}$	–	**26**	$(CH_3)_2$N–	–NH–	C_9H_{19}	1.9±0.4
8		–O–	C_8H_{17}	–	**27**	$(CH_3)_2$N–	–NH–	$C_{10}H_{21}$	11.6±2.2
9		–O–	$C_{10}H_{21}$	30.0±5.1	**28**[b]	$(CH_3)_2$N–	–NH–	$C_{12}H_{25}$	9.9±2.0
10		–O–	$C_{11}H_{23}$	–	**29**		–NH–	$C_{10}H_{21}$	–
11		–O–	$C_{12}H_{25}$	11.2±2.1	**30**		–NH–	$C_{12}H_{25}$	5.0±1.1
12		–O–	C_8H_{17}	6.0±1.1	**31**		–NH–	C_8H_{17}	–
13		–O–	2-C_8H_{17}	–	**32**		–NH–	C_9H_{19}	–
14		–O–	C_9H_{19}	–	**33**		–NH–	$C_{10}H_{21}$	–
15		–O–	$C_{10}H_{21}$	5.6±1.1	**34**		–NH–	$C_{12}H_{25}$	5.0±1.1
16		–O–	$C_{11}H_{23}$	3.0±0.6					

[a]Values taken from the literature;[3] [b]mentioned in patents[14,15]

DISCUSSION

The results of the determination of the percutaneous permeation enhancing activity of the prepared compounds showed that substitution of ester moiety with the isosteric amide group led to significant activity loss. This fact is probably not only due to a decrease of the overall lipophilicity of such amides in comparison to the isosteric esters, but more to the presence of an additional hydrogen bond donor site in the CONH moiety and possibly also to the higher melting points of the amides (*e.g.*, m.p. 48–49 °C for 6-(dimethylamino)*N*-dodecyl-hexanamide (**28**), while the isosteric dodecyl 6-dimethylaminohexanoate is a liquid at room temperature). These changes of the physicochemical properties could lead to a higher phase transition temperature of the lipid bilayers of cell membranes of SC of a skin treated with an appropriate amide in comparison with that of a skin treated with the isosteric ester, partially due to the lower SC uptake of the amidic enhancer (comp.[13,14]). In addition, an exchange of the terminal dimethylamino group with any other tertiary amino function, either acyclic diethylamino group, or five- to six-membered saturated basic rings, caused a decrease in the activity. Differences between the enhancing effect of the esters of 6-(piperidin-1-yl)hexanoic acid and the isosteric esters of 6-(morpholin-4-yl)hexanoic acid (the *ER* values of the decyl esters **15** and **20** are 5.6 and 15.0, respectively) suggest that not only the bulkiness of the basic substituent at the terminal position of the chain of hexanoic acid itself, but also its lipophilicity and/or the presence of additional hydrogen bond acceptor site (ethereal oxygen of the morpholine ring) could influence the activity (comp.[15]). However, also the influence of the different basicity of both heterocyclic substituents cannot be excluded (the pK_a of *N*-alkylpiperidines ranges between 9 and 10, while the pK_a of *N*-alkylmorpholines varies from 7 to 8). The overall basicity optimum could be found at a pK_a slightly under 9, which is the value of the most potent 6-(dimethylamino)-hexanoic acid derivative (pK_a of 6-(dimethylamino)*N*-dodecyl-hexanamide (**28**) is 8.8[11]). As far as the alkyl chain length is concerned, the alkyls with 10 and 12 carbon atoms of both prepared esters and amides seem to be more advantageous than those with 8, 9 or 11 carbon atoms, but more data are required for a more concrete statement. In general, the structural changes realized in this study led to compounds with reduced activities.

EXPERIMENTAL

General

The ^{1}H- and ^{13}C-NMR spectra were obtained using a Varian Mercury 300 MHz or Varian Gemini 200 MHz FT-NMR spectrometer in deuterated chloroform or dimethyl sulfoxide. The IR spectra were measured on a Nicolet Impact FTIR spectrometer. Melting points were determined on a Boetius apparatus Nagema (Rapido Wägetechnik, Radebeul, Germany) and are uncorrected. Elemental analyses (C, H, N, O) were performed on a Perkin–Elmer 2400 CHNS/O analyzer. All the presented reaction yields are preparative. Determination of trans-

dermal permeation enhancing activity was performed on the set of cells according to Franz[10] manufactured in the workshops of the Faculty of Pharmacy of the Charles University in Hradec Králové, Czech Republic. The HPLC analyses were performed on the chromatographic system consisting of the isocratic pump LCP 4001(Ecom, Prague, Czech Republic), injector LCI 30 (Laboratorni pristroje, Prague, Czech Republic), column LiChroCart 125-4 (LiChrospher 100, RP 18, 5 μm, Merck, Darmstadt, Germany), an SP 8440 UV detector (Spectra Physics) and the integrating software CSW 1.7 (Data Apex, Prague, Czech Republic), the mixture methanol:water 1:1 was used as the mobile phase at a flow rate 1ml/min. The effluent was monitored at 272 nm. The retention time of theophylline was 2.70±0.02 min.

*Synthesis of esters of 6-(diethylamino)hexanoic acid (**1**, **5–7**), 6-(pyrrolidin-1-yl)hexanoic acid (**2**,**8–11**), 6-(piperidin-1-yl)hexanoic acid (**3**, **12–17**) and 6-(morpholin-4-yl)hexanoic acid (**4**,**18–22**)*

A mixture of 0.500 mol (112 g) of ethyl 6-bromohexanoate and 1.5 mol of the appropriate secondary amine was refluxed under stirring for 24 h. After cooling, the reaction mixture was diluted with 100 ml of diethyl ether and left in a refrigerator until crystals of hydrobromide of the appropriate secondary amine formed. This salt was filtered off, the diethyl ether was evaporated and the residue was distilled under reduced pressure. A reduced pressure distillation of the reaction mixture after alkylation of pyrrolidine with ethyl 6-bromohexanoate also gave a small amount of 1,6-bis(pyrrolidin-1-yl)hexan-1-one (**2a**) as a by-product, probably originating by the direct aminolysis of ethyl 6-(pyrrolidin-1-yl)hexanoate with pyrrolidine.

A solution of 0.020 mol of (**1**), (**2**) (**3**) or (**4**) and 0.10 mol of an appropriate alkanol was heated to 90 °C and then 0.010 mol of sodium was dissolved in it. This mixture was heated to boiling and kept boiling under continuous distilling off of the formed ethanol through a 10 cm long Vigreux column for 6 h. The unreacted alkanol was then distilled off, the liquid residue was diluted with 4.0 ml of 0.50 M aqueous acetic acid, and this mixture was vigorously stirred and then extracted with 3×20 ml of diethyl ether. The combined ethereal extracts were dried with sodium sulfate, the diethyl ether was evaporated and the pure long-chain alkyl ester was obtained by distillation of the liquid residue under reduced pressure.

Alkylamides of 6-(dimethylamino)hexanoic acid

A mixture of 20 mmol ethyl 6-(dimethylamino)hexanoate (**23**), prepared by Eschweiler–Clarke reductive methylation followed by direct esterification with ethanol,[3] and 22 mmol of an appropriate aminoalkane, was heated under stirring at 180 °C for 2.5 h. After cooling, the reaction mixture was distilled under reduced pressure to remove both unreacted **23** and alkylamine and to isolate the desired alkyamide (**24**–**27**). *N*-Decyl-6-(dimethylamino)hexanamide (**27**), which spontaneously solidified at room temperature after it had been isolated by distillation, was additionally recrystallized from hexane. 6-(dimethylamino)*N*-dodecyl-hexanamide (**28**) could not be isolated by distillation under reduced pressure due to its to high boiling temperature, for this reason it was isolated by recrystallization of the residue after dodecylamine and **23** had been distilled off.

Alkylamides of 6-(piperidin-1-yl)hexanoic acid and 6-(morpholin-4-yl)hexanoic acid

A mixture of 0.020 mol of **3** or **4** and 0.022 mol of an alkylamine was heated to a temperature near to the boiling point of the amine for 4 h, then the mixture was distilled under reduced pressure, or it was dissolved in hexane and left to crystallize in a refrigerator to give the corresponding alkylamide.

Evaluation of the activity of the prepared compounds

Testing of transdermal permeation enhancing activity of the prepared compounds was performed by the same manner as was previously described for alkyl esters of 6-(dimethylamino)hexanoic acid.[3]

CONCLUSIONS

32 novel long-chain alkyl esters and *N*-alkylamides of 6-aminohexanoic acids with an acyclic or cyclic tertiary amino group and with alkyl chains in the range from octyl to dodecyl were prepared (compound **28**, 6-(dimethylamino) *N*-dodecyl-hexanamide, which was previously patented in different contexts,[11,12] was also prepared as a member of the homologous series). Thirteen of the prepared compounds were tested on their transdermal permeation enhancement activity *in vitro* using excised human skin with theophylline as the model permeant. All the evaluated substances showed an enhancing effect. The highest activity, characterized by *ER* = 30 was exhibited by compound **9**, *i.e.*, decyl 6-(pyrrolidin-1-yl)-hexanoate. In general, the esters were more potent than the amides. Comparison of the activities of the tested compounds, including the previously prepared alkyl 6-(dimethylamino)hexanoates,[3] suggested that increasing bulkiness of the terminal basic substituent leads to a decrease of the activity and, in addition, a basicity optimum exists in region of pK_a slightly under 9.

Acknowledgements. This work was supported by the Research Project MSM0021620822 of the Ministry of Education of the Czech Republic.

ИЗВОД

ЕСТРИ И АМИДИ ХЕКСАНСКЕ КИСЕЛИНЕ СУПСТИТУИСАНИ ТЕРЦИЈАРНОМ АМИНО ГРУПОМ У ТЕРМИНАЛНОМ ПОЛОЖАЈУ И ЊИХОВА АКТИВНОСТ У ПОВЕЋАЊУ ТРАНСДЕРМАЛНЕ ПРОПУСТЉИВОСТИ

OLDŘICH FARSA[1], PAVEL DOLEŽAL[2] и ALEXANDR HRABÁLEK[3]

[1]*Institute of Chemical Drugs, Faculty of Pharmacy, University of Veterinary and Pharmaceutical Sciences Brno, Palackého 1/3, 612 42 Brno* [2]*Department of Pharmaceutical Technology, Faculty of Pharmacy, Charles University, Hradec Králové и* [3]*Department of Inorganic and Organic Chemistry, Faculty of Pharmacy, Charles University, Hradec Králové, Czech Republic*

Серија алкил естара 6-(диетиламино)-, 6-(пиролидин-1-ил)-, 6-(пиперидин-1-ил) и 6-(морфолин-4-ил)хексанских киселина и алкиламида 6-(диметиламино)-, 6-(пиперидин-1-ил) и 6-(морфолин-4-ил)хексанских киселина, који садрже 8–12 угљеникових атома у алкил- низу, добијена је класичним органским синтезама. Одговарајући секундарни амин алкилован је етил-6-бромхексаноатом (**1**) да би се добио естар *ω*-супституисане хексанске киселине, осим етил-6-(диметиламино)хексаноата, који је добијен Ешвајлер–Кларковим (Eschweiler–Clarke) метиловањем праћеним директном естерификацијом са етанолом. Добијени естри *ω*-супституисане хексанске киселине подвргнути су директној трансестерификацији са алкохолима дугачког низа да би се добили жељени амино естри, или су третирани алкиламинима са дугачким низом да би се добили секундарни амиди одговарајућих хетероцикличних хексанских киселина. Активност ових прозвода у повећању трансдермалне пропустљивости тестирана је *in vitro* на узорцима људске коже, са теофилином као моделом пропустљивости. За

оцену активности коришћен је параметар односа пропустљивости (*ER*), дефинисан као однос укупне количине супстанце која пролази кроз кожу уз присуство испитиваних једињења и без њих. Децил-6-(пиролидин-1-ил)хексаноат (**9**) са *ER* = 30 показао је највећу активност. Ефекти естара у повећању пропустљивости били су, генерално, бољи него ефекти амида.

(Примљено 27. маја 2009, ревидирано 4. јануара 2010)

REFERENCES

1. B. M. Magnusson, K. A. Walters, M. S. Roberts, *Adv. Drug Deliv. Rev.* **50** (2001) 205
2. C. H. Purdon, C. G. Azzi, J. Zhang, E. W. Smith, H. I. Maibach, *Crit. Rev. Ther. Drug Carrier Syst.* **21** (2004) 97
3. A. Hrabálek, P. Doležal, O. Farsa, Z. Šklubalová, *Pharmazie* **55** (2000) 759
4. A. Hrabálek, K. Vávrová, P. Doležal, M. Macháček, *J. Pharm. Sci.* **94** (2005) 1494
5. A. Hrabálek, P. Doležal, M. Roman, M. Macháček, Z. Šklubalová, *Pharmazie* **49** (1994) 325
6. K. Vávrová, K. Lorencová, J. Novotný, A. Holý, A. Hrabálek, *Eur. J. Pharm. Biopharm.* **70** (2008) 901
7. J. Novotný, P. Kovaříková, M. Novotný, B. Janůšová, A. Hrabálek, K. Vávrová, *Pharm. Res.* **26** (2009) 811
8. F. Franke, M. Klepel, H. Lehman, C. Schromm, B. Braemer, (Fahlberg List), DD 201371 (1983)
9. R. Fusco, G. Palazzo, S. Chavarelli, D. Bovet, *Gazz. Chim. Ital.* **79** (1949) 836
10. T. J. Franz, *J. Invest. Dermatol.* **64** (1975) 190
11. V. Böllert, U. Curtius, G. Fritz, J. Nentwig, (Bayer Leverkusen), DE 1418849 (1969)
12. J. Conrad, H. Schnegelberger, H.-W. Eckert, F. Saygin, G. Koppensteiner, (Henkel), DE 2355026 (1975)
13. J. Hadgraft, J. Peck, D. G. Williams, W. J. Pugh, G. Allan, *Int. J. Pharm.* **141** (1996) 17
14. K. M. B. Mackay, A. C. Williams, B. W. Barry, *Int. J. Pharm.* **228** (2001) 89
15. Y. Song, C. Xiao, R. Mendelsohn, T. Zheng, L. Strekowski, B. Michniak, *Pharm. Res.* **22** (2005) 1918
16. P. A. Barett, (Wellcome Foundation), GB 682160 (1952)
17. P. Barczynski, Z. Dega-Szafran, E. Dulewicz, M. Petryna, M. Szafran, *Pol. J. Chem.* **74** (2000) 1149
18. Y. K. Lu, O. Y. Magidson, *Zh. Obshch. Khim.* **29** (1959) 3299
19. T. Abe, H. Baba, K. Okuhara, H. Fukaya, *J. Fluorine Chem.* **111** (2001) 115.

Journal of the Serbian Chemical Society
JSCS@tmf.bg.ac.rs • www.shd.org.rs/JSCS

J. Serb. Chem. Soc. 75 (5) S1–S10 (2010)
JSCS–3990

UDC 547.295.2+547.288.2+542.913+
547:616.032:611.778
Supplementary material

SUPPLEMENTARY MATERIAL TO

Esters and amides of hexanoic acid substituted with tertiary amino group in terminal position and their activity as transdermal permeation enhancers

OLDŘICH FARSA[1]*, PAVEL DOLEŽAL[2] and ALEXANDR HRABÁLEK[3]

[1]*Institute of Chemical Drugs, Faculty of Pharmacy, University of Veterinary and Pharmaceutical Sciences Brno, Palackého 1/3, 612 42 Brno,* [2]*Department of Pharmaceutical Technology, Faculty of Pharmacy, Charles University, Hradec Králové and* [3]*Department of Inorganic and Organic Chemistry, Faculty of Pharmacy, Charles University, Hradec Králové, Czech Republic*

J. Serb. Chem. Soc. 75 (5) (2010) 605–613

*Ethyl 6-(diethylamino)hexanoate (**1**).* Yield 50 %; b.p. 104–109 °C at 0.7–0.9 kPa (137–140 °C at 1.86 kPa[16]). IR ($CHCl_3$, cm^{-1}): 2973, 2838, 1727, 1466, 1375, 1300, 1270. ^{1}H-NMR (300 MHz, $CDCl_3$, δ / ppm): 4.13 (2H, *q*, *J* = 14.5, 7.4 Hz, $CH_3C\mathbf{H}_2O$), 2.49 (4H, *q*, *J* = 14.0, 6.9 Hz, $(CH_3C\mathbf{H}_2)_2N$), 2.40 (2H, *t*, *J* = = 7.2 Hz, CH_2CO), 2.30 (2H, *t*, *J* = 7.5 Hz, NCH_2 acyl), 1.70–1.58 (2H, *m*, CH_2 acyl), 1.52–1.38 (2H, *m*, CH_2 acyl), 1.36–1.20 (5H, *m*, CH_2 acyl + $C\mathbf{H}_3CH_2O$), 1.00 (6H, *t*, *J* = 6.5 Hz, $(C\mathbf{H}_3CH_2)_2N$). ^{13}C-NMR (75 MHz, δ / ppm): 173.45 (CO), 60.07 (OCH_2), 52.70 (CH_2N acyl), 46.80 ($(CH_2)_2N$), 34.28 ($\mathbf{C}H_2CO$), 27.22 ($\mathbf{C}H_2CH_2N$), 26.73 ($\mathbf{C}H_2(CH_2)_2CO$), 24.95 ($\mathbf{C}H_2CH_2CO$), 14.25 ($\mathbf{C}H_3CH_2O$) 11.68 ($(\mathbf{C}H_3CH_2)_2N$).

*Ethyl 6-(pyrrolidin-1-yl)hexanoate (**2**).* Yield 53 %; b.p. 106–112 °C at 0.5––0.6 kPa (143–146°C at 2.0 kPa[16]). IR ($CHCl_3$, cm^{-1}): 2965, 2938, 2880, 2865, 2800, 1727, 1464, 1375, 1301, 1271. ^{1}H-NMR (200 MHz, $CDCl_3$, δ / ppm): 4.11 (2H, *q*, *J* = 14.3, 7.3 Hz, OCH_2), 2.55–2.36 (6H, *m*, $(CH_2)_3N$), 2.29 (2H, *t*, *J* = = 7.51 Hz, CH_2CO), 1.82–1.30 (10H, *m*, $5CH_2$), 1.24 (3H, *t*, *J* = 7.1 Hz, CH_3). ^{13}C-NMR (50 MHz, δ / ppm): 173.67 (CO), 60.10 (OCH_2) 56.40 (NCH_2 acyl), 54.18 ($(CH_2)_2N$ pyrr.), 34.30 ($\mathbf{C}H_2CO$), 28.65 (CH_2), 27.25 (CH_2), 24.92 (CH_2), 23.43 (CH_2), 14.20 (CH_3).

*1,6-Bis(pyrrolidin-1-yl)hexan-1-one (**2a**), a side product.* Yield 3 %; b.p. 178–183 °C at 0.06–0.08 kPa; Anal. Calcd. for $C_{14}H_{26}N_2O$: C, 70.54; H, 10.99; N, 11.75; O, 6.71 %. Found: C, 70.61; H, 11.05; N, 11.69; O, 6.80 %. IR ($CHCl_3$,

* Corresponding author. E-mail: farsao@vfu.cz

cm^{-1}): 2973, 2936, 2879, 2800, 1624, 1448, 1343, 1328, 1294, 1270, 1252. ^{1}H-NMR (200 MHz, $CDCl_3$, δ / ppm): 3.40 (4H, *qi*, 2 CH_2); 2.58–2.37 (6H, *m*, $(CH_2)_3N$) acyl); 2.24 (2H, *t*, *J* = 7.5 Hz, CH_2CO), 2.00–1.15 (14H, *m*, 7 CH_2). ^{13}C-NMR (50 MHz, δ / ppm): 171.55 (CO), 56.43 (NCH_2 acyl), 54.16 ($(CH_2)_2N$ pyrr-acyl), 46.50 ($CON(\mathbf{C}H_2)_2$), 45.48 (CH_2), 34.63 ($\mathbf{C}H_2CO$), 28.81 (CH_2), 27.55 (CH_2), 26.06 (CH_2), 24.77 (CH_2), 24.33 (CH_2), 23.38 (CH_2).

*Ethyl 6-(piperidin-1-yl)hexanoate (**3**)*. Yield 55 %, b.p. 120–124 °C at 0.13 kPa (114–115 °C at 0.11 kPa[17]). IR ($CHCl_3$, cm^{-1}): 2938, 2865, 2800, 1727, 1464, 1375, 1271. ^{1}H-NMR (200 MHz, $CDCl_3$, δ / ppm): 4.11 (2H, *q*, *J* = 14.3, 7.3 Hz, OCH_2) 2.43–2.20 (4H, *m*, NCH_2 + CH_2CN acyl), 2.3 (4H, *4t*, *J* = 7.0 Hz, 2 CH_2N piperid.), 1.77–1.30 (12H, *m*, β+γ CH_2 piperid. + β+γ+δ CH_2 acyl), 1.24 (3H, *t*, *J* = 7.1 Hz, CH_3). ^{13}C-NMR (50 MHz, δ / ppm): 173.67 (CO), 60.10 (OCH_2), 59.35 (NCH_2 acyl), 54.63 ($(CH_2)_2N$ piperid), 34.33 ($\mathbf{C}H_2CO$), 27.33 ($NCH_2\mathbf{C}H_2$), 26.04 (CH_2), 25.02 ($\mathbf{C}H_2CH_2CO$), 14.20 (CH_3).

*Ethyl 6-(morpholin-4-yl)hexanoate (**4**)*. Yield: 82 %; b.p. 120–123 °C at 0.4 kPa (140–144 °C at 0.53 kPa,[18] 150–153 °C at 0.53 kPa[19]). IR ($CHCl_3$, cm^{-1}): 2941, 2863, 1727, 1458, 1375, 1256. ^{1}H-NMR (300 MHz, $CDCl_3$, δ / ppm): 4.11 (2H, *q*, *J* = 14.4, 7.5 Hz, $CH_3C\mathbf{H}_2O$), 3.70 (4H, *t*, *J* = 4.7 Hz, $O(C\mathbf{H}_2CH_2)_2N$), 2.40 (4H, *t*, *J* = 4.4 Hz, $O(CH_2C\mathbf{H}_2)_2N$), 2.35–2.25 (4H, *m*, CH_2CO + NCH_2 acyl), 1.73–1.41 (6H, *m*, $(3CH_2)$), 0.87 (3H, *t*, *J* = 6.7 Hz, CH_3). ^{13}C-NMR (75 MHz, $CDCl_3$, δ / ppm): 173.28 (CO), 66.82 ($(CH_2)_2O$ morph.), 60.04 ($\mathbf{C}H_2OCO$), 58.74 (CH_2N acyl), 53.64 ($(CH_2)_2N$ morph.), 34.15 ($\mathbf{C}H_2CO$), 26.93 ($\mathbf{C}H_2CH_2N$ acyl), 26.16 ($\mathbf{C}H_2(CH_2)_2CO$), 24.79 ($\mathbf{C}H_2CH_2CO$), 14.21 (CH_3).

*Octyl 6-(diethylamino)hexanoate (**5**)*. Yield 67 %; b.p. 134–138 °C at 0.035 kPa; Anal. Calcd. for $C_{18}H_{37}NO_2$: C, 72.19; H, 12.45; N, 4.68; O, 10.68 %. Found: C, 72.25; H, 12.35; N, 4.59; O, 10.80 %. IR ($CHCl_3$, cm^{-1}): 2930, 2856, 1727, 1465, 1378, 1271. ^{1}H-NMR (300 MHz, $CDCl_3$, δ / ppm): 4.04 (2H, *t*, *J* = 6.9 Hz, OCH_2), 2.50 (4H, *q*, *J* = 7.1, 14.3 Hz, $(CH_3C\mathbf{H}_2)_2N$), 2.36 (2H, *t*, *J* = 7.7 Hz, $NC\mathbf{H}_2CH_2$), 2.29 (2H, *t*, *J* = 7.6 Hz, CH_2CO), 1.68–1.25 (18H, *m*, 9 CH_2), 0.99 (6H, *t*, *J* = 7.1 Hz, $(C\mathbf{H}_3CH_2)_2N$), 0.87 (3H, *t*, *J* = 6.7 Hz, CH_3 octyl). ^{13}C-NMR (75 MHz, δ / ppm): 174.12 (CO), 64.66 (OCH_2), 52.98 (NCH_2), 47.07 ($(CH_3\mathbf{C}H_2)_2N$), 34.58 ($\mathbf{C}H_2CO$), 32.01 (CH_2), 29.44 ($\mathbf{C}H_2CO$), 29.41 ($\mathbf{C}H_2CO$), 28.86 ($\mathbf{C}H_2CO$), 27.48 ($\mathbf{C}H_2CO$), 26.94 ($\mathbf{C}H_2CO$), 26.16 ($\mathbf{C}H_2CO$), 25.23 (CH_2CO), 22.65 ($\mathbf{C}H_2CH_3$ octyl), 14.32 (CH_3 octyl). 11.87 ($(\mathbf{C}H_3CH_2)_2N$).

*Decyl 6-(diethylamino)hexanoate (**6**)*. Yield 52 %; b.p. 154–158 °C at 0.018 kPa. Anal. calcd. for $C_{20}H_{41}NO_2$: C, 73.34; H, 12.62; N, 4.28; O, 9.77 %. Found: C, 73.25; H, 12.54; N, 4.17; O, 9.66 %. IR ($CHCl_3$, cm^{-1}): 2933, 2859, 1727, 1458, 1378, 1270. ^{1}H-NMR (300 MHz, $CDCl_3$, δ / ppm): 4.05 (2H, *t*, *J* = 6.8 Hz, OCH_2), 2.51 (4H, *q*, *J* = 7.1, 14.3 Hz, $(CH_3C\mathbf{H}_2)_2N$), 2.37 (2H, *t*, *J* = 7.7 Hz, $NC\mathbf{H}_2CH_2$), 2.29 (2H, *t*, *J* = 7.6 Hz, CH_2CO), 1.69–1.23 (20H, *m*, 10 CH_2), 0.99 (6H, *t*, *J* = 7.1 Hz, $(C\mathbf{H}_3CH_2)_2N$), 0.87 (3H, *t*, *J* = 6.7 Hz, CH_3 decyl). ^{13}C-NMR

(75 MHz, δ / ppm): 173.91 (CO), 64.48 (OCH_2), 52.69 (NCH_2), 46.80 ((CH_3**C**H_2)$_2$N), 29.31 (CH_2), 29.22 (CH_2), 28.59 (CH_2), 27.21 (CH_2); 26.66 (CH_2), 25.89 (CH_2), 24.96 (CH_2), 22.65 (CH_2), 14.15 (CH_3 decyl), 11.59 (($\mathbf{C}H_3CH_2$)$_2$N).

*Dodecyl 6-(diethylamino)hexanoate (**7**)*. Yield: 52 %; b.p. 162–166 at 0.02 kPa. Anal. Calcd. for $C_{22}H_{45}NO_2$: C, 74.31; H, 12.76; N, 3.94; O, 9.0 %. Found: C, 74.27; H, 12.64; N, 4.02; O, 8.92 %. IR ($CHCl_3$, cm^{-1}): 2931, 2859, 1727, 1465, 1378, 1270. ^{1}H-NMR (300 MHz, $CDCl_3$, δ / ppm): 4.03 (2H, *t*, *J* = 6.7 Hz, OCH_2), 2.50 (4H, *q*, *J* = 14.3, 7.1 Hz, ($CH_3C\mathbf{H}_2$)$_2$N), 2.38 (2H, *t*, *J* = 7.6 Hz, $NC\mathbf{H}_2CH_2$), 2.30 (2H, *t*, *J* = 7.6 Hz, CH_2CO), 1.63–1.56 (2H, *m*, $OCH_2C\mathbf{H}_2$), 1.49–1.35 (2H, *m*, CH_2), 1.32–1.24 (18H, *m*, 9 CH_2), 0.99 (6H, *t*, *J* = 7.1 Hz, ($C\mathbf{H}_3CH_2$)$_2$N), 0.88 (3H, *t*, *J* = 6.7 Hz, CH_3 dodecyl). ^{13}C-NMR (75 MHz, δ / / ppm): 173.83 (CO), 64.38 (OCH_2), 52.69 (NCH_2), 46.79 ((CH_3**C**H_2)$_2$N), 34.30 (**C**H_2CO), 29.60 (CH_2), 29.59 (CH_2), 29.54 (CH_2), 29.49 (CH_2), 29.31 (CH_2), 29.22 (CH_2), 28.59 (CH_2), 27.21 (CH_2), 26.66 (CH_2), 25.89 (CH_2), 24.96 (**C**H_2CH_2CO), 22.65 (**C**H_2CH_3 dodecyl), 14.08 (CH_3 dodecyl), 11.59 (($\mathbf{C}H_3CH_2$)$_2$N).

*Octyl 6-(pyrrolidin-1-yl)hexanoate (**8**)*. Yield: 71 %; b.p. 127–136 °C at 0.03 kPa. Anal. Calcd. for $C_{18}H_{35}NO_2$: C, 72.68; H, 11.86; N, 4.71; O, 10.76 %. Found: C, 72.56; H, 11.92; N, 4.61; O, 10.82 %. IR ($CHCl_3$, cm^{-1}): 2930, 2858, 2801, 1724, 1466, 1352, 1270. ^{1}H-NMR (300 MHz, $CDCl_3$, δ / ppm): 4.04 (2H, *t*, *J* = 6.7 Hz, OCH_2), 2.51–2.35 (6H, *m*, (CH_2)$_2$N pyrr. + NCH_2 acyl), 2.30 (2H, *t*, *J* = 7.5 Hz, CH_2CO), 1.79–1.73 (4H, *m*, 2 C*H*$_2$), 1.69–1.46 (6H, *m*, 3 CH_2), 1.40–1.19 (14H, *m*, 7 CH_2), 0.87 (3H, *t*, *J* = 6.9 Hz, CH_3). ^{13}C-NMR (75 MHz, δ / ppm): 173.59 (CO), 64.40 (OCH_2), 56.40 (NCH_2 acyl), 54.20 ((CH_2)$_2$N pyrr.), 34.30 (**C**H_2CO), 31.79 (**C**$H_2CH_2CH_3$), 29.22 (CH_2 alkyl), 29.20 (CH_2 alkyl), 28.80 ($OCH_2\mathbf{C}H_2$), 28.66 (NCH_2CH_2 acyl), 27.29 (**C**H_2(CH_2)$_2$CO), 25.95 (O(CH_2)$_2\mathbf{C}H_2$), 24.99 (**C**H_2CH_2CO), 23.40 (($\mathbf{C}H_2$)$_2CH_2$N pyrr., *i.e.*, 2 βCH_2 pyrr.), 22.66 (**C**H_2CH_3), 14.13 (CH_3).

*Decyl 6-(pyrrolidin-1-yl)hexanoate (**9**)*. Yield: 62 %; b.p.150–155 °C at 0.02 kPa. Anal. Calcd. for $C_{20}H_{39}NO_2$: C, 73.79; H, 12.08; N, 4.30; O, 9.83 %. Found: C, 73.67; H, 12.15; N, 4.21; O, 9.91 %. IR ($CHCl_3$, cm^{-1}): 2929, 2858, 2800, 1724, 1467, 1353, 1272. ^{1}H-NMR (300 MHz, $CDCl_3$, δ / ppm): 4.07 (2H, *t*, *J* = 6.8 Hz, OCH_2), 2.51–2.34 (6H, *m*, (CH_2)$_2$N pyrr.+ NCH_2 acyl), 2.29 (2H, *t*, *J* = 7.5 Hz, CH_2CO), 1.79–1.73 (4H, *m*, 2 CH_2), 1.68–1.45 (6H, *m*, 3 CH_2), 1.41–1.16 (16H, *m*, 8 CH_2), 0.87 (3H, *t*, *J* = 6.7 Hz, CH_3). ^{13}C-NMR (75 MHz, δ / ppm): 173.61 (CO), 64.40 (OCH_2), 56.42 (NCH_2 acyl), 54.21((CH_2)$_2$N pyrr.), 34.33 (**C**H_2CO), 31.92 (**C**$H_2CH_2CH_3$), 29.66 (CH_2 alkyl), 29.62 (CH_2 alkyl), 29.57 (CH_2 alkyl), 29.35 (CH_2 alkyl), 29.29 (CH_2 alkyl), 28.79 ($OCH_2\mathbf{C}H_2$), 28.68 ($NCH_2\mathbf{C}H_2$ acyl), 27.31 (**C**H_2(CH_2)$_2$CO), 25.98 (O(CH_2)$_2\mathbf{C}H_2$), 25.01 (**C**H_2CH_2CO), 23.42 (($\mathbf{C}H_2$)$_2CH_2$N pyrr., *i.e.*, 2 βCH_2 pyrr.), 22.73 (**C**H_2CH_3), 14.18 (CH_3).

*Undecyl 6-(pyrrolidin-1-yl)hexanoate (**10**)*. Yield: 66 %; b.p. 169–170 °C at 0.04 kPa. IR ($CHCl_3$, cm^{-1}): 2928, 2856, 2801, 1724, 1466, 1352, 1275; ^{1}H--NMR (300 MHz, $CDCl_3$, δ / ppm): 4.04 (2H, *t*, *J* = 6.8 Hz, OCH_2), 2.51–2.35 (*m*, 6H, $(CH_2)_2N$ pyrr.+ NCH_2 acyl), 2.29 (2H, *t*, *J* = 7.5 Hz, CH_2CO), 1.81–1.71 (4H, *m*, 2 CH_2), 1.69–1.47 (6H, *m*, 3 CH_2); 1.40–1.18 (18H, *m*, 9 CH_2), 0.87 (3H, *t*, *J* = 6.6 Hz, CH_3). ^{13}C-NMR (75 MHz, δ / ppm): 173.57 (CO), 64.37 (OCH_2), 56.40 (NCH_2 acyl); 54.21 ($(CH_2)_2N$ pyrr.), 34.30 (**C**H_2CO), 31.92 (**C**$H_2CH_2CH_3$); 29.62 (CH_2 alkyl); 29.60 (CH_2 alkyl), 29.55 (CH_2 alkyl), 29.35 (CH_2 alkyl), 29.28 (CH_2 alkyl), 28.81 (OCH_2**C**H_2), 28.66 (NCH_2**C**H_2 acyl), 27.29 (**C**$H_2(CH_2)_2CO$), 25.96 ($O(CH_2)_2$**C**H_2), 25.00 (**C**H_2CH_2CO), 23.41 ((**C**$H_2)_2CH_2N$ pyrr., *i.e.*, 2 βCH_2 pyrr.), 22.71 (**C**H_2CH_3), 14.17 (CH_3).

*Dodecyl 6-(pyrrolidin-1-yl)hexanoate (**11**)*. Yield 49 %; b.p. 182–183 °C at 0.04 kPa. Anal. Calcd. for $C_{22}H_{43}NO_2$: C, 74.73; H, 12.26; N, 3.96; O, 9.05 %. Found: C, 74.68; H, 12.35; N, 3.89; O, 9.11 %. IR ($CHCl_3$, cm^{-1}): 2928, 2856, 2801, 1724, 1466, 1352, 1275. ^{1}H-NMR (300 MHz, $CDCl_3$, δ / ppm): 4.04 (2H, *t*, *J* = 6.8 Hz, OCH_2), 2.52–2.37 (6H, *m*, $(CH_2)_2N$ pyrr. + NCH_2 acyl), 2.30 (2H, *t*, *J* = 7.4 Hz, CH_2CO), 1.81–1.71 (4H, *m*, 2 CH_2), 1.70–1.46 (6H, *m*, 3 CH_2), 1.42–1.17 (20H, *m*, 10 CH_2), 0.87 (3H, *t*, *J* = 6.8 Hz, CH_3). ^{13}C-NMR (75 MHz, δ / ppm): 173.61 (CO). 64.40 (OCH_2), 56.42 (NCH_2 acyl), 54.22 $(CH_2)_2N$ pyrr.), 34.33 (**C**H_2CO), 31.95 (**C**$H_2CH_2CH_3$), 29.69 (CH_2 alkyl), 29.67 (CH_2 alkyl), 29.62 (CH_2 alkyl), 29.57 (CH_2 alkyl), 29.39 (CH_2 alkyl), 29.30 (CH_2 alkyl), 28.81 (OCH_2CH_2), 28.69 (NCH_2CH_2 acyl), 27.32 ($CH_2(CH_2)_2CO$), 25.98 ($O(CH_2)_2CH_2$), 25.02 (**C**H_2CH_2CO), 23.43 ((**C**$H_2)_2CH_2N$ pyrr., *i.e.*, 2 βCH_2 pyrr.), 22.74 (**C**H_2CH_3), 14.19 (CH_3).

*Octyl 6-(piperidin-1-yl)hexanoate (**12**)*. Yield: 62 %; b.p.163 °C at 0.04–0.05 kPa; Anal. Calcd. for $C_{19}H_{37}NO_2$: C, 73.26; H, 11.97; N, 4.50; O, 10.27 %. Found: C, 73.18; H, 12.05; N, 4.43; O, 10.39 %. IR ($CHCl_3$, cm^{-1}): 2934, 2858, 1724, 1469, 1456, 1378, 1271, 1258. ^{1}H-NMR (300 MHz, $CDCl_3$, δ / ppm): 4.04 (2H, *t*, *J* = 6.5 Hz, OCH_2), 2.41–2.20 (8H, *m*, (4 CH_2), 1.69–1.37 (12H, *m*, 6 CH_2), 1.36–1.20 (12H, *m*, 6 CH_2), 0.88 (3H, *t*, *J* = 6.8 Hz, CH_3). ^{13}C-NMR (75 MHz, $CDCl_3$, δ / ppm): 173.61 (CO); 64.39 (OCH_2), 59.35 (NCH_2 acyl), 54.63 ($(CH_2)_2N$ piperid.), 34.33 (**C**H_2CO), 31.81 (CH_2); 29.25 (CH_2) 29.22 (CH_2), 28.67 (CH_2), 27.33 (NCH_2**C**H_2), 26.68 (CH_2); 26.04 (CH_2), 25.97 (CH_2), 25.02 (**C**H_2CH_2CO), 24.54 (CH_2), 22.68 (**C**H_2CH_3); 14.15 (CH_3).

*2-Octyl 6-(piperidin-1-yl)hexanoate (**13**)*. Yield: 68 %; pale yellow oil. Anal. Calcd. for $C_{19}H_{37}NO_2$: C, 73.26; H, 11.97; N, 4.50; O, 10.27 %. Found: C, 73.21; H, 12.08; N, 4.41; O, 10.34 %. IR ($CHCl_3$, cm^{-1}): 2936, 2858, 1725, 1469, 1456, 1378, 1271, 1257. ^{1}H-NMR (300 MHz, $CDCl_3$, δ / ppm): 4.98–4.82 (1H, *m*, OCH), 2.43–2.20 (8H, *m*, 4 CH_2) 1.69–1.37 (12H, *m*, 6 CH_2), 1.36–1.13 (13H, *m*, 5 CH_2 + CH**C**H_3), 0.87 (3H, *t*, *J* = 6.80 Hz, terminal CH_3). ^{13}C-NMR (75 MHz, $CDCl_3$, δ / ppm) 173.17 (CO), 70.71 (OCH), 59.37 (NCH_2 acyl), 54.63

((CH_2)$_2$N piperid.), 35.96 (OCH**C**H_2), 34.69 (**C**H_2CO), 31.78 (CH_2), 29.14 (CH_2), 27.32 (NCH_2**C**H_2), 26.70 (CH_2), 26.04 (CH_2), 25.41 (OCHCH_2**C**H_2), 25.10 (**C**H_2CH_2CO), 24.54 (**C**H_2(CH_2)$_2$ piperid.), 22.62 (**C**H_2CH_3), 20.06 (OCH**C**H_3), 14.13 (CH_2**C**H_3).

*Nonyl 6-(piperidin-1-yl)hexanoate (**14**)*. Yield: 47 %; pale yellow oil. Anal. Calcd. for $C_{20}H_{39}NO_2$: C, 73.79; H, 12.08; N, 4.30; O, 9.83 %. Found: C, 73.69; H, 12.15; N, 4.24; O, 9.94 %. IR ($CHCl_3$, cm^{-1}): 2934, 2857, 1724, 1468, 1456, 1378, 1271, 1257. ^{1}H-NMR (300 MHz, $CDCl_3$, δ / ppm): 4.03 (2H, *t*, *J* = 6.7 Hz, OCH_2), 2.41–2.21 (8H, *m*, 4 CH_2), 1.70–1.18 (26H, *m*, 13 CH_2), 0.86 (3H, *t*, *J* = = 6.7 Hz, CH_3). ^{13}C-NMR (75 MHz, $CDCl_3$, δ / ppm): 173.81 (CO), 64.38 (OCH_2), 59.30 (NCH_2 acyl), 54.57 ((CH_2)$_2$N piperid.), 34.25 (**C**H_2CO), 31.80 (CH_2), 29.43 (CH_2), 29.20 (CH_2), 29.19 (CH_2), 28.58 (CH_2), 27.24 (CH_2), 26.56 (CH_2), 25.91 (CH_2), 25.88 (CH_2), 24.92 (**C**H_2CH_2CO), 24.42 (*C*H_2), 22.61 (**C**H_2CH_3), 14.06 (CH_3).

*Decyl 6-(piperidin-1-yl)hexanoate (**15**)*. Yield: 55 %; pale yellow oil. Anal. Calcd. for $C_{21}H_{41}NO_2$: C, 74.28; H, 12.17; N, 4.13; O, 9.42 %. Found: C, 74.18; H, 12.25; N, 4.07; O, 9.53 %. IR ($CHCl_3$ cm^{-1}): 2931, 2857, 1724, 1468, 1456, 1378, 1271, 1258. ^{1}H-NMR (300 MHz, $CDCl_3$, δ / ppm): 4.04 (2H, *t*, *J* = 6.7 Hz, OCH_2), 2.38–2.30 (4H, *m*, 2 CH_2), 2.26 (2H, *t*, *J* = 7.7 Hz, CH_2CO), 1.67–1.48 (10H, *m*, 5 CH_2), 1.35–1.24 (20H, *m*, 10 CH_2), 0.87 (3H, *t*, *J* = 6.7 Hz, CH_3). ^{13}C-NMR (75 MHz, $CDCl_3$, δ / ppm): 173.86 (CO), 64.41 (OCH_2), 59.36 (NCH_2 acyl), 54.62 ((CH_2)$_2$N piperid.), 34.29 (**C**H_2CO), 31.89 (CH_2), 29.62 (CH_2), 29.61 (CH_2), 29.55 (CH_2), 29.51 (CH_2), 29.33 (CH_2), 29.24 (**C**H_2); 28.61 (CH_2), 27.27 (CH_2), 26.62 (CH_2), 25.97 (CH_2), 25.91 (CH_2), 24.95 (**C**H_2CH_2CO), 24.47 (CH_2), 22.66 (**C**H_2CH_3), 14.10 (CH_3).

*Undecyl 6-(piperidin-1-yl)hexanoate (**16**)*. Yield 53 %; pale yellow oil. Anal. Calcd. for $C_{22}H_{43}NO_2$: C, 74.73; H, 12.26; N, 3.96; O, 9.05 %. Found: C, 74.68; H, 12.35; N, 3.88; O, 9.12 %. IR ($CHCl_3$, cm^{-1}): 2927. 2856, 1724, 1468, 1457, 1378, 1271, 1258. ^{1}H-NMR (300 MHz, $CDCl_3$, δ / ppm): 4.04 (2H, *t*, *J* = 6.7 Hz, OCH_2), 2.40–2.24 (8H, *m*, 4 CH_2), 1.68–1.25 (30H, *m*, 15 CH_2), 0.87 (3H, *t*, *J* = = 6.6 Hz, CH_3). ^{13}C-NMR (75 MHz, $CDCl_3$, δ / ppm): 174.11 (CO), 64.67 (OCH_2), 59.57 (NCH_2 acyl), 54.84 ((CH_2)$_2$N piperid.), 34.54 (**C**H_2CO), 32.14 (CH_2), 31.82 (CH_2), 29.84 (CH_2); 29.81 (CH_2), 29.76 (CH_2), 29.57 (CH_2), 29.49 (CH_2), 28.87 (CH_2), 27.52 (CH_2), 26.83 (CH_2), 26.18 (CH_2), 25.20 (CH_2), 24.69 (CH_2), 22.89 (**C**H_2CH_3); 14.36 (CH_3).

*Dodecyl 6-(piperidin-1-yl)hexanoate (**17**)*. Yield: 78 %; pale yellow oil. Anal. Calcd. for $C_{23}H_{45}NO_2$: C, 75.15; H, 12.34; N, 3.81; O, 8.70 %. Found: C, 75.08; H, 12.42; N, 3.75; O, 8.79 %. IR ($CHCl_3$, cm^{-1}): 2930, 2856, 1724, 1468, 1457, 1378, 1271, 1258; ^{1}H-NMR (300 MHz, $CDCl_3$, δ / ppm): 4.05 (2H, *t*, *J* = = 6.7 Hz, OCH_2), 2.40–2.24 (8H, *m*, 4 CH_2), 1.69–1.26 (32H, *m*, 16 CH_2), 0.88 (3H, *t*, *J* = 6.6 Hz, CH_3). ^{13}C-NMR (75 MHz, $CDCl_3$, δ / ppm): 173.86 (CO),

64.41 (OCH_2), 59.36 (NCH_2 acyl), 54.62 (($CH_2)_2$N piperid.), 34.29 (**C**H_2CO), 31.89 (CH_2), 29.62 (CH_2), 29.61 (CH_2), 29.55 (CH_2), 29.51 (CH_2), 29.33(CH_2), 29.23 (CH_2), 28.61 (CH_2), 27.27 (NCH_2**C**H_2 acyl), 26.62 (CH_2), 25.97 (CH_2), 25.91 (CH_2), 24.95 (**C**H_2CH_2CO), 24.47 (CH_2), 22.66 (**C**H_2CH_3), 14.10 (CH_3).

*Octyl 6-(morpholin-4-yl)hexanoate (**18**)*. Yield: 58 %, b.p. 161–163 °C at 0.04–0.05 kPa. Anal. Calcd. for $C_{18}H_{35}NO_3$: C, 68.97; H, 11.25; N, 4.47; O, 15.31 %. Found: C, 69.08; H, 11.33; N, 4.38; O, 15.39 %. IR ($CHCl_3$, cm^{-1}): 2930, 2859, 1724, 1468, 1373, 1287, 1258. ^{1}H-NMR (300 MHz, $CDCl_3$, δ / ppm): 4.04 (2H, *t*, *J* = 6.7 Hz, OCH_2 alkyl), 3.70 (4H, *t*, *J* = 4.6 Hz, O(C**H**$_2CH_2)_2$N), 2.41 (4H, *t*, O(CH_2C**H**$_2)_2$N), 2.30–2.26 (4H, *m*, CH_2CO + NCH_2 acyl), 1.73–1.41 (6H, *m*, 3 CH_2), 1.40–1.18 (12H, *m*, 6 CH_2), 0.87 (3H, *t*, *J* = 6.8 Hz, CH_3). ^{13}C-
-NMR (75 MHz, $CDCl_3$, δ / ppm): 173.53 (CO), 66.93 (($CH_2)_2$O morph.), 64.41 (OCH_2), 58.86 (NCH_2 acyl), 53.74 (($CH_2)_2$N morph.), 34.28 (**C**H_2CO), 31.79 (**C**$H_2CH_2CH_3$), 29.23 (CH_2), 29.21 (CH_2), 28.66 (OCH_2**C**H_2), 27.05 (NCH_2**C**H_2 acyl), 26.26 (**C**$H_2(CH_2)_2$CO), 25.95 (O($CH_2)_2$**C**H_2), 24.93 (**C**H_2CH_2CO), 22.67 (**C**H_2CH_3), 14.15 (CH_3).

*Nonyl 6-(morpholin-4-yl)hexanoate (**19**)*. Yield 56 %; b.p. 175–179 °C at 0.04–0.06 kPa. Anal. Calcd. for $C_{19}H_{37}NO_3$: C, 69.68; H, 11.39; N, 4.28; O, 14.66 %. Found: C, 69.78; H, 11.43; N, 4.19; O, 14.69 %. IR ($CHCl_3$, cm^{-1}): 2928, 2858, 1725, 1467, 1375, 1287, 1259. ^{1}H-NMR (300MHz, $CDCl_3$, δ / ppm): 4.15–3.95 (2H, *m*, OCH_2), 3.70 (4H, *t*, *J* = 6.8 Hz, O(C**H**$_2CH_2)_2$N), 2.41 (4H, *t*, *J* = 4.5 Hz, O(CH_2C**H**$_2)_2$N), 2.34–2.24 (4H, *m*, CH_2CO + NCH_2 acyl), 1.70–1.43 (6H, *m*, 3 CH_2), 1.39–1.19 (14H, *m*, 7 CH_2), 0.87 (3H, *t*, *J* = 6.8 Hz, CH_3). ^{13}C-NMR (75 MHz, $CDCl_3$, δ / ppm): 173.52 (CO), 66.94 (($CH_2)_2$O morph.), 64.41 (OCH_2), 58.87 (NCH_2 acyl), 53.75 (($CH_2)_2$N morph.), 34.28 (**C**H_2CO), 31.91 ($CH_2CH_2CH_3$), 29.55 (CH_2), 29.33 (CH_2), 29.27 (CH_2), 28.66 (OCH_2CH_2), 27.05 (NCH_2**C**H_2 acyl), 26.27 (**C**$H_2(CH_2)_2$CO), 25.96 (O($CH_2)_2$**C**H_2), 24.94 (**C**H_2CH_2CO), 22.71 (**C**H_2CH_3), 14.17 (CH_3).

*Decyl 6-(morpholin-4-yl)hexanoate (**20**)*. Yield 48 %; b.p. 150 °C at 0.02 kPa. Anal. Calcd. for $C_{20}H_{39}NO_3$: C, 70.33; H, 11.51; N, 4.10; O, 14.05 %. Found: C, 70.44; H, 11.63; N, 4.08; O, 14.11 %. IR ($CHCl_3$, cm^{-1}): 2929, 2857, 1724, 1467, 1375, 1287, 1258. ^{1}H-NMR (300 MHz, $CDCl_3$, δ / ppm): 4.05 (2H, *t*, *J* = 6.7 Hz, OCH_2), 3.71 (4H, *t*, *J* = 5.0 Hz, O(C**H**$_2CH_2)_2$N), 2.42 (4H, *t*, *J* = = 4.5 Hz, O(CH_2C**H**$_2)_2$N), 2.35–2.27 (4H, *m*, CH_2CO + NCH_2 acyl), 1.72–1.44 (6H, *m*, 3 CH_2), 1.42–1.17 (16H, *m*, 8 CH_2), 0.87 (3H, *t*, *J* = 6.7 Hz, CH_3). ^{13}C-
-NMR (75 MHz, $CDCl_3$, δ / ppm): 173.52 (CO), 66.93 (($CH_2)_2$O morph.), 64.41 (OCH_2), 58.85 (NCH_2 acyl), 53.74 (($CH_2)_2$N morph.), 34.26 (**C**H_2CO), 31.86 (**C**$H_2CH_2CH_3$), 29.50 (CH_2), 29.44 (CH_2), 29.27 (CH_2), 29.25 (CH_2), 28.66 (OCH_2**C**H_2), 27.04 (NCH_2**C**H_2 acyl), 26.26 (**C**$H_2(CH_2)_2$CO), 25.95 (O($CH_2)_2$**C**H_2), 24.93 (**C**H_2CH_2CO), 22.69 (**C**H_2CH_3), 14.16 (CH_3).

*Undecyl 6-(morpholin-4-yl)hexanoate (**21**)*. Yield 43 %; b.p. 180 °C at 0.055 kPa. Anal. Calcd. for $C_{21}H_{41}NO_3$: C, 70.94; H, 11.62; N, 3.94; O, 13.50 %. Found: C, 71.08; H, 11.73; N, 3.82; O, 13.59 %. IR ($CHCl_3$, cm^{-1}): 2928, 2857, 1725, 1467, 1375, 1287, 1259. ^{1}H-NMR (300 MHz, $CDCl_3$, δ / ppm): 4.07 (2H, *t*, *J* = 6.8 Hz, OCH_2), 3.71 (4H, *t*, *J* = 4.9 Hz, $O(C\mathbf{H}_2CH_2)_2N$), 2.41 (4H, *t*, *J* = = 5.7 Hz, $O(CH_2C\mathbf{H}_2)_2N$), 2.35–2.23 (4H, *m*, CH_2CO + NCH_2 acyl), 1.73–1.42 (6H, *m*, 3 CH_2), 1.40–1.15 (18H, *m*, 9 CH_2), 0.86 (3H, *t*, *J* = 7.0 Hz, CH_3). ^{13}C--NMR (75 MHz, $CDCl_3$, δ / ppm): 173.48 (CO), 66.92 ($(CH_2)_2O$ morph.), 64.38 (OCH_2), 58.81 (NCH_2 acyl), 53.73 ($(CH_2)_2N$ morph.), 34.25 ($\mathbf{C}H_2CO$), 31.91 ($\mathbf{C}H_2CH_2CH_3$), 29.69 (CH_2), 29.61 (CH_2), 29.52 (CH_2), 29.36 ($O(CH_2)_3\mathbf{C}H_2$), 29.26 ($\mathbf{C}H_2(CH_2)_2CH_3$), 28.64 ($OCH_2\mathbf{C}H_2$), 27.03 ($NCH_2\mathbf{C}H_2$ acyl), 26.22 ($\mathbf{C}H_2(CH_2)_2CO$), 25.94 ($O(CH_2)_2\mathbf{C}H_2$), 24.98 ($\mathbf{C}H_2CH_2CO$), 22.73 ($\mathbf{C}H_2CH_3$), 14.18 (CH_3).

*Dodecyl 6-(morpholin-4-yl)hexanoate (**22**)*. Yield 29 %; b.p. 178–182 °C at 0.03 kPa. Anal. Calcd. for $C_{22}H_{43}NO_3$: C, 71.5; H, 11.73; N, 3.79; O, 12.99 %. Found: C, 71.58; H, 11.81; N, 3.65; O, 13.09 %. IR ($CHCl_3$, cm^{-1}): 2927, 2856, 1724, 1467, 1374, 1287, 1257. ^{1}H-NMR (300 MHz, $CDCl_3$, δ / ppm): 4.05 (2H, *t*, *J* = 6.8 Hz, OCH_2), 3.71 (4H, *t*, *J* = 4.9 Hz, $O(C\mathbf{H}_2CH_2)_2N$), 2.42 (4H, *t*, *J* = = 4.4 Hz, $O(CH_2C\mathbf{H}_2)_2N$), 2.35–2.27 (4H, *m*, CH_2CO + NCH_2 acyl), 1.73–1.43 (6H, *m*, 3 CH_2), 1.41–1.19 (20H, *m*, 10 CH_2), 0.88 (3H, *t*, *J* = 6.7 Hz, CH_3). ^{13}C--NMR (75 MHz, $CDCl_3$, δ / ppm): 173.47 (CO), 66.92 ($(CH_2)_2O$ morph.), 64.38 (OCH_2), 58.84 (NCH_2 acyl), 53.73 ($(CH_2)_2N$ morph.), 34.25 ($\mathbf{C}H_2CO$), 31.91 ($\mathbf{C}H_2CH_2CH_3$), 29.65 (CH_2), 29.64 (CH_2), 29.58 (CH_2), 29.54 (CH_2), 29.36 ($O(CH_2)_3\mathbf{C}H_2$), 29.26 ($\mathbf{C}H_2(CH_2)_2CH_3$), 28.65 ($OCH_2\mathbf{C}H_2$), 27.03 ($NCH_2\mathbf{C}H_2$ acyl), 26.26 ($\mathbf{C}H_2(CH_2)_2CO$), 25.94 ($O(CH_2)_2\mathbf{C}H_2$), 24.92 ($\mathbf{C}H_2CH_2CO$), 22.70 ($\mathbf{C}H_2CH_3$), 14.16 (CH_3).

6-(Dimethylamino)-N-*octyl-hexanamide (**24**)*. Yield: 77 %; b.p.: 152 °C at 0.4 kPa. Anal. Calcd. for $C_{16}H_{34}N_2O$: C, 71.06; H, 12.67; N, 10.36; O, 5.92 %. Found: C, 71.12; H, 12.75; N, 10.54; O, 6.01 %. IR (KBr, cm^{-1}): 3449, 2930, 2859, 1660, 1518, 1467, 1378. ^{1}H-NMR (300 MHz, $CDCl_3$, δ / ppm): 5.60 (1H, *s*, CONH), 3.21 (2H, *q*, *J* = 7.0, 13.1 Hz, CH_2), 2.25–2.12 (10H, *m*, $(CH_3)_2N$ + 2 CH_2), 1.68–1.58 (2H, *m*, CH_2) 1.48–1.41 (4H, *m*, 2 CH_2), 1.36–1.25 (12H, *m*, 6 CH_2), 0.88 (3H, *t*, *J* = 6.7 Hz, CH_3 octyl). ^{13}C-NMR (75 MHz, $CDCl_3$, δ / ppm): 172.83 (CO), 59.52 ($(CH_3)_2N\mathbf{C}H_2$), 45.56 ($(CH_3)_2N$), 39.46 ($CONH\mathbf{C}H_2$), 36.74 (CH_2), 31.74 (CH_2), 29.65 (CH_2), 29.22 (CH_2), 29.17 (CH_2), 27.38 (CH_2), 26.98 (CH_2), 26.89 (CH_2), 25.60 (CH_2), 22.59 (CH_2), 14.05 (CH_3).

6-(Dimethylamino)-N-*(1-methylheptyl)-hexanamide (**25**)*. Yield: 54 %; b.p.: 176–178 °C at 0.6–0.8 kPa. Anal. Calcd. for $C_{16}H_{34}N_2O$: C, 71.06; H, 12.67; N, 10.36; O, 5.92 %. Found: C, 71.10; H, 12.73; N, 10.45; O, 5.87 %. IR (KBr, cm^{-1}): 3436, 2931, 2860, 1656, 1511, 1466, 1379. ^{1}H-NMR (300 MHz, $CDCl_3$, δ / / ppm): 5.31 (1H, *d*, *J* = 8.8 Hz, CONH), 4.08–3.88 (1H, *m*, $NHC\mathbf{H}(CH_3)CH_2$),

2.32–2.20 (8H, *m*, $(CH_3)_2N + CH_2$), 2.15 (2H, *t*, *J* = 7.3 Hz, CH_2CO), 1.73–1.35 (16H, *m*, 8 CH_2), 1.11 (3H, *d*, *J* = 6.6 Hz, $NHCH(C\mathbf{H}_3)CH_2$), 0.88 (3H, *t*, *J* = 6.4 Hz, CH_3 terminal). ^{13}C-NMR (75 MHz, $CDCl_3$, δ / ppm): 172.05 (CO), 59.57 ($(CH_3)_2N\mathbf{C}H_2$), 45.38 ($CONH\mathbf{C}H$), 45.08 ($(CH_3)_2N$), 37.05 ($CONHCH(CH_3)\mathbf{C}H_2$), 36.94 ($\mathbf{C}H_2CO$), 31.75 ($CH_2$), 29.14 ($CH_2$), 27.34 ($CH_2$), 27.00 ($CH_2$), 25.97 ($CH_2$), 25.67 ($CH_2$), 22.53 ($CH_2$), 21.02 ($CONHCH(\mathbf{C}H_3)CH_2$), 13.97 ($CH_3$ terminal).

6-(Dimethylamino)-N-*nonyl-hexanamide* (***26***). Yield 59 %; b.p. 211–212 °C at 0.7–0.8 kPa. Anal. Calcd. for $C_{17}H_{36}N_2O$: C, 71.77; H, 12.76; N, 9.85; O, 5.62 %. Found: C, 71.70; H, 12.81; N, 9.91; O, 5.55 %. IR (KBr, cm^{-1}): 3449, 2930, 2858, 1660, 1518, 1467, 1378. ^{1}H-NMR (300 MHz, $CDCl_3$, δ / ppm): 5.64 (1H, *s*, CONH); 3.21 (2H, *q*, *J* = 7.0, 13.1 Hz, CH_2), 2.24–2.11 (10H, *m*, $(CH_3)_2N$ + 2 CH_2), 1.67–1.57 (2H, *m*, CH_2), 1.50–1.42 (4H, *m*, 2 CH_2), 1.40–1.23 (14H, *m*, 7 CH_2), 0.85 (3H, *t*, *J* = 6.7 Hz, CH_3 nonyl). ^{13}C-NMR (75 MHz, $CDCl_3$, δ / ppm): 173.10 (CO), 59.78 ($(CH_3)_2N\mathbf{C}H_2$); 45.71 ($(CH_3)_2N$) 39.72 ($CONH\mathbf{C}H_2$), 36.98 (CH_2), 32.07 (CH_2), 29.91 (CH_2), 29.73 (CH_2), 29.53 (CH_2), 29.46 (CH_2), 27.64 (CH_2), 27.24 (CH_2), 27.16 (CH_2), 25.87 (CH_2), 22.87 (CH_2), 14.33 (CH_3).

6-(Dimethylamino)-N-*decyl-hexanamide* (***27***). Yield 69 %; colorless powder, m.p. 36–40 °C, b.p. 173–175 °C at 0.03 kPa. Anal. Calcd. for $C_{18}H_{38}N_2O$: C, 72.42; H, 12.83; N, 9.38; O, 5.36 %. Found: C, 72.35; H, 12.81; N, 9.45; O, 5.28 %. IR (KBr, cm^{-1}): 3449, 2928, 2856, 1660, 1518, 1467, 1378. ^{1}H-NMR (300 MHz, $CDCl_3$, δ / ppm): 5.60 (1H, *s*, (CONH), 3.21 (2H, *q*, *J* = 7.0, 13.2 Hz, CH_2), 2.26–2.13 (10H, *m*, ($(CH_3)_2N$ + 2 CH_2), 1.67–1.57 (2H, *m*, CH_2), 1.49–1.40 (4H, *m*, 2 CH_2), 1.38–1.21 (16H *m*, 8 CH_2), 0.87 (3H, *t*, *J* = 6.7 Hz, CH_3 decyl). ^{13}C--NMR (75 MHz, $CDCl_3$, δ / ppm): 172.82 (CO), 59.51 ($(CH_3)_2N\mathbf{C}H_2$) 45.45 ($(CH_3)_2N$), 39.46 ($CONH\mathbf{C}H_2$), 36.74 ($\mathbf{C}H_2CO$), 29.05 (CH_2), 29.12 (CH_2), 29.27 (CH_2), 29.48 (CH_2), 27.37 (CH_2), 26.97 (CH_2), 26.90 (CH_2), 25.60 (CH_2), 22.64 (CH_2), 14.09 (CH_3).

6-(Dimethylamino)-N-dodecyl-hexanamide (***28***). Yield 40 %; colorless powder, m.p. 48–49 °C (48–50 °C).[12] IR (KBr, cm^{-1}): 3449, 2927, 2856, 1660, 1518, 1467, 1377. ^{1}H-NMR (300 MHz, $CDCl_3$, δ / ppm): 5.57 (1H *s*, (CONH), 3.21 (2H, *q*, *J* = 7.0, 13.1, CH_2), 2.25–2.12 (10H, *m*, $(CH_3)_2N$ + 2 CH_2), 1.68–1.58 (2H, *m*, CH_2), 1.51–1.36 (2H, *m*, CH_2), 1.35–1.23 (22H, *m*, 11 CH_2), 0.86 (3H, *t*, *J* = 6.6 Hz, CH_3 dodecyl). ^{13}C-NMR (75 MHz, $CDCl_3$, δ / ppm): 172.82 (CO), 59.51 ($(CH_3)_2N\mathbf{C}H_2$), 45.45 ($(CH_3)_2N$), 39.46 ($CONH\mathbf{C}H_2$), 36.74 ($\mathbf{C}H_2CO$) 31.87 (CH_2), 29.65 (CH_2), 29.61 (CH_2), 29.59 (CH_2), 29.58 (CH_2), 29.55 (CH_2), 29.31 (CH_2), 29.27 (CH_2), 27.37 (CH_2), 26.97 (CH_2), 26.90 (CH_2), 25.60 (CH_2), 22.64 (CH_2), 14.09 (CH_3).

N-*Decyl-6-(piperidin-1-yl)hexanamide* (***29***). Yield: 40 %; colorless powder, m.p. 36–40 °C. Anal. Calcd. for $C_{21}H_{42}N_2O$: C, 74.5; H, 12.5; N, 8.27; O, 4.73 %. Found: C, 74.39; H, 12.53; N, 8.38; O, 4.61 %. IR ($CHCl_3$, cm^{-1}): 3450, 2930,

2856, 1660, 1518, 1468, 1377. ^{1}H-NMR (300 MHz, $CDCl_3$, δ / ppm): 5.51 (1H, *s*, NH), 3.24–3.17 (2H, *q*, CH_2), 2.33 (4H, *s*, 2 CH_2), 2.25 (2H, *t*, J = 7.7 Hz, NCH_2), 2.14 (2H, *t*, J = 7.6 Hz, CH_2CO), 1.68–1.23 (28H, *m*, 14 CH_2), 0.86 (3H, *t*, J = 6.6 Hz, CH_3). ^{13}C-NMR (75 MHz, $CDCl_3$, δ / ppm): 172.84 (CO), 59.34 ($CH_2(CH_2CH_2)_2N$), 54.61 (NCH_2 acyl), 39.45 (CONH**C**H_2), 36.74 (**C**H_2CO), 31.84 (CONHCH$_2$**C**H_2), 29.65 (CH_2), 29.50 (CH_2), 29.27 (CH_2), 27.30 (CH_2), 26.89 (CH_2), 26.63 (CH_2), 25.95 (CH_2), 25.70 (CH_2), 24.44 (CH_2), 22.64 (**C**H_2CH_3), 14.08 (CH_3).

N-*Dodecyl-6-(piperidin-1-yl)hexanamide* (***30***). Yield: 38 %; colorless powder, m.p. 45–49 °C. Anal. Calcd. for $C_{23}H_{46}N_2O$: C, 75.35; H, 12.65; N, 7.64; O, 4.36 %. Found: C, 75.28; H, 12.73; N, 7.74; O, 4.29 %. IR ($CHCl_3$, cm^{-1}): 3449, 2931, 2856, 1660, 1518, 1468, 1377. ^{1}H-NMR (300 MHz, $CDCl_3$, δ / ppm): 5.50 (1H, *s*, NH), 3.24–3.18 (2H, *q*, CH_2), 2.33 (4H, *s*, 2 CH_2), 2.26 (2H, *t*, J = 7.8 Hz, NCH_2), 2.14 (2H, *t*, J = 7.6 Hz, CH_2CO), 1.68–1.24 (32H, *m*, 16 CH_2), 0.86 (3H, *t*, J = 6.7 Hz, CH_3). ^{13}C-NMR (75 MHz, $CDCl_3$, δ / ppm): 172.83 (CO), 59.35 ($CH_2(CH_2$**C**$H_2)_2N$), 54.62 (NCH_2 acyl), 39.46 (CONH**C**H_2), 36.76 (**C**H_2CO), 31.88 (CONHCH$_2$**C**H_2), 29.66 (CH_2), 29.61 (CH_2), 29.60 (CH_2), 29.55 (CH_2), 29.52 (CH_2), 29.31 (CH_2), 29.28 (CH_2), 27.30 (CH_2), 26.90 (CH_2), 26.64 (CH_2), 25.96 (CH_2), 25.70 (CH_2), 24.45 (CH_2), 22.65 (**C**H_2CH_3), 14.10 (CH_3).

6-(Morpholin-4-yl)-N-*octyl-hexanamide* (***31***). Yield 28 %; b.p. 225–230 °C at 0.2 kPa. Anal. Calcd. for $C_{18}H_{36}N_2O_2$: C, 69.18; H, 11.61; N, 8.96; O, 10.24 %. Found: C, 69.28; H, 11.73; N, 9.04; O, 10.29 %. IR ($CHCl_3$, cm^{-1}): 3449, 2930, 2857, 1660, 1518, 1467, 1459, 1373. ^{1}H-NMR (300 MHz, $CDCl_3$, δ / / ppm): 5.58 (1H, *s*, CONH), 3.72 (4H, *t*, O(C**H**$_2CH_2)_2N$), 3.20 (2H, *q*, J = 7.2, 12.8 Hz, CH_2), 2.39 (4H, *t*, J = 4.5 Hz, $O(CH_2C$**H**$_2)_2N$), 2.32 (2H, *t*, J = 7.7 Hz, NCH_2 acyl), 2.13 (2H, *t*, J = 7.6 Hz, CH_2CO), 1.70–1.55 (2H, *m*, C**H**$_2CH_2CO$), 1.52–1.41 (4H, *m*, 2 CH_2), 1.38–1.25 (12H, *m*, 6 CH_2), 0.88 (3H, *t*, J = 6.7 Hz, CH_3). ^{13}C-NMR (75 MHz, $CDCl_3$, δ / ppm): 172.72 (CO), 66.75 ($O(CH_2CH_2)_2N$), 58.80 (NCH_2 acyl), 53.54 ($O(CH_2CH_2)_2N$), 39.44 (CONH**C**H_2), 36.55 (**C**H_2CO), 31.82 (CH_2), 29.71 (CH_2), 29.48 (CH_2), 29.28 (CH_2), 27.11 (CH_2), 26.86 (CH_2), 26.19 (CH_2), 25.63 (CH_2), 22.60 (CH_2), 14.05 (CH_3).

6-(Morpholin-4-yl)-N-*nonyl-hexanamide* (***32***). Yield 41 %; colorless powder, m.p. 41–47 °C, b.p. 201–203 °C at 0.05 kPa. Anal. Calcd. for $C_{19}H_{38}N_2O_2$: C, 69.89; H, 11.73; N, 8.58; O, 9.80 %. Found: C, 69.95; H, 11.83; N, 8.64; O, 9.91 %. IR ($CHCl_3$, cm^{-1}): 3449, 2930, 2858, 1661, 1518,1467, 1459, 1375. ^{1}H--NMR (300 MHz, $CDCl_3$, δ / ppm): 5.45 (1H, *s*, CONH), 3.70 (4H, *t*, J = 4.7 Hz, O(C**H**$_2CH_2)_2N$), 3.21 (2H, *q*, J = 7.1, 12.9, CH_2), 2.40 (4H, *t*, J = 4.4 Hz, $O(CH_2C$**H**$_2)_2N$), 2.31 (2H, *t*, J = 7.7 Hz, NCH_2 acyl), 2.14 (2H, *t*, J = 7.6 Hz, CH_2CO), 1.69–1.59 (2H, *m*, C**H**$_2CH_2CO$), 1.54–1.44 (4H, *m*, 2 CH_2), 1.37–1.24 (14H, *m*, 7 CH_2), 0.86 (3H, *t*, J = 6.7 Hz, CH_3). ^{13}C-NMR (75MHz, $CDCl_3$, δ /

/ ppm): 172.73 (CO), 66.95 (O(**C**$H_2CH_2)_2N$), 58.88 (NCH_2 acyl), 53.73 (O(CH_2**C**$H_2)_2N$), 39.46 (CONH**C**H_2), 36.73 (**C**H_2CO), 31.81 (CH_2), 29.65 (CH_2), 29.47 (CH_2), 29.26 (CH_2), 29.20 (CH_2), 27.11 (CH_2), 26.88 (CH_2), 26.27 (CH_2), 25.65 (CH_2), 22.62 (**C**H_2CH_3), 14.08 (CH_3).

N-*Decyl-6-(morpholin-4-yl)hexanamide (**33**)*. Yield 44 %; colorless powder, m.p. 45–48 °C. Anal. Calcd. for $C_{20}H_{40}N_2O_2$: C, 70.54; H, 11.84; N, 8.23; O, 9.40 %. Found: C, 70.65; H, 11.75; N, 8.14; O, 9.51 %. IR ($CHCl_3$, cm^{-1}): 3449, 2930, 2857, 1660, 1518, 1467, 1459, 1378. ^{1}H-NMR (300 MHz, $CDCl_3$, δ / / ppm): 5.45 (1H, *s*, CONH), 3.70 (4H, *t*, *J* = 4.7 Hz, O(C**H**$_2CH_2)_2N$), 3.21 (2H, *q*, *J* = 7.1, 12.9 Hz, CH_2), 2.40 (4H, *t*, *J* = 4.4 Hz, O($CH_2CH_2)_2N$), 2.31 (2H, *t*, *J* = 7.7 Hz, NCH_2 acyl), 2.14 (2H, *t*, *J* = 7.6 Hz, CH_2CO), 1.69–1.59 (2H, *m*, C**H**$_2CH_2CO$), 1.54–1.44 (4H, *m*, 2 CH_2), 1.37–1.24 (14H, *m*, 7 CH_2), 0.86 (3H, *t*, *J* = 6.7 Hz, CH_3). ^{13}C-NMR (75 MHz, $CDCl_3$, δ / ppm): 172.72 (CO), 66.74 (O(**C**$H_2CH_2)_2N$), 58.76 (NCH_2 acyl), 53.60 (O(CH_2**C**$H_2)_2N$), 39.43 (CONH**C**H_2), 36.60 (**C**H_2CO), 31.80 (CH_2), 29.59 (CH_2), 29.47 (CH_2), 29.46 (CH_2), 29.43 (CH_2), 29.22 (CH_2), 26.98 (CH_2), 26.85 (CH_2), 26.05 (CH_2), 25.55 (CH_2), 22.59 (**C**H_2CH_3), 14.04 (CH_3).

N-*Dodecyl-6-(morpholin-4-yl)hexanamide (**34**)*. Yield 50 %; colorless powder, m.p. 48–53 °C. Anal. Calcd. for $C_{22}H_{44}N_2O_2$: C, 71.69; H, 12.03; N, 7.6; O, 8.68 %. Found: C, 71.58; H, 11.93; N, 7.54; O, 8.71 %. IR ($CHCl_3$, cm^{-1}): 3449, 2930, 2858, 1660, 1518, 1467, 1459, 1376. ^{1}H-NMR (300 MHz, $CDCl_3$, δ / ppm): 5.56 (1H, *s*, CONH), 3.77 (4H, *t*, *J* = 4.6 Hz, O(C**H**$_2CH_2)_2N$), 3.22 (2H, *q*, *J* = = 13.2 Hz, 6.6 Hz, CH_2), 2.43 (4H, *t*, *J* = 7.5 Hz, O(CH_2C**H**$_2)_2N$), 2.34 (2H, *t*, *J* = = 4.6 Hz, NCH_2 acyl), 2.17 (2H, *t*, *J* = 7.51 Hz, CH_2CO), 1.65–1.12 (26H, *m*, 13 CH_2), 0.87 (3H, *t*, *J* = 6.42, CH_3). ^{13}C-NMR (75 MHz, $CDCl_3$, δ / ppm): 172.70 (CO), 66.43 (O(**C**$H_2CH_2)_2N$), 58.65 (NCH_2 acyl), 53.49 (O(CH_2**C**$H_2)_2N$), 39.55 (CONH**C**H_2), 36.55 (**C**H_2CO), 31.88 (CH_2), 29.69 (CH_2), 29.59 (CH_2), 29.55 (CH_2), 29.30 (CH_2), 29.01 (CH_2), 28.93 (CH_2), 27.82 (CH_2), 26.93 (CH_2), 26.56 (CH_2), 25.64 (CH_2), 25.43 (CH_2), 22.64 (**C**H_2CH_3), 14.03 (CH_3).

Journal of the Serbian Chemical Society
JSCS@tmf.bg.ac.rs • www.shd.org.rs/JSCS

J. Serb. Chem. Soc. 75 (5) 605–614 (2010)
JSCS–3991

UDC 677.027.423.1/.2:535.683+535.685
Original scientific paper

Synthesis, characterization and dyeing assessment of novel acid azo dyes and mordent acid azo dyes based on 2-hydroxy-4-methoxybenzophenone on wool and silk fabrics

BHARAT C. DIXIT[1]*, HITENDRA M. PATEL[1], RITU B. DIXIT[2] and DHIRUBHAI J. DESAI[1]

[1]*Department of Chemistry, V. P. & R. P .T. P Science College, Vallabh Vidyanagar-388 120, Gujarat and* [2]*Ashok & Rita Patel Institute of Integrated Study & Research in Biotechnology and Allied Sciences, New Vallabh Vidyanagar-388 120, Gujarat State, India*

(Received 4 July 2009, revised 21 January 2010)

Abstract: Novel acid mono azo and mordent acid mono azo dyes were synthesised by the coupling of diazonium salt solution of different aromatic amines with 2-hydroxy-4-methoxybenzophenone. The resulting dyes were characterized by spectral techniques, *i.e*., elemental analysis, IR, ^{1}H-NMR and UV––visible spectroscopy. The dyeing performance of all the dyes was evaluated on wool and silk fabrics. The dyeing of chrome pre-treated wool and silk fabrics showed better hues on mordented fabrics. Dyeing of wool and silk fabrics resulted in pinkish blue to red shades with very good depth and levelness. The dyed fabrics showed excellent to very good light, washing, perspiration, sublimation and rubbing fastness. The results of antibacterial studies of chrome pre-treated fabrics revealed that the toxicity of mordented dyes against *Escherichia coli*, *Staphylococcus aureus*, *Salmonella typhi*, *Bacillus subtilis* bacteria was fairly good.

Keywords: acid azo dye; mordent acid azo dye; light fastness; washing fastness.

INTRODUCTION

Traditionally, azo dyes are the most important class of commercial dyes, occupying more than half of the dye chemistry, which contain phenols as intermediates.[1–6] If they contain sodium salts of a sulphonic acid group in addition to a phenolic group, they are referred as an acid azo dye. All such dyes having phenolic and sulphonic acid moieties, contain hydroxyl (–OH) and sulphonic ($–SO_3H$) groups as auxochromic groups. Such an auxochromic (–OH) and chromophoric (C=O) groups-containing compound, *i.e*., 2-hydroxy-4-methoxybenzophenone, has shown wide applications as a polymer additive.[7–9] It is also known for its ex-

* Corresponding author. E-mail: dixits20002003@yahoo.co.in
doi: 10.2298/JSC090704039D

cellent UV absorbing capacity, as it prevents the photo-degradability of most vinyl polymers.[10–12] The acid mono azo dyes and mordent mono azo dyes formation based on this compound has not been developed except in a few patents.[13–16] Considering the above-mentioned importance of 2-hydroxy-4-methoxybenzophenone, it was planned to explore the field of acid azo dyes based on this compound, which may yield dyes with good hue properties.

Hence, in continuation of earlier work,[17,18] the present communication comprises the synthesis, characterization and dyeing assessment of novel acid mono azo and mordent acid mono azo dyes based on 2-hydroxy-4-methoxybenzophenone. The proposed synthetic route is shown in Scheme 1.

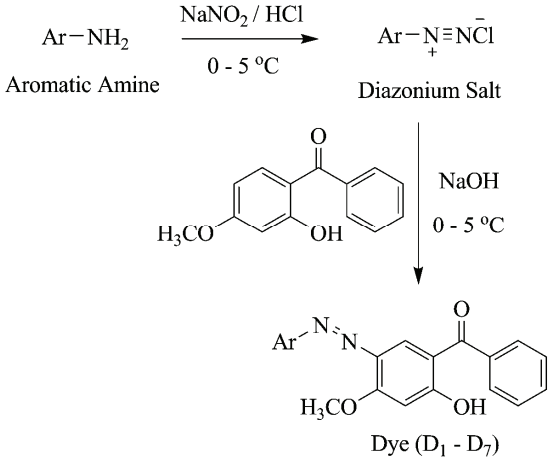

Scheme 1. Proposed synthetic route for the 2-hydroxy-4-methoxybenzophenone based dyes (**D_1**–**D_7**).

EXPERIMENTAL

All the employed chemicals were of analytical reagent grade. The aromatic amines shown in Table I were used for diazotization. Wool and silk fabrics were gifted by Color Tax (Pvt) Ltd., Surat, India. Melting points were determined by the open capillary method and are given uncorrected. The UV–visible absorption spectra were measured on a Carl Zeiss UV/Vis Specord spectrometer, and the elemental analysis was realized using a Perkin Elmer CHNS/O Analyzer 2400 Series II. The infrared spectra were recorded in KBr pellets on a Perkin–Elmer Spectrum GX FT-IR model. The ^{1}H-NMR spectra were recorded on Hitachi R-1500 (400 MHz) in DMSO-d_6 solvent and thin layer chromatography (TLC) was run on aluminium sheets pre-coated with silica gel 60 F_{254} (Merck, Germany) using a methanol–water–acetic acid (12:3:7) solvent system. The colour spots were visualized by a UV cabinet. A HTHP dyeing machine (model LL) was used for dyeing.

Synthesis of acid mono azo dyes

Diazotization. Diazotization of various aromatic amines (shown in Table I) was performed by a reported method.[19,20]

Accordingly, each of the aromatic amines (3.19 g, 0.010 mol) was mixed with HCl (25 mL, 37 %) in a mortar, transferred to a 3-neck round bottom flask, and additional HCl (20 mL, 37 %) was added. To the resultant suspension, crushed ice (25 g) and $NaNO_2$ (2.5 mL, 4 M) were added. Diazotization was realized over 0.5 h at 0–5 °C under continuous stirring. The complete synthetic route is shown in Scheme 1 and the structures of the various aromatic amines and the corresponding dyes are shown in Table I.

TABLE I. Structures of the aromatic amines and corresponding acid azo dyes

Dye	Aromatic amine	Acid azo dye structure
D$_1$	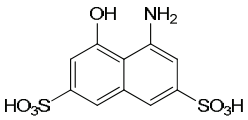	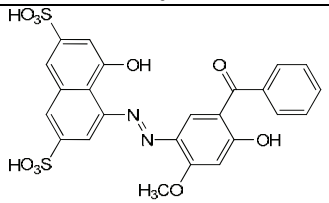
D$_2$	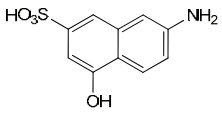	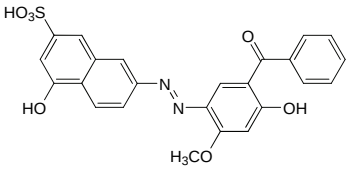
D$_3$	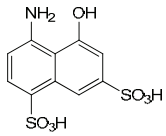	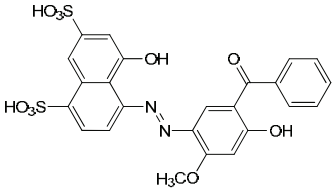
D$_4$	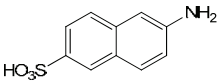	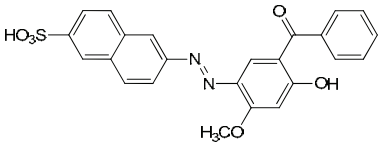
D$_5$	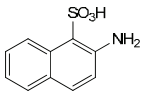	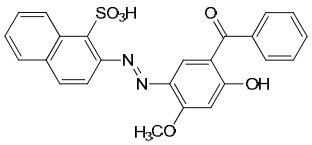
D$_6$	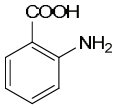	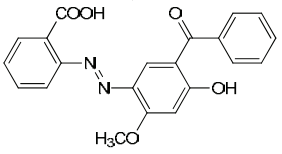
D$_7$	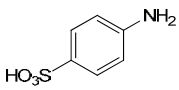	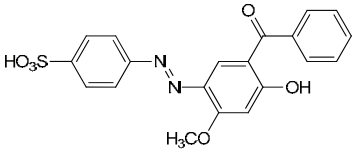

Coupling procedure. The coupling of above mentioned diazotized aromatic amines (as shown in Table I) was performed by a method reported in the literature.[19,20] The general procedure followed is given below: 2-hydroxy-4-methoxybenzophenone (2.15 g, 0.010 mol) was dissolved in aqueous sodium hydroxide (100 mL, 0.10 M) solution. The clear solution was cooled in an ice–salt bath and the diazonium salt solution of an aromatic amine was added dropwise over a period of 30 min under vigorous stirring. The pH was maintained between 2.0 to 3.0 by the simultaneous addition of 10 % w/v sodium carbonate solution. Stirring was continued for 2 h, allowing the temperature to rise to ambient. The dye was then filtered off and dissolved in distilled water. Then the acid azo dye was obtained by the evaporation procedure and subsequently dried at room temperature. The dyes were designated as acid mono azo dyes (**D_1**–**D_7**).

Acid mono azo dyeing method

Wool and silk fabrics are conveniently dyed in the laboratory at 90–130 °C and at a high pressure (166–207 kPa). A model glycerine-bath, high-temperature beaker and HTHP (model LL) dyeing machine were used. For this purpose, a paste of finely powdered acid azo dye (0.060 g) was prepared with a dispersing agent dodamol (0.090 g), wetting agent Tween-80 (0.0060 g) and water (2.0 mL) in a ball mill. Water (10 mL) was added to this paste under stirring and the pH was adjusted to 2.0–4.0 using acetic acid. This dye suspension (100 mL) was added to a beaker provided with a lid and a screw cap. A wetted pattern of wool or silk fabric was rolled into the beaker and the lid was placed on the beaker the metal cap tightened. The beaker was then placed vertically on the rotatory carrier inside the tank and the clamp plate was firmly tightened.

The rotatory carrier was then allowed to rotate in the glycerine-bath and the temperature was raised to 90 °C at a rate of 2 °C/min. The dyeing was continued for 1 h under pressure. After cooling for 1 h, the beaker was removed from the bath and washed with distilled water. The dyed pattern was thoroughly washed with cold water and dried at room temperature.

Mordent dyeing method

The wool and silk fabric dye pattern obtained from the above-mentioned process was treated with potassium dichromate solution equal to half of the weight of the dye and it was allowed to roll into the beaker and again the beaker was then placed vertically on the rotatory carrier inside the tank and the dyeing was continued for 1 h under pressure. After cooling for 1 h, the beaker was removed from the bath and washed with cold distilled water. The dyed pattern was thoroughly washed with warm water and air dried at room temperature.

Determination of the percentage exhaustion and fixation

The percentage exhaustion and fixation of the dyed fabrics were determined according to the reported methods.[21]

Fastness property

All the fastness properties of the synthesized dyes were assessed, *i.e.*, the light, sublimation and perspiration fastnesses according to the British standard: 1006-1978, the wash fastness according to the Indian standard: IS: 765-1979 and the rubbing fastness using a Crock meter (Atlas) AATCC-1961.

Antimicrobial activity

The *in vitro* antimicrobial activities of the acid azo chrome dyes were tested against *Escherichia coli*, *Staphylococcus aureus*, *Salmonella typhi* and *Bacillus subtilis* bacteria using agar nutrient as the medium. A stock solution of 250 ppm was prepared by dissolving the

compounds in 20 % DMSO solution. The antimicrobial activity was performed at a concentration 100 μg/ml, using the agar-cup method in which the well diameter was 4 mm,[22] with DMSO as the control.

RESULTS AND DISCUSSION

Physical properties of dyes

All the dyes obtained upon recrystallization from acetone were crystalline powders ranging in colour from pinkish blue to red. The purity of the dyes was checked by TLC using methanol–water–acetic acid (12:3:7) solvent system. A single spot was observed for each dye.

Analytical and spectral data of the dyes

*4-(5-Benzoyl-4-hydroxy-2-methoxyphenylazo)-5-hydroxy-2,7-naphthalenedisulphonic acid (**D1**)*. Yield: 78 %; m.p.: 146–150 °C; Rf. value: 0.78. Anal. Calcd. for $C_{24}H_{18}O_{10}N_2S_2$ (FW 558): C, 51.61; H, 3.32; N, 5.01; S, 11.46 %. Found: C, 51.59; H, 3.21; N, 5.00; S, 11.38 %. IR (KBr, cm^{-1}): 3463 (–OH), 3072 (=CH, aromatic), 1628 (C=O, diaryl), 1521 (N=N), 1520 (for naphthalene substitution), 1481 (C=C, aromatic), 1333 (C–N), 1101 (C–O), 1030, 650 (for sulphonic acid), 732, 584, 481 (for substituted benzene). ^{1}H-NMR (400 MHz, DMSO-d_6, δ / ppm): 3.82 (3H, *s*, Ar–OCH_3), 5.4 (2H, *s*, Ar–OH), 7.2–7.4 (11H, *m*, Ar–H), 8.0 (1H, *s*, –SO_3H), 8.2 (1H, *s*, –SO_3H).

*7-(5-Benzoyl-4-hydroxy-2-methoxyphenylazo)-4-hydroxy-2-naphthalenesulphonic acid (**D2**)*. Yield: 80 %; m.p.: 138–142 °C; Rf. value: 0.82. Anal. Calcd. for $C_{24}H_{18}O_7N_2S$ (FW 478): C, 60.25; H, 3.76; N, 5.85; S, 6.69 %. Found: C, 60.20; H, 3.72; N, 5.83; S, 6.61 %. IR (KBr, cm^{-1}): 3450 (–OH), 3082 (=CH, aromatic), 1624 (C=O, diaryl), 1540 (for naphthalene substitution), 1522 (N=N), 1490 (C=C, aromatic), 1345 (C–N), 1101 (C–O), 1032, 653 (for sulphonic acid), 744, 564, 478 (for substituted benzene). ^{1}H-NMR (400 MHz, DMSO-d_6, δ / ppm): 3.81 (3H, *s*, Ar–OCH_3), 7.2–7.5 (12H, *m*, Ar–H), 5.42 (1H, *s*, Ar––OH), 6.3 (1H, *s*, Ar–OH), 8.2 (1H, *s*, –SO_3H).

*4-(5-Benzoyl-4-hydroxy-2-methoxyphenylazo)-5-hydroxy-1,7-naphthalenedisulphonic acid (**D3**)*. Yield: 79 %; m.p.: 142–146 °C; Rf. value: 0.77. Anal. Calcd. for $C_{24}H_{18}O_{10}N_2S_2$ (FW 558): C, 51.61; H, 3.32; N, 5.01; S, 11.46 %. Found: C, 51.58; H, 3.19; N, 4.97; S, 11.34 %. IR (KBr, cm^{-1}): 3481 (–OH), 3070 (=CH, aromatic), 1632 (C=O, diaryl), 1542 (N=N), 1525 (for naphthalene substitution), 1483 (C=C, aromatic), 1337 (C–N), 1103 (C–O), 1029, 650 (for sulphonic acid), 737, 562, 472 (for substituted benzene). ^{1}H-NMR (400 MHz, DMSO-d_6, δ / ppm): 3.82 (3H, *s*, Ar–OCH_3), 7.1–7.3 (11H, *m*, Ar–H), 5.5 (2H, *s*, Ar–OH), 7.9 (1H, *s*, –SO_3H), 8.35 (1H, s, –SO_3H).

*6-(5-Benzoyl-4-hydroxy-2-methoxyphenylazo)-2-naphthalenesulphonic acid (**D4**)*. Yield: 81 %; m.p.: 131–135 °C; Rf. value: 0.84. Anal. Calcd. for $C_{24}H_{18}O_6N_2S$ (FW 462): C, 62.33; H, 3.89; N, 6.06; S, 6.92 %. Found: C, 62.27;

H, 3.83; N, 6.00; S, 6.89 %. IR (KBr, cm^{-1}): 3633 (–OH), 3080 (=CH, aromatic), 1652 (C=O, diaryl), 1560 (for naphthalene substitution), 1532 (N=N), 1473 (C=C, aromatic), 1338 (C–N), 1104 (C–O), 1032, 653 (for sulphonic acid), 782, 741, 583, 485 (for substituted benzene). ^{1}H-NMR (400 MHz, DMSO-d_6, δ / / ppm): 3.83 (3H, *s*, Ar–OCH_3), 7.2–7.4 (13H, *m*, Ar–H), 6.10 (1H, *s*, Ar–OH), 8.1 (1H, *s*, –SO_3H).

*2-(5-Benzoyl-4-hydroxy-2-methoxyphenylazo)-1-naphthalenesulphonic acid (**D$_5$**)*. Yield: 79 %; m.p.: 136–141 °C; Rf. value: 0.82. Anal. Calcd. for $C_{24}H_{18}O_6N_2S$ (FW 462): C, 62.33; H, 3.89; N, 6.06; S, 6.92 %. Found: C, 62.26; H, 3.84; N, 6.01; S, 6.88 %. IR (KBr, cm^{-1}): 3580 (–OH, phenolic), 3070 (=CH, aromatic), 1621 (C=O, diaryl), 1575 (for naphthalene substitution), 1531 (N=N), 1482 (C=C, aromatic), 1463 (C–N), 1338 (C–O), 1034, 650 (for sulphonic acid), 1103, 732, 574, 473 (for substituted benzene). ^{1}H-NMR (400 MHz, DMSO-d_6, δ / ppm): 3.82 (3H, Ar–OCH_3), 7.1–7.5 (13H, *m*, Ar–H), 6.3 (1H, *s*, Ar–OH), 8.2 (1H, s, –SO_3H).

*2-(5-Benzoyl-4-hydroxy-2-methoxyphenylazo)benzoic acid (**D$_6$**)*. Yield: 78 %; m.p.: 145–148 °C; Rf. value: 0.83. Anal. Calcd. for $C_{21}H_{16}O_5N_2$ (FW 376): C, 67.02; H, 4.25; N, 7.44 %. Found: C, 67.01; H, 4.18; N, 7.39 %. IR (KBr, cm^{-1}): 3430 (–OH, phenolic), 3540 (–OH, acidic), 3062 (=CH, aromatic), 1634 (C=O, diaryl), 1678 (C=O, carboxylic acid), 1581 (N=N), 1483 (C=C, aromatic), 1352 (C–N), 1103 (C–O), 1100, 850 (for carboxylic acid), 783, 741, 583, 482 (for substituted benzene). ^{1}H-NMR (400 MHz, DMSO-d_6, δ / ppm): 3.82 (3H, *s*, Ar–OCH_3), 7.1–7.5 (11H, *m*, Ar–H), 5.5 (1H, *s*, Ar–OH), 10.9 (1H, *s*, –COOH).

*4-(5-Benzoyl-4-hydroxy-2-methoxyphenylazo)benzenesulphonic acid (**D$_7$**)*. Yield: 83 %; m.p.: 150–154 °C; Rf. value: 0.85. Anal. Calcd. for $C_{20}H_{16}O_6N_2S$ (FW 412): C, 58.25; H, 3.88; N, 6.79; S, 7.76 %. Found: C, 58.18; H, 3.82; N, 6.71; S, 7.70 %. IR (KBr, cm^{-1}): 3590 (–OH), 3063 (=CH, aromatic), 1632 (C=O, diaryl), 1533 (N=N), 1471 (C=C, aromatic), 1324 (C–N), 1103 (C–O), 1031, 652 (for sulphonic acid), 780, 744, 586, 475 (for substituted benzene). ^{1}H--NMR (400 MHz, DMSO-d_6, δ / ppm): 3.82 (3H, *s*, Ar–OCH_3), 7.2–7.4 (11H, *m*, Ar–H), 6.1 (1H, *s*, Ar–OH), 7.9 (1H, *s*, –SO_3H).

The results of elemental analyses of each acid azo dye were consistent with the predicted structure, as shown in Table I. The number of azo group was almost one for each dye. The nitrogen content and number of azo group for each dye are co-related with each other. The IR spectrum of each dye comprised the important features of aromatic, azo, hydroxyl, keto and carboxylic acid groups.

The ^{1}H-NMR spectra of all the dye compounds based on 2-hydroxy-4-methoxybenzophenone shows important signals at their respective positions, confirming the structures of various acid azo dyes, as shown in Table I. One of the –OH protons in the **D$_1$** and **D$_3$** dyes might be merged with the aromatic protons, while the other –OH protons in the other dyes resonated as a singlet between 5.4

to 6.3 δ. In the **D_6** dye, the –COOH proton gave a singlet at 10.9 δ. The singlet of the $–SO_3H$ proton resonated between 7.9 to 8.35 δ and $–OCH_3$ protons resonated as a singlet around 3.8 δ in all the acid azo dyes.

The visible absorption spectroscopic properties of the dyes were recorded in DMF. The absorption maxima (λ_{max}) of all the dyes falls in the range 422–465 nm in DMF, and the values are given in Table II. The values of the logarithm of molar extinction coefficient (log ε) of all the dyes were in the range of 4.21–4.60, consistent with their high absorption intensity. Moreover, the presence of electron donating or electron attracting groups did not bring about any marked increase or decrease in λ_{max} in the visible region and log ε remained nearly constant. However, an electron attracting substituent, such as $–SO_3H$, in the structure of the coupler increases the polarizability and will results in bathochromic shifts. This leads to a decrease in the energy between the highest occupied molecular orbital and lowest unoccupied molecular orbital and thus the $\pi \rightarrow \pi^*$ electronic transition occurs with a lower frequency photon, resulting in a bathochromic shift of the visible absorption band.

TABLE II. Absorption maxima in DMF (λ_{max}), intensities (log ε), exhaustion (E) and fixation (F) of acid mono azo dyes on wool and silk fabrics

Dye	λ_{max} / nm	log ε	Acid azo dyeing on wool		Acid azo dyeing on silk	
			E / %	F / %	E / %	F / %
D_1	465	4.60	80	89	72	90
D_2	445	4.36	75	94	75	87
D_3	450	4.45	72	90	80	92
D_4	435	4.27	85	89	76	88
D_5	430	4.20	74	86	82	91
D_6	420	4.18	71	88	75	89
D_7	422	4.21	85	92	78	90

Dyeing properties of dyes

The acid mono azo dyes were applied at a 2 % depth on wool and silk fabrics. Their dyeing properties are shown in Tables III–VI. These dyes gave a wide range of colours varying from pinkish blue to red shades with good levelness, brightness and depth on the fabrics. The variation in the shades of the dye fabric results from both the nature and position of the substituent present on the diazotized compound. The dyeing showed excellent fastness to light, with a very good to excellent washing, perspiration, rubbing and sublimation fastnesses.

A remarkable degree of smoothness after washing was observed. This may be attributed to the good penetration into and affinity of the dye molecule for the structure of the fabrics. The most prominent feature of these dyes is that the dye patterns treated with Cr(III) salt solution afforded an excellent shining shade of the dyes. This might be due to chrome complex formation on the fabric matrix.

TABLE III. Results of acid mono azo dyeing and various fastness properties of dyes on wool fabrics (grading: 5 – excellent, 4 – very good, 3 – good, 2 – fair, 1 – poor)

Dye	Colour shades on wool	Light fastness	Washing fastness	Perspiration fastness		Sublimation fastness	Rubbing fastness	
				Acid	Alkaline		Dry	Wet
D_1	Pinkish blue	5	5	4	5	4	4	4
D_2	Pinkish blue	5	4	5	4	4	4	4
D_3	Reddish brown	5	5	5	5	5	5	4
D_4	Yellowish pink	4	5	4	5	4	4	3
D_5	Chocolate brown	4	4	5	5	4	5	4
D_6	Red	5	5	5	5	5	4	3
D_7	Red	5	4	5	5	4	5	4

TABLE IV. Results of acid mono azo dyeing and various fastness properties of dyes on silk fabrics (grading: 5 – excellent, 4 – very good, 3 – good, 2 – fair, 1 – poor)

Dye	Colour shades on silk	Light fastness	Wash fastness	Perspiration fastness		Sublimation fastness	Rubbing fastness	
				Acid	Alkaline		Dry	Wet
D_1	Pinkish blue	5	4	4	5	5	4	3–4
D_2	Pinkish blue	5	4	5	4	4	4	3
D_3	Reddish brown	4	4	4	5	5	4	4
D_4	Yellowish pink	4	4	4	4	4	4	3–4
D_5	Chocolate brown	5	5	4	4	4	5	4
D_6	Red	5	4	4	4	5	4	4
D_7	Red	5	4	4	4	5	5	3–4

TABLE V. Results of mordent acid azo dyeing and various fastness properties of dyes on wool fabrics (grading: 5 – excellent, 4 – very good, 3 – good, 2 – fair, 1 – poor)

Dye	Colour shades on wool	Light fastness	Washing fastness	Perspiration fastness		Sublimation fastness	Rubbing fastness	
				Acid	Alkaline		Dry	Wet
D_1	Pinkish blue	5	5	4	5	5	5	4
D_2	Pinkish blue	5	5	5	4	5	4	4
D_3	Reddish brown	5	5	5	5	5	5	4
D_4	Yellowish pink	5	5	5	5	5	5	4
D_5	Chocolate brown	5	4	5	5	4	5	4
D_6	Red	5	5	5	5	5	4	4
D_7	Red	5	5	5	5	5	5	4

The antibacterial activities of the chrome complexes of the dyes (**D_1**–**D_7**) were monitored against the various pathogens. The results (Table VII) showed that the **D_1**, **D_3** and **D_7** dyes had moderate to high, **D_6** weak to moderate and the other dyes weak activity against all the tested microorganisms. The dye pattern of the chrome-treated dye may be tolerable for the human body.

TABLE VI. Results of mordent acid azo dyeing and various fastness properties of dyes on silk (grading: 5 – excellent, 4 – very good, 3 – good, 2 – fair, 1 – poor)

Dye	Colour shades on silk	Light fastness	Wash fastness	Perspiration fastness		Sublimation fastness	Rubbing fastness	
				Acid	Alkaline		Dry	Wet
D_1	Pinkish blue	5	5	5	5	5	5	4
D_2	Pinkish blue	5	5	5	5	5	4	4
D_3	Reddish brown	5	4	5	5	5	4	4
D_4	Yellowish pink	5	5	5	5	4	5	5
D_5	Chocolate brown	5	5	5	5	4	5	4
D_6	Red	5	5	5	5	5	4	4
D_7	Red	5	5	5	4	5	5	4

TABLE VII. Antibacterial activity of the acid azo chrome dyes (100 μg/mL)

Dye	Zone of inhibition, mm			
	E. coli	*S. aureus*	*S. typhi*	*B. subtilis*
D_1	>21	16–20	16–20	16–20
D_2	11–15	11–15	11–15	11–15
D_3	>21	16–20	16–20	16–20
D_4	11–15	11–15	11–15	11–15
D_5	11–15	11–15	11–15	11–15
D_6	16–20	16–20	11–15	16–20
D_7	>21	>21	16–20	16–20

CONCLUSIONS

All newly synthesized acid mono azo dyes and mordent acid mono azo dyes exhibited very good to excellent fastness to light, sublimation, perspiration and rubbing. The remarkable degree of levelness after dyeing indicates good penetration into, and affinity of these dyes for the fabric matrix. They give deep and bright hues with levelling dyeing. The nature of the substituent in the coupling component has little influence on the UV–visible absorption and shade of the dyeing. A comparison of the acid mono azo and the mordent acid azo dyes revealed that the mordent acid mono azo dyes have better shades than the acid azo dyes. Of the acid azo chrome dyes (**D_1**–**D_7**), the dyes **D_1**, **D_3** and **D_7** showed moderate to high antibacterial activity against all the tested microorganisms.

Acknowledgments. The authors are thankful to the principal, V. P. & R. P. T. P. Science College and C. V. M. for providing the necessary research facilities. The authors are also thankful to Mr. Ashok C. Kapadia and Mr. Pradeep N. Mistry of the Color Tax (Pvt) Ltd., Surat, India, for characterization of the azo group and giving the standard of fastness properties and to Raju Mehta of G.P.C.B., Surat, India, for providing useful chemicals.

ИЗВОД

СИНТЕЗА, КАРАКТЕРИЗАЦИЈА И ИСПИТИВАЊЕ БОЈЕЊА ВУНЕНИХ И СВИЛЕНИХ ТКАНИНА НОВИМ КИСЕЛИМ И МОЧИЛСКИМ АЗО БОЈАМА НА БАЗИ 2-ХИДРОКСИ-4-МЕТОКСИБЕНЗОФЕНОНА

BHARAT C. DIXIT[1], HITENDRA M. PATEL[1], RITU B. DIXIT[2] и DHIRUBHAI J. DESAI[1]

[1]*Department of Chemistry, V. P. & R. P .T. P Science College, Vallabh Vidyanagar-388 120. Gujarat и* [2]*Ashok & Rita Patel Institute of Integrated Study & Research in Biotechnology and Allied Sciences, New Vallabh Vidyanagar-388120, Gujarat State, India*

Нове киселе и мочилске моноазо боје су синтетизоване куповањем диазонијумових соли различитих ароматичних амина са 2-хидрокси-4-метоксибензофеноном. Добијене боје су окарактерисане елементарном анализом, ИЦ, ^{1}H-NMR и UV–Vis техникама. Својства бојења су испитана на вуненим и свиленим тканинама. Бојење вунених и свилених тканина претходно третираних хромом дало је боље обојење. Обојеност бојених вунених и свилених тканина се кретала од плавичасто розе до црвене нијансе. Обојене тканине су показале веома добру постојаност на светлост, прање, зној, сублимацију и трење. Резултати антибактеријских испитивања својстава тканина претходно третираних хромом указала су на релативно добру токсичност мочилских боја према *Escherichia coli*, *Staphylococcus aureus*, *Salmonella typhi* и *Bacillus subtilis*.

(Примљено 4. јула 2009, ревидирано 21. јануара 2010)

REFERENCES

1. W. M. Cumming, G. J. Howie, *J. Chem. Soc*. (1933) 133
2. A. T. Peters, D. Walker, *J. Chem. Soc*. (1956) 429
3. A. I. Vogel, *A Textbook of Practical Organic Chemistry*, 3rd ed., Longman, London, 1961, p. 620
4. P. F. Gordon, P. Gregory, *Organic Chemistry in Colour*, 1st ed., Springer-Verlag, Berlin, 1983, p. 60
5. S. K. Mohamed, A. M. Nour El-Din, *J. Chem. Res*. **8** (1999) 508
6. R. D. Naik, C. K. Desai, K. R. Desai, *Orient. J. Chem*. **16** (2000) 159
7. S. Yurteri, A. Onen, Y. Yagci, *Eur. Polym. J*. **38** (2002) 1845
8. W. Huang, B. Hou, *Tribology Lett*. **18** (2005) 445
9. E. Eltayeb, M. Barikani, A. R. Mahdavian, H. Honarkar, *Iranian Polym. J*. **18** (2009) 753
10. M. Johnson, R. G. Hauserman, *J. Appl. Polym. Sci*. **21** (1977) 3457
11. H. Kamogawa, M. Nanasawa, Y. Uehara, *J. Polym. Sci. A* **15** (1977) 675
12. K. Allmer, A. Hult, B. Ranby, *J. Polym. Sci*. **27** (1989) 3419
13. V. Frantisek, N. Hana, *Czech patent*: 176, 377 (1979) [CA 91:P58685x]
14. B. Raouf, *US patent* 4,066,388 (1978)
15. B. Brian, C. Donald, *A. G.* Sandoz, *DE patent* 3,417,782 (1984)
16. R. T. Markus, K. Jakob, *Eur. Patent (EP)* 169,808 (1986)
17. B. C. Dixit, H. M. Patel, D. J. Desai, *J. Serb. Chem. Soc*. **72** (2007) 119
18. B. C. Dixit, H. M. Patel, D. J. Desai, R. B. Dixit, *E-J. Chem*. **6** (2009) 315
19. H. E. Frirz-David, L. Blengy, *Fundamental Process of Dye Chemistry*, 3rd Ed., Wiley, New York, 1949, p. 241
20. M. Szymczyk, A. E. Shafei, H. S. Freeman, *Dyes Pigm*. **72** (2007) 8
21. R. M. E. Shishtawy, Y. A. Youssef, N. S. E. Ahmed, A. A. Mousa, *Dyes Pigm*. **72** (2007) 57
22. M. J. Pelzar, E. C. S. Chan, N. R. Krieg, *Antibiotics and Other Chemotherapeutic Agents in Microbiology*, 5th ed., Blackwell Science, New York, 1998.

Journal of the Serbian Chemical Society
JSCS@tmf.bg.ac.rs • www.shd.org.rs/JSCS

J. Serb. Chem. Soc. 75 (5) 615–627 (2010)
JSCS–3992

UDC 665+54–188:62–436.1
Original scientific paper

Preparation of microcapsules containing different contents of different kinds of oils by a segregative coacervation method and their characterization

VERICA J. SOVILJ*#, JADRANKA L. MILANOVIĆ, JAROSLAV M. KATONA and LIDIJA B. PETROVIĆ

Faculty of Technology, Department of Applied and Engineering Chemistry, University of Novi Sad, Bul. cara Lazara 1, 21000 Novi Sad, Serbia

(Received 8 October, revised 17 December 2009)

Abstract: Microencapsulation of different oils was performed using a segregative coacervation method. In order to microencapsulate, 20 % oil-in-water (O/W) emulsions were prepared in a continuous phase consisting of a 1 % mixture of hydroxypropylmethylcellulose (HPMC)/sodium carboxymethylcellulose (NaCMC) mass ratio (0.7/0.3) and various concentrations (0, 0.35 and 1 %) of the anionic surfactant sodium dodecylsulfate (SDS). Various interactions between the components occur in the continuous phase of emulsions, which influence the structure and properties of the adsorption layer around the oil droplets. The formed HPMC/SDS complexes in the presence of NaCMC molecules undergo segregative phase separation and form a coacervate which adsorbs onto the oil droplets, forming the wall of the microcapsules. Sunflower oil, pumpkin seed oil and a mixture of sunflower and linseed oil were used as the core material. Microcapsules in the solid form were obtained by spray drying the emulsions. The stability of the emulsions, the particle size and particle size distribution of the emulsions and suspensions of microcapsules and the oil content of the microcapsules were determined. The influence of the oil kind on the properties of the microcapsules was also investigated. It was found that at 0.35 % SDS, a coacervate layer around the oil droplets forms a stabile, compact microcapsules wall, which prevents oil extraction. The kind of oil influences the properties of the emulsions and microcapsules, which is important in the selection of oils for microencapsulation by this method.

Keywords: microencapsulation; coacervation; segregation; emulsions; oil content.

* Corresponding author. E-mail: vsovilj@uns.ac.rs
# Serbian Chemical Society member.
doi: 10.2298/JSC091008042S

INTRODUCTION

Microencapsulation is an effective method to wrap a liquid and/or a solid material by polymers and has extensive potential applications in the fields of food, pharmaceutics, cosmetics, pesticides, biotechnology, catalysis and many other areas.[1] Recently, microencapsulation techniques were adopted for the production of polymer-coated nanoparticles for electronic paper application[2] or for the production of electrorheological fluids.[3] The reason for microencapsulation of food ingredients is to protect sensitive food components, improve the stability of reactive or volatile additives (such as vitamins, flavors, *etc*.), mask unpleasant taste and flavor of certain ingredients, incorporate time-release mechanisms into the formulation or simply convert liquids to solid.[4,5] In recent years, the controlled release concept of encapsulated ingredients at the right time and in the right place has increased more and more.[6] Microencapsulated medical plant extracts can be used as supplements in functional food. Such microcapsules can improve the effectiveness of food designed for a health diet and for a food targeted to certain risk groups.

Among different techniques for microencapsulation of functional food ingredients, coacervation (phase separation) is the most common one applied in the food industry.[7] The term coacervation was suggested for the first time by Bungenberg de Jong[8] to explain the phenomenon of phase separation in a macromolecular system in which two phases are formed. Simple coacervation refers to phase separation brought about by reducing the solubility of a polymer by changing the temperature, adding non-solvents or "salting-out" by electrolytes, while complex coacervation or "associative" phase separation involves the addition of another oppositely charged macromolecule.[1,9,10] As a consequence, the system demixes into two phases: a solvent-rich phase containing a very small amount of polymer and a polymer-rich phase – coacervate. "Segregative" phase separation occurs due to the thermodynamic incompatibility of two polymers, which results in system demixing into two phases, each phase rich with one of the two polymers.[11]

In microencapsulation processes by a coacervation method, the material to be encapsulated is emulsified or dispersed in a solution of a polymer, and by changing the temperature, pH value or adding another polymer or non-solvent, coacervation can be induced, where the coacervate deposits at the surfaces of the dispersed particles and forms a thin coating. After further treatment, in order to solidify the polymeric wall, microcapsules can be obtained and separated from the system.[5,12,13] The coacervation method of microencapsulation was recently adopted for coating nanoparticles for electronic paper application. The most commonly used wall materials in microencapsulation by coacervation processes are proteins, gums, carbohydrates and various synthetic polymers.[5,7]

In recent years, hydroxypropylmethylcellulose (HPMC), a water soluble, non-ionic cellulose derivative, has been widely used in food products.[14] The presence of hydroxypropyl and methyl groups renders the cellulose molecules hydrophobic and makes them surface active.[15] The hydroxypropyl and methyl groups represent potential sites for adsorption of low molar mass surfactants, such as sodium dodecylsulfate (SDS), which results in the formation of a polymer–surfactant complex. This is of practical interest in dispersed systems, since such interactions affect the structure of the adsorption layer around oil droplets. It was shown in a previous investigation[16] that HPMC–SDS interactions affect the emulsion stability and adsorption layer formation. Since, the HPMC/SDS complex bears a net negative charge and behaves like a polyelectrolyte, the addition of an oppositely charged polyelectrolyte, such as sodium carboxymethylcellulose (NaCMC), causes electrostatic repulsion and "segregative" phase separation.[17] The system separates into an HPMC/SDS complex-rich phase, *i.e.*, coacervate and a NaCMC-rich phase, *i.e.*, supernatant.[18] This is a method of coacervate formation by thermodynamic incompatibility where one polyelectrolyte is actually a polymer–surfactant complex, formed through the interaction. If coacervation occurs in the continuous phase of an emulsion, it results in the adsorption of the coacervate around oil droplets and microcapsules wall formation.

The aim of the present work was to investigate the influence of coacervate formation in the continuous phase of emulsions in the system HPMC/SDS/ /NaCMC on wall formation around oil droplets, *i.e.*, microencapsulation, as well as on the properties of the microcapsules. In addition, the influence of the kind of oil on the properties of the microcapsules was investigated. Different properties of emulsions and microcapsules, such as stability, particle size and particle size distribution, redispersibility in water and encapsulation efficiency, were determined.

EXPERIMENTAL

Materials

Hydroxypropylmethylcellulose (HPMC), (trade name Methocel K4M CR, methoxyl content: 22.7 %, hydroxypropyl content: 8.9 %), pharmaceutical grade, was obtained from Colorcon Ltd., England. The viscosity average molecular mass was $\overline{M}_v$ = 91500 g/mol, determined at 20 °C, and the critical overlap concentration c^* = 0.127 %. Sodium carboxymethylcellulose (NaCMC), *DS* = 0.77, purity >96 %, was obtained from "Milan Blagojević" Lučani, Serbia. The viscosity average molecular mass was $\overline{M}_v$ = 116000 g/mol, determined at 25 °C, and the critical overlap concentration c^* = 0.187 %. Sodium dodecylsulfate (SDS), purity > 99 %, was obtained from Merck, Germany. As core materials, sunflower oil ("Sunce", Sombor, Serbia), pumpkin seed oil ("Banat", Nova Crnja, Serbia) and a mixture of cold pressed linseed/sunflower oil (mass ratio 0.2:0.8) were used. Cyclohexane was obtained from "Kemika", Zagreb, Croatia.

Preparation of the solutions

Stock solutions of HPMC and NaCMC were prepared at concentrations of 2.56 % (w/w) and 2.4 % (w/w), respectively, by dispersing the required amount of HPMC and NaCMC in bidistilled water at 80 °C (above the gel point of HPMC, which is approximately 70 °C) and 20 °C, respectively, by gentle stirring. The stock solutions were left for 24 h at room temperature before further use. A stock solution of SDS was prepared at a concentration of 7 % (w/v). Bidistilled water was used as the solvent.

Preparation of the emulsions

Stock emulsions of different oils 22.22 % (w/w) in a binary mixture HPMC/SDS (continuous phase) were prepared by homogenization using an Ultraturrax T-25 (Janke & Kunkel, Germany) at 4700 rpm for 3 min. The emulsification temperature was 25 °C. Binary mixtures were composed of 0.8 % w/w HPMC (based on the mass of the continuous phase) and various concentrations of SDS. The final emulsion was prepared by careful addition (drop by drop) of 10 g of a 2.4 % w/w NaCMC solution into 90 g of the stock emulsion stirred on a magnetic stirrer. In this way, 20 % w/w oil-in-water (O/W) final emulsions with continuous phases composed of a 1 % mixture HPMC/NaCMC (mass ratio 0.7:0.3) and SDS (0, 0.35 and 1 % SDS) were obtained.

Stability test

For the stability test, the emulsions were transferred into graduated cylinders and stored at room temperatures for 60 days. During storage, the emulsions separated into a cream layer at the top, and a transparent serum layer at the bottom of the cylinder. The total height of the emulsion, H_E, and the height of the serum layer, H_S, were measured during time. The extent of creaming was characterized by the creaming index, H, given by:[19]

$$H = 100\frac{H_S}{H_E} \tag{1}$$

The higher creaming index, H, the worse is the emulsion stability.

Spray drying of the emulsions

The emulsions were spray dried in a Mini Spray Dryer (Büchi 190, Switzerland), whereby microcapsules in the form of a powder were obtained. The drying parameters during the process, such as air flow, aspiration and feeding were controlled to keep 150 °C inlet and 100 °C outlet temperature.

Determination of the particle size and particle size distribution

Particle size and particle size distribution of the emulsions and suspensions of microcapsules in water were determined by the microscopic image analysis technique, using "QWin" software (Leica).[20] The volume–surface mean diameter, d_{vs} / μm, and standard deviation, σ / / μm, were calculated.

Encapsulation efficiency

The encapsulation efficiency was determined by extraction of the encapsulated oil with cyclohexane. Microcapsules (1 g) were dispersed in 100 ml of cyclohexane and left for 40 min on a magnetic stirrer. The samples were then filtered and the amount of released oil was determined spectrophotometrically, at 234 nm for the sunflower oil and the mixture of linseed/sunflower oil, and at 274 nm for the pumpkin seed oil, using a Hewlett Packard 8452A Diode Array spectrophotometer.

RESULTS AND DISCUSSION

Deposition of coacervate at the surface of the oil droplets in the emulsions

Since the emulsions were prepared by dispersing the oils in continuous phases consisting of HPMC molecules or HPMC–SDS mixtures, to which NaCMC molecules were subsequently added, various interactions occurred in the continuous phase of the emulsions, *i.e.*, HPMC–NaCMC, HPMC–SDS, and HPMC–SDS––NaCMC, which could affect the properties of the emulsions and the obtained microcapsules.

The interactions between HPMC and SDS molecules were previously investigated by various methods: conductometry, viscometry and rheology.[16,18,21,22] It was shown that binding of the SDS molecules onto the HPMC molecules starts with a hydrophobic interaction mechanism when the surfactant concentration reaches the critical aggregation concentration (*CAC*). The interaction causes an increase in viscosity and after reaching the maximum, when a three-dimensional network with a negative net charge had been created, the viscosity decreases with increasing SDS concentration until the end of interaction, *i.e.*, at an SDS concentration called the polymer saturation point (*PSP*). After *PSP*, the viscosity remains constant and is lower than the viscosity of the pure HPMC solution.[16,21]

The addition of the anionic polymer NaCMC to an emulsion having HPMC/ /SDS complexes in the continuous phase results in electrostatic repulsion between the same charged groups of the NaCMC molecules and HPMC/SDS complexes, which leads to phase separation and coacervate formation. The formed coacervate deposits around the oil droplets. A schematic diagram of the procedure for emulsion preparation with a coacervate layer around the oil droplet, *i.e.*, microcapsule formation, is presented in Fig. 1.

The results of previous investigations[15,16] showed that, depending on the mass ratio of the components in the HPMC/SDS/NaCMC system, complexes with different structures were obtained, which influence the properties of the adsorption layer around the oil droplets and, hence, microcapsules with different wall properties could be expected.

In the present study, a 1 % solution of HPMC/NaCMC mass ratio 0.7:0.3 was chosen, which gives a coacervate having the largest volume in the presence of SDS.[17,18] The concentrations of SDS were 0, 0.35 and 1 %, which cover different regions of HPMC–SDS interaction. With 0 % SDS in the continuous phase of emulsion, only the complex HPMC/NaCMC is present and there is no coacervate formation. With 0.35 % SDS, the HPMC/SDS complex in the continuous phase forms the most entangled negatively charged network, and after addition of NaCMC molecules, the polymer–polymer incompatibility results and the continuous phase separates into an HPMC/SDS complex-rich phase, the coacervate, and a NaCMC-rich phase, the supernatant.[18] The formed coacervate adsorbs at the oil droplets surface forming a compact polymer layer. With 1 % SDS, the in-

teraction between HPMC and the SDS molecules is completed, the intermolecular network breaks down, the HPMC/SDS complex is solubilized with SDS and the formed coacervate layer is not compact.

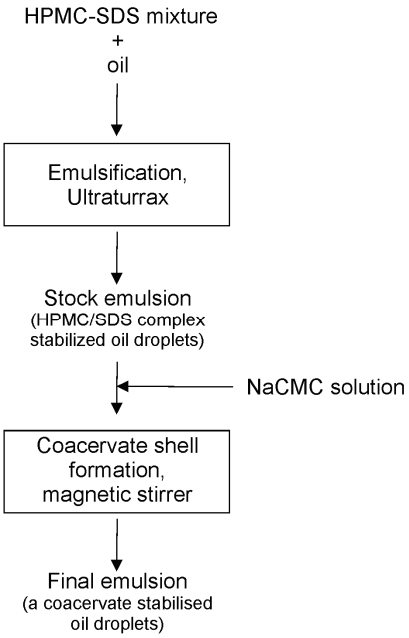

Fig. 1. Scheme of the preparation of coacervate stabilized emulsions.

Photographs of 20 % emulsions prepared with different kinds of oil at the chosen SDS concentrations after 24-h storage are shown in Fig. 2.

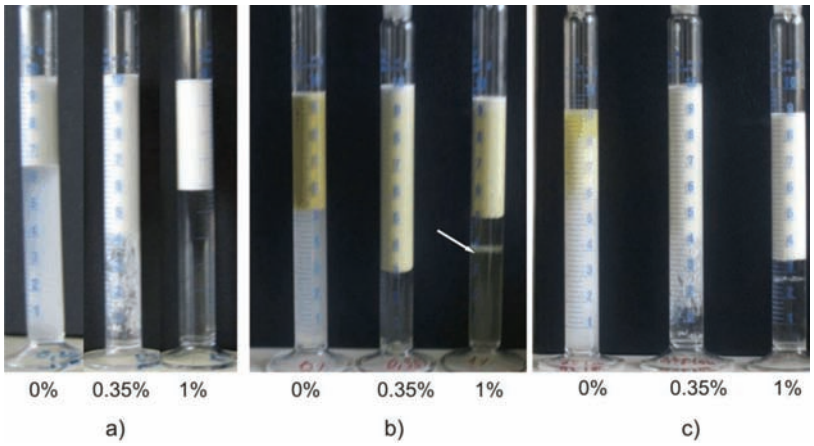

Fig. 2. Photographs of 20 % emulsions of a) sunflower oil, b) pumpkin seed oil and c) a mixture of linseed/sunflower oil (0.2/0.8) in a 1 % solution of HPMC/NaCMC (0.7/0.3) at the investigated SDS concentrations after 24 hours of storage.

It can be seen that in all emulsions, the highest volume of the cream layer was obtained at an SDS concentration of 0.35 %, *i.e.*, at the maximum coacervation. At this SDS concentration, the formed HPMC/SDS complex separated from the continuous phase after addition of NaCMC molecules and deposited around the oil droplets as a compact coacervate layer. Therefore, cream layers were formed immediately after preparation of the emulsions and the creaming index did not change with time, Fig. 3, except for the emulsion of the pumpkin seed oil. At the bottom of the cylinders, Fig. 2, there is no evidence of any coacervate sediment, indicating that all of the formed coacervate was adsorbed around the oil droplets, which contributes to the cream height, and thus the emulsions have the lowest creaming index, *H*, Fig. 3. The serum layers of the emulsions are clear, while in the emulsions of sunflower oil and mixture of linseed/ /sunflower oil some of the rest cream remains stuck to the wall at the lower part of the cylinders, Fig. 2.

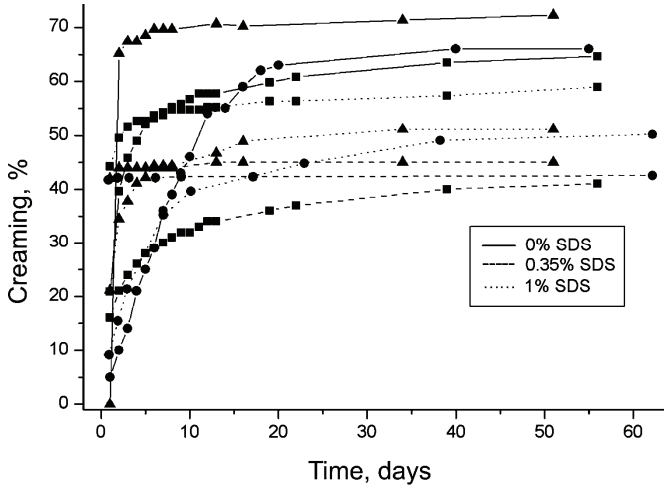

Fig. 3. Creaming index of 20 % emulsions prepared with different oils (■, pumpkin seed oil, ▲, linseed/sunflower oil (0.2/0.8), ●, sunflower oil) at the investigated SDS concentrations as a function of time.

Emulsions without SDS, *i.e.*, without a coacervate, exhibited typical sedimentation instability with a turbid serum layer due to the polydispersity of the emulsions and slow migration of the small oil droplets through the viscous continuous phase containing the HPMC/NaCMC complex.[18] The creaming indexes, *H*, of all emulsions with 0 % SDS were the highest and changed with time, Fig. 3. The emulsion of linseed/sunflower oil was found to be the least stable and separated in five days. In the emulsions of pumpkin seed oil and the mixture of linseed/sunflower oil without SDS, the cream layers were more intensely colored, compared to the corresponding cream layers of the emulsions with SDS, in-

dicating that in the absence of a coacervate shell, the adsorption layer around the oil droplets was thin. Therefore, the characteristic color of the used oils was visible.

At an SDS concentration of 1 %, the volume of the cream layer of emulsions was smaller, *i.e.*, the creaming index, *H*, was higher than that with 0.35 % SDS, indicating that the formed coacervate, which consisted of a solubilized HPMC/ /SDS complex, was partly desorbed from the oil droplets surface and was visible lower in the cylinders as a transparent sediment, arrow in Fig. 2. The creaming indexes of emulsions with 1 % SDS were between those with 0 and 0.35 % SDS and changed with time, Fig. 3, due to the slow process of desorption and stabilization of the adsorption layers in the emulsions.

It is evident that the thickness and the composition of the adsorption layers around the oil droplets depended on the SDS concentration, which suggests that microcapsules of different wall properties could be obtained after spray drying of the emulsions. In addition, the different appearance of the pumpkin seed oil emulsion with 0.35 % SDS and the linseed oil emulsion with no SDS, when compared to the corresponding sunflower oil emulsions, Fig. 2, indicates that the kind of oil also affects the properties of the adsorption layer and, hence, the properties of the emulsions and microcapsules.

Particle size distribution of the emulsions and suspensions of microcapsules

The prepared emulsions were spray dried and microcapsules in powder form were obtained. The particle size and particle size distribution of the emulsions and the suspensions of microcapsules in water were determined, Table I.

TABLE I. Parameters of the particle size distribution of the emulsions and suspensions of microcapsules in water

Parameter	Sunflower oil			Pumpkin seed oil			Linseed/sunflower oil (0.2/0.8)		
	c_{SDS} / %								
	0.00	0.35	1.00	0.00	0.35	1.00	0.00	0.35	1.00
Emulsions									
d_{vs} / μm	20.53	3.42	2.54	11.0	3.36	3.10	7.61	5.52	5.30
σ / μm	5.49	0.81	0.66	4.37	0.79	0.86	3.56	2.56	3.06
Suspensions									
d_{vs} / μm	4.14	4.63	8.24	5.88	6.56	7.79	7.81	4.94	10.42
σ /μm	1.83	1.58	3.77	2.83	2.93	3.54	3.48	1.71	4.52

It is evident that the presence of SDS significantly decreased the particle size in all emulsions. The best correlation, *i.e.*, the smallest difference in particle size distribution of the emulsions and the corresponding suspensions of microcapsules was obtained with SDS concentration of 0.35 %. At this SDS concentration, the formed HPMC/SDS complex was separated from the solution by addition of NaCMC and deposited on the surface of the oil droplets as a compact coacervate layer. This enabled microcapsules to be obtained with a stable wall and almost

the same particle size as in the original emulsion, indicating that at this SDS concentration, the drying conditions had an insignificant effect on the particle size of the microcapsules. These microcapsules had a more uniform particle size distribution (lower standard deviation, σ) and a better redispersibility in water, compared to the microcapsules obtained with 0 and 1.0 % SDS. The microcapsules prepared without SDS and with 1 % SDS had significantly different mean diameters to those of the corresponding emulsions, as a consequence of wall instability under the employed drying conditions.

The microphotographs of the sunflower oil emulsions, the microcapsules powders and the suspensions of the microcapsules in water, obtained at characteristic SDS concentrations, are presented in Fig. 4, while the particle size distributions of the sunflower oil emulsions and suspension of microcapsules in water are presented in Fig. 5.

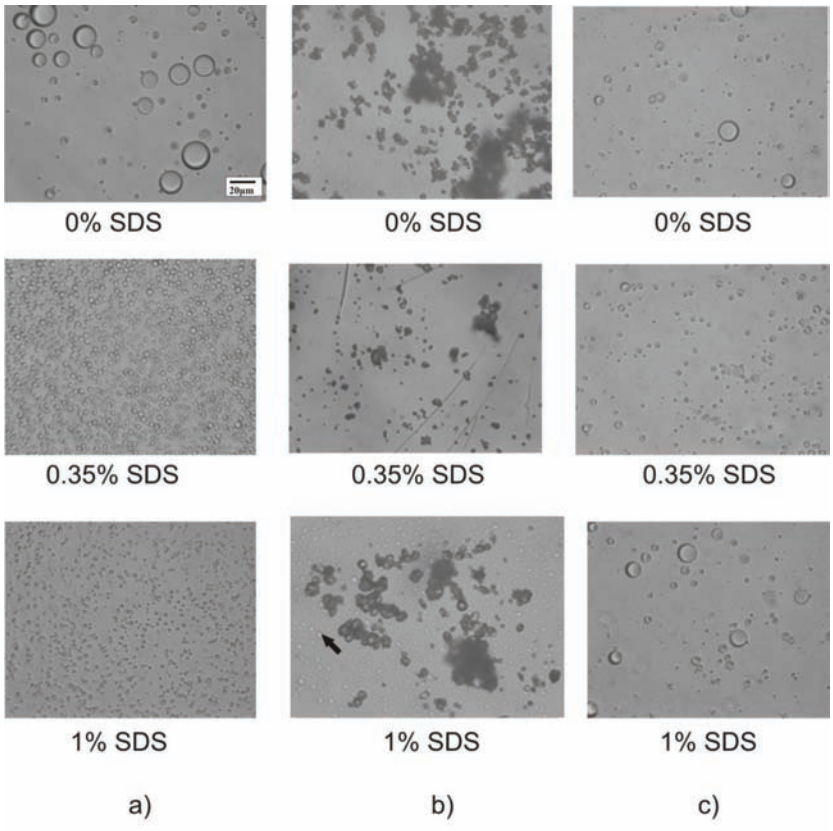

Fig. 4. Microphotographs of a) 20 % emulsions of sunflower oil in a 1 % solution of HPMC/NaCMC (0.7/0.3) at different SDS concentrations, b) the corresponding microcapsules powders and c) suspension of the microcapsules in water.

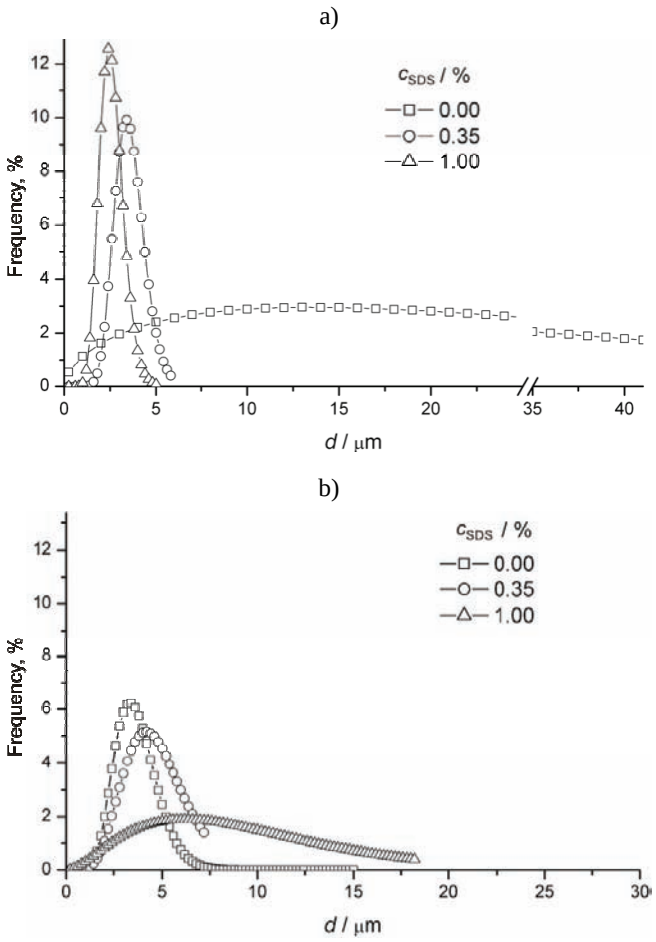

Fig. 5. Particle size distribution of a) emulsions and b) suspensions of the microcapsules in water, obtained at the investigated SDS concentrations.

The microphotographs and the particle size distributions show that the emulsions without SDS contained large droplets and were more polydisperse when compared to the emulsions with SDS. A similar behavior was found for the other investigated emulsions. During the spray drying of the emulsions without SDS, the large oil droplets stick or crack and remain on the spray cylinder wall, which results in a decrease in particle size of the microcapsules and a change in particle size distribution, Fig. 5. The exception is the microcapsules with the oil mixture, Table I, which have almost the same particle size as the corresponding emulsion. This is due to the significantly smaller d_{vs} of the emulsion droplets containing the linseed/sunflower oil mixture and hence better stability during the drying process. The lower d_{vs} value could be a consequence of the higher level of poly-

unsaturated fatty acids in linseed oil,[23] which contributed to the emulsification efficiency of the HPMC molecules.

An increase in the size of the microcapsules, compared to the corresponding emulsion, is evident for the sample containing 1 % SDS, Fig. 5, because of coalescence of the oil leached from microcapsules during their redispersion in water. Namely, the microcapsules readily cracked during the manipulation as indicated by the presence of free oil droplets (arrow) in the microphotograph of the microcapsules powder, Fig. 4, which indicates the instability of the wall of the microcapsules. Only the suspension of microcapsules obtained at 0.35 % SDS had almost the same particle size and particle size distribution, Table I and Fig. 5, as the corresponding emulsion, *i.e.*, firm and stable microcapsules walls which were resistant to the spray drying conditions.

Encapsulation efficiency

The encapsulation efficiency was determined spectrophotometrically after extraction of the oil from the microcapsules with cyclohexane. The results are presented in Fig. 6.

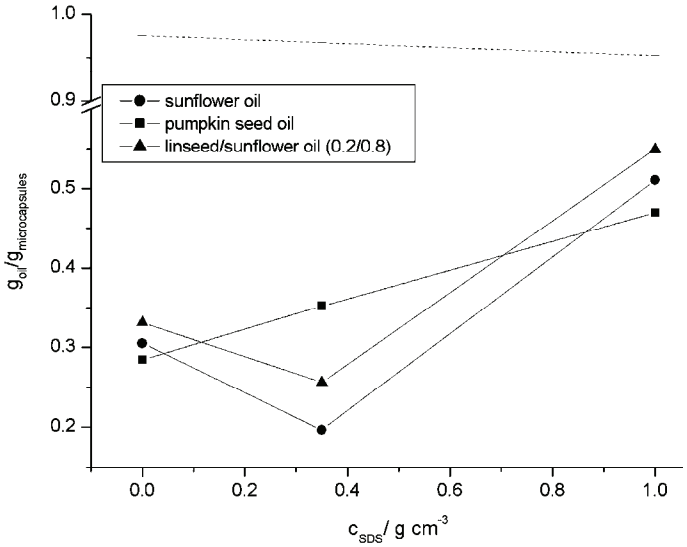

Fig. 6. Amount of oil extracted from the microcapsules as a function of SDS concentration and the theoretical amount of oil (---).

The lowest amount of extracted oil was found in the microcapsules containing sunflower and the mixture of linseed/sunflower oil (0.2/0.8) in the HPMC/ /SDS interaction region, *i.e.*, at 0.35 % SDS. This is most likely a consequence of the presence of the compact, networked coacervate layer around the oil surface, which forms a stable microcapsules wall and hinders oil extraction. The largest

amount of extracted oil was found at SDS concentration of 1 %, which is in agreement with the proposed permeable structure of microcapsules wall. In comparison with the theoretical amount of oil present in the microcapsules, Fig. 6, the amount of extracted oil suggests that some oil was still present in all microcapsules after extraction, and that the permeability depends on the wall structure, *i.e.*, the presence of the coacervate around the oil droplets. The exceptions were the microcapsules of pumpkin seed oil where the amount of extracted oil increased with increasing SDS concentration, indicating that the presence of coacervate has no influence on the transport of oil through the wall. The reason for this could be presence of sterols in high percent in pumpkin seed oil, which can be adsorbed onto the oil droplets surfaces[24] and influence the permeability of the adsorption layer.

As the nature of the encapsulated oil influences the microencapsulation process and the properties of microcapsules, for a detailed explanation of the different behaviors of the used oils, information about their chemical composition is necessary. Therefore, the physico-chemical characteristics of oils should be considered as an important parameter of microencapsulation by the presented method.

CONCLUSIONS

Due to the interaction of the components in the continuous phase of emulsions consisting of HPMC, NaCMC and SDS molecules, the formed anionic complex HPMC/SDS deposits around the oil droplets as a coacervate in the presence of NaCMC molecules and forms the microcapsules wall. The properties of the walls of the microcapsules depend on the SDS concentration. At 0.35 % SDS, the formed coacervate layer is compact and enables the formation of stable microcapsules with entrapped oil, which is difficult to extract. In addition, the oil characteristics affect the stability of the coacervate layer. For the microencapsulation of different oils, knowledge of their components is important for predicting their influence on the microencapsulation efficiency by the coacervation method.

Acknowledgement. This work was supported by the Ministry of Science and Technological Development of the Republic of Serbia, Project No. 20022.

И З В О Д

ДОБИЈАЊЕ И КАРАКТЕРИЗАЦИЈА МИКРОКАПСУЛА КОЈЕ САДРЖЕ РАЗЛИЧИТЕ ВРСТЕ УЉА ПРИМЕНОМ МЕТОДЕ СЕГРЕГАТИВНЕ КОАЦЕРВАЦИЈЕ

ВЕРИЦА Ј. СОВИЉ, ЈАДРАНКА Л. МИЛАНОВИЋ, ЈАРОСЛАВ М. КАТОНА и ЛИДИЈА Б. ПЕТРОВИЋ

Технолошки факултет, Катедра за примењене и инжењерске хемије, Универзитет у Новом Саду, Бул. цара Лазара 1, 21000 Нови Сад

Формиране су микрокапсуле уљног садржаја методом коацервације сегрегативног типа. Континуална фаза 20 % (w/w) емулзија уља у води, У/В, састојала се од 1 % (w/w) смеше хидроксипропилметил-целулозе (HPCMC) и натријум-карбоксиметил-целулозе (NaCMC) масеног односа 0,7/0,3, уз присуство анјонске површински активне материје, натријум-додецил

сулфата (SDS) концентрација: 0, 0,35 и 1 мас. %. Наведене концентрације SDS омогућавају формирање различитих структура адсорпционих слојева око диспергованих капљица уља сегрегативном коацервацијом комплекса HPMC/SDS у присуству молекула NaCMC, што је утицало на формирање и особине микрокапсула. Као уљна фаза коришћено је сунцокретово уље, бундевино уље и смеша сунцокретовог и ланеног уља. Микрокапсуле у облику праха добијене су распршивањем емулзија у Spray Dryer-у. Одређивана је стабилност, величина и расподела честица емулзија и одговарајућих суспензија микрокапсула у води, као и проценат енкапсулираног уља екстракцијом. Показало се да се стабилан компактан слој коацервата око капи формира при 0,35 % SDS, који спречава екстракцију уља из микрокапсула. Такође, на особине емулзија и микрокапсула утиче и врста уља тако што поједине компоненте уља мењају структуру адсорпционог слоја око капи и њихову стабилност, о чему треба водити рачуна при избору уља за микрокапсулацију овом методом.

(Примљено 8. октобра, ревидирано 17. децембра 2009)

REFERENCES

1. C. Thies, in *Microencapsulation: Methods and industrial applications*, S. Benita, Ed., Marcel Dekker, New York, Basel, 1996, p. 1
2. J. H. Park, M. A. Lee, B. J. Park, H. J. Choi, *Curr. Appl. Phys.* **7** (2007) 349
3. B. J. Park, M. S. Kim, H. J. Choi, *Mater. Lett.* **63** (2009) 2178
4. K. G. H. Desai, H. J. Park, *Drying Technol.* **23** (2005) 1361
5. A. Gharsallaoui, G. Roudaut, O. Chambin, A. Voilley, R. Saurel, *Food Res. Int.* **40** (2007) 1107
6. U. R. Pothakamury, G. V. Barbosa-Canovas, *Trends Food Sci. Technol.* **61** (1995) 397
7. S. Gouin, *Trends Food Sci. Technol.* **15** (2004) 330
8. D. J. Burgess, J. E. Carless, *J. Colloid Interface Sci.* **98** (1984) 1
9. H. S. Kas, L. Oner, in *Handbook of pharmaceutical controlled release technology*, D. L. Wies, Ed., CRC Press, London, 2000, p. 301
10. J. A. Bakan, J. L. Anderson, in *The theory and practice of industrial pharmacy*, H. A. Lieberman, J. L. Kanig, Eds., Lea and Febiger, Philadelphia, PA, 1976, p. 420
11. J. L. Doublier, C. Garnier, D. Renard, C. Sanchez, *Curr. Opin. Colloid Interface Sci.* **5** (2000) 202
12. K. S. Mayya, A. Bhattacharyya, J.-F. Argillier, *Polym. Int.* **52** (2003) 644
13. W. Li, G. Wu, H. Chen, M. Wang, *Colloids Surf., A* **333** (2009) 133
14. G. A. Burdock, *Food Chem. Toxicol.* **45** (2007) 2341
15. W. M. Kulicke, O. Arendt, M. Berger, *Colloid Polym. Sci.* **276** (1998) 101
16. V. J. Sovilj, L. B. Petrović, *Carbohydr. Polym.* **64** (2006) 41
17. V. J. Sovilj, L. B. Petrović, *Colloids Surf., A* **298** (2007) 94
18. J. Katona, V. J. Sovilj, L. B. Petrović, *Carbohydr. Polym.* **74** (2008) 193
19. D. Kelley, J. D. McClements, *Food Hydrocolloids* **17** (2003) 87
20. T. Moschakis, B. S. Murray, E. Dockinson, *J. Colloid Interface Sci.* **284** (2005) 714
21. V. J. Sovilj, L. B. Petrović, *Colloid Polym. Sci.* **284** (2005) 334
22. J. V. Šaletić, V. J. Sovilj, L. B. Petrović, *Hem. Ind.* **58** (2004) 521
23. M. G. Pereira, S. M. Mudge, J. Latchford, *Mar. Environ. Res.* **56** (2003) 367
24. Y. Barenholz, *Prog. Lipid Res.* **41** (2002) 1.

Journal of the Serbian Chemical Society
JSCS@tmf.bg.ac.rs • www.shd.org.rs/JSCS

J. Serb. Chem. Soc. 75 (5) 629–637 (2010)
JSCS–3993

UDC 546.733'763'723'+542.9+
547.571+547.511:615.28–188
Original scientific paper

Synthesis, physical characterization and antimicrobial activity of trivalent metal Schiff base complexes

GAJENDRA KUMAR[1], DHARMENDRA KUMAR[2], C. P. SINGH[2]*, AMIT KUMAR[1] and V. B. RANA[1]

[1]*Department of Chemistry Meerut College, Meerut, (UP) 250001 and* [2]*Department of Chemistry Sahu Jain College, Najibabad, (UP) 246763, India*

(Received 19 June, revised 16 November 2009)

Abstract: M(III) complexes of Cr, Mn and Fe with a Schiff base derived from 2-amino-4-ethyl-5-hydroxybenzaldehyde and thiocarbohydrazide were synthesized and characterized by several techniques, including elemental analysis (C,H,N), molar conductance measurements, magnetic measurements, and electronic, mass and IR spectral studies. Based on these studies, a five-coordinated square pyramidal geometry for all the complexes was proposed. The Schiff base ligand and the complexes were also tested for their antimicrobial activity (against the bacteria *Escherichia coli*, *Staphylococcus aureus*, *Pseudomonas aeruginosa* and *Bacillus megaterium*, and the fungi *Kluyveromyces fragilis*, *Rhodotorula rubra*, *Candida albicans* and *Trichoderma reesei*) to assess their inhibiting potential. An attempt was also made to correlate the antimicrobial activity with the geometry of the complexes. All complexes were found to be less active against the pathogens *E. coli*, *S. aureus* and *P. aeruginosa*. The Cr(III) complex showed the best antimicrobial activity, but the ligand alone was found to be active against the fungus *T. reesei*.

Keywords: Co (III), Cr (III) and Fe (III) complexes; Schiff Base; 2-amino-4--ethyl-5-hydroxybenzaldehyde; thiocarbohydrazide; antimicrobial activity.

INTRODUCTION

The field of Schiff base complexes is fast developing because of the wide variety of possible structures for the ligands, depending on the aldehyde and amine used. Many Schiff bases and their complexes have been widely studied because of their industrial and biological applications.[1,2] Some Schiff bases were tested for fungicidal activity, which is related to their chemical structure.[3] Schiff base compounds (–RC=N–) are usually formed by the condensation of a primary amine with an active carbonyl. The cross-linking agents can also be derived from

* Corresponding author. E-mail: gaj25chem@gmail.com
doi: 10.2298/JSC090704037K

metal complexes with O, N or S ligands. For example, an intracoordination salt such as salicylates or anthranilates and aliphatic or aromatic amines can form strong five- or six-membered chelate rings which are able to produce metal containing cross-linking agents with the required properties.[4–7] Synthesis of oxovanadium(IV) complexes of Schiff bases derived by the condensation of 2-aminobenzaldehyde with various diamines (1,2-diaminoethane, 1,2-diamino-propane, 1,3-diaminopropane) were characterized by elemental analysis, spectral data and electrochemical studies.[8] The complexes of Co(II), Ni(II), and Cu(II) ions with the Schiff bases derived from the condensation of salicylaldehyde and *o*-aminophenol or 2-aminobenzoic acid were synthesized and characterized by different techniques, in particular, elemental analysis and molar conductance measurements as well as IR and electronic spectroscopy.[9–11]

The aim of the present study was to prepare, characterize and determine the antimicrobial activity of Schiff base complexes derived from thiocarbohydrazide and 2-amino-4-ethyl-5-hydroxybenzaldehyde.

EXPERIMENTAL

Materials

All chemicals used in this work were of analytical reagent grade (anhydrous). $CrCl_3$, $MnCl_3$ and $FeCl_3$ were purchased from Aldrich (New Delhi, India); DMSO, DMF and ethanol were purchased from Sigma (New Delhi, India); 2-amino-4-ethyl-5-hydroxybenzaldehyde and thiocarbohydrazide were purchased from Fluka (Mumbai, India).

Synthesis of the Schiff base

The Schiff base (ligand) was prepared by mixing a warm dilute ethanolic solution of thio-carbohydrazide (5 mmol) with 2-amino-4-ethyl-5-hydroxy benzaldehyde (10 mmol) under reflux for 2 h (Scheme 1). The precipitate was then removed from the reaction mixture by filtration,[11,12] washed with ethanol and dried in a desiccator over anhydrous $CaCl_2$. The colour of the solid product was yellow (yield 65 %).

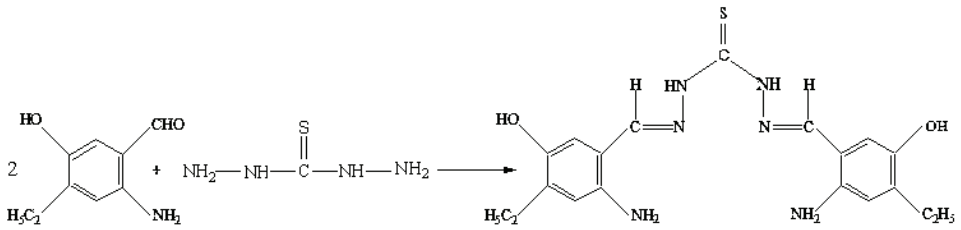

Scheme 1. Synthesis of the Schiff base ligand.

Synthesis of the complexes

The Schiff base was taken in ethanol (50 cm^3) and stirred gently for one hour to give a homogeneous solution and then trivalent chromium, manganese or iron chlorides salts (25 cm^3) were added (Scheme 2). The resulting solution was refluxed for 6–8 h. The mixture was concentrated to half its initial volume and kept in a desiccator for two days over anhydrous $CaCl_2$. The complexes were then filtered, washed with ethanol and dried. The complexes were

soluble in DMF and DMSO but insoluble in other common organic solvents and water. They were thermally stable up to 523–553 K and then decomposed.

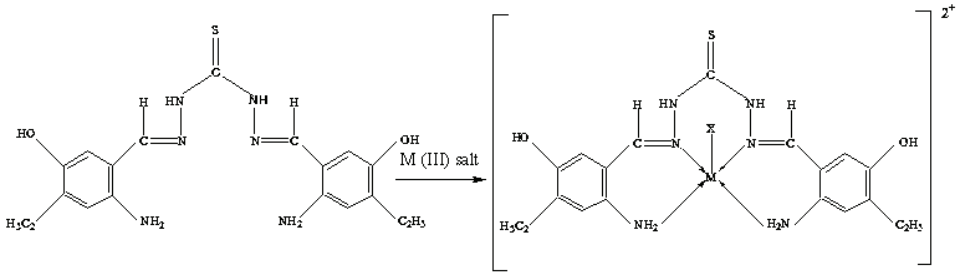

Scheme 2. Synthesis of the M(III) Schiff base complexes.

Methods and apparatus applied

The microanalyses for C, H, and N were estimated by an elemental analyzer (Perkin Elmer 2400), at SAIF, CDRI, Lucknow, India, and the metal contents of Mn(III), Co(III) and Fe(III) were determined using a Perkin Elmer 5000 atomic absorption spectrophotometer. Table I contains some physical properties of the prepared compounds. The conductivity was measured on a digital conductivity meter (HPG system, G-3001) in DMSO at room temperature. The magnetic susceptibility measurements were performed on a Vibrating Sample Magnetometer (Model PAR 155) at room temperature. The electronic spectra (in DMSO) were recorded on a Hitachi 330 spectrophotometer (5815–32573 cm^{-1}). The IR spectra were obtained using a Perkin Elmer 1650 FT-IR spectrophotometer in the wavenumber range 4000––200 cm^{-1} using Nujol Mull (the molar conductivities, magnetic moments and spectral data are given in Tables I and II). The FAB mass spectra (at room temperature) were recorded on a VG-70-S mass spectrometer. The purity of the Schiff base and its complexes were confirmed by TLC (microcrystalline cellulose (Merck) was used for the preparation of the thin layer, complete separation was achieved with the solvent system acetone/conc. HCl/water (86:8:7); the R_F values increased in the following order of M(II) complexes: Mn, Co, Cu (0.20, 0.34, 0.60)) and HPLC. The HPLC chromatographic instrument consisted of a Waters 600 pump with a Waters 600 controller, a Waters 2996 photodiode array detector with UV detection at 254 nm, a Discovery C_8 column, 15 cm×4.6 mm I.D., 5 µm particles. The mobile phase was methanol:25 mmol KH_2PO_4, pH 3 (20:80) at a flow rate of 1 ml min^{-1}.

Antimicrobial activity

The antibacterial and antifungal activities of the newly synthesized compounds were evaluated by the agar well diffusion method.[13] All the microbial cultures were adjusted to 0.5 McFarland Standard, which is visually comparable to a microbial suspension containing approximately 1.5×10^8 cfu/ml.[14] 20 ml of agar media was poured into each Petri plate and the plates were swabbed with 100 µl inocula of the test microorganisms and kept 15 min for adsorption. Using an 8 mm-diameter sterile cork borer, wells were bored into the seeded agar plates and these were loaded with 100 ml of a solution of each compound dissolved in the dimethyl sulphoxide (DMSO) at a concentration of 1.0 mg/ml. All the plates were incubated at 300 K for 24 h. The antimicrobial activity of all the synthesized compounds was evaluated by measuring the zone of growth inhibition against the test organisms with zone reader (Hi antibiotic zone scale). The medium with dimethyl sulphoxide (DMSO) as solvent was used as

a negative control whereas media with ciprofloxacin (standard antibiotic) and griseofulvin (standard antifungal drug) were used as the positive controls. The experiments were performed in triplicate.

The ligand HL and its Cr(III), Mn(III) and Fe(III) complexes were tested for their antibacterial and antifungal activity against the bacteria: *Escherichia coli*, *Staphylococcus aureus*, *Pseudomonas aeruginosa* and *Bacillus megaterium*, and the fungi: *Kluyveromyces fragilis*, *Rhodotorula rubra*, *Candida albicans* and *Trichoderma reesei* procured from Microbial Type Collection and Gene Bank, Institute of Microbial Technology (IMTECH), Chandigarh, India.

RESULTS AND DISCUSSION

The elemental analyses (C, H, N and M) data of the metal chelates, Table I, showed that they may be represented by the formula $[M(C_{19}H_{24}N_6O_2S)X]X_2$, (M(III) = Cr, Mn and Fe; X = Cl). The purity of the Schiff base and its complexes was confirmed by the TLC and HPLC techniques.

TABLE I. Elemental analysis, molar conductance and magnetic moment of the Schiff base ligand and its metal complexes

Compd.	Molecular formula	FW	Colour	Calcd. (Found)/ %				μ_{eff}	Λ_M
				C	H	N	M	μ_B	S cm^2 mol^{-1}
Ligand (HL)	$C_{19}H_{24}N_6O_2S$	506.62	Yellow	45.0 (45.4)	4.7 (4.8)	16.6 (15.9)	–	–	–
Cr complex	$[Cr(HL)X]X_2$	558.61	Greenish	40.8 (40.5)	4.3 (4.2)	15.0 15.0)	9.3 (9.4)	4.35	58.8
Mn complex	$[Mn(HL)X]X_2$	562.46	Dark brown	40.5 (40.6)	4.3 (4.2)	14.9 (15.1)	9.9 (9.8)	4.85	40.0
Fe complex	$[Fe(HL)X]X_2$	561.56	Orange red	40.6 (40.5)	4.3 (3.3)	15.0 (14.9)	9.8 (9.6)	5.78	32.5

The measurements of the molar conductance in DMSO, Table I, showed that these chelates were 1:2 type of electrolytes (the conductance values were 30–60 S cm^2 mol^{-1}, whereas the literature range is 30–180 S cm^2 mol^{-1}).[15] The tests for anions were positive before and after decomposition of the chelates with concentrated HNO_3, showing their presence outside as well as inside the coordination sphere. Several attempts to obtain a single crystal suitable for X-ray crystallography failed. However, the analytical, spectroscopic and magnetic data enabled the prediction of the possible structure of the synthesized complexes. The low molar conductance of the complexes might arise due to the large size of the cation coordination sphere, which might have a low ionic mobility; the values of molar conductance suggest that the complexes were electrolytes and that chloride was present as the counter ion.

The IR and electronic spectral data of the ligand and of the complexes are given in Table II.

The IR spectra provided valuable information regarding the nature of functional group attached to the metal atom. The presence of a single medium band in

the region 3250–3330 cm^{-1} in the complexes may be assigned to N–H stretching vibrations.[16,17] It was noted that a pair of bands corresponding to ν(NH_2) at 3245 and 3309 cm^{-1} were present in the spectra of the thiocarbohydrazide. The value of the ν(C=N) stretching vibration was found at a lower frequency (1520–1560 cm^{-1}) than the expected value (1580–1650 cm^{-1}). This may be explained based on a drift of the lone pair density of the azomethine nitrogen towards the metal atom,[18,19] indicating that coordination occurred through the nitrogen of the (C=N) groups. The bands present in the range 3020–3040 cm^{-1} may be assigned to (C–H) stretching vibrations of the benzil and naphthalene rings.[20] The C–N stretching was in the range 1000–1300 cm^{-1}. The band near 780 cm^{-1} in thiocarbohydrazide may be assigned to free ν(C=S). This band is also present in the spectra of all the complexes, which indicates that sulphur is not coordinating to the metal atom.[21,22] The band at 3292–3438 cm^{-1} is due to the presence of –OH groups in the complexes. The far IR spectra of the complexes show bands in the region 420–450 cm^{-1}, corresponding to ν(M–N) vibrations,[23–24] which identifies coordination of the azomethine nitrogen.[25] The bands present at 290–310 cm^{-1} may be assigned to ν(M–Cl) vibrations.[26,27]

TABLE II. IR spectral bands position (cm^{-1}) and electronic spectral data in DMSO (cm^{-1}) of the Schiff base ligand and its metal complexes

Compd.	ν (NH_2)	ν (C=N)	ν (C=S)	ν (M–Cl)	ν (M–N)	–OH str.	–OH ben.	UV–Vis maxima, cm^{-1} (extinction coefficients, $m^3\ mol^{-1}\ cm^{-1}$)
Ligand (HL)	3250	1560	740	295	410	3327	1350	27027 (35.8)
Cr complex	3280	1530	760	310	400	3292	1352	8950–9300 (24.5, 8.20)
Mn complex	3260	1560	730	290	440	3375	1380	22200–22575 (32.4, 12.6)
Fe complex	3310	1520	780	397	450	3438	1332	9540–9830 (18.3, 8.9)

The FAB mass spectra of the ligand and the Cr (III), Mn (III) and Fe (III) complexes were recorded. All the spectra exhibited parent peaks due to molecular ions (M^+). The proposed molecular formula of these complexes was confirmed by comparing their molecular formula weights with the *m*/*z* values. The molecular ion peaks obtained were as follows: *m*/*z* 506 (ligand), 558 (Cr(III) complex), 562 (Mn(III) complex) and 561 (Fe(III) complex). These data are in good agreement with the proposed molecular formula for these complexes, *i.e.*, $[M(C_{19}H_{24}N_6O_2S)X]X_2$, where M = Cr(III), Mn(III) and Fe(III), and X = = Cl^-. In addition to the peaks due to the molecular ions, the spectra exhibited peaks assignable to various fragments arising from the thermal cleavage of the complexes. The peak intensity suggested the stability of the fragments.

The electronic spectra of the Schiff base and its complexes were recorded in DMSO. The absorption spectra of free ligand consisted of an intense band centered at 370 nm (27027 cm^{-1}), attributed to the n → π* transition of the thioxo group. Another intense band in the higher energy region of the spectra of the free ligand was related to the n → π* transition of the benzene rings.[22]

Magnetic moment of the Cr(III) complex was 4.35 μ_B at room temperature, which is close to the predicted value for three unpaired electrons in the metal ion.[28] The electronic spectrum of the Cr(III) complex showed bands in the range 8950–9310 cm^{-1}. The spectral bands are consistent with that of a five-coordinated Cr(III) complex, the structure of which was confirmed by X-ray diffraction measurements.[29] Based on the analytical data, spectral studies and electrolytic nature of the complex, a square-pyramidal geometry may be assigned for this complex.[30] The electronic spectral bands may be assigned as: $^4B_1 \rightarrow {}^4E^a$, $^4B_1 \rightarrow$ $\rightarrow {}^4B_2$, $^4B_1 \rightarrow {}^4A_1$ and $^4B_1 \rightarrow {}^4E^b$.

The magnetic moment of the Mn(III) complex was 4.85 μ_B, which indicates a high spin d^4 system.[28] The electronic spectra of the manganese complex show three d–d bands, which lay in the range 12250–12590 cm^{-1} and may be assigned to charge transfer transitions. The spectrum resembles those reported for five coordinated, square pyramidal Mn(III) complexes.[30] This is further supported by the presence of a broad ligand field band at 20400 cm^{-1}. The various bands may be assigned as follows: $^5B_1 \rightarrow {}^5A_1$, $^5B_1 \rightarrow {}^5B_2$ and $^4B_1 \rightarrow {}^5E$. The band assignments in single electron transitions may be made as: $d_{z^2} \rightarrow d_{x^2-y^2}$, $d_{xy} \rightarrow d_{x^2-y^2}$ and d_{xy}, $d_{yz} \rightarrow d_{x^2-y^2}$, respectively, in order of increasing energy. However, the complex did not have idealized C_{4V} symmetry.

The magnetic moment of the Fe (III) complex was 5.78 μ_B, corresponding to five unpaired electrons and is close to the predicted high spin values for this metal ion.[28] The electronic spectra of the Fe (III) complex showed various bands in the range 9820–9970 cm^{-1}, which are consistent with the range of spectral bands reported for five coordinate square pyramidal Fe(III) complex.[31] The various bands can be assigned as: $d_{xy} \rightarrow d_{xz}$, d_{yz} and $d_{xy} \rightarrow d_{z^2}$. Any attempt to make accurate assignment was difficult due to the interactions of the metal–ligand π-bond systems lifting the degeneracy of the d_{xz} and d_{yz} pair.

Based on the various characterisation results, the structure shown in Scheme 2 may be proposed for all the complexes.

The antimicrobial results, Table III, showed that HL (ligand) exhibited moderate activity against all the tested bacteria and *C. albicans* fungus. HL showed high antifungal activity against *K. fragilis* and *T. reesei* but no activity against *R. rubra*. The Cr(III) complex showed high antibacterial and antifungal activity against *B. megaterium*, *K. fragilis*, *R. rubra* and *C. albicans*, moderate activity against *E. coli*, *S. aureus* and *P. aeruginosa*, but no activity against *T. reesei*. The Mn(III) complex exhibited moderate activity against *P. aeruginosa* and *B. megaterium*,

was highly effective against *K. fragilis*, *C. albicans* and *T. reesei*, but showed no activity against *E. coli*, *S. aureus* and *R. rubra*. The Fe(III) complex exhibited moderate activity against *S. aureus*, *P. aeruginosa*, *B. megaterium* and *T. reesei*, had a higher effect against *K. fragilis* and *C. albicans*, but no activity against *E. coli* and *R. rubra* microorganisms.

TABLE III. Antibacterial and antifungal activity of the standards, solvent, ligand and its metal complexes

Cmpd.	Inhibition zone, mm							
	E. coli	*S. aureus*	*P. aeruginosa*	*B. megaterium*	*K. fragilis*	*R. rubra*	*C. albicans*	*T. reesei*
Ligand (HL)	7	7	7	8	12	0	9	14
Cr complex	9	8	7	16	18	16	12	0
Mn complex	0	0	9	7	10	0	15	12
Fe complex	0	8	9	7	15	0	12	7
Ciprofloxacin	24	20	22	24	–	–	–	–
Griseofulvin	–	–	–	–	24	24	24	23
DMSO (control)	0	0	0	0	0		0	0

Antibacterial and antifungal activities of the ligand and its metal complexes were compared with those of the standard drugs ciprofloxacin and griseofulvin. The variation in the activity of different metal complexes against different microorganisms depends on the impermeability of the cell or differences in the ribosomes in the microbial cells.[32] The lipid membrane surrounding the cell favours the passage of any lipid soluble materials and it is known that liposolubility is an important factor controlling antimicrobial activity.[33,34]

In the present study, the low activity of the metal complexes may be due to their low lipophilicity, because of which penetration of the complex through the lipid membrane was decreased and hence, they could neither block nor inhibit the growth of the microorganisms.

CONCLUSIONS

The analytical data showed the presence of one metal ion per ligand molecule and suggested a mononuclear structure for the complexes $[M(C_{19}H_{24}N_6O_2S)X]X_2$. The electronic spectral data is in favour of a square pyramidal geometry of the complexes. The ligand and its Cr(III), Mn(III) and Fe(III) complexes were tested for antimicrobial activity against some pathogens. All the complexes were found to be less active against the bacteria *E. coli*, *S. aureus* and *P. aeruginosa*, whereas the Cr(III) complex showed the best antimicrobial activity against the bacterium *B. megaterium* and the fungi *K. fragilis* and *R.. rubra*. The free ligand ($C_{19}H_{24}N_6O_2S$) was found to be active against the fungus *T. reesei*.

Acknowledgements. The authors express their sincere thank to the head of the Department of Chemistry, the principal and college managing board of the Meerut College, Meerut, India, for their encouragement and providing the research facilities and to CDRI Lucknow and IIT Roorkee for providing the mass, electronic and IR spectral data.

ИЗВОД

СИНТЕЗА, ФИЗИЧКА КАРАКТЕРИЗАЦИЈА И АНТИМИКРОБНА АКТИВНОСТ ТРОВАЛЕНТНИХ МЕТАЛНИХ КОМПЛЕКСА СА ШИФОВИМ БАЗАМА

GAJENDRA KUMAR[1], DHARMENDRA KUMAR[2], C.P. SINGH[2], AMIT KUMAR[1] и V. B. RANA[1]

[1]*Department of Chemistry Meerut College, Meerut, (UP) 250001 u* [2]*Department of Chemistry, Sahu Jain College, Najibabad, (UP) 246763, India*

Синтетисани су M(III) комплекси Cr, Mn и Fe са Шифовим базама изведеним из 2-амино-4-етил-5-хидроксибензалдехида и тиокарбохидразида и окарактерисани помоћу неколико техника коришћењем елементалне анализе (C, H, N), моларне проводљивости, магнетним мерењима, електронским, масеним и IR спектралним проучавањима. На основу тога за ове комплексе је предложена пето-координациона квадратно-пирамидална геометрија и нађено да су потенцијални антимикробни агенси. Лиганд Шифове базе и комплекси су такође тестирани према бактеријама *Escherichia coli*, *Staphylococcus aureus*, *Pseudomonas aeruginosa* и *Bacillus megaterium*, и гљивицама *Kluyveromyces fragilis*, *Rhodotorula rubra*, *Candida albicans* и *Trichoderma reesei* да би се утврдила њихова инхибиторска моћ. Такође је покушано да се доведе у везу биолошка активност са геометријом комплекса. Нађено је да су сви комплекси били мање активни према патогенима *E. coli*, *S. aureus* и *P. aeruginosa*, док је Cr(III) комплекс био најактивнији, а сам слободни лиганд је показао активност према гљивици *T. reesei*.

(Примљено 19. јуна, ревидирано 16. новембра 2009)

REFERENCES

1. H. A. El-Borae, *J. Therm. Anal. Calorim.* **81** (2005) 339
2. Z. M. Zaki, S. S. Haggag, A. A. Sayed, *Spectrosc. Lett.* **31** (1998) 757
3. A. S. M. Al-Shiri, H. M. Abdel-Fattah, *J. Therm. Anal. Calorim.* **71** (2003) 643
4. A. V. Kurnoskin, *J. Macromol. Sci., Rev. Macromol. Chem. Phys.* **C36** (1996) 457
5. A. V. Kurnoskin, *Polym. Compos.* **14** (1993) 481
6. A. V. Kurnoskin, *Polymer* **34** (1993) 1060
7. A. V. Kurnoskin, *Ind. Eng. Chem. Res.* **31** (1992) 524
8. E. Canpolat, M. Kaya, *J. Coord. Chem.* **57** (2004) 1217
9. A. A. Maihub, M. M. El-Ajaily, S. M. Filog, *Asian J. Chem.* **17** (2005)
10. E. A. Elzahany, K. H. Hegab, S. K. H. Khalil, N. S. Youssef, *Aust. J. Basic Appl. Sci.* **2** (2008) 210
11. F. M. Morad, M. M. El-Ajaily, S. Ben Gweirif, *J. Sci. Appl.* **1** (2007) 72
12. R. Rajave, M. S. Vadivu, C. Anitha, *E-J. Chem.* **5** (2008) 620
13. I. Ahmad, A. J. Beg, *J. Ethnopharmacol.* **74** (2001) 113
14. J. M. Andrews, *J. Antimicrob. Chemother.* **48** (2001) 5
15. R. Kumar, R. Singh, *Turk. J. Chem.* **30** (2006) 77
16. G. A. Bain, D. X. West, J. Krejci, J. V. Martinez, S. H. Ortega R. A. Toscano, *Polyhedron* **16** (1997) 855

17. S. Chandra, S. D. Sharma, *Transition Met. Chem*. **27** (2002) 732
18. C. Lodeiro, R. Basitida, E. Bertolo, A. Macias, R. Rodriguez, *Transition Met. Chem*. **28** (2003) 388
19. D. P. Singh, R. Kumar, V. Malik, P. Tyagi, *Transition Met. Chem*. **32** (2007) 1051
20. O. V. Mikhailov, M. R. Kazymova, T. A. Shumilova, S. S. Solovieva, *Transition Met. Chem.* **20** (2004) 732
21. S. Chandra, S. Thakur, *Transition Met. Chem*. **29** (2004) 925
22. M. Shakir, O. S. M. Nasman, S. P. Varkey, *Polyhedron* **15** (1996) 309
23. M. Shakir, K. S. Islam, A. K. Mohamed, M. Shagufa, S. S. Hasan, *Transition Met. Chem.* **24** (1999) 577
24. S. Chandra, R. Kumar, *Transition Met. Chem*. **29** (2004) 269
25. V. B. Rana, D. P. Singh, P. Singh, M. P. Teotia, *Transition Met. Chem*. **7** (1982) 174
26. M. Shakir, K. S. Islam, A. K. Mohamed, N. Jahn, *Transition Met. Chem*. **22** (1997) 189
27. T. A. Khan, S. S. Hasan, S. P. Varkey, M. A. Rather, N. Jahan, M. Shakir, *Transition Met. Chem*. **22** (1997) 4
28. B. N. Figgis, J. Lewis, *Prog. Inorg. Chem.* **6** (1965) 37
29. J. S. Wood, *Prog. Inorg. Chem.* **16** (1972) 227
30. D. P. Singh, V. B. Rana, *Polyhedron* **14** (1995) 2901
31. A. B. P. Lever, *Inorganic Electronic Spectroscopy,* 2nd Ed., Elsevier, Amsterdam, 1984.
32. S. K. Sengupta, O. P. Pandey, B. K. Srivastava, V. K. Sharma, *Transition Met. Chem*. **23** (1998) 349
33. J. Parekh, P. Inamdhar, R. Nair, S. Baluja, S. Chandra, *J. Serb. Chem. Soc*. **70** (2005) 116
34. Y. Vaghasia, R. Nair, M. Soni, S. Baluja, S. Chandra, *J. Serb. Chem. Soc*. **69** (2004) 991.

Journal of the Serbian Chemical Society
JSCS@tmf.bg.ac.rs • www.shd.org.rs/JSCS

J. Serb. Chem. Soc. 75 (5) 639–648 (2010)
JSCS–3994

UDC 547.53'788+547.235:546.562'742'472
Original scientific paper

Benzothiazolylazo derivatives of some *β*-dicarbonyl compounds and their Cu(II), Ni(II) and Zn(II) complexes

KRISHNANNAIR KRISHNANKUTTY[1], MUHAMMED BASHEER UMMATHUR[2]* and DAMODARAN KAMALAKSHY BABU[3]

[1]*Department of Chemistry, University of Calicut, Kerala-673635,* [2]*Department of Chemistry, Unity Women's College, Manjeri, Kerala-676122 and* [3]*Department of Chemistry, Zamorin's Guruvayurappan College, Calicut, Kerala-673014, India*

(Received 16 August, revised 4 December 2009)

Abstract: The coupling of diazotized 2-aminobenzothiazole with 1,3-dicarbonyl compounds (benzoylacetone, methyl acetoacetate and acetoacetanilide) yielded a new series of tridentate ligand systems (HL). Analytical, IR, ^{1}H--NMR, ^{13}C-NMR and mass spectral data indicated that the compounds exist in the intramolecularly hydrogen bonded azo-enol tautomeric form in which one of the carbonyl groups of the dicarbonyl moiety had enolised and hydrogen bonded to one of the azo nitrogen atoms. The compounds formed stable complexes with Ni(II), Cu(II) and Zn(II) ions. The Cu(II) complexes conform to [CuL(OAc)] stoichiometry while the Ni(II) and Zn(II) complexes are in agreement with [ML_2] stoichiometry. Analytical, IR, ^{1}H-NMR, ^{13}C-NMR and mass spectral data of the complexes are consistent with the replacement of the chelated enol proton of the ligand with a metal ion, thus leading to a stable six--membered chelate ring involving a cyclic nitrogen, one of the azo nitrogens and the enolate oxygen. The Zn(II) chelates are diamagnetic while Cu(II) and Ni(II) complexes showed a normal paramagnetic moment.

Keywords: benzothiazolylazo-*β*-dicarbonyls; azo-enol form; Cu(II), Ni(II) and Zn(II) complexes; IR, mass and NMR spectral studies.

INTRODUCTION

The chemistry of 2-aminobenzothiazole has gained increasing interest in both synthetic organic chemistry and biological fields.[1] The substitution of an aryl diazonium group at the active methylenic carbon provides for the possibility of azo-hydrazone tautomerism.[2] In recent years, a significant number of tridentate azo compounds containing heteroaryl ring systems have been developed in order to improve the colouring properties and to achieve more specificity and selectivity in chemical analysis.[3] Metal dye complexes play a very important role in dye-

* Corresponding author. E-mail: mbummathur@gmail.com
doi: 10.2298/JSC090816040K

stuff technology[4] and find application in many other fields, especially in analytical chemistry.[5] However, structural aspect of many of these products and their metal derivatives have received only scanty attention. In continuation of studies on arylazo[6–11] derivatives of *β*-dicarbonyl compounds and their metal complexes, the synthesis and characterization of benzothiazolylazo derivatives of three *β*-dicarbonyl compounds: benzoylacetone, methyl acetoacetate and acetoacetanilide, are reported herein. Typical Cu(II), Ni(II) and Zn(II) complexes of these compounds were also synthesized and characterized.

EXPERIMENTAL

Methods, instruments and materials

Carbon, hydrogen and nitrogen contents were determined by microanalyses (Heraeus elemental analyzer from RSIC, Central Drug Research Institute, Lucknow, India, and Catalysis division, Department of Chemistry, Indian Institute of Technology, Chennai, India) and the metal contents of the complexes by AAS (Perkin Elmer 2380 spectrometer). The electronic spectra of the compounds in methanol (10^{-4} mol/L) were recorded on a 1601 Shimadzu UV–Vis. spectrophotometer, the IR spectra (KBr discs) on an 8101 Shimadzu FTIR spectrophotometer, the ^{1}H-NMR spectra ($CDCl_3$ or DMSO-d_6) on a Varian 300 NMR spectrometer and the mass spectra on a Jeol/SX-102 mass spectrometer (FAB using argon and *meta*--nitrobenzyl alcohol as the matrix). The molar conductance of the complexes was determined in DMF (≈10^{-3} mol/L) at room temperature (301±1 K). The magnetic susceptibilities were determined at room temperature on a Guoy type magnetic balance, Sherwood Scientific Ltd., England, at room temperature using $Hg[Co(NCS)_4]$ as the standard.

Benzoylacetone, methyl acetoacetate, acetoacetanilide, 2-aminobenzothiazole, methanol, urea and the metal acetates were of AR grade, purchased from Merck, Germany.

General procedure for the preparation of benzothiazolylazo derivatives of β-dicarbonyl compounds

An aqueous solution of 2-benzothiazolediazonium ion was prepared by a standard method.[12] To a solution of $NaNO_2$ (1.4 g) in H_2SO_4 (12 M, 20 mL), kept below 278 K, a cooled (≈278 K) solution of 2-aminobenzothiazole (1.5 g, 0.010 mol) in 15 mL DMF was added slowly under stirring. The stirring was continued for ≈1 h, after which the reaction mixture was filtered to obtain a clear yellow diazonium salt solution. After destroying the excess nitrous acid with urea, the diazonium salt solution (0.010 mol) was added slowly under stirring to an ice-cold (< 278 K) solution of the required *β*-dicarbonyl compound (benzoylacetone, methyl acetoacetate or acetoacetanilide, 0.010 mol in 25 mL ethanol). Cooled (< 278 K) NaOH solution (1.0 M, 20 mL) was added dropwise to maintain the pH of the mixture at around 5. Stirring was continued for about 30 min and the precipitated compound was filtered, washed several times with deionised water and recrystallized twice from hot methanol to obtain chromatographically pure material: 2-(2-benzothiazolylazo)-1-phenyl-1,3-butanedione (Hbba), methyl 2-(2-benzothiazolyazo)-3-oxobutanoate (Hbma) and 2-(2-benzothiazolylazo)--3-oxo-*N*-phenylbutanamide (Hban) (TLC on silica gel, acetone as the solvent). All the compounds were crystalline in nature with a reddish pink colour and were soluble in common polar and non-polar organic solvents, such as benzene, methanol, ethanol, chloroform and carbon tetrachloride. The compounds formed stable complexes with Ni(II), Cu(II) and Zn(II) ions.

Synthesis of the Ni(II), Cu(II) and Zn(II) complexes

A concentrated aqueous solution of metal(II) acetate (0.010 mol) was added under stirring to a methanolic solution of one of the ligands (0.020 mol, 20 mL). Stirring was continued for the following ≈2 h. The precipitated complex was filtered, washed with water, recrystallized from hot chloroform and dried under vacuum. The Ni(II), Cu(II) and Zn(II) complexes had a greenish black, dark violet and dull white colour, respectively. The complexes were well soluble in CH_3CN, DMSO and DMF but insoluble in methanol, ethanol, carbon tetrachloride and water.

Determination of magnetic susceptibility

A thin cylindrical glass tube filled with the sample was vertically suspended from the beam of a balance in a draught-free enclosure in such a way that its lower end lied between the poles of an electromagnet. The weight of the sample was determined with the field off and with the field on. Corrections for diamagnetism of the constituents were made using Pascal constants.[13] The effective magnetic moments were calculated using the formula μ_{eff} = = $2.83(\chi_M T)^{1/2}(9.274\times10^{-24})$ A m^2, where χ_M is the corrected molar susceptibility and T is temperature. The Zn(II) chelates were diamagnetic while the Cu(II) and Ni(II) complexes showed a normal paramagnetic moment.

RESULTS AND DISCUSSION

The observed elemental analytical data of the benzothiazolylazo derivatives (Table I) indicate that the diazo-coupling reaction between the diazotized 2-aminobenzothiazole and the β-dicarbonyl compounds occurred in the 1:1 mole ratio. The analytical data (Table I) together with non-electrolytic nature in DMF (specific conductance < 10 S cm^{-1}; 10^{-3} M solution) suggested the formula $[ML_2]$ for the complexes where M(II) = Zn and Ni, and [CuL(OAc)] for the Cu(II) complexes.

TABLE I. Physical and analytical data of the new benzothiazolylazo derivatives of β-dicarbonyl ligands and their metal complexes (Hbba: 2-(2-benzothiazolylazo)-1-phenyl-1,3-butanedione; Hbma: methyl 2-(2-benzothiazolylazo)-3-oxobutanoate; Hban: 2-(2-benzothiazolylazo)-3-oxo-*N*-phenylbutanamide; –OAc: acetate)

Compound	Yield	M.p.	$\mu_{eff}\times10^{24}$	Found (Calcd.), %			
Empirical formula	%	°C	A m^2	C	H	N	M
Hbba	60	180	–	63.10	3.98	12.98	–
$C_{17}H_{13}N_3SO_2$				(63.16)	(4.02)	(13.00)	
Hbma	70	98	–	51.88	3.99	15.05	–
$C_{12}H_{11}N_3SO_3$				(51.99)	(3.97)	(15.16)	
Hban	70	182	–	60.23	4.14	16.64	–
$C_{17}H_{14}N_4SO_2$				(60.36)	(4.14)	(16.57)	
$[Ni(bba)_2]$	60	170	25.8	58.20	3.48	11.98	8.50
$C_{34}H_{24}N_6NiS_2O_4$				(58.06)	(3.42)	(11.95)	(8.35)
$[Ni(bma)_2]$	65	>300	25.9	47.30	3.30	13.65	9.54
$C_{24}H_{20}N_6NiS_2O_6$				(47.16)	(3.27)	(13.75)	(9.61)
$[Ni(ban)_2]$	70	270	26.1	55.53	3.54	15.24	8.02
$C_{34}H_{26}N_8NiS_2O_4$				(55.68)	(3.55)	(15.29)	(8.01)

TABLE I. Continued

Compound Empirical formula	Yield %	M.p. °C	$\mu_{eff}\times10^{24}$ A m^2	Found (Calcd.)/ % C	H	N	M
[Cu(bba)(OAc)]	65	220	16.2	51.40	3.34	9.36	14.19
$C_{19}H_{15}CuN_3SO_4$				(51.29)	(3.37)	(9.45)	(14.29)
[Cu(bma)(OAc)]	65	>300	16.5	42.26	3.23	10.70	15.85
$C_{14}H_{13}CuN_3SO_5$				(42.15)	(3.26)	(10.54)	(15.94)
[Cu(ban)(OAc)]	72	>300	16.8	49.55	3.45	12.28	13.75
$C_{19}H_{16}CuN_4SO_4$				(49.61)	(3.48)	(12.19)	(13.83)
[Zn(bba)$_2$]	68	208	–	57.58	3.38	11.80	9.35
$C_{34}H_{24}N_6S_2O_4Zn$				(57.52)	(3.38)	(11.84)	(9.22)
[Zn(bma)$_2$]	72	>300	–	46.56	3.23	13.63	10.72
$C_{24}H_{20}N_6S_2O_6Zn$				(46.65)	(3.24)	(13.61)	(10.59)
[Zn(ban)$_2$]	68	225	–	55.28	3.53	15.03	8.75
$C_{34}H_{26}N_8S_2O_4Zn$				(55.18)	(3.52)	(15.15)	(8.84)

IR Spectra

The IR spectra of the benzothiazolylazo derivatives show a strong band at ≈1640 cm^{-1}, assignable to the stretching of the enolised acetyl carbonyl group[8] (Fig. 1). The free benzoyl, ester and anilide carbonyl bands of Hbba, Hbma and Hban were observed at 1650, 1738 and 1670 cm^{-1}, respectively.[14,15] In the spectra of all the compounds, two medium intensity bands were observed at ≈1280 and 1470 cm^{-1}, assignable to C–O–H in-plane bending and ν(N=N), respectively.[14,15] The aromatic ν(C=C) vibrations appeared at ≈1580 cm^{-1} and benzothiazole ring ν(C=N) was observed at ≈1620 cm^{-1}. The broad band in the range 2500–3300 cm^{-1} indicates the existence of strong intramolecular hydrogen bonding in these compounds. Thus, the IR spectra strongly support the existence of the compounds in the intramolecularly hydrogen-bonded azo-enol tautomeric form.

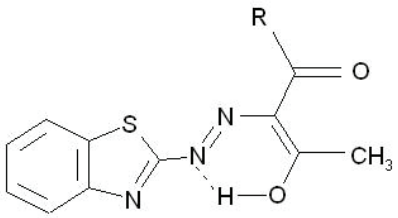

Fig. 1. Schematic view representing the geometry of the prepared benzothiazolylazo derivatives, where R = C_6H_5 (Hbba); OCH_3 (Hbma); NHC_6H_5 (Hban).

In the IR spectra of all the complexes, the broad free ligand band in the region 2500–3300 cm^{-1} had disappeared, indicating the replacement of the enol proton by a metal ion during complexation.[7,8] Several medium intensity bands were present in this region of the spectra due to various ν(C–H) vibrations. The absence of the free ligand band at ≈1270 cm^{-1} due to C–O–H bending also supports the replacement of the enol proton by a metal ion. The free carbonyl band of the compounds was only marginally shifted indicating that this carbonyl is not

involved in the coordination. However, the band due to the hydrogen bonded acetyl carbonyl group disappeared and instead a new band appeared at ≈1570 cm^{-1} in the spectra of all the complexes, supporting the involvement of the enolised carbonyl in the bonding with the metal ion.[16] In the spectra of all the complexes, the band at ≈1470 cm^{-1} due to ν(N=N) and the band due to benzothiazole ν(C=N) at ≈1620 cm^{-1} of the ligands were appreciably shifted (20–30 cm^{-1}) to lower wave numbers, indicating the involvement of these groups in the bonding with the metal ion, as shown in Figs. 2 and 3.

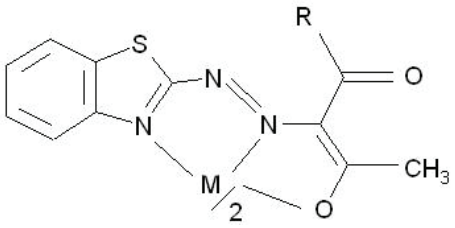

Fig. 2. Schematic view representing the proposed geometry of the metal complexes of the benzothiazolylazo derivatives within 1/2 molecules.

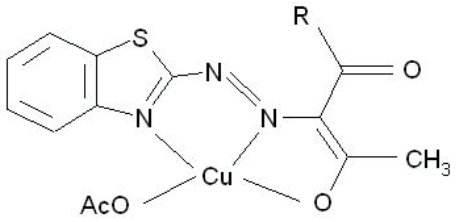

Fig. 3. Schematic view representing the proposed coordination in the Cu(II) complexes of the benzothiazolylazo derivatives.

As in the spectrum of the ligand, the complexes of Hban showed a band at ≈3400 cm^{-1} due to the NH group of anilide. In the spectra of the Cu(II) complexes, a comparatively strong band at ≈1625 cm^{-1} and a medium intensity band at ≈1310 cm^{-1} appeared due to the antisymmetric and symmetric stretching of the monodentate acetate group, respectively,[16,17] as in Fig. 3. The presence of new medium intensity bands in the 420–490 and 530–560 cm^{-1} regions, assignable to ν(M–O) and ν(M–N) in the spectra of all the complexes[16] also support Figs. 2 and 3. Important bands that appeared in the spectra are given in Table II.

NMR Spectra

The ^{1}H-NMR spectra of the benzothiazolylazo derivatives are characterized by the presence of a low field, one proton signal at δ 13 ppm, which is considerably lower than that reported for arylazo derivatives of β-diketones that exist in the hydrazone form.[9–11] Since azo-enol protons show a signal in the δ range 10–14 ppm, the signal at δ 13 ppm can be assigned to the intramolecularly hydrogen bonded enol proton of Fig. 1.[8,9,18] The integrated intensities of all other protons agree well with the structure of the compounds presented in Fig. 1. In the ^{1}H-NMR spectra of the diamagnetic Zn(II) complexes, the low field signal due to the chelated hydrogen disappeared, indicating its replacement by the metal ion during complexation.[8,19] The non-involvement of the ester carbonyl and the anilide NH groups in the coordination is evident from the observed position of the

OCH_3 and anilide NH resonance signals, which remain unaltered. The position of the signal of the methyl proton in the chelates is downfield shifted, indicating the involvement of the acetyl carbonyl in the coordination. The integrated intensities of all other protons agree well with the structure of the complexes presented in Fig. 2. The assignments of the various proton signals observed are assembled in Table III.

TABLE II. Characteristic IR stretching bands (cm^{-1}) of the ligands and their metal complexes (abbreviations as in Table I)

Compound	Free ν(C=O)	Chelated ν(C=O)	Acetate ν(C=O) and ν(C–O)	ν(C=N)	ν(N=N)	ν(M–N)	ν(M–O)
Hbba	1650	1640	–	1615	1468	–	–
$[Ni(bba)_2]$	1648	1572	–	1590	1440	548	420, 470
[Cu(bba)(OAc)]	1645	1566	1622, 1305	1593	1444	540	428, 490
$[Zn(bba)_2]$	1652	1570	–	1588	1446	548	420, 478
Hbma	1738	1644	–	1618	1460	–	–
$[Ni(bma)_2]$	1737	1574	–	1589	1435	555	430, 468
[Cu(bma)(OAc)]	1735	1566	1622, 1300	1590	1436	540	420, 485
$[Zn(bma)_2]$	1734	1568	–	1594	1438	540	420, 466
Hban	1670	1638	–	1615	1460	–	–
$[Ni(ban)_2]$	1665	1565	–	1590	1438	538	435, 488
[Cu(ban)(OAc)]	1666	1562	1620, 1305	1588	1440	545	422, 480
$[Zn(ban)_2]$	1668	1574	–	1592	1435	550	428, 477

TABLE III. ^{1}H-NMR spectral data (δ/ ppm) of the ligands and their Zn(II) complexes (abbreviations as in Table I)

Compound	OH	CH_3	R	Benzothiazolyl
Hbba	12.80 (1H, *s*, *br*)	2.61 (3H, *s*)	6.80–8.07 (9H, *m*)	
$[Zn(bba)_2]$	–	2.88 (6H, *s*)	6.98–8.02 (18H, *m*)	
Hbma	12.52 (1H, *s*, *br*)	2.45 (3H, *s*)	3.82 (3H, *s*)	6.90–7.50 (4H, *m*)
$[Zn(bma)_2]$	–	2.82 (6H, *s*)	3.85 (6H, *s*)	7.10–7.60 (8H, *m*)
Hban	12.99 (1H, *s*, *br*)	2.59 (3H, *s*)	7.15–7.81 (9H, *m*), 11.20 (1H, *s*, anilide NH)	
$[Zn(ban)_2]$	–	2.85 (6H, *s*)	7.20–8.01 (18H, *m*), 11.16 (2H, *s*, anilide NH)	

The ^{13}C-NMR spectrum of Hbma clearly indicates its existence in the azo--enol form. That the two carbonyl groups are in different electronic environments is evident from the large separation of the carbonyl carbon signals. The comparatively large chemical shift of the methyl carbon signal in the spectrum indicates the enolised nature of the acetyl group and its involvement in hydrogen bonding.[8] The involvement of the enolate oxygen and hetero nitrogen atoms in the bonding with the metal ion is evident from the position of the various signals in the ^{13}C--NMR spectrum of its Zn(II) complex (Table IV).

TABLE IV. ^{13}C-NMR spectral data (δ / ppm) of Hbma and its Zn(II) complex (abbreviations as in Table I)

Compound	C=O	CH_3	C–N	Benzothiazolyl
Hbma	196.7, 198.3	26.5, 30.8	165.3	121.7, 122.4, 124.9, 126.9, 132.1, 135.5, 141.7
$[Zn(bma)_2]$	195.7, 196.6	28.2, 33.1	147.2	118.9, 122.0, 124.0, 125.8, 126.6, 127.5, 131.5

Mass spectra

The formulation of the benzothiazolylazo derivatives as shown in Fig. 1 is clearly supported from the presence of an intense molecular ion peak in the mass spectra. The presence of peaks due to the elimination of ArN_2 from molecular ion, characteristic of tautomers,[9,20,21] in the spectra support the azo structure of the compounds. Fragments due to the elimination of RCO and CH_3CO are also present in the spectra of all the ligands. The origin of the peak at *m/z* 175 in the mass spectra of the compounds can be explained by the formation of the ion radical $BT–N_2CH]^+$ (BT = benzothiazole ring) through the elimination of CH_3CO and RCO from P^+. If the compounds existed in the hydrazone form, the most facile reaction would be the cleavage of the N–N bond[21] and an ion of *m/z* 175 could not be formed. Thus, all available evidences support the existence of the compounds in the azo-enol form rather than the keto-hydrazone form. The FAB mass spectra of the Cu(II) complexes showed molecular ion peaks corresponding to [CuL(OAc)] stoichiometry. Peaks corresponding to $[P–RCO]^+$, $[P–CH_3CO]^+$, $[RCO]^+$, $[CH_3CO]^+$, $[CuL]^+$, L^+ and fragments of L^+ were also present in the spectra. The spectra also showed peaks due to $[P–CH_3COO]^+$. The spectra of all the chelates contained a number of fragments containing copper in the 3:1 natural abundance of ^{63}Cu and ^{65}Cu isotopes (Table V).

TABLE V. Mass spectral data of the new ligands and their Cu(II) complexes (abbreviations as in Table I)

Compound	Mass spectral data (*m/z*)
Hbba	323, 280, 218, 175, 162, 161, 134, 105, 43
Hbma	277, 234, 218, 175, 162, 134, 115, 59, 43
Hban	338, 295, 218, 176, 175, 162, 134, 120, 43
[Cu(bba)(OAc)]	446, 444, 403, 401, 387, 385, 344, 342, 341, 339, 323, 280, 239, 237, 175, 162, 105
[Cu(bma)(OAc)]	400, 398, 341, 339, 357, 355, 282, 280, 277, 239, 237, 175, 162, 134, 115
[Cu(ban)(OAc)]	461, 459, 402, 400, 341, 339, 418, 416, 282, 280, 239, 237, 338, 295, 176, 175, 162, 120

Electronic spectral and magnetic measurements data

The UV spectra of the benzothiazolylazo derivatives show two broad bands with maxima at ≈380 nm and ≈270 nm due to various n → π* and π → π* transitions. The absorption maxima of the metal chelates bore close resemblance with those of the free ligands, which indicates that no structural alteration to the ligand had occurred during complexation. However, the values were shifted to slightly longer wavelength in the spectra of the metal complexes,[22] indicating the involvement of the carbonyl and azo groups in metal complexation. In the Cu(II) complexes, the presence of a broad visible band at ≈15,000 cm^{-1} (log ε ≈ ≈ 0.73) and the measured μ_{eff} values (Table I) support a square-planar structure.[23] The Ni(II) chelates showed three well-separated absorption bands in the spectra at λ_{max} ≈ 8100 (log ε = 0.67–0.72), ≈13200 (log ε = 0.69–0.84) and ≈24200 cm^{-1} (log ε = 0.77–0.82), corresponding to the transitions: $^3A_{2g} \rightarrow {}^3T_{2g}$; $^3A_{2g} \rightarrow {}^3T_{1g}(F)$ and $^3A_{2g} \rightarrow {}^3T_{1g}(P)$, respectively.[24] These, together with their measured μ_{eff} values (Table I), support the octahedral structure.

Thus, the observed analytical, IR, ^{1}H-NMR, ^{13}C-NMR and mass spectral data are in conformity with the structures given in Fig. 1 for the benzothiazolylazo derivatives and in Fig. 2 for their Ni(II) and Zn(II) complexes. The analytical and spectral data of the Cu(II) complexes are in agreement with Fig. 3.

CONCLUSIONS

Three new arylazo derivatives were prepared by coupling 2-benzothiazolediazonium ion with the active methylene group of the *β*-dicarbonyl compounds benzoylacetone, methyl acetoacetate and acetoacetanilide (HL). The analytical and spectral data of the compounds confirmed their existence in the azo-enol form in which one of the carbonyl groups of the dicarbonyl moiety was enolised and hydrogen bonded to one of the azo nitrogens. For the Cu(II) complexes, the formulas [CuL(OAc)] are assumed, while the Ni(II) and Zn(II) complexes are represented with [ML_2]. The analytical and spectral data clearly indicated the monobasic tridentate nature of the compounds and the involvement of the cyclic nitrogen, one of the azo nitrogens and the enolate oxygen in the bonding with the metal ion.

ИЗВОД

БЕНЗОТИОАЗОЛИЛАЗО ДЕРИВАТИ НЕКИХ *β*-ДИКАРБОНИЛ ЈЕДИЊЕЊА И ЊИХОВИХ Cu(II), Ni(II) И Zn(II) КОМПЛЕКСА

KRISHNANNAIR KRISHNANKUTTY[1], MUHAMMED BASHEER UMMATHUR[2] и DAMODARAN KAMALAKSHY BABU[3]

[1]Department of Chemistry, University of Calicut, Kerala-673635, [2]Department of Chemistry, Unity Women's College, Manjeri, Kerala-676122 и [3]Department of Chemistry, Zamorin's Guruvayurappan College, Calicut, Kerala-673014, India

Куповањем диазотованог 2-аминобензотиазола са 1,3-дикарбонилним једињењима (бензоилацетоном, метил-ацетоацетатом и ацетоацетанилидом) добијена је нова серија три-

дентатних лигандних система (HL). Аналитички, IR, ^{1}H-NMR, ^{13}C-NMR и масени спектрални подаци указују да једињења постоје у интрамолекулско водонично везаном азо-енол таутомерном облику у коме је једна од карболилних група у дикарбонилној околини енолизована и водонично везана за један од азо азота. Једињења су градила стабилне комплексе са Ni(II), Cu(II) и Zn(II) јонима. Cu(II) комплексима одговара [CuL(OAc)] стехиометрија, док су Ni(II) и Zn(II) комплекси у складу са [ML_2] стехиометријом. Аналитички, IR, ^{1}H-NMR, ^{13}C-NMR и масени спектрални подаци су у складу са заменом хелатног енолног протона лиганда металним јоном, што доводи до стабилног шесточланог хелатног прстена укључујући циклични азот, један од азо азота и енолатни кисеоник. Zn(II) хелати су дијамагнетични, док су Cu(II) и Ni(II) комплекси имали нормални парамагнетични момент.

(Примљено 16. августа, ревидирано 4. децембра 2009)

REFERENCES

1. a) S. Bondock, W. Fadaly, M. A. Metwally, *J. Sulfur Chem.* **30** (2009) 74; b) Q. Ding, X. He, J. Wu, *J. Comb. Chem.* **11** (2009) 587; c) A. E. Berns, P. Conte, H. Philipp, E. G. Witte, H. Lewandowski, *Vadose Zone J.* **8** (2009) 670; d) M. M. El-ajaily, F. I. El-moshaty, R. S. El-zweay, A. A. Maihub, *Int. J. Chem. Tech. Res.* **1** (2009) 80; e) C. Chorao, F. Charmantray, P. B. Hoggan, M. Sancelme, A. Cincilei, M. Traikia, G. Mailhot, A. M. Delort, *Chemosphere* **75** (2009) 121; f) S. D. Srivastava, J. P. Sen, *Indian J. Chem.* **47B** (2008) 1583
2. a) D. R. Matazo, R. A. Ando, A. C. Borin, P. S. Santos, *J. Phys. Chem. A.* **112** (2008) 4437; b) T. Hihara, Y. Okada, Z. Morita, *Dyes Pigments* **61** (2004) 199; c) T. Hihara, Y. Okada, Z. Morita, *Dyes Pigments* **59** (2003) 25; d) K. H. Saunders, R. L. M. Allen, *Aromatic Diazo compounds*, 3rd ed., Edward Arnold, London, 1985
3. a) T. Yasui, N. Komatsu, K. Egami, H. Yamada, A. Yuchi, *Anal. Sci.* **23** (2007) 1011; b) P. Manashi, D. Chayan, H. Chen-Hsiung, G. Sreebrata, *J. Chem. Sci.* **119** (2007) 3; c) C. Sudipta, S. Anasuya, H. Chen-Hsiung, G. Sreebrata, *Z. Anorg. Allg. Chem.* **663** (2007) 1775; d) C. P. Morley, S. Ford, M. D. Vaira, *Polyhedron* **23** (2004) 2967; e) M. G. B. Drew, B. Vickery, G. R. Willey, *J. Chem. Soc., Perkin Trans. 2.* **10** (1982) 1297
4. a) F. Zaubitzer, T. Riis-Johannessen, K. Severin, *Org. Biomol. Chem.* **7** (2009) 4598; b) X. Wang, L. Feng, *Spectrochim. Acta Part A. Mol. Biomol. Spectrosc.* **71** (2008) 1433; c) K. Venkataraman, *Chemistry of Synthetic Dyes*, Vol. 5, Academic Press, New York, 1977
5. a) M. A. Fox, J. K. Whitesell, D. Magde, L. Zhu, *Molecules* **14** (2009) 3851; b) R. Gup, E. Giziroglu, B. Kirkan, *Dyes Pigments* **73** (2007) 40; c) B. Salih, R. Zenobi, *Anal. Chem.* **70** (1998) 1536; d) R. R. Myers, J. L. Long, *Pigments, Part I*, Marcel Dekker, New York, 1975
6. K. Krishnankutty, M. B. Ummathur, D. K. Babu, *Indian J. Inorg. Chem.* **4** (2009) 83
7. a) K. Krishnankutty, M. B. Ummathur, P. Ummer, *J. Serb. Chem. Soc.***74** (2009) 1273; b) K. Krishnankutty, P. Sayudevi, M. B. Ummathur, *J. Serb. Chem. Soc.* **72** (2007) 1075; c) K. Krishnankutty, M. B. Ummathur, P. Sayudevi, *J. Indian Chem. Soc.* **86** (2009) 325; d) K. Krishnankutty, M. B. Ummathur, P. Sayudevi, *J. Indian Chem. Soc.* **85** (2008) 48; e) K. Krishnankutty, M. B. Ummathur, P. Sayudevi, *J. Indian Chem. Soc.* **84** (2007) 518; f) K. Krishnankutty, M. B. Ummathur, P. Sayudevi, *J. Indian Chem. Soc.* **84** (2007) 337
8. K. Krishnankutty, D. K. Babu, *J. Indian Chem. Soc.* **73** (1996) 379
9. K. Krishnankutty, V. T. Rema, *Synth. React. Inorg. Met.-Org. Chem.* **25** (1995) 243

10. a) K. Krishnankutty, J. Michael, *J. Indian Chem. Soc.* **70** (1993) 238; b) K. Krishnankutty, J. Michael, *J. Coord. Chem.* **28** (1993) 259; c) *ibidum.* **22** (1990) 327
11. K. Krishnankutty, P. Ummer, *J. Indian Chem. Soc.* **66** (1989) 194; b) K. Krishnankutty, P. Ummer, *J. Indian Chem. Soc*. **65** (1988) 213
12. R. C. Elderfield, *Heterocyclic Compounds*, Vol. 1, Wiley, New York, 1950, p. 555
13. E. König, *Magnetic Properties of Coordination and Organometallic Transition Metal Compounds*, Springer-Verlag, Berlin, 1966
14. L. J. Bellamy, *The Infrared Spectra of Complex Molecules*, Chapman and Hall, London, 1980
15. C. N. R. Rao, *Chemical Applications of Infrared Spectroscopy*, Academic Press, London, 1963
16. N. Nakamoto, *Infrared Spectra and Raman Spectra of Inorganic and Coordination Compounds*, 5th ed., Wiley, New York, 1997
17. K. Krishnankutty, M. B. Ummathur, *J. Indian Chem. Soc.* **83 (**2006) 639
18. A. Lycka, J. Jirman, A. Cee, *Magn. Reson. Chem.* **28** (1990) 408
19. a) N. Raman, V. Muthuraj, S. Ravichandran, A. Kulandaisamy, *Proc. Indian Acad. Sci. (Chem. Sci.)* **115** (2003) 161; b) S. Vineeta, G. Rekha, *J. Fluorine Chem.* **76** (1996) 149; c) D. C. Nonhebel, *Tetrahedron* **24** (1968) 1869
20. a) A. Farghaly, Z. A. Abdallah, *Arkivoc* **17** (2008) 295; b) H. Budzikiewicz, C. Djerassi, D. H. Williams, *Mass Spectrometry of Organic Compounds*, Holden Day, San Francisco, CA, 1967
21. a) C. Zhimin, W. Yiqun, G. Donghong, G. Fuxi, *Dyes Pigments* **76** (2008) 624; b) K. Kobayashi, K. Kurishara, K. Hirose, *Bull. Chem. Soc. Jpn.* **45** (1972) 3551
22. a) R. Bahari, M. N. Garif, M. Shamsudheen, *Malaysian J. Anal. Sci.* **12** (2008) 272; b) J. P. Fackler Jr., F. A. Cotton, D. W. Barnum, *Inorg. Chem.* **2** (1963) 97
23. a) K. Ray, T. Weyhermüller, F. Neese, K. Wieghardt, *Inorg. Chem.* **44** (2005) 5345; b) K. C. Joshi, V. N. Pathak, *Coord. Chem. Rev.* **22** (1977) 37
24. a) M. B. Ummathur, K. Krishnankutty, S. Balagopal, *J. Serb. Chem. Soc.* **74** (2009) 259; b) K. Krishnankutty, V. D. John, *Synth. React. Inorg. Met.-Org. Chem.* **33** (2003) 343.

Journal of the Serbian Chemical Society
JSCS@tmf.bg.ac.rs • www.shd.org.rs/JSCS

J. Serb. Chem. Soc. 75 (5) 649–657 (2010)
JSCS–3995

UDC 547.15+547.235'512:541.124
Original scientific paper

A theoretical study of the mechanism of the addition reaction between carbene and azacyclopropane

XIAOJUN TAN[1]*, PING LI[2], WEIHUA WANG[2], GENGXIU ZHENG[3] and QIUFEN WANG[3]

[1]*College of Medical and Life Science, University of Jinan, Jinan, Shandong, 250022,* [2]*Department of Chemistry, Qufu Normal University, Qufu, Shandong, 273165 and* [3]*College of Chemistry and Chemical Engineering, University of Jinan, Jinan, Shandong, 250022, P. R. China*

(Received 3 March, revised 15 December 2009)

Abstract: The mechanism of the addition reaction between carbene and azacyclopropane was investigated using the second-order Moller–Plesset perturbation theory (MP2). By using the 6-311+G* basis set, geometry optimization, vibrational analysis and the energy properties of the involved stationary points on the potential energy surface were calculated. From the surface energy profile, it can be predicted that there are two reaction mechanisms. The first one (1) is carbene attack at the N atom of azacyclopropane to form an intermediate, **1a** (IM1a), which is a barrier-free exothermic reaction. Then, IM1a can isomerize to IM1b *via* a transition state **1a** (TS1a), in which the potential barrier is 30.0 kJ/mol. Subsequently, IM1b isomerizes to a product (Pro1) *via* TS1b with a potential barrier of 39.3 kJ/mol. The other one (2) is carbene attack at the C atom of azacyclopropane, firstly to form IM2 *via* TS2a, the potential barrier is 35.4 kJ/mol. Then IM2 isomerizes to a product (Pro2) *via* TS2b with a potential barrier of 35.1 kJ/mol. Correspondingly, the reaction energy for the reactions (1) and (2) is –478.3 and –509.9 kJ/mol, respectively. Additionally, the orbital interactions are also discussed for the leading intermediate.

Keywords: carbene; azacyclopropane; addition reaction.

INTRODUCTION

Carbenes can be defined as divalent carbon intermediates, in which the carbene carbon is linked to two adjacent groups by covalent bonds and possesses two nonbonding electrons. Carbenes play an important role in organic chemistry, especially for the addition reaction between a carbene and a C=O double bond.[1–4] Therefore, they have attracted much attention not only from theoretical but also

* Corresponding author. E-mail: chm_tanxj@ujn.edu.cn
doi: 10.2298/JSC090303031T

applied chemists. For example, the study of carbene has provided simple and direct synthesis of small-ring, highly strained compounds, as well as those that can hardly be synthesized through conventional ways.[5] Lu *et al*. reported systematically the reactions between carbene or substituted carbenes with some small molecules using theoretical calculations.[6–8] Apeloig *et al*. extensively studied the mechanisms and stereoselectivity of carbene addition to olefins using experimental as well as theoretical methods.[9,10] However, the reaction between carbene and small-ring strained molecules, such as azacyclopropane, has not, to the best of our knowledge, been hitherto reported. As a representative small-ring molecule, azacyclopropane also plays an important role in organic and medical chemistry. Therefore, it is very important to study the addition reaction between carbene and azacyclopropane.

In the present study, the addition reaction between carbene and azacyclopropane was systematically investigated employing the MP2/6-311+G* level of theory. Intermediates (IM), transition states (TS) and products (Pro) were located on the potential energy surface. Possible reaction mechanisms have been proposed. Hopefully, the present results will be helpful for further experimental and theoretical studies on the similar addition reactions associated with carbene.

Calculation method

The second-order Moller–Plesset perturbation theory (MP2) method[11] combined with the 6-311+G* basis set was employed to locate all the stationary points along the reaction pathways. Frequency analyses were also performed to confirm the nature of the minima and transition states. Moreover, intrinsic reaction coordinate (IRC) calculations were performed to further validate the calculated transition states connecting the reactants and products. Additionally, relevant energy quantities, such as reaction energies and barrier energies, were rectified with zero-point vibrational energy (ZPVE) corrections.

All the calculations were realized using Gaussian 98 programs.[12]

RESULTS AND DISCUSSION

The following two pathways are possible for the addition reaction between carbene and azacyclopropane:

$$H_2C: + \text{azacyclopropane} \rightarrow \text{IM1a} \rightarrow \text{TS1a} \rightarrow \text{IM1b} \rightarrow \text{TS1b} \rightarrow \text{Pro1} \quad (1)$$

$$H_2C: + \text{azacyclopropane} \rightarrow \text{TS2a} \rightarrow \text{IM2} \rightarrow \text{TS2b} \rightarrow \text{Pro2} \quad (2)$$

Here, reaction (1) is carbene attack of the N atom of azacyclopropane to form an intermediate **1a** (IM1a), which is a barrier-free exothermic reaction. IM1a then isomerizes to IM1b *via* a transition state **1a** (TS1a). Subsequently, IM1b isomerizes to a product Pro1 *via* TS1b. Reaction (2) is carbene attack of a C atom of azacyclopropane, firstly to form IM2 *via* TS2a and then IM2 isomerizes to a product Pro2 *via* TS2b.

Reaction (1) between carbene and azacyclopropane

The selected geometrical parameters for the intermediates (IM1a, IM1b), transition states (TS1a, Ts1b), and product (Pro1) in reaction (1) are given in Fig. 1. Correspondingly, the relevant energy quantities are summarized in Table I. The potential energy profile of the reaction based on Table I is illustrated in Fig. 2. As can be seen in Fig. 2, reaction (1) consists of three steps: the first one is a barrier-free exothermic reaction of 204.2 kJ/mol, resulting in the intermediate IM1a; the second step is the isomerization of IM1a to intermediate IM1b *via* TS1a with a barrier of 30.0 kJ/mol. Subsequently, IM1b isomerizes to product Pro1 *via* TS1b with 39.3 kJ/mol barrier.

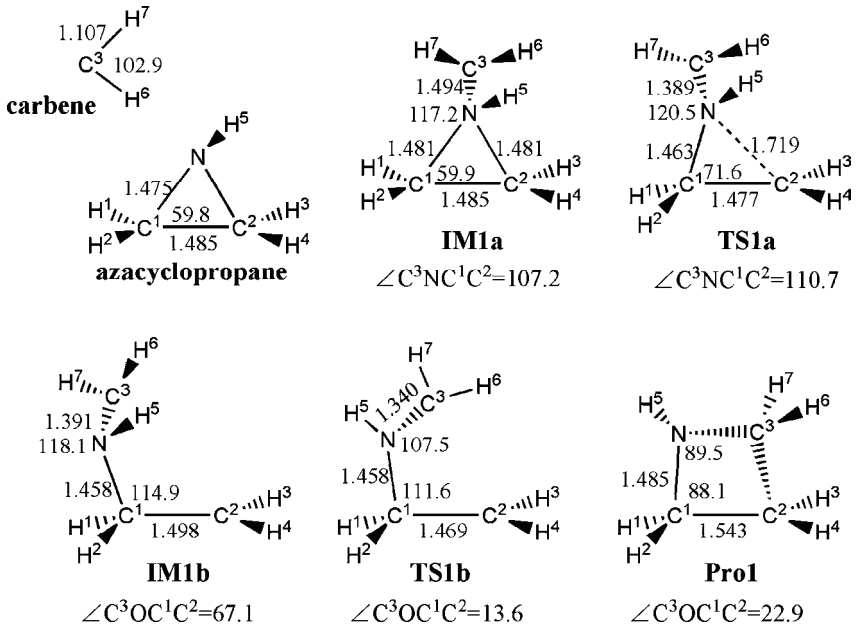

Fig. 1. Optimized structures of the reactants, intermediates (IM), transition states (TS), and product (Pro) of reaction (1) at the MP2/6-311+G* level of theory, where the bond lengths and bond angles are in angstroms and degrees, respectively.

When carbene approaches the N atom of azacyclopropane, it can form an intermediate (IM1a) with azacyclopropane, which is a barrier-free process. In IM1a, the conformation of azacyclopropane is changed slightly compared with that in the isolated azacyclopropane. For example, the bond length of C^1–C^2 and the bond angle of N–C^1–C^2 in IM1a and in isolated azacyclopropane are almost equal to each, whereas the bond length of N–C^1 is slightly prolonged by 0.006 Å, denoting a weakening of the N–C^1 bond. Based on population analyses, some electrons on atom N in isolated azacyclopropane have been transferred to atom C^3 in IM1a; *i.e.*, the Mulliken charges on N (C^3) are –0.291 (–0.392) and –0.039

(–0.962) for the isolated reactants and IM1a, respectively. To investigate this combined process of carbene and azacyclopropane interaction, the potential energy curve for IM1a was constructed along the distance between the two fragments. As shown in Fig. 3, the energy of the system decreases continuously before combination. Actually, to the best our ability, no transition state could be located for this combined process.

TABLE 1. The electronic structure energies (E_{SE}), zero-point energies (E_{ZP}), total energies (E_T) and relative energies (E_R) for the species of the addition reaction between carbene and azacyclopropane at the MP2/6-311+G* level of theory

Species	E_{SE} / a.u.	E_{ZP} / a.u.	E_T[a] / a.u.	E_R / kJ mol^{-1}
CH_2 + azacyclopropane	–192.3657253	0.075571	–172.416767	0.0
IM1a	–172.5933031	0.098745	–172.494559	–204.2
TS1a	–172.5790342	0.095911	–172.483123	–174.2
IM1b	–172.6006735	0.094209	–172.506464	–235.5
TS1b	–172.5846392	0.093144	–172.491495	–196.2
Pro1	–172.7004242	0.101444	–172.598980	–478.3
TS2a	–172.4950407	0.091775	–172.403266	35.4
IM2	–172.5979765	0.093005	–172.504972	–231.5
TS2b	–172.5844913	0.092897	–172.491594	–196.4
Pro2	–172.7101680	0.099146	–172.611022	–509.9

[a]$E_T = E_{SE} + E_{ZP}$

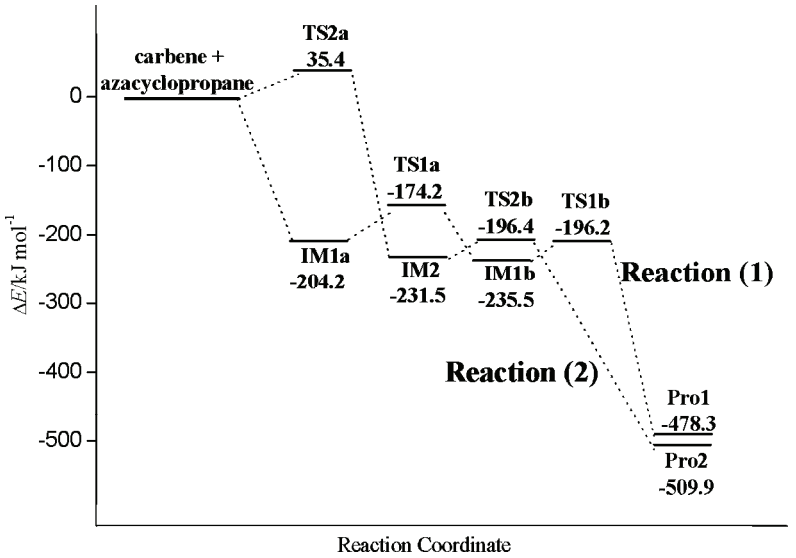

Fig. 2. Potential energy surface for the addition reaction between carbene and azacyclopropane at the MP2/6-311+G* level of theory.

As illustrated in Fig. 4, the formation mechanism of IM1a can be explained by frontier molecular orbital (MO) analysis. The unoccupied p orbital (main com-

ponent of the LUMO) of C^3 of carbene overlaps with the *p* electron at the N of azacyclopropane, consequently forming a p → p interaction in the N–C^3 donor––acceptor bond, which changed the two reactants into IM1a.

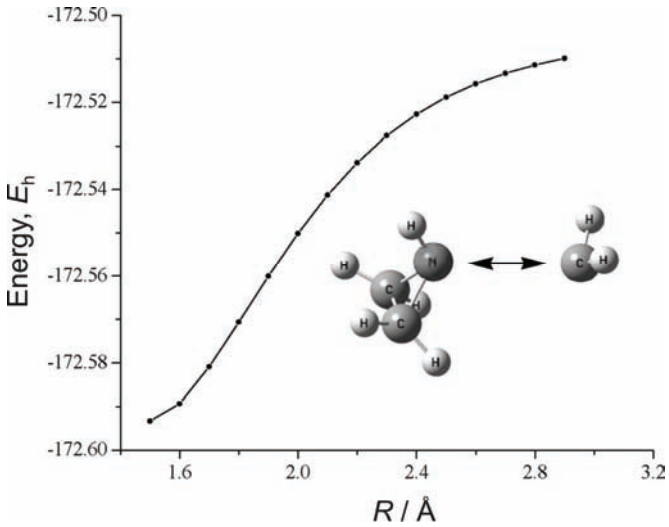

Fig. 3. Energy changes in the combined process of IM1a, together with the distance between two fragments at the MP2/6-311+G* level of theory.

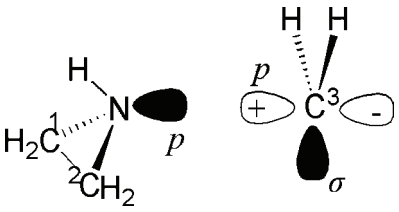

Fig. 4. Frontier molecular orbital (MO) symmetry--adoption of carbene and azacyclopropane.

The unique imaginary frequency of the transition state TS1a is 776.928i cm^{-1}, and the transition state can, therefore, be affirmed as real. According to the calculation of the IRC of TS1a and further optimization for the primary IRC results, TS1a connects IM1a and IM1b. In TS1a, the distance of N–C^1 and N–C^2 reached 1.463 and 1.719 Å, respectively. Compared with the IM1a, the N–C^1 and N–C^2 distances in TS1a are shortened slightly by 0.018 Å and elongated by 0.238 Å, respectively, which denote rupturing of the N–C^2 bond and destruction of the three-membered azacyclopropane ring. Simultaneously, the N–C^1–C^2 angle in TS1a is changed to 71.6°, which can decrease the angle tensility of N–C^1–C^2. Furthermore, the distance between C^3 and N is 1.389 Å, which is shortened by 0.105 Å compared with the corresponding distance in IM1a, suggesting that a new C^3–N bond is to be formed.

In intermediate IM1b, the N–C^1 distance is 1.458 Å, which is approximately the normal length of an N–C single bond. The distance between C^3 and N decreased to 1.391 Å, which is shortened by 0.103 Å compared with the corresponding distance in IM1a, suggesting the formation of a new C^3–N bond. Simultaneously, because of the release of the restriction of the small ring, the C^1–C^2 bond length is elongated to 1.498 Å, *i.e.*, by 0.013 Å compared with the corresponding distance in IM1a. The N–C^1–C^2 angle is 114.9°, meaning that the C^1 atom had adopted a normal sp^3 hybridization state. There is an unconjugated electron in C^2 and C^3, respectively. The dihedral angles of $H^3C^2C^1H^4$ and $H^6C^3NH^7$ are 166.0° and 144.2°, respectively. In contrast, the dihedral angle of H^1–C^1–C^2–H^2 is only 116.7°. Therefore, C^2 and C^3 adopt a sp^2 hybridization state. Since C^2 and C^3 has an unconjugated electron, the energy of IM1b is higher; therefore, it can transfer to the more stable conformer Pro1.

The unique imaginary frequency of the transition state TS1b, which connects IM1b and Pro1, is 730.712i cm^{-1}. In TS1b, the N–C^1–C^2 angle is 111.6°, which is reduced compared with the corresponding angle in IM1b (114.9°). Simultaneously, the dihedral angle of C^3–N–C^1–C^2 is 13.6°, which is significantly decreased compared with the corresponding dihedral angle in IM1b (67.1°), suggesting the planar structure Pro1 is to be formed.

In Pro1, three carbon atoms adopt sp^3 hybridization and the bond lengths of C–C and C–N are 1.543 and 1.485 Å, respectively. The angle tensility in a four--membered ring is smaller than that in a three-membered ring. Therefore, Pro1 is more stable than IM1b. Based on the calculated results, the energy of Pro1 is lower by 242.8 kJ/mol than IM1b.

Reaction (2) between carbene and azacyclopropane

When carbene approaches the carbon atom of azacyclopropane, it can form an intermediate (IM2) with azacyclopropane *via* TS2a, then IM2 can isomerize to Pro2 *via* TS2b. The geometrical parameters for the intermediate (IM2), transition state (TS2a, TS2b), and product (Pro2) in reaction (2) are given in Fig. 5. Correspondingly, the relevant energy quantities are summarized in Table I. The potential energy profile of reaction (2) based on Table 1 is illustrated in Fig. 2, from which, it can be directly seen that reaction (2) consists of two steps: the first one is carbene and azacyclopropane form IM2 *via* TS2a, for which the potential barrier is 35.4 kJ/mol; then, IM2 isomerizes to product Pro2 with a barrier of 35.1 kJ/mol.

The unique imaginary frequency of the transition state TS2a is 1286.34i cm^{-1}, therefore the transition state can be affirmed as real. According to the calculation of the IRC of TS2a, and further optimization for the primary IRC results, TS2a connects reactants and IM2. In TS2a, the distance of N–C^2 reached 1.696 Å, compared with isolated azacyclopropane, this distance is elongated by 0.221 Å.

Simultaneously, the N–C^1–C^2 angle reached to 70.7°, which is increased by 10.9° compared with that in isolated azacyclopropane. Therefore, the N–C^2 bond is to be ruptured and the three-membered azacyclopropane ring to be destroyed. In TS2a, the N–C^3 distance is 1.980 Å, which denotes an N-C^3 bond is to be formed.

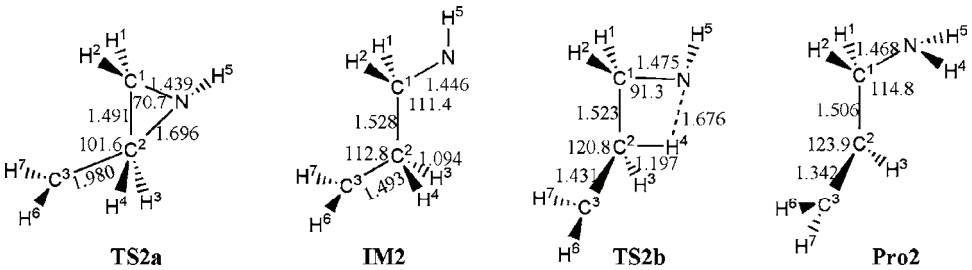

Fig. 5. Optimized structures of the intermediates (IM), transition states (TS), and product (Pro) of reaction (2) at the MP2/6-311+G* level of theory, where the bond lengths and bond angles are in angstrom and degree, respectively.

In IM2, both C^1 and C^2 adopt the sp^3 hybridized state. The N–C^1–C^2 angle is 111.4°, which denotes that the three-membered ring of azacyclopropane is unfolded. Simultaneously, there is an unconjugated electron in N and C^3, respectively. Therefore, IM2 has a higher energy and it can transfer to the more stable conformer Pro2.

The unique imaginary frequency of the transition state TS2b, which connects IM2 and Pro2, is 778.737i cm^{-1}. In TS2b, the C^2–C^3 distance is shortened to 1.431 Å, denoting a double C^2–C^3 bond is to be formed. The C^2–H^4 distance is about 1.197 Å, which is prolonged by 0.103 Å compared with that in IM2. Simultaneously, the N–H^4 distance attains 1.676 Å, which is shortened largely compared with that in IM2. Thus, in the TS2b, a new N–H^4 bond is to be formed and the C^2–H^4 bond is to be broken simultaneously.

In Pro2, the N–H^4 distance is shortened to 1.014 Å, denoting that the atom H^4 has been transferred to the N atom and a new N–H^4 bond is formed. Both the C^2 and C^3 atoms adopt an sp^2 hybridized state and the C^1–C^2–C^3angle is 123.9°. The C^2–C^3 distance is 1.342 Å, which is the normal C=C double bond length.

A comparison between the two reaction pathways indicates that the two potential barriers along reaction (1) is 30.0 (IM1a → IM1b) and 39.3 (IM1b → Pro1) kJ/mol, respectively, which is similar to that along reaction (2) (reactants → → IM2, 35.4 kJ/mol, and IM2 → Pro2, 35.1 kJ/mol). Hence, it can be predicated that reactions (1) and (2) should be the parallel reactions from the viewpoint of kinetics. However, the energy of reaction (1) is –478.3 kJ/mol, which is lower than that of reaction (2) (–509.9 kJ/mol). Therefore, from the thermodynamic viewpoint, Pro2 should be the dominant product.

CONCLUSIONS

In the present study, the mechanism of the addition reaction between carbene and azacyclopropane was investigated at the MP2/6-311+G* level of theory. Geometry optimization, vibrational analysis, and relevant energy properties for the involved stationary points on the potential energy surface were calculated. Two reactions, (1) and (2), were found. Reaction (1) is carbene attack of the N atom of azacyclopropane to form an intermediate **1a** (IM1a), which is a barrier--free exothermic reaction. IM1a then isomerizes to IM1b *via* a transition state **1a** (TS1a), where the potential barrier is 30.0 kJ/mol. Subsequently, IM1b can isomerize to a product Pro1 *via* TS1b with a potential barrier of 39.3 kJ/mol. The orbital interactions are also discussed to explain the combined process of the leading intermediate. Reaction (2) is carbene attack of the C atom of azacyclopropane, firstly to form IM2 *via* TS2a, the potential barrier of which is 35.4 kJ/mol. Then IM2 isomerizes to a product Pro2 *via* TS2b with a potential barrier of 35.1 kJ/mol. The reaction energies for reactions (1) and (2) are –478.3 and –509.9 kJ/mol, respectively. From the kinetic viewpoint, reactions (1) and (2) should be the parallel reactions. However, from the thermodynamic viewpoint, Pro2 should be the dominant product. Hopefully, the present results will fill a void in the available data in the study of the interactions between carbene and the small-ring strained molecules.

Acknowledgements. This work was supported by the Scientific Research Foundation of Jinan University (XKY0709).

И З В О Д

ТЕОРИЈСКО ПРОУЧАВАЊЕ МЕХАНИЗМА АДИЦИЈЕ КАРБЕНА НА АЗАЦИКЛОПРОПАН

XIAOJUN TAN[1], PING LI[2], WEIHUA WANG[2], GENGXIU ZHENG[3] и QIUFEN WANG[3]

[1]College of Medical and Life Science, University of Jinan, Jinan, Shandong, 250022, [2]Department of Chemistry, Qufu Normal University, Qufu, Shandong, 273165 и [3]College of Chemistry and Chemical Engineering, University of Jinan, Jinan, Shandong, 250022, P. R. China

Испитиван је механизам адиције карбена на азациклопропан помоћу Moller–Plesset-ове пертурбационе теорије другог реда (MP2). Применом базног сета 6-311+G* извршена је оптимизација геометрије, вибрациона анализа и одређене енергетске особине стационарних тачака на хиперповршини потенцијалне енергије. На основу енергетског профила предвиђено је да постоје два реакциона механизма, (1) и (2). У првом (1), карбен напада N атом азациклопропана и гради интермедијер **1a** (IM1a), што је егзотермна реакција без баријере. Затим се IM1a изомеризује у IM1b преко прелазног стања **1a** (TS1a), где потенцијална баријера износи 30,0 kJ/mol. После тога, IM1b се изомеризује у продукт (Pro1) преко TS1b са потенцијалном баријером од 39,3 kJ/mol. У другом механизму (2), карбен напада C атом азациклопропана, прво градећи IM2 преко TS2a, са потенцијалном баријером од 35,4 kJ/mol. Затим се IM2 изомеризује у продукт (Pro2) преко TS2b са потенцијалном баријером од 35,1 kJ/mol. Доследно томе, енергије реакција (1) и (2) су –478,3 и –509,9 kJ/mol, редом. Осим тога, разматрана је и интеракција између орбитала код главних интермедијера.

(Примљено 3. марта, ревидирано 15. децембра 2009)

REFERENCES

1. M. Mitani, Y. Kobanashi, K. Koyama, *J. Chem. Soc., Perkin Trans* **1** (1995) 653
2. M. Garcia, C. D. Campo, E. F. Llama, *Tetrahedron Lett.* **49** (1993) 8433
3. M. Garcia, C. D. Campo, E. F. Llama, *J. Chem. Soc., Perkin Trans* **1** (1995) 1771
4. R. R. Kostikov, A. F. Khlebnikov, V. Y. Bespalov, *J. Phys. Org. Chem.* **6** (1993) 83
5. Y. Wang, H. Li, *Acta Phys. Chim. Sin.* **20** (2004) 1339
6. P. J. Stang, *J. Am. Chem. Res.* **15** (1982) 348
7. X. H. Lu, Y. X. Wang, *J. Phys. Chem. A* **107** (2003) 7885
8. X. H. Lu, Y. X. Wang, *J. Mol. Struct. (THEOCHEM)* **686** (2004) 207
9. Y. Apeloig, M. Karni, P. J. Stang, *J. Am. Chem. Soc.* **105** (1983) 4781
10. D. P. Fox, P. J. Stang, Y. Apeloig, M. Karni, *J. Am. Chem. Soc.* **108** (1986) 750
11. L. A. Curtis, K. Raghavachari, J. A. Pople, *J. Chem. Phys.* **66** (1981) 2153
12. *Gaussian 98*, Gaussian Inc, Pittsburgh, PA, 1998.

Journal of the Serbian Chemical Society
JSCS@tmf.bg.ac.rs • www.shd.org.rs/JSCS

J. Serb. Chem. Soc. 75 (5) 659–667 (2010)
JSCS–3996

UDC 546.57.027:534.1/.2:539.2
Original scientific paper

Franck–Condon factors and observed band strength distribution in the vibrational structure of the Ag_2 *D-X* band system

ANKICA ANTIĆ-JOVANOVIĆ[1*#], MILOŠ MOMČILOVIĆ[1], VOJISLAV BOJOVIĆ[1], MURTADHA A. KHAKOO[2] and RUSS R. LAHER[3]

[1]Faculty of Physical Chemistry, University of Belgrade, P. O. Box 47, 11158 Belgrade, Serbia, [2]Department of Physics, California State University Fullerton, CA 92834 and [3]Spitzer Science Center, California Institute of Technology, M/S 314-6, Pasadena, CA 91125, USA

(Received 8 June 2009, revised 1 February 2010)

Abstract: Potential curves for the $X^1\Sigma_g^+$ and $D^1\Sigma_u^+$states of three diatomic silver isotopomers, $^{107}Ag_2$, $^{107}Ag^{109}Ag$ and $^{109}Ag_2$, were determined from the best available molecular constants by the Rydberg–Klein–Rees method. From these potentials, Franck–Condon factors and band-origin wavenumbers were computed, and the reliability of the obtained values was verified by comparison with the observed band strength distribution and the measured band origin positions in a previously recorded *D-X* spectrum. The ratios of the Franck–Condon factors to those of corresponding isotopic bands were found to be very close to unity, revealing only a very small isotopic effect on the Franck–Condon factors of Ag_2 *D-X* bands. The isotopic shifts of the calculated band origins agree well with previously measured displacements of band heads.

Keywords: Franck–Condon factors; band strength distribution; Ag_2 *D-X* band system; isotopic effect.

INTRODUCTION

The electronic spectrum of the silver dimer, Ag_2, as known to date, consists of six well-developed systems with the red degraded bands between 160–540 nm having a common lower state, $^1\Sigma_g^+$, which is the ground state of the molecule. The systems were identified to belong to: $A^1\Sigma_u^+$–$X^1\Sigma_g^+$ (400–540 nm), $B^1\prod_u$–$X^1\Sigma_g^+$ (275–295 nm), $C^1\prod_u$–$X^1\Sigma_g^+$ (264–271 nm), $D^1\Sigma_u^+$–$X^1\Sigma_g^+$ (256–261 nm), $E^1\prod_u$–$X^1\Sigma_g^+$ (247–256 nm) and $H^1\Sigma_u^+$–$X^1\Sigma_g^+$ (169–173 nm) transitions, and all, with the exception of the *H-X* system, were observed in absorption and partly in emission as early as the 1950s.[1–3] Kleman and Lindkvist[2] gave the most complete data for bands of the *A-X* system, while the work of Ruamps[3] provided a better description of the *B-X*, *C-X*, *D-X* and *E-X* systems. About twenty years

* Corresponding author. E-mail: ankica@ffh.bg.ac.rs
# Serbian Chemical Society member.
doi: 10.2298/JSC090608035A

later, Brown and Ginter[4] re-photographed these bands in absorption and recorded, for the first time, the *H*-*X* transition in the vacuum ultraviolet, in addition to the known systems. Due to the limited spectral resolution in the conventional absorption and emission spectroscopy used in their experiments, the authors were able to perform only a vibrational analysis of the bands, which was supported by Srdanov and Pesić based on isotope shift measurements.[5,6] At the beginning of 1990s, several authors analyzed a few highly resolved bands of the *A*-*X*, *B*-*X* and *E*-*X* systems, obtained by new laser spectroscopic techniques, and derived very accurate rotational constants for all states involved in the transitions.[7–9] Some Ag_2 band systems were also investigated in matrix environments, in both absorption and emission.[10–16] In all the aforementioned studies, the attention was focused on the analysis of the bands to yield accurate molecular constants and correct assignment of the involved electronic states. However, information on the transition probability parameters for these bands, at least the Franck–Condon factors (FCFs), which may be the governing parameters for the determination of band strength distributions in the vibrational structure of band systems, is scarce. The only existing sets of FCFs for Ag_2 bands from the early work were those for the *B*-*X* and *C*-*X* bands reported by Vujisić and Pešić.[17] The authors performed FCF calculations using Morse potential energy functions in a formalism developed by Fraser and Jerman[18,19] and molecular constants were obtained from their analysis of the spectrum;[5,20] these were later corrected by Beutel *et al.*[9]

Due to the important role of FCFs and related quantities for the prediction of vibrational band strength distributions in molecular band systems and for an explanation of the experimentally observed intensity pattern, recently an evaluation of transition probability parameters for all band systems of diatomic silver were undertaken. It was hoped that the obtained data would be useful for both experimentalists and theoreticians in future research on the Ag_2 spectrum, which is of interest in many areas, such as studies of small silver clusters, catalysis and surface science.

In the first paper of this series, a large set of FCFs and *r*-centroids for the *E*-*X* bands based on Morse and Rydberg–Klein–Rees (RKR) potentials were reported, and it was shown that both sets of data agreed fairly well for transitions involving low vibrational levels with ν’ and ν’’ up to 6, while both sets followed the same intensity pattern.[21] In the following papers, all relevant transition probability parameters for the *A*-*X* bands were calculated, including FCFs, *r*-centroids, electronic transition moment function (ETMF), Einstein coefficients and absorption band oscillator strengths, and the results of a comparison of theoretical and experimental data.[22,23] The last study involved the experimental and theoretical study of absorption band strengths in the *B*-*X* system of Ag_2 isotopomers.[24]

In the present paper, for the first time, the FCFs for the rather weak *D*-*X* bands appearing in the transition between the vibronic levels of the lower $X^1\Sigma_g^+$

and the upper $D^1\Sigma_u^+$ states are reported. FCF computation was performed using RKR potential energy curves separately for three diatomic silver isotopomers, $^{107}Ag_2$, $^{107}Ag^{109}Ag$ and $^{109}Ag_2$, which are always present in the gas-phase spectrum of diatomic natural silver. The aim was to analyze the band strength distribution in the experimental spectrum using computed FCFs, and also to see whether isotopic substitution causes a shift in the values of FCFs of isotopic Ag_2 molecules,[25,26] which is of interest in intensity analysis of unresolved isotopic bands and in the determination of the abundances of isotopic molecules present using intensity measurements of resolved isotopic bands.

METHOD OF COMPUTATION

The theoretical background for the present computation can be found in previous papers.[21-23] Briefly, neglecting the effect of rotational–vibrational interaction and assuming a constant ETMF over the range of internuclear distances encountered in the detected transitions (*i.e.*, the *r*-centroid approximation), the measured band strength signal, $I_{v',v''}$, in the absorption electronic spectrum of the diatomic molecule is given by:[27]

$$I_{v',v''} = DN_{v''}\nu_{v',v''}R_e^2(\int \Psi_{v'}\Psi_{v''}dr)^2 \quad (1)$$

where D is a constant, $N_{v''}$ is the population in the lower vibronic state, $\nu_{v',v''}$ is the frequency of the $v'' \rightarrow v'$ transition, R_e is the average ETMF, which is conventionally used as an approximation in the cases where the function varies sufficiently slowly with internuclear distance, and $(\int \Psi_{v'}\Psi_{v''}dr)^2$ is the square of the overlap integral or FCF, $q_{v',v''}$, associated with the $v'' \rightarrow v'$ transition. The wavefunctions $\Psi_{v'}$ and $\Psi_{v''}$ are those for the rotationless ($J = 0$) vibrational states.

The computational accuracy of the FCFs depends primarily on the choice of the potential energy functions. Usually, Morse potential functions and Morse wavefunctions can be taken as a fairly satisfactory approximation of the realistic wavefunctions, especially for low vibrational levels. However, since the recorded *D*-*X* system includes transitions between relatively high vibrational levels with $v' = 14$ and $v'' = 17$ (in the *X* state these levels cover about 22 % of the full potential and about 37 % in the *D* state), RKR potential curves were used for both the *X* and *D* states (Fig. 1) in the radial Schrödinger Equation to solve for $\Psi_{v'}$ and $\Psi_{v''}$ in order to obtain reliable FCF values.

The molecular constants required for the $^{107}Ag^{109}Ag$ calculation are listed in Table I together with the constants for the less abundant isotopomers, $^{107}Ag_2$ and $^{109}Ag_2$, which were derived from the constants of $^{107}Ag^{109}Ag$ using isotope relations:[27]

$$\omega_e^i = \omega_e(\mu/\mu^i)^{1/2};\ \omega_e^i x_e^i = \omega_e x_e(\mu/\mu^i);\ \omega_e^i y_e^i = \omega_e y_e(\mu/\mu^i)^{3/2} \quad (2)$$

$$B_e^i = B_e(\mu/\mu^i);\ \alpha_e^i = \alpha_e(\mu/\mu^i)^{3/2} \quad (3)$$

where μ is the reduced mass of $^{107}Ag^{109}Ag$ and μ^i is the reduced mass of the less abundant molecules.

The calculation of the RKR potential-FCFs was performed for transitions involving v' and v'' levels up to 21 using the RKR/FCF computer program developed by Espy.[28]

RESULTS AND DISCUSSION

Portions of the 15×21 arrays of the calculated FCFs for all three diatomic silver isotopomers together with computed band-origin wavenumbers of the corres-

ponding bands are contained in Table I (Supplementary material). The FCFs for the transitions v'' (from 11 to 21) $\rightarrow$ v' (from 0 to 6) are negligibly small and they are not presented in Table I, nor are those for the transitions $v'' > 15 \rightarrow v'$ (from 0 to 21).

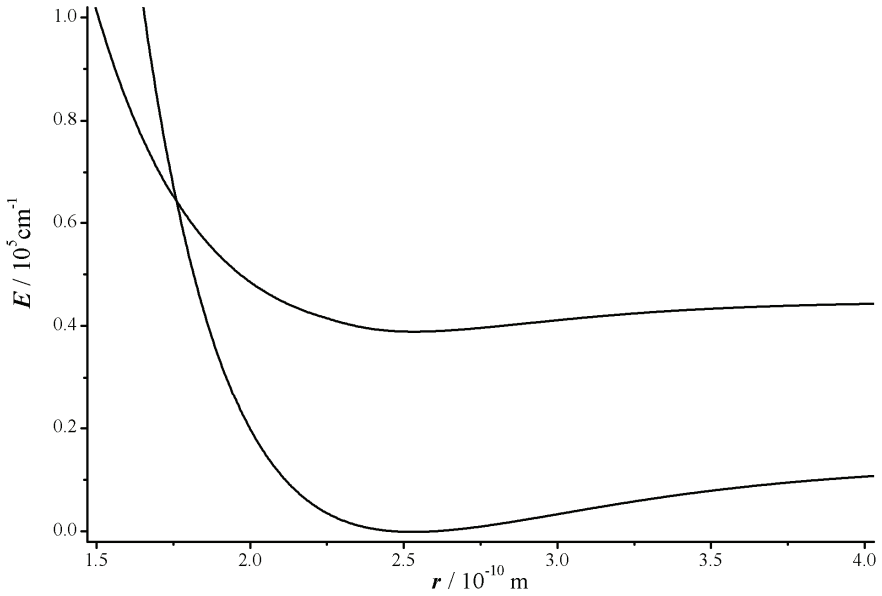

Fig. 1. RKR Potential energy curves for the *X* (lower curve) and *D* (upper curve) states of the $^{107,109}Ag_2$ molecule.

TABLE I. Molecular constants (cm^{-1}) of the Ag_2 $X^1\Sigma g^+$ and $D^1\Sigma u^+$ states used in the RKR computations (The constants for $^{107}Ag_2$ and $^{109}Ag_2$ were calculated from the isotopic relations (2) and (3); μ ($^{107}Ag^{109}Ag$) = 53.94783 amu; μ ($^{107}Ag2$) = 53.45255 amu; μ ($^{109}Ag2$) = = 54.452378 amu)

Constant	$X^1\Sigma_g^+$			$D^1\Sigma_u^+$		
	$^{107}Ag^{109}Ag$	$^{107}Ag_2$	$^{109}Ag_2$	$^{107}Ag^{109}Ag$	$^{107}Ag_2$	$^{109}Ag_2$
T_e	–96.039[a]	–96.039	–96.039	38918.4	38918.4	38918.4
ω_e	192.40[b]	193.289	191.506	168.2[c]	168.977	167.419
$\omega_e x_e$	0.643[b]	0.649	0.637	1.20[c]	1.210	1.189
$\omega_e y_e$	0.0003[b]	0.000304	0.000296			
D_e	13403.1	13404.9	13404.0	5894.3	5899.0	5893.6
B_e	0.04881[d]	0.04926	0.04836	0.04865[d]	0.04910	0.04820
$\alpha_e \times 10^{-4}$	2.08[c]	2.11	2.05	2.82[c]	2.86	2.78

[a]Re-adjusted T_e such that T_0 (v' = 0) = 0 for $\nu_0(0,0)$ = 39002.2 cm^{-1} of Brown and Ginter; [b]Ref. 2; [c]Ref. 3; [d]Ref. 9

A close survey of Table I reveals that the prominent FCFs form a narrow Franck–Condon envelope with a concentration of the highest values on the dia-

gonal axis of the matrix, which is typical for transitions between electronic states having a similar equilibrium distance r_e (see B_e for both states given in Table I).

The distribution of the FCF values in the v',v'' scheme indicates the appearance of a $\Delta v = 0$ sequence as the strongest one in the system, followed by the much weaker bands of a few other sequences with low $\Delta v = v' - v''$ values. Very small FCFs for the transitions $v'' > v' + 1 \rightarrow v'$ (from 0 to 1), $v'' > v' + 2 \rightarrow v'$ (from 2 to 3), $v'' > v' + 3 \rightarrow v'$ (from 4 to 5) and $v'' > v' + 4 \rightarrow v'$ (from 6 to 7) suggest the absence a few first members in the $\Delta v = -1, -2, -3$ and -4 sequences.

To verify the reliability of the calculated FCFs, data previously reported by Srdanov and Pešić[5] on the *D-X* system was used. They listed band heads for 41 bands of the $^{107}Ag^{109}Ag$ isotopomer belonging to five sequences ($\Delta v = 0, -1, -2, -3$ and -4), which are included in the v', v'' scheme shown in Fig. 2. The bands of the $\Delta v = 0$ sequence were visually estimated by the authors as the most intense in the system, while all other bands were estimated to be much weaker.

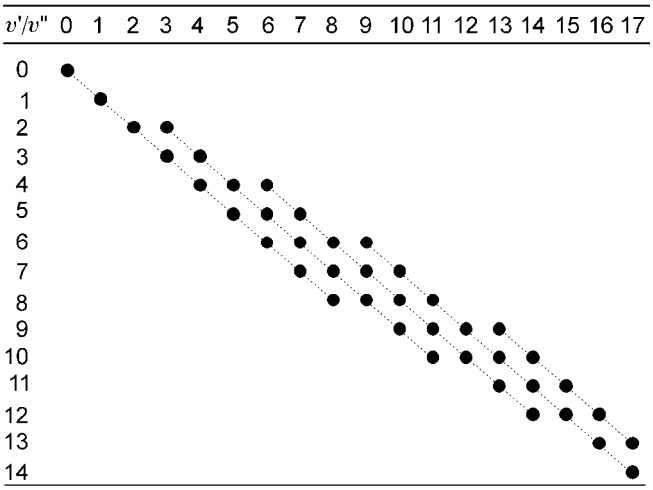

Fig. 2. Recorded *D-X* bands of $^{107}Ag^{109}Ag$.

As can be seen from Fig. 2, the distribution of the bands in the v',v'' scheme is generally consistent with that of the prominent FCFs in Table I. The recorded bands form a narrow envelope with the first two members missing in the $\Delta v = -1$ sequence, the first four missing in the $\Delta v = -2$ sequence, the first six and the first eight members missing in the $\Delta v = -3$ and $\Delta v = -4$ sequences, respectively. The absence of these features was predicted by the computed FCFs.

An attempt was made to judge more directly the agreement between experimental and theoretical results by comparing the ratios of the measured relative bands strengths of the bands having a common lower vibrational level with those theoretically computed for the same bands using the computed FCFs and quoted

wavenumbers. For this purpose, a portion of the *D*-*X* system containing the bands of the $\Delta v = 0$ and $\Delta v = -1$ sequences was recorded in absorption as described elsewhere.[22] The microphotometer tracing of the recorded bands is shown in Fig. 3.

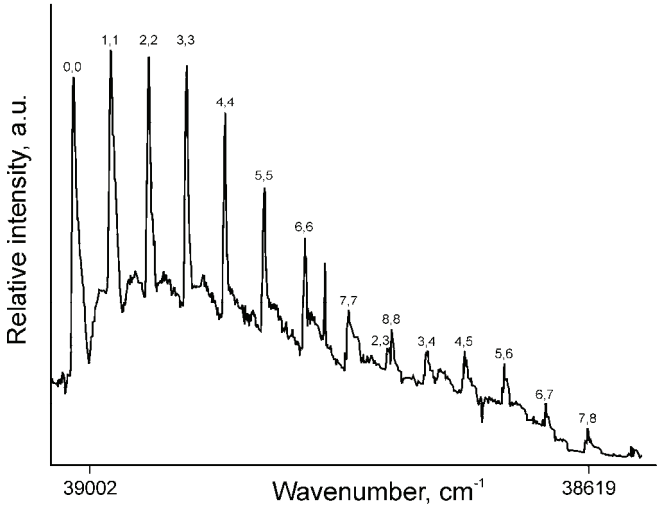

Fig. 3. Microphotometer trace of the recorded Ag_2 *D*-*X* bands of the $\Delta v = 0$ and –1 sequences.

However, due to the very low band strengths of the $\Delta v = -1$ sequence bands and, consequently, very low accuracy of the measurement of their intensity, the attempt was not successful. Therefore, as an additional check on the accuracy of the RKR calculations, a comparison of the band origin wavenumbers obtained in this study were compared with those measured by Brown and Ginter[4] at the positions of the intensity minima clearly seen in several bands of the $\Delta v = 0$ sequence (these wavenumbers are given in the note of Table I).

In addition, the isotopic shifts calculated in the present work were compared with those measured by Srdanov and Pešić,[5] in whose spectrum the heads of 19 bands belonging to three diatomic silver isotopomers, $^{107}Ag_2$, $^{107}Ag^{109}Ag$ and $^{109}Ag_2$, were resolved.[5] In both cases, agreement within experimental error was found. The isotope shifts of the calculated band origins, $\Delta\nu^i_0 = \nu_0(^{107}Ag_2 - \nu_0(^{107}Ag^{109}Ag)$ and $\Delta\nu^i_0 = \nu_0(^{109}Ag_2 - \nu_0(^{107}Ag^{109}Ag)$, as well as the isotopic displacements of the band heads, $\Delta\nu^i_h = \nu_h(^{107}Ag_2 - \nu_h(^{107}Ag^{109}Ag)$ and $\Delta\nu^i_h = \nu_h(^{109}Ag_2 - \nu_h(^{107}Ag^{109}Ag)$ measured by Srdanov and Pešić, are presented in Table II.

Finally, it is worthwhile to point out the very small isotopic effect seen in the FCFs of the *D*-*X* bands of Ag_2 isotopomers. As follows from Table I, the ratios $q(^{107}Ag_2)/q(^{107}Ag^{109}Ag)$ and $q(^{109}Ag_2)/q(^{107}Ag^{109}Ag)$ are very close to unity for all the observed bands, with discrepancies at the third decimal place. This is of interest to know for intensity analysis of unresolved isotopic bands, since, in

such cases, the measured strength signal contains contributors from all isotopemers present, as well as for the study of abundances of the isotope species present based on intensity measurements of isotopic resolved bands.

TABLE II. Isotope shifts $\Delta\nu_0^{i}$ and $\Delta\nu_h^{i}$ in cm^{-1} for the resolved bands of the Ag_2 *D-X* system ν_0, $\nu_0^{i(1)}$ and $\nu_0^{i(2)}$ – calculated band-origin wavenumbers of $^{107}Ag^{109}Ag$, $^{107}Ag_2$ and $^{109}Ag_2$, respectively; ν_h, $\nu_h^{i(1)}$ and $\nu_h^{i(2)}$ – measured band-head wavenumbers of $^{107}Ag^{109}Ag$, $^{107}Ag_2$ and $^{109}Ag_2$, respectively)

v',v''	$\Delta\nu_0^{i} = \nu_0^{i(1)} - \nu_0$	$\Delta\nu_h^{i} = \nu_h^{i(1)} - \nu_h$	$\Delta\nu_0^{i} = \nu_0^{i(2)} - \nu_0$	$\Delta\nu_h^{i} = \nu_h^{i(2)} - \nu_h$
5,5	–0.75	–0.8	+0.77	+0.8
6,6	–0.90	–1.0	+0.96	+1.0
7,7	–1.08	–1.2	+1.13	+1.2
8,8	–1.25	–1.4	+1.32	+1.4
3,4	–1.29	–1.3	+1.30	+1.3
4,5	–1.42	–1.5	+1.44	+1.4
5,6	–1.56	–1.6	+1.61	+1.6
6,7	–1.71	–1.8	+1.76	+1.8
7,8	–1.87	–2.0	+1.93	+1.8
8,9	–2.04	–2.2	+2.11	+2.1
9,10	–2.22	–2.4	+2.30	+2.4
4,6	–2.23	–2.3	+2.28	+2.2
5,7	–2.37	–2.4	+2.41	+2.4
6,8	–2.51	–2.6	+2.56	+2.8
7,9	–2.65	–2.7	+2.71	+2.8
8,10	–2.81	–2.9	+2.89	+3.0
9,11	–2.97	–3.1	+3.07	+3.2
10,12	–3.15	–3.3	+3.26	+3.4
11,13	–3.33	–3.6	+3.46	+3.6

CONCLUSIONS

In this paper, FCFs for the *D-X* bands of three diatomic silver isotopomers were derived for the first time using the RKR approach. The reliability of the obtained values was verified by comparison of the predicted band strength distribution based on the calculated FCFs and band-origin wavenumbers with those observed in the experimental *D-X* spectrum.

Comparison of the isotopic shifts of the calculated band origins with experimentally measured band heads in a previously recorded *D-X* spectrum further supports the accuracy of the present RKR-based calculations. The isotope effect on Ag_2 *D-X* FCFs was also examined and found to be negligible.

SUPPLEMENTARY MATERIAL

Band-origin wavenumbers in cm^{-1} and FCFs for the $D^1\Sigma_u^+ – X^1\Sigma_g^+$ bands of $^{107}Ag_2$, $^{107}Ag^{109}Ag$ and $^{109}Ag_2$ (Table I) can be found in the electronic version of the paper as Supplementary material (http://www.shd.org.rs/JSCS/), from the office of the Serbian Chemical Society (JSCS@shd.org.rs) or from the corresponding author upon request.

Acknowledgments. This work was supported by the Ministry of Science and Technological Development of the Republic of Serbia, Project No. 142065.

ИЗВОД

ФРАНК-КОНДОНОВИ ФАКТОРИ И ЗАПАЖЕНА РАСПОДЕЛА ЈАЧИНЕ ТРАКА У ВИБРАЦИОНОЈ СТРУКТУРИ Ag_2 *D-X* ТРАКАСТОГ СИСТЕМА

АНКИЦА АНТИЋ-ЈОВАНОВИЋ[1], МИРОСЛАВ КУЗМАНОВИЋ[1], ВОЈИСЛАВ БОЈОВИЋ[1], MURTADHA A. KHAKOO[2] и RUSS R. LAHER[3]

[1]*Факултет за физичку хемију, Универзитет у Београду, п. пр. 47, 11158 Београд,* [2]*Department of Physics, California State University Fullerton, CA 92834 и* [3]*Spitzer Science Center, California Institute of Technology, M/S 314-6, Pasadena, CA 91125, USA*

Користећи најбоље расположиве спектроскопске константе за основно $X^1\Sigma_g^+$и побуђено $D^1\Sigma_u^+$стање Ag_2 молекула израчунате су Ридберг–Клајн–Рисове (РКР) потенцијалне криве за оба електронска стања, на којима је засновано израчунавање Франк–Кондонових (ФК) фактора и положаја почетака *D-X* трака. Поменути параметри израчунати су за три изотопна двоатомска молекула, $^{107}Ag_2$, $^{107}Ag^{109}Ag$ и $^{109}Ag_2$, увек присутна у парној фази природног сребра на високим температурама, који је смеша два изотопа: ^{107}Ag (≈51,5 %) и ^{109}Ag (≈48,5 %). Добијене вредности упоређене су са расподелом релативних интензитета трака у експерименталном спектру. Утврђено је да појава интензивних *D-X* трака $\Delta v = 0$ секвенције и много слабијих трака секвенција Δv од 1 до 4, као и њихови релативни интензитети следе предвиђену расподелу интензитета на основу ФК фактора и фреквенција прелаза. Слагање изотопских померања израчунатих почетака трака изотопних молекула и померања раније измерених чела трака додатно су потврдили исправност наших РКР-израчунавања. Односи ФК фактора мање обилних изотопних молекула, $^{107}Ag_2$ и $^{109}Ag_2$, и ФК фактора обилнијег изотопа, $^{107}Ag^{109}Ag$, врло блиских јединици, указали су да изотопска замена има занемарљиво мали ефекат на вредности ФК фактора Ag_2 *D-X* трака.

(Примљено 8. јуна 2009, ревидирано 1. фебруара 2010)

REFERENCES

1. J. Ruamps, *C. R. Acad. Sci.* **238** (1954) 1489
2. B. Kleman, S. Lindkvist, *Ark. Fys.* **9** (1955) 385
3. J. Ruamps, *Ann. Phys. Paris* **4** (1959) 1111
4. C. M. Brown, M. L. Ginter, *J. Mol. Spectrosc*. **69** (1978) 25
5. V. I. Srdanov, D. S. Pešić, *Bull. Soc. Chim. Belgrade* **44** (1979) 281
6. D. S. Pešić, V. I. Srdanov, *J. Mol. Spectrosc*. **90** (1981) 27
7. B. Simmard, P. A. Hackett, A. M. James, P. R. Langridge-Smith, *Chem. Phys Lett.* **186** (1991) 415
8. H. G. Kramer, V. Beutel, K. Weyers, W. Demtroder, *Chem. Phys. Lett.* **193** (1992) 331
9. V. Beutel, H. G. Kramer, G. L. Bhale, M. Kuhn, K. Weyers, W. Demtroder, *J. Chem. Phys.* **98** (1993) 2699
10. G. A. Ozin, H. Huber, *Inorg. Chem.* **17** (1979) 155
11. S. A. Mitchell, G. A. Kenney-Wallace, G. A. Ozin, *J. Am. Chem. Soc*. **103** (1981) 6030
12. R. Ginter, *Chem. Phys*. **102** (1986) 187
13. M. D. Morse, *Chem. Rev*. **86** (1986) 1049
14. T. Hebert, H. Wiggenbauser, D. M. Kolb, *J. Chem. Phys*. **91** (1989) 1417
15. L. König, I. Rabin, W. Schulze, G. Ertl, *Science* **276** (1996) 1353

16. I. Rabin, W. Schulze, G. Ertl, *J. Chem. Phys.* **108** (1998) 5137
17. B. R. Vujisić, D. S. Pešić, *Spectrosc. Lett.* 23 (1990) 1081
18. P. A. Freser, *Can. J. Phys.* **32** (1954) 515
19. R. W. Nicholls, W. R. Jermain, *Proc. Phys. Soc.* **LXIX 3-A** (1955) 253
20. D. S. Pešić, B. R. Vujisić, *J. Mol. Spectrosc.* 146 (1991) 516
21. M. Kuzmanović, M. A. Khakoo, V. Bojović, A. Antić-Jovanović, *Russ. J. Phys. Chem.* **81** (2007) 1438
22. A. Antić-Jovanović, M. Kuzmanović, V. Bojović, M. A. Khakoo, R. R. Laher, *Chinese Phys. Lett*. **24** (2007) 2566
23. R. R. Laher, M. A. Khakoo, A. Antić-Jovanović, *J. Mol. Spectrosc*. **248** (2008) 111
24. A. Antić-Jovanović, M. Kuzmanović, V. Bojović, M. A. Khakoo, R. R. Laher (2009), submitted to Journal of Atomic, Molecular and Optical Physics
25. M. Halmann, I. Laulicht, *J. Chem. Phys*. **44** (1966) 2398
26. N. E. Kuz'menko, L. A. Kiznecova, Y. Y. Kuzjakov, *Frank–Condon Factors of two-atom molecules*, MGU, Moscow, 1984 (in Russian)
27. G. Herzberg, *Spectra of diatomic molecules*, Van Nostrand-Reinhold, New York, 1951
28. F. R. Gilmore, R. R. Laher, P. J. Espy, *J. Phys Chem. Ref. Data* **21** (1992)1005.

Journal of the Serbian Chemical Society
JSCS@tmf.bg.ac.rs • www.shd.org.rs/JSCS
J. Serb. Chem. Soc. 75 (5) S11–S22 (2010) UDC 546.57.027:534.1/.2:539.2
JSCS–3996 *Supplementary material*

SUPPLEMENTARY MATERIAL TO

Franck–Condon factors and observed band strength distribution in the vibrational structure of the Ag_2 *D*-*X* band system

ANKICA ANTIĆ-JOVANOVIĆ[1*#], MILOŠ MOMČILOVIĆ[1], VOJISLAV BOJOVIĆ[1], MURTADHA A. KHAKOO[2] and RUSS R. LAHER[3]

[1]Faculty of Physical Chemistry, University of Belgrade, P. O. Box 47, 11158 Belgrade, Serbia, [2]Department of Physics, California State University Fullerton, CA 92834 and [3]Spitzer Science Center, California Institute of Technology, M/S 314-6, Pasadena, CA 91125, USA

J. Serb. Chem. Soc. 75 (5) 659–667 (2010)

TABLE I. Band-origin wavenumbers in cm^{-1} and FCFs for the $D1\Sigma u+ - X1\Sigma g+$ bands of 107Ag2, 107Ag109Ag and 109Ag2 (wavenumbers of the origins of the (0,0), (1,1), (2,2), (3,3) and (4,4) bands reported in Ref. 4 are: 39002.2, 38977.2, 38951.1, 38923.6 and 38894.4 cm^{-1}, respectively)

v'/v''	0	1	2	3	4	5	6
			0				
			ν_0 / cm^{-1}				
$^{107}Ag^{109}Ag$	39002.11	38810.99	38621.16	38432.61	38245.34	38059.35	37874.64
$^{107}Ag_2$	39002.05	38810.06	38619.36	38429.96	38241.85	38055.03	37869.49
$^{109}Ag_2$	39002.17	38811.93	38622.97	38435.28	38248.86	38063.70	37879.82
			FCFs				
$^{107}Ag^{109}Ag$	9.9416E–1	3.6158E–3	2.2152E–3	2.3866E–7	9.1935E–6	1.7943E–7	9.4644E–8
$^{107}Ag_2$	9.9414E–1	3.6365E–3	2.2146E–3	2.4550E–7	9.1849E–6	1.7964E–7	9.4733E–8
$^{109}Ag_2$	9.9400E–1	3.7753E–3	2.2153E–3	3.6381E–7	9.1155E–6	1.6912E–7	9.2336E–8
			1				
			ν_0 / cm^{-1}				
$^{107}Ag^{109}Ag$	39167.90	38976.79	38786.96	38598.41	38411.14	38225.14	38040.43
$^{107}Ag_2$	39168.60	38976.61	38785.91	38596.51	38408.40	38221.58	38036.04
$^{109}Ag_2$	39167.20	38976.97	38788.01	38600.32	38413.89	38228.74	38044.85
			FCFs				
$^{107}Ag^{109}Ag$	4.1626E–3	9.7813E–1	1.0452E–2	7.1925E–3	1.0020E–5	4.9550E–5	7.0147E–7
$^{107}Ag_2$	4.1862E–3	9.7805E–1	1.0513E–2	7.1930E–3	1.0148E–5	4.9517E–5	7.0166E–7
$^{109}Ag_2$	4.3427E–3	9.7759E–1	1.0804E–2	7.1970E–3	1.1467E–5	4.9227E–5	6.5526E–7

* Corresponding author. E-mail: ankica@ffh.bg.ac.rs
# Serbian Chemical Society member.

TABLE I-S. Continued

v'/v''	0	1	2	3	4	5	6
				2			
				ν_0 / cm^{-1}			
$^{107}Ag^{109}Ag$	39331.29	39140.18	38950.35	38761.80	38574.53	38388.54	38203.82
$^{107}Ag_2$	39332.73	39140.74	38950.04	38760.64	38572.53	38385.70	38200.17
$^{109}Ag_2$	39329.86	39139.62	38950.66	38762.97	38576.55	38391.39	38207.51
				FCFs			
$^{107}Ag^{109}Ag$	1.5542E–3	1.3464E–2	9.4843E–1	2.0726E–2	1.5583E–2	7.3186E–5	1.6288E–4
$^{107}Ag_2$	1.550E3–3	1.3541E–2	9.4823E–1	2.0846E–2	1.5589E–2	7.3923E–5	1.6284E–4
$^{109}Ag_2$	1.5328E–3	1.3907E–2	9.4744E–1	2.1275E–2	1.5597E–2	7.9038E–5	1.6199E–4
				3			
				ν_0 / cm^{-1}			
$^{107}Ag^{109}Ag$	39492.29	39301.17	39111.34	38922.79	38735.52	38549.53	38364.81
$^{107}Ag_2$	39494.44	39302.44	39111.75	38922.34	38734.23	38547.41	38361.88
$^{109}Ag_2$	39490.13	39299.90	39110.94	38923.25	38736.82	38551.67	38367.78
				FCFs			
$^{107}Ag^{109}Ag$	1.2340E–4	4.1802E–3	2.9945E–2	9.0288E–1	3.4075E–2	2.8062E–2	2.9612E–4
$^{107}Ag_2$	1.2382E–4	4.1658E–3	3.0114E–2	9.0251E–1	3.4272E–2	2.8083E–2	2.9880E–4
$^{109}Ag_2$	1.2438E–4	4.1121E–3	3.0717E–2	9.0141E–1	3.4800E–2	2.8092E–2	3.1146E–4
				4			
				ν_0 / cm^{-1}			
$^{107}Ag^{109}Ag$	39650.87	39459.76	39269.93	39081.38	38894.11	38708.12	38523.40
$^{107}Ag_2$	39653.72	39461.73	39271.03	39081.63	38893.52	38706.70	38521.17
$^{109}Ag_2$	39648.03	39457.80	39268.83	39081.14	38894.72	38709.56	38525.68
				FCFs			
$^{107}Ag^{109}Ag$	1.7837E–8	6.0355E–4	7.1447E–3	5.5441E–2	8.4026E–1	4.9485E–2	4.5217E–2
$^{107}Ag_2$	2.1241E–8	6.0549E–4	7.1103E–3	5.5748E–2	8.3965E–1	4.9766E–2	4.5263E–2
$^{109}Ag_2$	2.7485E–8	6.0653E–4	7.0069E–3	5.6578E–2	8.3833E–1	5.0339E–2	4.5252E–2
				5			
				ν_0 / cm^{-1}			
$^{107}Ag^{109}Ag$	39807.06	39615.95	39426.12	39237.57	39050.30	38864.31	38679.59
$^{107}Ag_2$	39810.59	39618.60	39427.90	39238.50	39050.39	38863.56	38678.03
$^{109}Ag_2$	39803.55	39613.31	39424.35	39236.66	39050.24	38865.08	38681.20
				FCFs			
$^{107}Ag^{109}Ag$	4.0384E–7	1.5698E–6	1.7843E–3	9.5640E–3	9.1202E–2	7.6068E–1	6.5298E–2
$^{107}Ag_2$	4.0146E–7	1.6523E–6	1.7895E–3	9.4987E–3	9.1692E–2	7.5979E–1	6.5655E–2
$^{109}Ag_2$	3.9588E–7	1.7547E–6	1.7884E–3	9.3434E–3	9.2701E–2	7.5838E–1	6.6201E–2
				6			
				ν_0 / cm^{-1}			
$^{107}Ag^{109}Ag$	39960.85	39769.74	39579.91	39391.36	39204.09	39018.10	38833.38
$^{107}Ag_2$	39965.04	39773.04	39582.35	39392.94	39204.83	39018.01	38832.48
$^{109}Ag_2$	39956.69	39766.45	39577.49	39389.80	39203.38	39018.22	38834.34

TABLE I-S. Continued

v'/v''	0	1	2	3	4	5	6
			6				
			FCFs				
$^{107}Ag^{109}Ag$	2.8789E–8	2.3924E–6	1.6219E–5	4.0827E–3	1.0590E–2	1.3746E–1	6.6593E–1
$^{107}Ag_2$	2.8955E–8	2.3727E–6	1.6752E–5	4.0928E–3	1.0486E–2	1.3816E–1	6.6473E–1
$^{109}Ag_2$	2.8922E–8	2.3351E–6	1.7201E–5	4.0825E–3	1.0292E–2	1.3927E–1	6.6343E–1
			7				
			ν_0 / cm^{-1}				
$^{107}Ag^{109}Ag$	40112.24	39921.13	39731.29	39542.75	39355.48	39169.49	38984.77
$^{107}Ag_2$	40117.06	39925.07	39734.37	39544.97	39356.86	39170.04	38984.51
$^{109}Ag_2$	40107.45	39917.22	39728.26	39540.56	39354.14	39168.98	38985.10
			FCFs				
$^{107}Ag^{109}Ag$	4.0775E–11	2.9622E–7	7.6689E–6	8.5869E–5	7.9027E–3	9.6717E–3	1.9298E–1
$^{107}Ag_2$	4.4198E–11	2.9770E–7	7.5793E–6	8.8010E–5	7.9175E–3	9.5282E–3	1.9391E–1
$^{109}Ag_2$	4.8857E–11	2.9604E–7	7.4464E–6	8.9088E–5	7.8851E–3	9.3252E–3	1.9497E–1
			8				
			ν_0 / cm^{-1}				
$^{107}Ag^{109}Ag$	40261.23	40070.11	39880.28	39691.73	39504.46	39318.47	39133.76
$^{107}Ag_2$	40266.67	40074.67	39883.98	39694.57	39506.46	39319.64	39134.11
$^{109}Ag_2$	40255.83	40065.76	39876.64	39688.95	39502.52	39317.37	39133.48
			FCFs				
$^{107}Ag^{109}Ag$	5.4023E–11	2.4622E–9	1.6238E–6	1.6979E–5	3.1759E–4	1.3499E–2	6.8577E–3
$^{107}Ag_2$	5.3659E–11	2.5648E–9	1.6302E–6	1.6692E–5	3.2409E–4	1.3513E–2	6.6923E–3
$^{109}Ag_2$	5.1421E–11	2.6265E–9	1.6159E–6	1.6376E–5	3.2545E–4	1.3441E–2	6.5245E–3
			9				
			ν_0 / cm^{-1}				
$^{107}Ag^{109}Ag$	40407.82	40216.70	40026.87	39838.32	39651.05	39465.06	39280.35
$^{107}Ag_2$	40413.85	40221.86	40031.16	39841.76	39653.65	39466.83	39281.29
$^{109}Ag_2$	40401.84	40211.60	40022.64	39834.95	39648.53	39463.37	39279.49
			FCFs				
$^{107}Ag^{109}Ag$	1.3094E–12	4.4891E–10	3.4203E–8	6.2887E–6	2.7559E–5	9.3070E–4	2.0807E–2
$^{107}Ag_2$	1.3265E–12	4.4131E–10	3.5248E–8	6.3058E–6	2.6853E–5	9.4697E–4	2.0807E–2
$^{109}Ag_2$	1.2777E–12	4.2218E–10	3.5342E–8	6.2354E–6	2.6316E–5	9.4606E–4	2.0676E–2
			10				
			ν_0 / cm^{-1}				
$^{107}Ag^{109}Ag$	40552.00	40360.89	40171.06	39982.51	39795.24	39609.25	39424.53
$^{107}Ag_2$	40558.62	40366.62	40175.90	39986.52	39798.41	39611.59	39426.06
$^{109}Ag_2$	40545.46	40355.23	40166.27	39978.56	39792.16	39607.00	39423.12
			FCFs				
$^{107}Ag^{109}Ag$	6.3339E–13	4.4600E–11	1.5572E–9	2.5729E–7	1.9170E–5	3.1446E–5	2.3047E–3
$^{107}Ag_2$	6.4400E–13	4.4829E–11	1.5017E–9	2.6370E–7	1.9191E–5	3.0113E–5	2.3397E–3
$^{109}Ag_2$	6.1430E–13	4.3337E–11	1.4318E–9	2.6172E–7	1.8946E–5	2.9492E–5	2.3280E–3

TABLE I-S. Continued

v'/v''	0	1	2	3	4	5	6
			11				
			ν_0 / cm^{-1}				
$^{107}Ag^{109}Ag$	40693.79	40502.68	40312.85	40124.30	39937.03	39751.04	39566.32
$^{107}Ag_2$	40700.96	40508.97	40318.27	40128.87	39940.76	39753.94	39568.40
$^{109}Ag_2$	40686.71	40496.48	40307.52	40119.83	39933.40	39748.25	39564.37
			FCFs				
$^{107}Ag^{109}Ag$	2.0755E–13	2.3530E–12	4.6084E–10	2.2871E–9	1.3371E–6	4.8567E–5	1.9692E–5
$^{107}Ag_2$	2.1710E–13	2.3877E–12	4.6076E–10	2.0920E–9	1.3655E–6	4.8520E–5	1.7965E–5
$^{109}Ag_2$	2.0106E–13	2.2625E–12	4.4573E–10	1.9795E–9	1.3473E–6	4.7853E–5	1.7567E–5
			12				
			ν_0 / cm^{-1}				
$^{107}Ag^{109}Ag$	40833.18	40642.06	40452.23	40263.68	40076.41	39890.42	39705.71
$^{107}Ag_2$	40840.88	40648.89	40458.20	40268.79	40080.68	39893.86	39708.33
$^{109}Ag_2$	40825.58	40635.35	40446.39	40258.70	40072.27	39887.12	39703.24
			FCFs				
$^{107}Ag^{109}Ag$	2.9055E–15	3.2095E–12	6.0764E–13	2.8550E–9	1.0253E–11	5.3902E–6	1.0533E–4
$^{107}Ag_2$	3.6157E–15	3.3225E–12	6.1062E–13	2.8392E–9	2.5195E–11	5.4890E–6	1.0495E–4
$^{109}Ag_2$	2.6965E–15	3.1121E–12	5.4329E–13	2.7483E–9	1.8188E–11	5.3958E–6	1.0341E–4
			13				
			ν_0 / cm^{-1}				
$^{107}Ag^{109}Ag$	40970.17	40779.05	40589.22	40400.67	40213.40	40027.41	39842.70
$^{107}Ag_2$	40978.39	40786.40	40595.70	40406.30	40218.18	40031.36	39845.83
$^{109}Ag_2$	40962.08	40771.84	40582.88	40395.19	40208.77	40023.61	39839.73
			FCFs				
$^{107}Ag^{109}Ag$	5.1114E–16	3.8581E–13	1.6432E–11	3.9492E–11	1.2119E–8	2.1381E–8	1.7931E–5
$^{107}Ag_2$	4.2185E–16	4.1490E–13	1.6939E–11	4.0094E–11	1.1970E–8	2.4722E–8	1.8214E–5
$^{109}Ag_2$	5.1247E–16	3.7086E–13	1.5863E–11	3.9152E–11	1.1606E–8	2.4084E–8	1.7900E–5
			14				
			ν_0 / cm^{-1}				
$^{107}Ag^{109}Ag$	41104.75	40913.64	40723.81	40535.28	40347.99	40162.00	39977.28
$^{107}Ag_2$	41113.47	40921.48	40730.78	40541.38	40353.27	40166.45	39980.92
$^{109}Ag_2$	41096.19	40905.96	40716.99	40529.30	40342.88	40157.72	39973.84
			FCFs				
$^{107}Ag^{109}Ag$	1.0469E–15	1.8575E–17	2.8457E–12	4.5915E–11	7.8835E–10	3.7719E–8	2.9638E–7
$^{107}Ag_2$	1.0610E–15	1.8756E–16	3.0359E–12	4.7056E–11	7.9716E–10	3.6895E–8	3.2024E–7
$^{109}Ag_2$	1.0404E–15	8.5242E–19	2.7415E–12	4.4044E–11	7.7003E–10	3.5897E–8	3.1105E–7
			15				
			ν_0 / cm^{-1}				
$^{107}Ag^{109}Ag$	41236.94	41045.83	40856.00	40667.45	40480.18	40294.20	40109.47
$^{107}Ag_2$	41246.14	41054.15	40863.45	40674.05	40485.93	40299.11	40113.58
$^{109}Ag_2$	41227.93	41037.69	40848.73	40661.04	40474.62	40289.46	40105.58
			FCFs				
$^{107}Ag^{109}Ag$	2.5699E–15	2.0713E–14	1.6784E–16	1.6100E–11	5.9965E–11	6.2840E–9	8.7173E–8
$^{107}Ag_2$	2.5665E–15	2.0428E–14	1.3919E–15	1.6974E–11	6.0876E–11	6.3305E–9	8.3939E–8
$^{109}Ag_2$	2.5072E–15	2.0414E–14	5.1069E–17	1.5475E–11	5.6757E–11	6.1057E–9	8.4409E–8

TABLE I-S. Continued

v'/v''	7	8	9	10
		0		
		ν_0 / cm^{-1}		
$^{107}Ag^{109}Ag$	37691.21	37509.04	37328.14	37148.51
$^{107}Ag_2$	37685.26	37502.29	37320.61	37140.20
$^{109}Ag_2$	37697.19	37515.82	37335.71	37156.85
		FCFs		
$^{107}Ag^{109}Ag$	1.0115E–8	2.4440E–9	4.6757E-10	1.1121E–10
$^{107}Ag_2$	1.0160E–8	2.4570E–9	4.7137E–10	1.1230E–10
$^{109}Ag_2$	9.7111E–9	2.3571E–9	4.4814E–10	1.0646E–10
		1		
		ν_0 / cm^{-1}		
$^{107}Ag^{109}Ag$	37857.00	37674.83	37493.93	37314.30
$^{107}Ag_2$	37851.83	37668.84	37487.16	37306.75
$^{109}Ag_2$	37862.22	37680.85	37500.74	37321.88
		FCFs		
$^{107}Ag^{109}Ag$	6.5187E–7	6.8620E–8	2.0323E–8	4.1707E–9
$^{107}Ag_2$	6.5234E–7	6.8909E–8	2.0422E–8	4.2029E–9
$^{109}Ag_2$	6.3795E–7	6.5818E–8	1.9629E–8	3.9991E–9
		2		
		ν_0 / cm^{-1}		
$^{107}Ag^{109}Ag$	38020.39	37838.22	37657.32	37477.69
$^{107}Ag_2$	38015.93	37832.97	37651.28	37470.88
$^{109}Ag_2$	38024.88	37843.51	37663.39	37484.54
		FCFs		
$^{107}Ag^{109}Ag$	1.3736E–6	2.6254E–6	2.5781E–7	9.4377E–8
$^{107}Ag_2$	1.3718E–6	2.6272E–6	2.5882E–7	9.4798E–8
$^{109}Ag_2$	1.2532E–6	2.5754E–6	2.4691E–7	9.1294E–8
		3		
		ν_0 / cm^{-1}		
$^{107}Ag^{109}Ag$	38181.38	37999.21	37818.31	37638.68
$^{107}Ag_2$	38177.64	37994.67	37812.99	37632.59
$^{109}Ag_2$	38185.15	38003.78	37823.67	37644.81
		FCFs		
$^{107}Ag^{109}Ag$	4.2201E–4	1.4958E–6	8.1025E–6	6.9989E–7
$^{107}Ag_2$	4.2208E–4	1.4878E–6	8.1081E–6	7.0248E–7
$^{109}Ag_2$	4.2053E–4	1.3001E–6	7.9664E–6	6.6878E–7
		4		
		ν_0 / cm^{-1}		
$^{107}Ag^{109}Ag$	38339.97	38157.80	37976.90	37797.27
$^{107}Ag_2$	38336.93	38153.96	37972.28	37791.88
$^{109}Ag_2$	38343.05	38161.68	37981.57	37802.71

TABLE I-S. Continued

v'/v''	7	8	9	10
		4		
		FCFs		
$^{107}Ag^{109}Ag$	8.7347E–4	9.4741E–4	5.2799E–7	2.1304E–5
$^{107}Ag_2$	8.8090E–4	9.4805E–4	5.1575E–7	2.1322E–5
$^{109}Ag_2$	9.0736E–4	9.4505E–4	3.6822E–7	2.0993E–5
		5		
		ν_0 / cm^{-1}		
$^{107}Ag^{109}Ag$	38496.16	38313.99	38133.09	37953.46
$^{107}Ag_2$	38493.79	38310.83	38139.14	37948.74
$^{109}Ag_2$	38498.57	38317.20	38137.08	37958.23
		FCFs		
$^{107}Ag^{109}Ag$	6.7365E–2	2.1083E–3	1.9270E–3	4.1798E–7
$^{107}Ag_2$	6.7451E–2	2.1257E–3	1.9294E–3	4.4132E–7
$^{109}Ag_2$	6.7414E–2	2.1705E–3	1.9236E–3	6.5563E–7
		6		
		ν_0 / cm^{-1}		
$^{107}Ag^{109}Ag$	38649.95	38467.78	38286.88	38107.25
$^{107}Ag_2$	38648.24	38465.27	38283.59	38103.20
$^{109}Ag_2$	38651.71	38470.34	38290.23	38111.37
		FCFs		
$^{107}Ag^{109}Ag$	7.9326E–2	9.4400E–2	4.4054E–3	3.6400E–3
$^{107}Ag_2$	7.9735E–2	9.4538E–2	4.4411E–3	3.6465E–3
$^{109}Ag_2$	8.0230E–2	9.4437E–2	4.5072E–3	3.6352E–3
		7		
		ν_0 / cm^{-1}		
$^{107}Ag^{109}Ag$	38801.34	38619.17	38438.27	38258.64
$^{107}Ag_2$	38800.26	38617.30	38435.62	38255.22
$^{109}Ag_2$	38802.47	38621.10	38440.99	38262.13
		FCFs		
$^{107}Ag^{109}Ag$	5.5968E–1	8.9165E–2	1.2552E–1	8.2379E–3
$^{107}Ag_2$	5.5818E–1	8.9585E–2	1.2572E–1	8.3036E–3
$^{109}Ag_2$	5.5706E–1	8.9987E–2	1.2551E–1	8.3893E–3
		8		
		ν_0 / cm^{-1}		
$^{107}Ag^{109}Ag$	38950.33	38768.16	38587.26	38407.63
$^{107}Ag_2$	38949.87	38766.91	38585.22	38404.82
$^{109}Ag_2$	38950.85	38769.48	38589.37	38410.52
		FCFs		
$^{107}Ag^{109}Ag$	2.5472E–1	4.4725E–1	9.2560E–2	1.5909E–1
$^{107}Ag_2$	2.5584E–1	4.4550E–1	9.2936E–2	1.5934E–1
$^{109}Ag_2$	2.5681E–1	4.4474E–1	9.3245E–2	1.5900E–1

TABLE I-S. Continued

v'/v''	7	8	9	10
		9		
		ν_0 / cm^{-1}		
$^{107}Ag^{109}Ag$	39096.91	38914.74	38733.85	38554.22
$^{107}Ag_2$	39097.05	38914.09	38732.41	38552.00
$^{109}Ag_2$	39096.86	38915.49	38735.38	38556.52
		FCFs		
$^{107}Ag^{109}Ag$	3.0731E–3	3.1780E–1	3.3549E–1	8.7994E–2
$^{107}Ag_2$	2.9284E–3	3.1901E–1	3.3362E–1	8.8267E–2
$^{109}Ag_2$	2.8226E–3	3.1980E–1	3.3328E–1	8.8514E–2
		10		
		ν_0 / cm^{-1}		
$^{107}Ag^{109}Ag$	39241.10	39058.93	38878.03	38698.40
$^{107}Ag_2$	39241.82	39058.85	38877.17	38696.77
$^{109}Ag_2$	39240.49	39059.11	38879.00	38700.15
		FCFs		
$^{107}Ag^{109}Ag$	2.9285E–2	2.5077E–4	3.7559E–1	2.3185E–1
$^{107}Ag_2$	2.9245E–2	2.0070E–4	3.7676E–1	2.3000E–1
$^{109}Ag_2$	2.9049E–2	1.7845E–4	3.7736E–1	2.3006E–1
		11		
		ν_0 / cm^{-1}		
$^{107}Ag^{109}Ag$	39382.89	39200.72	39019.82	38840.19
$^{107}Ag_2$	39384.16	39201.20	39019.52	38839.11
$^{109}Ag_2$	39381.73	39200.36	39020.25	38841.40
		FCFs		
$^{107}Ag^{109}Ag$	5.0032E–3	3.7826E–2	1.2614E–3	4.2055E–1
$^{107}Ag_2$	5.0695E–3	3.7707E–2	1.4097E–3	4.2149E–1
$^{109}Ag_2$	5.0347E–3	3.7453E–2	1.4499E–3	4.2198E–1
		12		
		ν_0 / cm^{-1}		
$^{107}Ag^{109}Ag$	39522.28	39340.11	39159.21	38979.58
$^{107}Ag_2$	39524.09	39341.12	39159.44	38979.04
$^{109}Ag_2$	39520.60	39339.23	39159.12	38980.27
		FCFs		
$^{107}Ag^{109}Ag$	6.0827E–7	9.7515E–3	4.4813E–2	9.4610E–3
$^{107}Ag_2$	2.2017E–7	9.8633E–3	4.4566E–2	9.9287E–3
$^{109}Ag_2$	2.2334E–7	9.7792E–3	4.4285E–2	9.9637E–3
		13		
		ν_0 / cm^{-1}		
$^{107}Ag^{109}Ag$	39659.26	39477.09	39296.19	39116.56
$^{107}Ag_2$	39661.59	39478.63	39296.94	39116.54
$^{109}Ag_2$	39657.10	39475.73	39295.61	39116.76

TABLE I-S. Continued

v'/v''	7	8	9	10
		13		
		FCFs		
$^{107}Ag^{109}Ag$	1.9829E–4	4.1910E–5	1.7306E–2	4.8389E–2
$^{107}Ag_2$	1.9686E–4	4.8085E–5	1.7474E–2	4.7968E–2
$^{109}Ag_2$	1.9423E–4	4.6745E–5	1.7307E–2	4.7722E–2
		14		
		ν_0 / cm^{-1}		
$^{107}Ag^{109}Ag$	39793.85	39611.68	39430.78	39251.15
$^{107}Ag_2$	39796.68	39613.71	39432.027	39251.63
$^{109}Ag_2$	39791.21	39609.84	39429.73	39250.87
		FCFs		
$^{107}Ag^{109}Ag$	5.1135E–5	3.2535E–4	3.4282E–4	2.8225E–2
$^{107}Ag_2$	5.1816E–5	3.2145E–4	3.6733E–4	2.8446E–2
$^{109}Ag_2$	5.0745E–5	3.1766E–4	3.5768E–4	2.8163E–2
		15		
		ν_0 / cm^{-1}		
$^{107}Ag^{109}Ag$	39926.04	39743.87	39562.97	39383.34
$^{107}Ag_2$	39929.34	39746.38	39564.69	39384.29
$^{109}Ag_2$	39922.95	39741.58	39561.47	39382.61
		FCFs		
$^{107}Ag^{109}Ag$	1.8942E–6	1.2774E–4	4.6041E–4	1.3308E–3
$^{107}Ag_2$	2.0026E–6	1.2912E–4	4.5171E–4	1.3955E–3
$^{109}Ag_2$	1.9287E–6	1.2637E–4	4.4783E–4	1.3598E–3

v'/v''	11	12	13	14	15	16	17
				7			
				ν_0 / cm^{-1}			
$^{107}Ag^{109}Ag$	38080.28	37903.19	37727.36	37552.80	37379.50	37207.45	37036.66
$^{107}Ag_2$	38076.09	37898.26	37721.69	37546.40	37372.38	37199.64	37028.16
$^{109}Ag_2$	38084.53	37908.20	37733.11	37559.28	37386.69	37215.35	37045.26
				FCFs			
$^{107}Ag^{109}Ag$	6.4776E–3	5.8373E–5	2.2843E–4	5.0418E–6	1.1708E–5	2.0874E–6	1.1209E–6
$^{107}Ag_2$	6.4928E–3	5.9253E–5	2.2890E–4	5.0426E–6	1.1749E–5	2.1003E–6	1.1289E–6
$^{109}Ag_2$	6.4704E–3	6.2454E–5	2.2633E–4	4.6766E–6	1.1432E–5	1.9987E–6	1.0808E–6
				8			
				ν_0 / cm^{-1}			
$^{107}Ag^{109}Ag$	38229.264	38052.18	37876.35	37701.80	37528.49	37356.44	37185.65
$^{107}Ag_2$	38225.70	38047.86	37871.30	37696.01	37521.99	37349.24	37177.76
$^{109}Ag_2$	38232.92	38056.59	37881.50	37707.66	37535.08	37363.74	37193.64
				FCFs			
$^{107}Ag^{109}Ag$	1.4065E–2	1.0950E–2	2.0163E–4	4.5232E–4	4.6287E–6	2.4131E–5	3.6875E–6
$^{107}Ag_2$	1.4175E–2	1.0981E–2	2.0427E–4	4.5353E–4	4.6127E–6	2.4217E–5	3.7091E–6
$^{109}Ag_2$	1.4272E–2	1.0937E–2	2.1066E–4	4.4874E–4	4.1764E–6	2.3611E–5	3.5254E–6

TABLE I-S. Continued

v'/v''	11	12	13	14	15	16	17
				9			
				ν_0 / cm^{-1}			
$^{107}Ag^{109}Ag$	38375.85	38198.77	38022.94	37848.38	37675.07	37503.03	37332.24
$^{107}Ag_2$	38372.88	38195.05	38018.48	37843.19	37669.17	37496.43	37324.95
$^{109}Ag_2$	38378.92	38202.59	38027.50	37853.67	37681.08	37509.74	37339.65
				FCFs			
$^{107}Ag^{109}Ag$	1.9253E–1	2.2189E–2	1.7684E–2	5.5039E–4	8.6242E–4	2.3327E–6	4.8032E–5
$^{107}Ag_2$	1.9281E–1	2.2359E–2	1.7743E–2	5.5707E–4	8.6527E–4	2.2988E–6	4.8214E–5
$^{109}Ag_2$	1.9233E–1	2.2451E–2	1.7662E–2	5.6757E–4	8.5643E–4	1.9363E–6	4.7093E–5
				10			
				ν_0 / cm^{-1}			
$^{107}Ag^{109}Ag$	38520.04	38342.96	38167.13	37992.56	37819.26	37647.22	37476.43
$^{107}Ag_2$	38517.65	38339.81	38163.25	37987.96	37813.94	37641.19	37469.71
$^{109}Ag_2$	38522.55	38346.22	38171.13	37997.29	37824.77	37653.37	37483.27
				FCFs			
$^{107}Ag^{109}Ag$	7.5260E–2	2.2242E–1	3.2615E–2	2.7360E–2	1.2878E–3	1.5896E–3	7.9356E–9
$^{107}Ag_2$	7.5386E–2	2.2267E–1	3.2855E–2	2.7460E–2	1.3027E–3	1.5959E–3	4.2198E–9
$^{109}Ag_2$	7.5618E–2	2.2208E–1	3.2924E–2	2.7318E–2	1.3170E–3	1.5797E–3	5.8962E–9
				11			
				ν_0 / cm^{-1}			
$^{107}Ag^{109}Ag$	38661.83	38484.74	38308.92	38134.35	37961.05	37789.00	37618.22
$^{107}Ag_2$	38659.98	38482.16	38305.59	38130.30	37956.28	37783.53	37612.05
$^{109}Ag_2$	38663.80	38487.46	38312.38	38138.54	37965.96	37794.62	37624.52
				FCFs			
$^{107}Ag^{109}Ag$	1.4332E–1	5.5944E–2	2.4482E–1	4.4820E–2	4.0602E–2	2.6880E–3	2.8379E–3
$^{107}Ag_2$	1.4167E–1	5.5910E–2	2.4497E–1	4.5134E–2	4.0761E–2	2.7182E–3	2.8511E–3
$^{109}Ag_2$	1.4202E–1	5.6170E–2	2.4433E–1	4.5162E–2	4.0526E–2	2.7332E–3	2.8214E–3
				12			
				ν_0 / cm^{-1}			
$^{107}Ag^{109}Ag$	38801.21	38624.13	38448.30	38273.74	38100.44	37928.39	37757.60
$^{107}Ag_2$	38799.91	38622.08	38445.52	38270.22	38096.21	37923.46	37751.98
$^{109}Ag_2$	38802.67	38626.44	38451.25	38277.41	38104.83	37933.49	37763.39
				FCFs			
$^{107}Ag^{109}Ag$	4.4534E–1	7.5243E–2	3.3569E–2	2.5580E–1	5.7636E–2	5.7804E–2	5.1181E–3
$^{107}Ag_2$	4.4583E–1	7.3933E–2	3.3413E–2	2.5576E–1	5.8008E–2	5.8039E–2	5.1740E–3
$^{109}Ag_2$	4.4639E–1	7.4422E–2	3.3703E–2	2.5518E–1	5.7991E–2	5.7675E–2	5.1823E–3
				13			
				ν_0 / cm^{-1}			
$^{107}Ag^{109}Ag$	38938.20	38761.12	38585.29	38410.73	38237.42	38065.38	37894.59
$^{107}Ag_2$	38937.42	38759.58	38583.02	38407.73	38233.71	38060.96	37889.48
$^{109}Ag_2$	38939.16	38762.83	38587.74	38413.90	38241.32	38069.98	37899.88

TABLE I-S. Continued

v'/v''	11	12	13	14	15	16	17
				13			
				FCFs			
$^{107}Ag^{109}Ag$	2.7898E–2	4.4434E–1	2.9987E–2	1.3347E–2	2.5227E–1	6.9215E–2	7.8888E–2
$^{107}Ag_2$	2.8796E–2	4.4419E–1	2.9131E–2	1.3160E–2	2.5195E–1	6.9609E–2	7.9206E–2
$^{109}Ag_2$	2.8722E–2	4.4503E–1	2.9564E–2	1.3422E–2	2.5159E–1	6.9565E–2	7.8682E–2
				14			
				ν_0 / cm^{-1}			
$^{107}Ag^{109}Ag$	39072.79	38895.71	38719.88	38545.32	38372.01	38199.96	38029.18
$^{107}Ag_2$	39072.50	38894.67	38718.10	38542.81	38368.79	38196.05	38024.57
$^{109}Ag_2$	39073.27	38896.94	38721.85	38548.02	38375.43	38204.09	38034.00
				FCFs			
$^{107}Ag^{109}Ag$	4.6967E–2	5.8209E–2	4.1516E–1	6.4559E–3	1.2802E–3	2.3288E–1	7.7215E–2
$^{107}Ag_2$	4.6349E–2	5.9601E–2	4.1426E–1	6.0704E–3	1.1960E–3	2.3223E–1	7.7572E–2
$^{109}Ag_2$	4.6211E–2	5.9305E–2	4.1561E–1	6.3077E–3	1.3060E–3	2.3221E–1	7.7550E–2
				15			
				ν_0 / cm^{-1}			
$^{107}Ag^{109}Ag$	39204.98	39027.82	38852.07	38677.50	38504.20	38332.15	38161.37
$^{107}Ag_2$	39205.17	39027.33	38850.77	38675.48	38501.46	38328.71	38157.23
$^{109}Ag_2$	39205.01	39028.68	38853.59	38679.76	38507.17	38335.83	38165.74
				FCFs			
$^{107}Ag^{109}Ag$	4.2534E–2	3.9902E–2	9.9603E–2	3.5991E–1	1.4988E–6	2.7456E–3	1.9878E–1
$^{107}Ag_2$	4.2781E–2	3.9109E–2	1.0146E–1	3.5828E–1	9.5897E–7	2.9082E–3	1.9779E–1
$^{109}Ag_2$	4.2362E–2	3.9141E–2	1.0088E–1	3.6025E–1	3.3826E–7	2.6984E–3	1.9822E–1

v'/v''	18	19	20	21
		7		
		ν_0 / cm^{-1}		
$^{107}Ag^{109}Ag$	36867.14	36698.86	36531.83	36366.06
$^{107}Ag_2$	36857.94	36688.99	36521.31	36354.90
$^{109}Ag_2$	36876.41	36708.80	36542.44	36377.32
		FCFs		
$^{107}Ag^{109}Ag$	3.7084E–7	1.5533E–7	6.1116E–8	2.5378E–8
$^{107}Ag_2$	3.7446E–7	1.5711E–7	6.1951E–8	2.5769E–8
$^{109}Ag_2$	3.5507E–7	1.4860E–7	5.8255E–8	2.4129E–8
		8		
		ν_0 / cm^{-1}		
$^{107}Ag^{109}Ag$	37016.12	36847.84	36680.82	36515.05
$^{107}Ag_2$	37007.55	36838.60	36670.92	36504.51
$^{109}Ag_2$	37024.79	36857.18	36690.82	36525.70
		FCFs		
$^{107}Ag^{109}Ag$	2.3811E–6	7.8391E–7	3.5361E–7	1.4392E–7
$^{107}Ag_2$	2.3974E–6	7.9137E–7	3.5753E–7	1.4583E–7
$^{109}Ag_2$	2.2993E–6	7.5075E–7	3.3858E–7	1.3727E–7

TABLE I-S. Continued

v'/v''	7	8	9	10
		9		
		ν_0 / cm^{-1}		
$^{107}Ag^{109}Ag$	37162.71	36994.43	36827.41	36661.64
$^{107}Ag_2$	37154.73	36985.79	36818.10	36651.69
$^{109}Ag_2$	37170.80	37003.19	36836.83	36671.71
		FCFs		
$^{107}Ag^{109}Ag$	5.9403E–6	4.8096E–6	1.5427E–6	7.5515E–7
$^{107}Ag_2$	5.9723E–6	4.8417E–6	1.5570E–6	7.6321E–7
$^{109}Ag_2$	5.6659E–6	4.6516E–6	1.4776E–6	7.2377E–7
		10		
		ν_0 / cm^{-1}		
$^{107}Ag^{109}Ag$	37306.90	37138.62	36971.60	36805.83
$^{107}Ag_2$	37299.45	37130.55	36962.87	36796.46
$^{109}Ag_2$	37314.42	37146.82	36980.45	36815.33
		FCFs		
$^{107}Ag^{109}Ag$	9.3125E–5	8.6832E–6	9.3480E–6	2.8471E–6
$^{107}Ag_2$	9.3513E–5	8.7243E–6	9.4088E–6	2.8728E–6
$^{109}Ag_2$	9.1478E–5	8.2529E–6	9.0562E–6	2.7267E–6
		11		
		ν_0 / cm^{-1}		
$^{107}Ag^{109}Ag$	37448.68	37280.41	37113.38	36947.62
$^{107}Ag_2$	37441.84	37272.89	37105.21	36938.80
$^{109}Ag_2$	37455.67	37288.07	37121.70	36956.58
		FCFs		
$^{107}Ag^{109}Ag$	6.3486E–6	1.7688E–4	1.1343E–5	1.7651E–5
$^{107}Ag_2$	6.5770E–6	1.7770E–4	1.1384E–5	1.7766E–5
$^{109}Ag_2$	7.3761E–6	1.7405E–4	1.0721E–5	1.7131E–5
		12		
		ν_0 / cm^{-1}		
$^{107}Ag^{109}Ag$	37588.07	37419.79	37252.77	37087.00
$^{107}Ag_2$	37581.77	37412.82	37245.14	37078.72
$^{109}Ag_2$	37594.54	37426.94	37260.57	37095.45
		FCFs		
$^{107}Ag^{109}Ag$	4.9102E–3	4.5232E–5	3.3019E–4	1.2796E–5
$^{107}Ag_2$	4.9360E–3	4.6269E–5	3.3193E–4	1.2817E–5
$^{109}Ag_2$	4.8827E–3	4.8302E–5	3.2539E–4	1.1984E–5
		13		
		ν_0 / cm^{-1}		
$^{107}Ag^{109}Ag$	37725.06	37556.78	37389.76	37223.99
$^{107}Ag_2$	37719.27	37550.32	37382.64	37216.23
$^{109}Ag_2$	37731.03	37563.43	37397.06	37231.94

TABLE I-S. Continued

v'/v''	7	8	9	10
		13		
		FCFs		
$^{107}Ag^{109}Ag$	9.0071E–3	8.2303E–3	1.6939E–4	6.0652E–4
$^{107}Ag_2$	9.1029E–3	8.2779E–3	1.7259E–4	6.1012E–4
$^{109}Ag_2$	9.0910E–3	8.1845E–3	1.7588E–4	5.9842E–4
		14		
		ν_0 / cm^{-1}		
$^{107}Ag^{109}Ag$	37859.65	37691.37	37524.34	37358.58
$^{107}Ag_2$	37854.35	37685.41	37517.73	37351.31
$^{109}Ag_2$	37865.15	37697.54	37531.18	37366.06
		FCFs		
$^{107}Ag^{109}Ag$	1.0303E–1	1.4766E–2	1.3350E–2	4.7992E–4
$^{107}Ag_2$	1.0342E–1	1.4918E–2	1.3433E–2	4.8812E–4
$^{109}Ag_2$	1.0273E–1	1.4867E–2	1.3274E–2	4.9140E–4
		15		
		ν_0 / cm^{-1}		
$^{107}Ag^{109}Ag$	37991.83	37823.56	37656.56	37490.77
$^{107}Ag_2$	37987.02	37818.07	37650.39	37483.98
$^{109}Ag_2$	37996.89	37829.28	37662.92	37497.80
		FCFs		
$^{107}Ag^{109}Ag$	7.9252E–2	1.2843E–1	2.2643E–2	2.0921E–2
$^{107}Ag_2$	7.9502E–2	1.2887E–1	2.2866E–2	2.1058E–2
$^{109}Ag_2$	7.9576E–2	1.2803E–1	2.2756E–2	2.0799E–2

Journal of the Serbian Chemical Society
JSCS@tmf.bg.ac.rs • www.shd.org.rs/JSCS

J. Serb. Chem. Soc. 75 (5) 669–679 (2010)
JSCS–RN3997

UDC 546.73'74'48'47+66–914.7:547.652:543.421
Original scientific paper

Preconcentration of Co, Ni, Cd and Zn on naphthalene–2,4,6-trimorpholino-1,3,5-triazin adsorbent and flame atomic absorption determination

TAYYEBEH MADRAKIAN*, MOHAMMAD ALI ZOLFIGOL and FATHEMEH ABOULGHAZI

Faculty of Chemistry, Bu-Ali Sina University, Hamadan 65174, Iran

(Received 4 April, revised 24 November 2009)

Abstract: A preconcentration method was developed for the determination of trace amounts of Co, Ni, Cd and Zn by atomic absorption spectrometry. The method is based on the retention of the metal cations by naphthalene–2,4,6-trimorpholino-1,3,5-triazin adsorbent in a column. The adsorbed metals were then eluted from the column with hydrochloric acid and the Co, Ni, Cd and Zn were determined by flame atomic absorption spectrometry. The optimal extraction and elution conditions were studied. The effects of diverse ions on the preconcentration were also investigated. A preconcentration factor of 250 for Co(II), Ni(II) and Zn(II), and 400 for Cd(II) can easily be achieved. Calibration graphs were obtained and the detection limits of the method for Co(II), Ni(II), Cd(II) and Zn(II) were 0.51, 0.49, 0.17 and 0.10 ng mL^{-1}, respectively. The relative standard deviations (*RSD*) of 0.37–2.31 % for Co, 0.37–3.73 % for Ni, 2.20–2.40 % for Cd and 1.50–2.56 % for Zn were obtained. The method was also used for the simultaneous preconcentration of these elements and the method was successfully applied to their preconcentration and determination. The method was applied to the determination of Co, Ni, Cd and Zn in several real samples.

Keywords: 2,4,6-trimorpholino-1,3,5-triazin; solid–liquid extraction; environmental samples; naphthalene.

INTRODUCTION

The determination of metal ions in natural samples such as waters, soils and biological fluids is a very important part of environmental and public health studies. However, the direct determination of metal ions at trace level is limited due to their low concentration and matrix interferences. Flame atomic absorption spectrometry (FAAS), which is often used for the determination of trace metal ions, suffers from insufficient sensitivity for the direct determination of metal

* Corresponding author. E-mail: madrakian@basu.ac.ir
doi: 10.2298/JSC090404032M

ions in environmental samples. Therefore, a preconcentration or separation step is frequently necessary to improve the detection limit and sensitivity. For this purpose, several separation and preconcentration procedures have been developed for trace metal ion determination involving different analytical strategies. To accomplish this task, solvent extraction, co-precipitation or solid phase preconcentration technique can be applied.

Solid phase extraction is a sensitive, fast and economic preconcentration method for traces of analyte ions in various materials, including natural waters, ores, biological samples, *etc*. Of all separation-enrichment separation procedures, solid phase extraction possesses several advantages: large preconcentration factors, simplicity of phase separation and suitability for automation.[1–3]

A variety of solid materials, such as modified ion exchange resins,[4–6] zeolites,[7] silica gel,[8] activated carbon,[9] C60–C70 fullerene[10] and microcrystalline naphthalene,[11–13] have been used for preconcentration of trace metals. It was shown that the type of employed support material is a critical factor in the performance of the resulting supported reagent or catalyst. Two main factors should be considered when employing a material as a support. First, the material needs to be stable both thermally and chemically during the reaction process. Secondly, the structure of the support needs to be such that the active sites are well dispersed on its surface and that these sites are easily accessible.

Solid–liquid extraction of metals with microcrystalline naphthalene is a very rapid and convenient method, which can be used for many types of metal complexes.[14–16] Under selected experimental conditions, the analyte can be adsorbed on the adsorbent and subsequently washed off using an inorganic acid.

In this study, a simultaneous solid-phase preconcentration method for the determination of cadmium, cobalt, nickel and zinc by atomic absorption is described. The method is based on the adsorption of these ions on 2,4,6-trimorpholino-1,3,5-triazin supported on naphthalene, used as an adsorbent in a column. The metal ions adsorbed on the adsorbent are then eluted with hydrochloric acid solution and determined by FAAS. The method was applied to the determination of Ni, Co, Zn and Cd in tap water, spring water, apple leaves, multi-vitamin tablets and B_{12} vitamin samples.

EXPERIMENTAL

Apparatus

A Shimadzu model 670 atomic absorption spectrometer was used for the determination of the preconcentrated metal ions. The employed conditions are given in Table I. The flow rates of air and acetylene were set as recommended by the manufacturer.

Reagents

Triply distilled water was used and analytical reagent grade chemicals were purchased from Merck and Aldrich Chemical Companies. 2,4,6-Trimorpholino-1,3,5-triazin was prepared and purified according to a literature method.[17]

TABLE I. Operating parameters for the flame atomic absorption spectroscopic determination of cations

Element	Current, mA	Wavelength, nm	Slit, nm
Ni	4.0	232.0	0.15
Co	6.0	240.7	0.20
Zn	4.0	213.9	0.50
Cd	4.0	228.8	0.30

Preparation of the adsorbent

A 0.010 g of synthesized ligand was dissolved in acetone at 40 °C under vigorous stirring. After dissolving 0.20 g naphthalene in the above solution, 20 mL triply distilled water was added slowly to obtain adsorbent particles with suitable sizes. Then, the mixture was stirred for 1 h, at 40 °C. The product was filtered and the adsorbent was dried to use.

Analytical procedure

An accurately weighed amount of adsorbent was transferred into a glass column of 4 cm length and 0.8 cm diameter. The column was washed with triply distilled water. The pH of an optimized volume of metal ion solution was adjusted by the drop wise addition of dilute HNO_3. The solution was then passed through the column at a flow rate of 5 mL min^{-1}. Metal ion adsorbed on the column was then eluted with 2.0 mL of 1.0 mol L^{-1} HCl solution at an elution rate of 1 mL min^{-1}. The metal concentration in the eluted solution was determined by FAAS.

Determination of nickel and zinc in apple leaves

A 1.0 g sample was taken in a beaker and dissolved in 20 mL concentrated nitric acid with heating. The solution was cooled, diluted and filtered. The pH of the final solution was adjusted to 5 by suitable addition of an NH_3 solution and the solution was finally diluted to 250 mL with distilled water in a volumetric flask.[18] The nickel and zinc content of the solution was then determined after preconcentration as described above.

Determination of cobalt in pharmaceutical samples

The contents of vitamin B_{12} in four ampoules for injection were determined as cobalt. The contents of the ampoules were decomposed in a 50 mL round-bottom flask by heating with 5.0 mL of a mixture containing concentrated nitric and sulfuric acid (10:1) on a hot plate until near dryness.[19] The drop-wise addition of concentrated nitric acid was required to obtain a colorless residue. The residue was neutralized with a dilute sodium hydroxide solution and was then diluted to an appropriate volume (50 mL). The cobalt contents were analyzed by the recommended procedure.

Determination of zinc in a milk sample

A sample of powdered milk (1.0 g) was heated in a beaker containing a mixture of concentrated sulfuric acid (10 mL) and nitric acid (4.0 mL) until a clear solution was obtained. This was allowed to cool and most of the acid was neutralized with sodium hydroxide. The pH was adjusted to the optimum value and the volume was made up to 500 mL.[20] The concentration of zinc was estimated by passing the solution through the column. The metal ion was eluted from the column using 2.0 mL of 1.0 mol L^{-1} HCl and determined using FAAS.

Determination of zinc in multivitamin tablets

Ten multivitamin tablets were weighed, ground, placed in a conical flask and treated with 20 mL of 0.10 mol L^{-1} HCl. The solution was shaken mechanically and filtered, the pre-

cipitate was thoroughly washed with deionized water and then the combined filtrates were transferred into a 100 mL volumetric flask and diluted to the mark with deionized water.[21] The zinc content of the solution was then determined after preconcentration as described above.

RESULTS AND DISCUSSION

Adsorption of each ion was investigated separately. Ions from solutions with different concentrations of cations were adsorbed on the sorbent. Different parameters were optimized. The pH of the sample solution, the type and concentration of the eluent, the effect of sample and eluent flow rates on the extraction efficiency, the interference effect of foreign species and the capacity factor of the sorbent for metal ions recovery were studied. The optimization procedure was performed by varying one parameter while keeping the others constant.

Effect of variables on the preconcentration

The effect of pH on the preconcentration of the cations was examined in the range 3.0–7.0, and the results are shown in Fig. 1. The results show that in the pH range of 4.0–5.5, the analytes were quantitatively adsorbed on microcrystalline naphthalene and the recovery was more than 90 %. In order to obtain the best conditions for the determination after preconcentration, pH 4.5 was chosen.

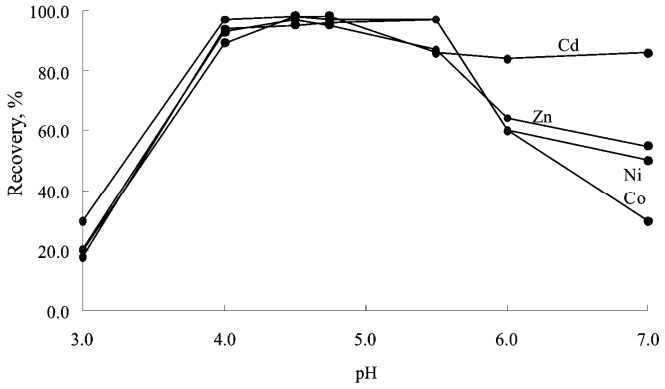

Fig. 1. Effect of pH of the metal ions solution on the percent of retention on sorbent. Experimental conditions: 10.0 mL 5.0 ng mL^{-1} metal ion solution at different pH, 0.21 g sorbent.

The percent sorption of 10.0 mL of 5.0 μg mL^{-1} of the solutions of the cations at pH 4.5 on the sorbent surface as a function of the flow rate of the sample solution was examined in the range of 0.5–15.0 mL min^{-1}. The results indicated that at flow rates lower than 10 mL min^{-1}, complete sorption of each cation on sorbent was achieved. However at flow rates greater than 10 mL min^{-1}, there was a decrease in the percentage sorption. This may be due to insufficient equilibration of the sample solution with the sorbent. Thus a flow rate of 10 mL min^{-1} was chosen for further studies.

In order to choose an appropriate eluent for desorbing the cations from the sorbent surface, a series of selected mineral acids, *i.e.*, hydrochloric nitric and sulfuric acid were used. Aliquots of 10.0 mL of 2.0 μg mL^{-1} of each cation solution were passed through a series of columns containing 0.21 g of adsorbent. A total of 2.0 mL of 1.0 mol L^{-1} of the above-mentioned eluents was used for desorption of the adsorbed cations. The amount of cation back-extracted into the liquid phase by each eluent was measured using FAAS. Percent recoveries of cations were calculated for each sample. The results show that the recovery was the best when hydrochloric acid solution was used as the eluent. Therefore, hydrochloric acid was selected as the eluent.

For desorbing metal ions already adsorbed on the adsorbent, different concentrations of the eluent, in the range 0.05–2.00 mol L^{-1} HCl, were used. As is shown in Fig. 2, at concentrations greater than 1.00 mol L^{-1}, HCl completely desorbed the metal ions from the sorbent surface. Therefore, a concentration of 1.0 mol L^{-1} of HCl was selected for further studies.

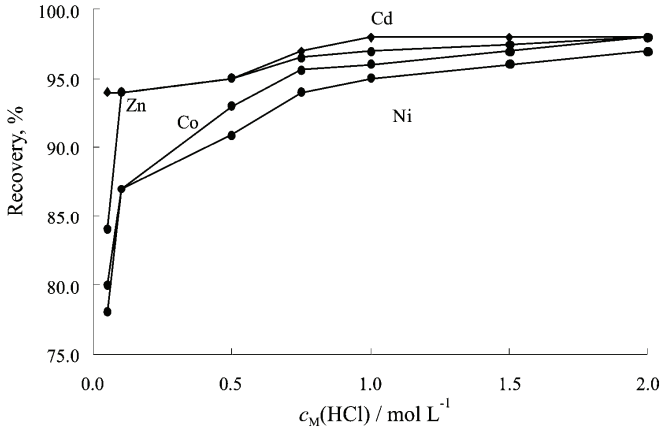

Fig. 2. Effect of eluent concentration on percent recovery of metal ions. Experimental conditions: 10.0 mL 5.0 ng mL^{-1} metal ions solution at pH 4.5, 0.21 g sorbent with different concentration of eluent.

The effect of the volume of the eluent solution was also studied. The results are shown in Fig. 3. The percent of recovery of cations increased with increasing volume of HCl up to 2.0 mL and thereafter remained constant. Therefore, the optimum volume of the eluent was chosen as 2.0 mL. The flow rate of eluent was 1.0 mL min^{-1}.

The prepared sorbent was subjected to several loadings with the sample solution and subsequent elution with the eluent. The capacity of the adsorbent had not changed after 5 cycles of sorption and desorption.

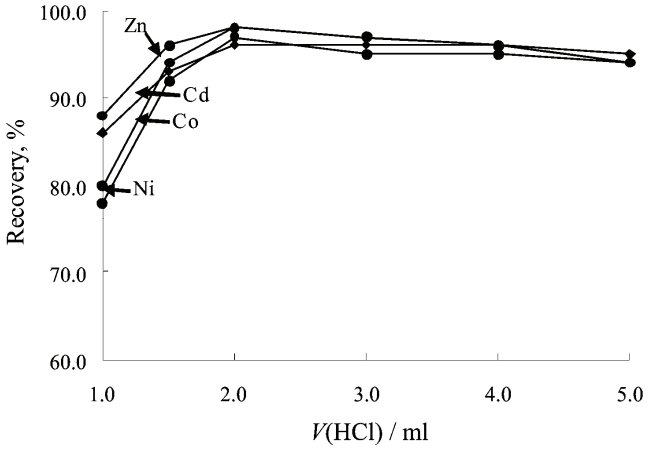

Fig. 3. Effect of the volume of eluent on percent of recovery of metal ions. Experimental conditions: 10.0 mL 5.0 ng mL^{-1} metal ions solution at pH 4.5, 0.21 g sorbent with different volumes.

The effect of the sample volume on the adsorption of cations on 0.21 g of sorbent was studied by passing sample volumes of 10–1000 mL containing the same amount of cation (10 μg) through the column and the signal of each eluted solution was compared with calibration curve data, which was achieved from the determination method. The obtained signals of concentrated cation solutions showed that a preconcentration factor of 250 for Ni(II), Co(II) and Zn(II), and 400 for Cd(II) can be achieved by this method.

Retention capacity of the adsorbent

The retention capacity of adsorbent was determined by the batch method. A 20 mL solution of 0.10 μg mL^{-1} of each cation at pH 4.5 was transferred into a separating funnel and 0.12 g adsorbent was added. The separating funnel was shaken vigorously for 30 min. The concentration of the cations in the filtrate was determined according to the calibration curves and then the adsorbed amount of each cation was calculated. The retention capacity (μg adsorbed cation/g adsorbent) was obtained and the results showed that the capacity factors were 102, 51.5, 7305, and 100 μg g^{-1} for Cd(II), Co(II), Ni(II) and Zn(II), respectively.

Effect of foreign ions

The effects of different cations and anions were investigated from the percentage recovery of 0.20 μg mL^{-1} of each metal ion in 10 mL of solution by the proposed method. The following ions did not interfere at a concentration of 1000 μg mL^{-1} with the preconcentration and determination of 0.20 μg mL^{-1} of the studied metal ions: K^+, SO_4^{2-}, NO_3^-, Br^-, CrO_4^{2-}, PO_4^{3-}, $S_2O_3^{2-}$, CH_3COO^-, F^-, SCN^-, $NH_4^+$and Cl^-. Hg^{2+}, MoO_4^- and Na^+ interfered at a concentration of 300

μg mL^{-1}, Sr^{2+} interfered at 20 μg mL^{-1}, Ca^{2+} interfered at 10.0 μg mL^{-1} with the determination of the studied cations but the presence of fluoride ion did not interfere up to 100 μg mL^{-1}. Mg^{2+}, Pb^{2+} and Mn^{2+} interfered at 10 μg mL^{-1} with the determination of the cations. The results indicate that high concentrations of all the tested ions did not interfere with separation and determination of the studied cations.

Analytical characteristics

Calibration graphs were constructed from measurements made under the optimum conditions described above. The calibration equations are given in Table II. The limit of detection and limit of quantification are defined as $c_{LOD} = 3S_B/m$ and $c_{LOQ} = 10S_B/m$, where S_B and m are the standard deviation of the blank and the slope of the calibration graph, respectively. To evaluate the accuracy and precision of the method, two different concentrations of each of the standard samples were repeated several times. The results are given in Table III, which shows that the relative standard deviation (*RSD*) for the determination of different concentrations of the cations was in the range 0.37–3.73 %.

TABLE II. Analytical features of the proposed method

Cation	Equation	Linear range ng mL^{-1}	*LOD*[a] ng mL^{-1}	*LOQ*[b] ng mL^{-1}	R^2 (n = 8)
Cd(II)	$A = 0.0094c + 0.0023$	1.00–8.00	0.17	0.56	0.9995
Co(II)	$A = 0.0031c + 0.0007$	3.00–60.00	0.51	1.70	0.9993
Ni(II)	$A = 0.0032c + 0.0009$	4.00–100.00	0.49	1.63	0.9986
Zn(II)	$A = 0.0084c + 0.0105$	0.40–50.00	0.10	0.33	0.9983

[a]Limit of detection, [b]limit of quantification

TABLE III. Accuracy and precision of the proposed method

Cation	c / ng mL^{-1}	Relative error, %	*RSD* / % (n = 5)
Cd(II)	5.00	–1.86	2.40
	50.00	0.62	2.20
Co(II)	5.00	–0.54	2.31
	50.00	–0.19	0.37
Ni(II)	5.00	2.16	3.73
	50.00	0.16	0.37
Zn(II)	1.00	1.64	2.56
	25.00	1.27	1.50

Simultaneous preconcentration

A solution (500 mL) containing 30.0, 35.0, 25.0 and 10.0 ng mL^{-1} of Cd, Co, Ni and Zn ions, respectively, was prepared and passed through the column. The metal ions were eluted with 4.0 mL of HCl solution (1.0 mol L^{-1}) and Cd, Co, Ni and Zn were determined by FAAS. The results are given in Table IV and

indicate the proposed method is suitable for the simultaneous preconcentration and separation of Cd, Co, Ni and Zn and allows the determination of trace amounts of these elements by FAAS, which is a technique available in almost every laboratory.

TABLE IV. Simultaneous preconcentration of the studied cations by the proposed method

Cation	c / ng mL^{-1}	Recovery, %
Cd(II)	30.0	93.4
Co(II)	35.0	99.2
Ni(II)	25.0	92.6
Zn(II)	10.0	94.8

Analytical application

The suitability of the proposed method for the analysis of natural water samples was checked by spiking samples of spring water and tap water with different concentrations of cations. The results are given in Table V. The accuracy and applicability of the proposed method were tested by its application to the determination of Zn and Cd in tap and spring water samples, Zn in powdered milk, Zn in multi-vitamin tablets, Ni and Zn in apple leaves, and Co in vitamin B_{12}. The results are given in Table VI and they indicate the successful applicability of the proposed method for the determination of these cations in real samples.

TABLE V. Determination of the studied cations in natural water samples by the proposed method (n = 5)

Cation	Amount of cation, μg L^{-1}				Recovery, %	
	Added		Found			
	Tap water	Spring water	Tap water	Spring water	Tap water	Spring water
Ni(II)	0.0	0.00	4.36 ± 0.21	5.54 ± 0.27	–	–
	10.00	10.00	14.60 ± 0.22	15.45 ± 0.45	102.4	99.1
	20.00	20.00	24.40 ± 0.47	25.50 ± 0.48.	100.2	99.8
Cd(II)	0.00	0.00	n.d[a]	n.d	–	–
	10.00	10.00	9.50 ± 0.46	10.73 ± 49	95.0	107.3
	20.00	20.00	19.83 ± 0.91	20.50 ± 0.66	99.2	102.5
Co(II)	0.00	0.00	n.d	n.d	–	–
	10.00	10.00	9.64 ± 0.25	10.47 ± 0.38	96.4	104.7
	20.00	20.00	19.45 ± 0.61	20.36 ± 0.47	97.3	101.8
Zn(II)	0.00	0.00	28.43 ± 0.39	10.50 ± 0.36	–	–
	10.00	10.00	38.30 ± 0.64	20.34 ± 0.45	98.7	98.4
	20.00	20.00	48.20 ± 0.57.	30.61 ± 0.81	98.9	100.5

[a]Not detected

TABLE VI. Application of the proposed method to real samples (n = 5)

Cation	Added, μg L^{-1}	Found, μg L^{-1}	Recovery, %
Co(II) in orange juice	0.00	7.36 ± 0.32	–
	10.00	17.09 ± 0.76	97.3
	20.00	27.43 ± 0.84	100.3
Zn(II) in apple leaves	0.00	18.30 ± 0.46	–
	10.00	28.14 ± 0.48	98.4
	20.00	37.83 ± 0.59	97.7
Zn(II) in powdered milk	0.00	25.20 ± 0.96	–
	10.00	35.05 ± 1.00	98.5
Zn(II) in multi vitamin tablets	0.00	36.80 ± 1.21	–
	10.00	46.90 ± 1.49	101.0
Ni(II) in apple leaves	0.00	4.69 ± 0.19	–
	10.00	14.28 ± 0.26	95.9
	20.00	24.27 ± 0.57	97.9
Ni(II) in orange juice	0.00	14.30 ± 0.38	–
	10.00	24.24 ± 0.55	99.4
	20.00	34.25 ± 0.49	99.8
Co(II) in vitamin B_{12}	0.00	46.22 ± 1.03	–
	10.00	55.92 ± 1.73	97.0

CONCLUSIONS

Solid–liquid extraction with microcrystalline naphthalene is an effective separation and preconcentration technique for trace elements. This proposed preconcentration method has a high enrichment factor, which opens the possibility of determining concentration levels of cations as low as sub-micro amounts. In it is suitable for the simple and accurate determination of these elements in a variety of real samples giving satisfactory results. A comparison between the proposed method and some existing methods reported for preconcentration of metal ions by the solid phase extraction method[20,22–26] is given in Table VII. As Table VII shows, the proposed method exhibits a comparable capacity level, a lower detection limit and a wider linear range, as well as being a convenient, safe, simple, rapid and inexpensive method for the determination of trace quantities of the studied cations in real samples giving satisfactory results.

TABLE VII. Comparison of the proposed method with some other SPE methods

Matrix	Detection limit, μg L^{-1}	Application	Ref.
Modified silica gel with aminothioamidoanthraquinone	Ni = 2.90 Co = 0.95 Cd = 1.95	Natural waters	22
Cellulose functionalized with 8-hydroxyquinoline	Zn = 0.84 Ni = 1.61 Co = 1.09 Cd = 2.59	Natural waters and Co in drugs	23

TABLE VII. Continued

Matrix	Detection limit, μg L^{-1}	Application	Ref.
o-Aminobenzoic acid-functionalized XAD-4 copolymer resin	Zn = 2.50 Ni = 5.00 Co = 6.50 Cd = 2.50	Natural waters	24
4,6-Dihydroxy-2-mercaptopyrimidine (DHMP) loaded on activated carbon	Ni = 3.80 Co = 3.40	Natural waters and spinach	25
Glycerol–silica gel	Co = 1.00	Natural waters	26
2-{[1-(2-Hydroxynaphthyl)-methylidene]amino}-benzoic acid (HNMABA)	Zn = 5.00 Ni = 20.00 Co = 8.00 Cd = 10.00	Natural waters, Co in B_{12} vitamin, Zn in powdered milk	20
Modified microcrystal naphthalene with 2,4,6-trimorpholino--1,3,5-triazin	Zn = 0.10 Ni = 0.49 Co = 0.51 Cd = 0.17	Natural waters, Co in B_{12} vitamin, Zn in powdered milk, Zn and Ni in apple leaves	Proposed method

ИЗВОД

ПРЕКОНЦЕНТРАЦИЈА Co, Ni, Cd И Zn НА АДСОРБЕНТУ НАФТАЛЕН–2,4,6-ТРИМОРФОЛИНО-1,3,5-ТРИАЗИНА И ОДРЕЂИВАЊЕ ПЛАМЕНОМ АТОМСКОМ АПСОРПЦИОНОМ СПЕКТРОМЕТРИЈОМ

TAYYEBEH MADRAKIAN, MOHAMMAD ALI ZOLFIGOL и FATHEMEH ABOULGHAZI

Faculty of Chemistry, Bu-Ali Sina University, Hamedan 6517838683, Iran

За одређивање трагова Co, Ni, Cd и Zn пламеном атомском апсорпционом спектрометријом развијена је метода преконцентрисања, која се заснива на ретенцији катјона на стубу адсорбенса нафтален–2,4,6-триморфолино-1,3,5-триазина. Адсорбовани катјони се потом елуирају са колоне помоћу хлороводоничне киселине, а Co, Ni, Cd и Zn одређују пламеном атомском апсорпционом спектрометријом. Испитивани су оптимални услови екстракције и елуције. Испитиван је такође и ефекат страних јона на преконцентрацију. Постигнут је фактор преконцентрисања од 250 за Co(II), Ni(II), Zn(II) и 400 за Cd(II). Детекционе границе методе за Co(II), Ni(II), Cd(II) и Zn(II) износе: 0.51, 0.49, 0.17 и 0.10 ng mL^{-1}, а добијена је релативна стандардна девијација (*RSD*) за Co, 0,37–2,31 %, за Ni, 0,37–3,73 %, за Cd, 2,20––2,40 % и Zn, 1,50–2,56 %. Метода је успешно примењена за одређивање Co, Ni, Cd и Zn у неколико различитих реалних узорака.

(Примљено 4. априла, ревидирано 24. новембра 2009)

REFERENCES

1. S. H. Lee, H. S. Choi, *B. Kor. Chem. Soc*. **24** (2003) 1705.
2. D. Kara, N. Tekin, *Microchim. Acta* **149** (2005) 193
3. G. Her, H. S. Choi, *J. Korean Chem. Soc*. **49** (2005) 145
4. M. C. Yebra, J. Salgado, L. Ouig, A. Moreno-Cid, *Anal. Bioanal. Chem*. **374** (2002) 530
5. A. Uzan, M. Soylak, L. Elci, *Talanta* **54** (2001) 197
6. S. Sarac, L. Olu, L. Elci, *Anal. Chim. Acta* **452** (2002) 77

7. Y. P. D. Pena, W. Lopez, J. L. Burguera, M. Burguera, M. Gallignani, R. Brunetto, P. Carrero, C. Rondon, F. Imbert, *Anal. Chim. Acta* **403** (2000) 249
8. M. A. A. Akl, I. M. M. Kenawy, R. R. Lasheen, *J. Microchem.* **78** (2004) 143
9. K. Jankowski, J. Yao, K. Kasiura, A. Jackowska, A. Sieradzka, *Spectrochim. Acta B* **60** (2005) 369
10. J. R. Baena, M. Gallego, M. Valcarcel, *Anal. Chem.* **74** (2002) 1519
11. D. Thorburn Burns, N. Tungkananuruk, *Anal. Chim. Acta* **189** (1986) 383
12. B. K. Puri, S. Balani, *Talanta* **42** (1995) 337
13. N. Pourreza, H. Zavvar Mousavi, *Anal. Chim. Acta* **503** (2004) 279
14. C. Xiong, Z. Jiang, B. Hu, *Anal. Chim. Acta* **559** (2006) 113
15. M. A. Taher, *Anal. Chim. Acta* **408** (2000) 153
16. M. A. Taher, *Talanta* **52** (2000) 301
17. D. Azarifar, M. A. Zolfigol, A. Forghaniha, *Hetrocycles* **63** (2004) 1897
18. S. Akman, N. Tokman, *Talanta* **60** (2003) 199
19. M. I. Toral, P. Richter, L. Silva, *Talanta* **40** (1993) 1405
20. K. Kiran, K. Suresh Kumar, K. Suvardhan, K. Janardhanam, P. Chiranjeevi, *J. Hazardous Mater.* **147** (2007) 15
21. W. Thanasarakhan, S. Liawruangrath, S. Wangkarn, B. Liawruangrath, *Talanta* **71** (2007) 1849
22. W. Ngeontae, W. Aeungmaitrepirom, T. Tuntulani, *Talanta* **71** (2007) 1075
23. V. Gurnani, A. K. Singh, B. Venkataramani, *Anal. Chim. Acta* **485** (2003) 221
24. S. D. Çekiç, H. Filik, R. Apak, *Anal. Chim. Acta* **505** (2004) 15
25. M. Ghaedi, F. Ahmadi, A. Shokrollahi, *J. Hazard. Mater*. 142 (2006) 272
26. A. Safavi, N. Iranpoor, N. Saghir, S. Momeni, *Anal. Chim. Acta* **569** (2006) 139.

Journal of the Serbian Chemical Society
JSCS@tmf.bg.ac.rs • www.shd.org.rs/JSCS

J. Serb. Chem. Soc. 75 (5) 681–687 (2010)
JSCS–3998

UDC 632.95+546.185+541.135.5–039.26+543.552
Short communication

SHORT COMMUNICATION

Voltammetric determination of the neonicotinoid insecticide thiamethoxam using a tricresyl phosphate-based carbon paste electrode

ZSIGMOND J. PAPP[1#], VALÉRIA J. GUZSVÁNY[1*#], SZYMON KUBIAK[2], ANDRZEJ BOBROWSKI[2] and LUKA J. BJELICA[1#]

[1]*Department of Chemistry, Biochemistry and Environmental Protection, Faculty of Sciences, University of Novi Sad, Trg D. Obradovića 3, 21000 Novi Sad, Serbia and* [2]*Department of Building Materials Technology, Faculty of Materials Science and Ceramics, AGH-University of Science and Technology, Mickiewicza 30, 30-059 Krakow, Poland*

(Received 24 June, revised 26 November 2009)

Abstract: The objective of the work was to investigate the possibility of using a tricresyl phosphate-based carbon paste electrode for the direct voltammetric determination of the neonicotinoid insecticide thiamethoxam. The analyte was determined by differential pulse voltammetry in Britton–Robinson buffer pH 7.0 in the concentration range of 3.72–41.5 μg mL^{-1}. The reproducibility of the analytical signal at the 7.29 μg mL^{-1} level was characterized by a relative standard deviation of 1.3 %. The applicability of the developed method was evaluated by determining thiamethoxam in a river water sample and a commercial formulation Actara 25 WG.

Keywords: pesticide; thiamethoxam; differential pulse voltammetry; carbon paste electrode; tricresyl phosphate.

INTRODUCTION

Neonicotinoids are among the most effective insecticides for the control of sucking insect pests, such as aphids, whiteflies, leaf- and plant-hoppers, thrips, some micro lepidoptera and a number of coleopteran pests. Their broad spectrum of efficacy, together with their systemic and translaminar action, pronounced residual activity and unique mode of action make neonicotinoids the most rapidly expanding class of insecticidals.[1,2]

Launched in 1998 by Syngenta, thiamethoxam ((*EZ*)-3-(2-chloro-1,3-thiazol-5-ylmethyl)-5-methyl-1,3,5-oxadiazinan-4-ylidene(nitro)amine) is marketed

* Corresponding author. E-mail: valeria.guzsvany@dh.uns.ac.rs
# Serbian Chemical Society member.
doi: 10.2298/JSC090624033P

as Actara for foliar and as Cruiser for seed-treatment uses. To date, thiamethoxam holds registration for 115 crop uses in at least 64 countries on a wide range of crops, such as vegetables, potatoes, rice, cotton, fruit, tobacco and cereals. It is the second biggest neonicotinoid in terms of sales.[1,2]

Due to its wide and constantly expanding areas of application, there is a growing need for new analytical methods for the determination of thiamethoxam, both in commercial formulations and real environmental samples, using simple and cost-effective instrumental techniques.

Analytical techniques that are employed most frequently for the determination of thiamethoxam include high-performance liquid chromatography (HPLC) with a diode array detector (DAD),[3,4] mass spectrometric,[5–7] thermal lens spectrometric[8] and electrochemical detection.[9] Ultra-sensitive automated flow fluorescent immunoassay[10] has also been employed for the rapid, selective and sensitive analysis of different samples containing thiamethoxam. Several electroanalytical methods, such as cyclic voltammetry (CV),[11] differential-pulse polarography (DPP)[12] and differential-pulse voltammetry (DPV),[13–15] have also been employed for the determination of thiamethoxam in model solutions and some real samples.

Over the last five decades, carbon paste, a mixture of carbon powder and pasting liquid, has become one of the widely used electrode materials for the preparation of various electrodes, sensors, and detectors. In 2008, the 50th anniversary of the introduction of carbon paste electrode (CPE) was celebrated and corresponding reviews appeared.[16,17] On the other hand, to the best of our knowledge, there is only one publication dealing with the application of a CPE in the analysis of neonicotinoids. Namely, imidacloprid was determined by DPV in different samples using a tricresyl phosphate-based CPE (TCP–CPE).[18]

In this work, a voltammetric investigation of thiamethoxam was performed at a TCP–CPE and an electroanalytical method was developed for its DPV determination in an aqueous Britton–Robinson buffer solution (pH 7.0) as the supporting electrolyte. The developed voltammetric procedure was tested by determining thiamethoxam in a river water sample and the commercial formulation Actara 25 WG. The results of the developed electroanalytical method were compared with those obtained by HPLC/DAD.

EXPERIMENTAL

Chemicals and solutions

All employed chemicals were of analytical reagent grade and the solutions were prepared in doubly distilled water. The analytical standard of thiamethoxam (Sigma-Aldrich Laborchemikalien GmbH, Germany) was of 99.7 % purity. The concentration of the thiamethoxam stock solution was 186.9 μg mL^{-1}, which was further diluted as required. Britton–Robinson buffer solutions for voltammetric characterization and determination were prepared from a stock solution 0.040 M phosphoric (Merck, Germany), boric (Merck) and acetic (Merck) acid, by

adding 0.20 M sodium hydroxide (Merck) to obtain the required pH value. For the preparation of the mobile phase in the HPLC experiments, acetonitrile (J. T. Baker, The Netherlands, purity 99.8 %) and 0.20 % phosphoric acid (made by diluting phosphoric acid (Centrohem, Serbia)) were used. The commercial formulation of thiamethoxam was Actara 25 WG (Syngenta Crop Protection AG, Switzerland). The river water sample was collected from the Danube River (Novi Sad, Serbia) and stored in the dark at 4 °C for one week before analysis.

Apparatus

Voltammetric experiments were performed on an Autolab (PGSTAT12, Ecochemie, The Netherlands) electrochemical analyzer operated *via* GPES 4.9 software (Ecochemie). The cell stand included a three-electrode system with a CPE as working, a saturated calomel electrode (SCE) (Amel, Italy) as the reference, and a platinum (Amel) auxiliary electrode. All potentials are quoted *vs*. SCE as reference.

Comparative HPLC measurements were performed using an Agilent 1100 liquid chromatograph (Agilent Technologies Inc., USA), Zorbax Eclipse XDB-C18 (4.6 mm×250 mm, 3.5 μm) column, equipped with a DAD.

Procedures

Preparation of the CPE. Carbon paste was made by intimate hand-mixing of CR 5 graphite powder (Maziva Týn, the Czech Republic) with tricresyl phosphate (mixture of isomers, Sigma-Aldrich Chemie GmbH, Switzerland) as the pasting liquid. The detailed procedure of the electrode preparation was described earlier.[18]

Voltammetry on CPEs. In the model systems and real samples, thiamethoxam was measured in 5.00 mL of solution of different concentrations, to which 5.00 mL of Britton–Robinson buffer solution was added. The scan rate in the cyclic voltammetry (CV) was 50 mV s^{-1}. The DPV measurement parameters were as follows: pulse amplitude 50 mV, pulse width 50 ms, scan rate 25 mV s^{-1}.[13-15] The deaerated solutions (nitrogen stream, 10 min) were measured at ambient temperature without filtering.

Chromatography. For the HPLC/DAD analysis, all aliquots were filtered through Millex 0.22 μm syringe filters. The mobile phase was a mixture of water (0.20 % phosphoric acid) and acetonitrile (70:30, v/v).[4,12] The separation was performed isocratically at a flow rate of 1.0 mL min^{-1}. The column temperature was held at 25 °C. Thiamethoxam was detected at a working wavelength of 252 nm and a retention time of 2.5 min. The concentration of the investigated compound was determined from the area of the corresponding peak.

Sample preparation. The commercial formulation Actara 25 WG was powdered and homogenized in a porcelain mortar and then dissolved in doubly distilled water. This solution was diluted stepwise to the required concentration. Aliquots of the river water sample were spiked with the standard solution of thiamethoxam and kept in the dark at 4 °C for 1 h before analysis, without any sample pretreatment. Filtering was performed only for HPLC measurements.

RESULTS AND DISCUSSION

Voltammetric investigation of thiamethoxam at CPE

Relying on previous polarographic investigations,[12] the detection of thiamethoxam was based on the irreversible reduction of its nitro group. Before applying TCP–CPE for quantitative determinations, it was necessary to perform characterization of the compound. The CV (Fig. 1) and DPV (Fig. 2) curves were

recorded in the pH range from 2.0 to 8.0 to study the pH dependence of the peak potentials, which shifted to more negative values with increasing pH. The sharpest, most symmetrical and intense peaks were obtained in the neutral and slightly alkaline solutions (pH 7.0 and 8.0), which is in good agreement with previous voltammetric investigations of neonicotinoids with a nitro-group.[11–15,18–21] Based on these results and with the aim of avoiding possible hydrolysis of the TCP binder in alkaline media, pH 7.0 was chosen for the determinations. Studies of the reproducibility of the TCP–CPE signals were also performed, first to check the signal stability and possible changes in its shape during the measurement. Voltammograms obtained for a 7.29 μg mL^{-1} solution of thiamethoxam showed good reproducibility of the analytical signal during approximately 30 min.

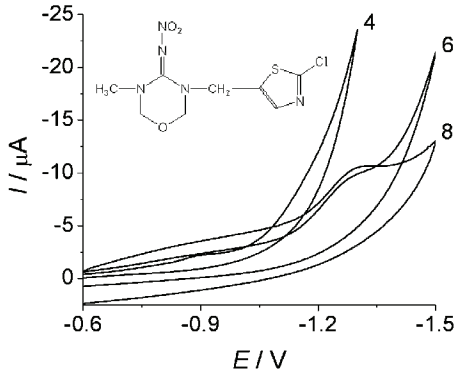

Fig. 1. Influence of pH on the CV signals of thiamethoxam (the pH values of the solutions are indicated at the curves). The inset shows the structural formula of thiamethoxam. Measurement parameters: v = 50 mV s^{-1}, c = 31.6 μg mL^{-1}.

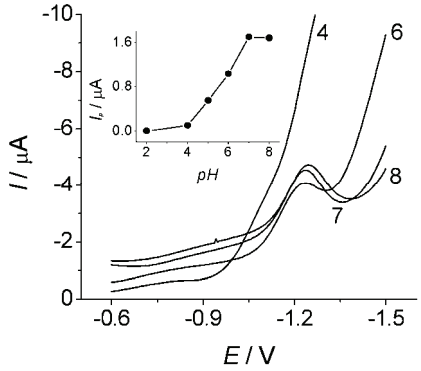

Fig. 2. Influence of pH on DPV signals of thiamethoxam (the pH values of the solutions are indicated at the curves). The inset shows the dependence of the peak current on pH. Measurement parameters: v = 25 mV s^{-1}, pulse amplitude: 50 mV, pulse width: 50 ms, c = 31.6 μg mL^{-1}.

Purging the solutions with nitrogen (10 min) led to a lower background current and better reproducibility of determination in this fairly negative potential region. It was shown earlier that the use of membrane plasticizers (*e.g.*, TCP, dioctyl phthalate) in CPEs as the pasting liquids instead of the usual binders, such as Nujol or silicone oil, can significantly reduce the amount of oxygen absorbed in the graphite.[22] Hence, no special attention was paid to the oxygen in the paste. The electrochemical properties of the TCP–CPE were improved and stabilized by potential cycling. In the study, all electrodes were subjected to electrochemical activation by potential cycling in the range from –0.60 to –1.50 V (10 cycles) prior to the measurements. Increasing the number of potential cycles lead neither to a further widening of the potential window nor a lowering of the background current or signal stabilization.

Determination of thiamethoxam in model systems and selected real samples

The quantitative DPV determination of thiamethoxam at a TCP-CPE in model systems (Fig. 3) is based on the linear relationship between the peak current intensity ($|I_p|$) and the thiamethoxam concentration (c). For the tested range of 3.72–41.5 μg mL^{-1}, the following equation was obtained:

$$|I_p| = 0.07516c - 0.04634, \; r = 0.999$$

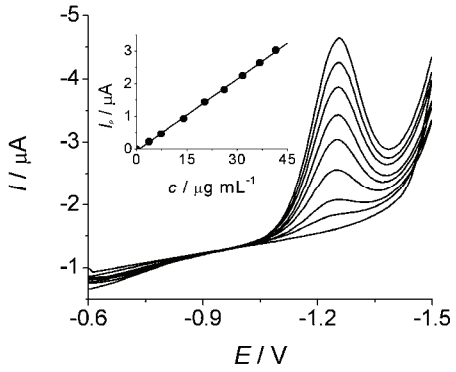

Fig. 3. Differential pulse voltammograms recorded at the TCP–CPE for different concentrations of thiamethoxam (3.72, 7.29, 14.0, 20.3, 26.2, 31.6, 36.7 and 41.5 μg mL^{-1}) in Britton–Robinson buffer solution. The inset shows the corresponding calibration plot.

The reproducibility of the analytical response was assessed by comparing peak the heights of six replicate recordings at a thiamethoxam concentration level of 7.29 μg mL^{-1}. The obtained *RSD* value of 1.3 % indicates a relatively good precision of the developed method.

The applicability of the elaborated voltammetric procedure was tested by determining the thiamethoxam concentration in several real samples. As can be seen from Fig. 4, the matrix from the river water sample (the Danube) and the

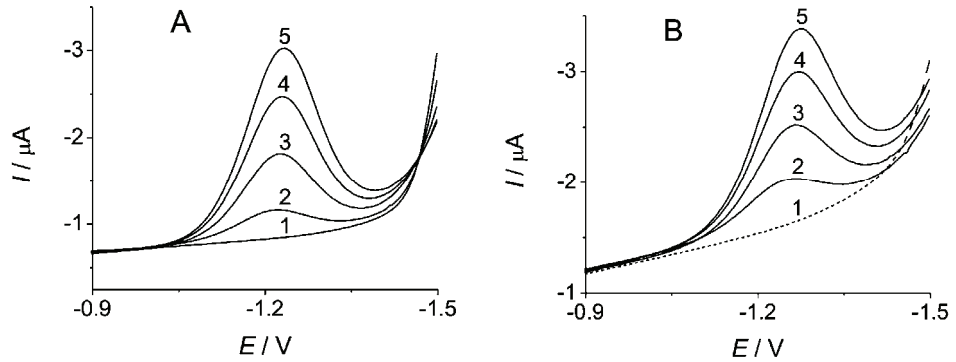

Fig. 4. Determination of thiamethoxam in real samples. River water (A): sample (1), spiked sample (2), successive standard additions (8.82, 16.9 and 24.2 μg mL^{-1}; 3–5), and the commercial formulation Actara 25 WG (B): baseline (1), sample (2), and successive standard additions (7.15, 13.8 and 20.0 μg mL^{-1}; 3–5).

commercial formulation Actara 25 WG did not block the electrode surface and did not show voltammetric interferences, which are favorable facts for the determination. The standard addition method was applied for the determination of the active compound in real samples. The good correlation between the determined and declared/added amounts, as well as the low *RSD* values reflects the high accuracy and precision of the proposed method (Table I). On the other hand, the somewhat lower precision observed for the commercial formulation in comparison with that for model solutions and river water probably arises from the incomplete homogenization of the solid sample. Furthermore, the insecticide concentrations determined by DPV agreed well with the results of the comparative HPLC/ /DAD analysis (Table I). The determination of lower concentrations of the target compound, especially in the case of river water samples, can be achieved, *e.g.*, by applying different preconcentration or extraction methods before the analysis.

TABLE I. Assay of thiamethoxam in real samples (n = 5)

Analyte	Method of determination			
	DPV		HPLC/DAD	
	Found	*RSD* / %	Found	*RSD* / %
Danube water[a]	7.90 μg mL^{-1}	3.0	8.06 μg mL^{-1}	0.53
Actara 25 WG[b]	23.6 %	4.9	23.4 %	1.0

[a]The added value: 8.12 μg mL^{-1}; [b]nominal value: 25±6 %

CONCLUSIONS

This study confirmed the applicability of a TCP–CPE for the direct cathodic voltammetric determination of the insecticide thiamethoxam. DPV in Britton–Robinson buffer solution of pH 7.0 was found to be suitable for the determination of thiamethoxam with a linear response in the concentration range of 3.72–41.5 μg mL^{-1}. The developed procedure might be applied for the determination of thiamethoxam in selected real samples. The voltammetric results were validated by comparative HPLC/DAD measurements. Voltammetry using a TCP–CPE can be a fast and inexpensive tool for obtaining information about insecticide concentrations, especially in commercial formulations in which the analyte concentration is higher.

Acknowledgements. The authors would like to acknowledge the financial support from the Ministry of Science and Technological Development of the Republic of Serbia (Project No. 142029), the Secretariat for Science and Technological Development of AP Vojvodina, Republic of Serbia (Grants No. 114-451-00663/2009-01 and 114-451-02011/2007-02) and Central European Exchange Programme for University Studies (Project No. CII-CZ-0212-02--0910).

ИЗВОД

ВОЛТАМЕТРИЈСКО ОДЕЂИВАЊЕ НЕОНИКОТИНОИДНОГ ИНСЕКТИЦИДА ТИАМЕТОКСАМА ПРИМЕНОМ ЕЛЕКТРОДЕ ОД УГЉЕНИЧНЕ ПАСТЕ НА БАЗИ ТРИКРЕЗИЛ-ФОСФАТА

ZSIGMOND J. PAPP, SZYMON KUBIAK, VALÉRIA J. GUZSVÁNY, ANDRZEJ BOBROWSKI и ЛУКА Ј. БЈЕЛИЦА

[1]Департман за хемију, биохемију и заштиту животне средине, Природно–математички факултет, Универзитет у Новом Саду, Трг Д. Обрадовића 3, 21000 Нови Сад и [2]Department of Building Materials Technology, Faculty of Materials Science and Ceramics, AGH-University of Science and Technology, Mickiewicza 30, 30-059 Krakow, Poland

Циљ рада је био да се испита могућност примене електроде од угљеничне пасте на бази трикрезил-фосфата за директно волтаметријско одређивње неоникотиноидног инсектицида тиаметоксама. Аналит је одређиван диференцијалном пулсном волтаметријом у Британ–Робинсон пуферу, pH 7,0, у концентрационом опсегу 3,72−41,50 μg mL^{-1}. Репродуктивност аналитичког сигнала карактерише релативна стандардна девијација (на нивоу од 7,29 μg mL^{-1}) од 1,3 %. Применљивост развијене методе је проверена одређивањем тиаметоксама у речној води и комерцијалној формулацији инсектицида Actara 25 WG.

(Примљено 24. јуна, ревидирано 26. новембра 2009)

REFERENCES

1. P. Jeschke, R. Nauen, *Pest Manag. Sci.* **64** (2008) 1084
2. A. Elbert, M. Haas, B. Springer, W. Thielert, R. Nauen, *Pest Manag. Sci.* **64** (2008) 1099
3. E. Watanabe, K. Baba, H. Eun, *J. Agric. Food Chem.* **55** (2007) 3798
4. S. Seccia, P. Fidente, D. Montesano, P. Morrica, *J. Chromatogr. A* **1214** (2008) 115
5. S. Seccia, P. Fidente, D. Attard Barbini, P. Morrica, *Anal. Chim. Acta* **553** (2005) 21
6. P. Fidente, S. Seccia, F. Vanni, P. Morrica, *J. Chromatogr. A* **1094** (2005) 175
7. A. Di Muccio, P. Fidente, D. A. Barbini, R. Dommarco, S. Seccia, P. Morrica, *J. Chromatogr. A* **1108** (2006) 1
8. V. Guzsvány, A. Madžgalj, P. Trebše, F. Gaál, M. Franko, *Environ. Chem. Lett.* **5** (2007) 203
9. M. Rancan, S. Rossi, A. G. Sabatini, *J. Chromatogr. A* **1123** (2006) 60
10. H. J. Kim, W. L. Shelver, E. C. Hwang, T. Xu, Q. X. Li, *Anal. Chim. Acta* **571** (2006) 66
11. V. Guzsvány, F. Gaál, L. Bjelica, S. Ökrész, *J. Serb. Chem. Soc.* **70** (2005) 735
12. V. Guzsvány, M. Kádár, F. Gaál, K. Tóth, L. Bjelica, *Microchim. Acta* **154** (2006) 321
13. V. Guzsvány, M. Kádár, F. Gaál, L. Bjelica, K. Tóth, *Electroanal.* **18** (2006) 1363
14. V. Guzsvány, M. Kádár, F. Gaál, L. Bjelica, K. Tóth, in: *Sensing in Electroanalysis*, Vol. 2, K. Vytřas, K. Kalcher, Eds., University of Pardubice, Pardubice, 2007, p. 75
15. F. Gaál, V. Guzsvány, L. Bjelica, *J. Serb. Chem. Soc.* **72** (2007) 1465
16. I. Švancara, K. Vytřas, K. Kalcher, A. Walcarius, J. Wang, *Electroanal.* **21** (2009) 7
17. K. Vytřas, I. Švancara, R. Metelka, *J. Serb. Chem. Soc.* **74** (2009) 1021
18. Z. Papp, I. Švancara, V. Guzsvány, K. Vytřas, F. Gaál, *Microchim. Acta* **166** (2009) 169
19. A. Navalón, R. El-Khattabi, A. González-Casado, J. L. Vilchez, *Microchim. Acta* **130** (1999) 261
20. A. Guiberteau, T. Galeano, N. Mora, P. Parrilla, F. Salinas, *Talanta* **53** (2001) 943
21. V. Guzsvány, M. Kádár, Z. Papp, L. Bjelica, F. Gaál, K. Tóth, *Electroanal.* **20** (2008) 291
22. I. Švancara, K. Vytřas, *Anal. Chim. Acta* **273** (1993) 195.

Journal of the Serbian Chemical Society
JSCS@tmf.bg.ac.rs • www.shd.org.rs/JSCS

J. Serb. Chem. Soc. 75 (5) 689–701 (2010)
JSCS–3999

UDC 665.941+547.281+661.717.52–12:66.095.26:543.51
Original scientific paper

Molar-mass distribution of urea–formaldehyde resins of different degrees of polymerisation by MALDI-TOF mass spectrometry

IVANA GAVRILOVIĆ-GRMUŠA[1]*, OLIVERA NEŠKOVIĆ[2], MILANKA ĐIPOROVIĆ-MOMČILOVIĆ[1] and MLAĐAN POPOVIĆ[1]

[1]*Faculty of Forestry, University of Belgrade, Kneza Viseslava 1, 11030 Belgrade and* [2]*Department of Physical Chemistry, Institute "Vinča" Belgrade, Mike Petrovića-Alasa 12–14, 11351 Belgrade, Serbia*

(Received 30 October 2009, revised 25 January 2010)

Abstract: This paper describes some results obtained in an investigation of urea–formaldehyde (UF) resins of different degrees of polymerisation by matrix-assisted laser desorption/ionisation time-of-flight (MALDI-TOF) mass spectrometry (MS). MALDI-TOF MS proved to be an appropriate technique for analyzing these types of polymers, bearing in mind that the results of the analysis correspond with previous physical and chemical measurements. This technique enables a relatively swift determination of the degree of polymerrisation through the monitoring of key changes in the structure of a polymer. Thus, in the analysis of UF resins, it may be possible to monitor a decrease in the intensity of the monohydroxymethyl urea (MMU) signal, which corresponds to an increase of the mass spectra values in the mass range of higher homologues, above 1000 g mol^{-1}. A noticeable difference concerns the signal intensities in the higher mass ranges (up to 1400 g mol^{-1}), which corresponds to more branched and longer homologues of the polymers. Especially, a significantly more intensive signal of MMU was registered. The average molecular weight (*MW)* of the examined samples was between 936 and 1324 g mol^{-1}, with a maximal deviation of 20 %, depending on the ratios of the reactants.

Keywords: urea-formaldehyde resins; molar ratio; molecular structure; degree of polymerisation; MALDI-TOF.

INTRODUCTION

Urea–formaldehyde, UF, resins are the most important type of adhesives in the wood industry. They are widely used for the production of wood-based composite panels, such as particleboards, fibreboards and plywood.[1]

* Corresponding author. E-mail: ivana.grmusa@sfb.rs
doi: 10.2298/JSC091030036G

UF resins are based on a manifold reaction of two monomers, urea and formaldehyde.[2] By using different reaction and preparation conditions, a more or less innumerable variety of condensed structures is possible.[3] In the application stage, UF resins are still soluble or dispersed in water. They also can be supplied in the form of spray-dried water-soluble powders. Such structures consist of linear or branched polymeric molecules of various molecular masses. After hardening, UF resins form insoluble three-dimensional networks of thermosetting duromers.[4]

Although UF resins consist of only two main components, *i.e.*, urea and formaldehyde, they present a broad variety of possible reactions and structures.[5] This variety leads to a wide range of molar mass distributions in UF resins, from low molar mass molecules up to more or less polymeric structures. The highest molar masses in UF resin cannot be clearly determined, but it is estimated that molar masses of 100000 to 500000 g mol^{-1} can successfully describe the macromolecule structure of UF resins.[3,6–8]

From the viewpoint of end-use applications of UF resins, the molar mass distribution is a very important chemical characteristic, having an influence on several important properties of the resin, such as: viscosity, flow ability, penetration into the wood surface,[9,10] distribution on the wood furnish (particles or fibres), water dilute ability,[11] *etc*. The molar mass distribution can be determined by means of gel permeation chromatography (GPC),[12] but it is very difficult because an increase in the molecular weight of the soluble macromolecules and in the degree of branching leads to the formation of insoluble products.[13] In addition, analysis of the structural components can be performed by various spectroscopic methods, such as: infrared (IR);[14–19] nuclear magnetic resonance (NMR), *i.e.*, ^{1}H-NMR,[20–23] ^{13}C-NMR,[14,24–28] ^{15}N-NMR[9,30] and Raman spectroscopy.[31]

Matrix-assisted laser desorption/ionisation time-of-flight (MALDI-TOF) mass spectrometry has greatly expanded the use of mass spectrometry towards large molecules and has been demonstrated to be a powerful method for the characterization of both synthetic and natural polymers. This technique is usually combined with a time-of-flight (TOF) mass analyzer, which has the advantages of being capable of providing a complete mass spectrum per event, having a virtually unlimited mass range, requiring a small amount of analyte and relatively low cost equipment.[32–34]

Generally, the polycondensation structures of UF resins have not been studied thoroughly by the MALDI-TOF technique. Therefore, the objective of this research was a MALDI-TOF investigation of the molar mass distribution of UF resin samples obtained from the same reactor batch, but having three different degrees of polymerisations.

EXPERIMENTAL

Preparation of urea–formaldehyde (UF) resins with various viscosities

Urea–formaldehyde resins were synthesized *via* the reaction between formalin at a concentration of 47.69 % and urea by DUKOL Ostrava (the Czech Republic). Four samples of about 1 L, designated as I, II, III and IV, were taken from the same reactor batch when the viscosity values showed that different degrees of polymerisation had been attained. Samples I–III were prepared at an F:U molar ratio of 2:1. Sample IV was prepared by modification of sample III by the addition of formaldehyde to give an F:U ratio of 1.45:1. All the samples were kept in a refrigerator before further use.

The samples were tested for viscosity, dry matter content, pH value, gel time and pot life. The obtained results are presented in Table I.

In order to determine the dry matter content, 2.0 g of resin were dried in a laboratory oven at 105 ± 2 °C until constant mass was reached.

The viscosity of the four UF resins was determined by the Brookfield method. The test values registered on the Brookfield instrument together with factors based on the employed combination of the type of rotating spindle and the rotation speed were used to calculate the viscosity in Pa s.

The pH value of each UF resin sample was determined by inserting a glass electrode directly into the emulsion.

The gel time of the resins containing hardener was determined by the boiling water test. The time measurement began when a test tube containing approximately 2.0 g of resin together with the hardener ammonium sulphate (1 % based on the adhesive dry matter) was immersed into boiling water. The resin in the test tube was gently stirred throughout the test. The gel time was taken as the time elapsed from immersion of the test tube until hardening of the resin, when stirring was no longer possible.

The densities of the resins were determined at 20 °C using a pycnometer of 25 mL nominal volume, the exact volume of which was determined using distilled water.

Preparation of the MALDI matrix

A saturated solution of α-cyano-4-hydroxycinnamic acid (CHCA) was prepared by dissolving the matrix in 50 % acetonitrile with 0.10 % trifluoracetic acid. The solution was vortexed thoroughly and sonicated in a water bath for several minutes at room temperature. The solution was used for the preparation of samples for MALDI-TOF MS. All employed chemicals were of p.a. purity, originating from Sigma-Aldrich (St. Louis, WI, USA).

Matrix-assisted laser desorption/ionisation time-of-flight mass spectrometry

An aliquot of each sample solutions containing an internal standard was combined 1:1 with the CHCA matrix and mixed thoroughly. Aliquots (0.50 μL) of the mixtures were spotted onto a 100-spot sample plate (Applied Biosystems) and air-dried. Mass analysis was performed in the positive ion reflector mode using a 200 Hz frequency pulsed N_2 laser operating at 327 nm. Five spectra at each of 10 randomly selected positions were accumulated per spot between 170 and 500 g mol^{-1} using the MS positive ion reflector mode acquisition method. Calibration of the instrument was realised using Calibration mixture 2 as the external standard. To generate spectra with high mass accuracy, an internal calibration was performed.

Sample preparation

For the analysis of silver clusters, 1.0 mg mL^{-1} solutions in 0.10 % trifluoracetic acid were prepared. 0.50 μL of these solutions was placed onto 0.50 μL of CHCA solution on the target.

Data analysis

Samples of the UF resins (I–IV) were mixed with the CHCA matrix in ratios of 1:100 and 1:10, v/v. The concentration of CHCA was 10 mg mL^{-1}, diluted in a 1:1 acetonitrile and water solution. After dilution, 0.50 μL volumes of samples were placed on the MALDI plate. Samples were air dried and analyzed on a 4800 Plus MALDI TOF/TOF analyser (Applied Biosystems, Foster City, CA, USA) in the positive mode. Data Explorer, version 4.9, was used for the analysis of the recorded spectra. Ions of the CHCA matrix were used for internal calibration, based on the theoretically calculated masses of CHCA monomers, dimers and trimers at *m*/*z* 190.05 (molecular formula $C_{10}H_7NO_3$), 379.09 (molecular formula $C_{20}H_{14}N_2O_6$) and 568.14 (molecular formula $C_{30}H_{21}N_3O_9$), respectively. The mass spectrum of the matrix alone was recorded in order to eliminate the signals generated by the matrix itself. Baseline correction and Gaussian smoothing was applied to each mass spectrum.

Positively charged ions were analysed in the reflector mode using delayed ion extraction. The spectra were recorded with a 200 Hz frequency data-sampling rate. Unless otherwise stated, the extraction delay time was 150 ns and deflection was used to suppress ions up to *m*/*z* 500. The spectra were recorded using the reflector mode of the TOF analyzer under delayed extraction conditions, thus improving the mass accuracy and resolution. The extraction voltage was 20 kV in all cases. Other instrument parameters were tuned for optimal resolution. All instrument high voltages were left on between all analyses to ensure a stable instrument performance. After short interruptions (< 7 min), while exchanging the sample plate, the high voltages of the instrument were switched on 50 min prior to spectra acquisition. The applied laser intensity was between 10 and 30 % of the maximum available laser power.

The spectra were acquired without a low mass gate and each spectrum represents an average of at least 100 single laser shots.

RESULTS AND DISCUSSION

Physical characteristics of UF resins

The characteristics of UF resins (Table I) showed no significant differences between samples I–III, except for the viscosity, sample III having a viscosity of 555 mPa s, while the viscosities of samples I and II were 218 and 281 mPa s, respectively. All the determined physical properties were significantly increased for sample IV in comparison to the other samples, which clearly distinguishes sample IV from samples I–III. The viscosity of sample IV was 2052 mPa s, a value 3 to 9 times higher when compared with the other samples. It will be quite evident later that increased content of higher homologues increased the viscosity of this resin.

TABLE I. The characteristics of the UF resins (Samples I–IV)

No.	Property	UF Sample			
		I	II	III	IV
1	Dry matter, %	53.7	53.6	53.8	65.6
2	Brookfield viscosity (at 20 °C), mPa s	218	282	555	2052
3	pH	7.8	7.9	8.0	7.7
4	Gel time, s	58	59	58	59
5	Density, g cm^3	1.24	1.24	1.25	1.30

Degree of polymerisation

The recorded spectra of samples I–IV (Figs. 1 and 2), obtained on the MALDI-TOF/TOF instrument, implicate a close relationship between viscosity, dry matter content and degree of polymerisation of the UF resin samples. A comparison of spectra revealed sample I had the lowest degree of polymerisation and also the lowest viscosity.

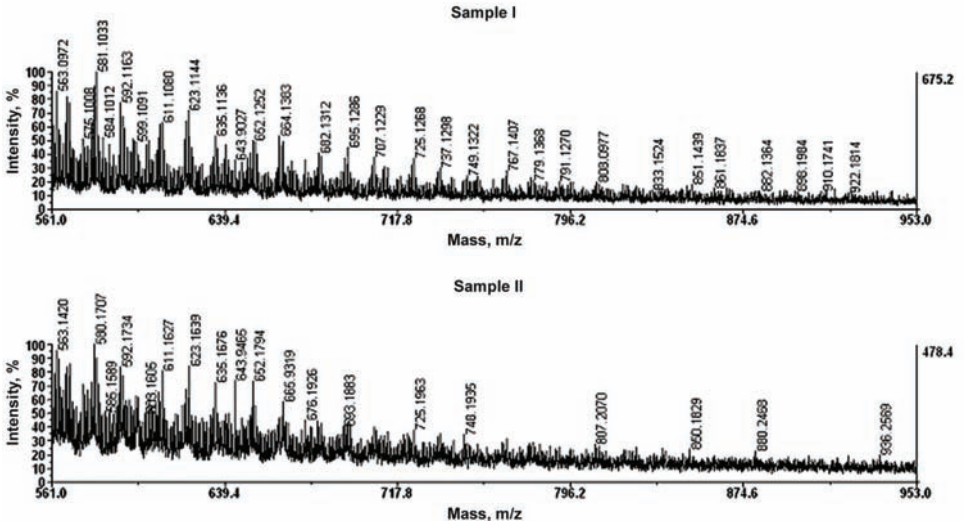

Fig. 1. MALDI-TOF Mass spectra of samples I and II in the *m*/*z* range 561–953.

Results of the analysis showed that samples I and II had similar degrees of polymerisation, but with a slightly higher amount of branching in sample I, as indicated by its more pronounced mass signals in the *m*/*z* range 561–953 (Fig. 1). Although, both samples had a similar dry matter content, they differed in viscosity, with sample II having an approximately 30 % higher viscosity than sample I.

Due to its higher viscosity, an increased amount of homologues with a higher degree of polymerisation is to be expected in sample II. However, the difference between the signal intensity of the higher homologues in samples I and II was negligible (also when compared with samples III and IV).

The dry matter content of samples I, II and III were similar. On the other hand, the viscosity of sample III was almost twice that of samples I and II. A higher viscosity implies a higher degree of polymerisation, which can be observed in the mass spectrum of sample III, shown in Fig. 2.

In addition, three times more intense signals in the same mass range of the higher polymerisation homologues were registered for sample III (data not given) than for samples I and II (shown in Fig. 1).

According to its physical and chemical parameters, sample IV had no similarities with samples I–III, having an almost one order of magnitude higher viscosity compared with the other three samples, a 10 % higher dry matter content and a significantly increased degree of polymerisation of higher homologues, as shown in Fig. 2.

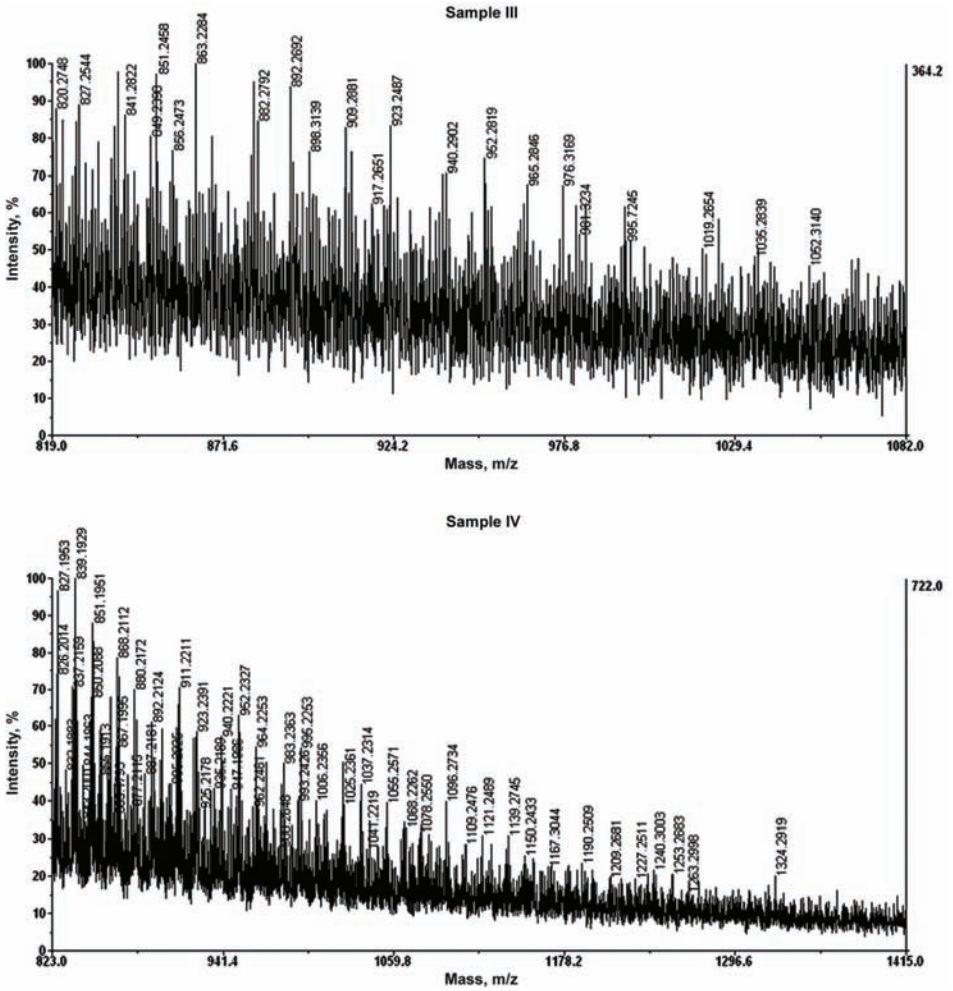

Fig. 2. MALDI-TOF Mass spectra of sample III (maximum registered polymer mass 1052 g mol^{-1}) and sample IV (maximum registered polymer mass 1324 g mol^{-1}).

Comparison of the polymer structures of samples I, II, III and IV

Higher homologue products of the polymerisation processes, which are registered in the *m*/*z* range 200–1200, may be described through a combination of the residues in the general structure. Confirmation of such structures was based

on both external and internal calibration. The external calibration was applied on the mass spectra shown in Figs. 1 and 2, with an experimental error of 0.10 g mol^{-1} of the mass value. In addition, the mass spectra were internally calibrated (see later in the text Figs. 5–7) using signals originating from the ions of the CHCA matrix, which increased the mass measurement accuracy to 5 ppm (third of the four decimal digits of the mass value). Accurate mass measurement leads to a better determination of the elemental ion composition and, in this sense, the molecular formula of a link can be established. As the polymers consisted of a series of links, it was impossible to determine the molecular formulas of all the polymers. However, it was possible to determine the constitutive elements of the polymer structure.

The true mass and molecular formula were determined using the signals of the highest intensity in order to identify the structure of the higher homologues. Within the observed mass range and according to the signal intensity, it is possible to determine the type of homologue and the preferred form of branching. NMR research indicated that the formation of mono-, di- and tri-hydroxymethyl urea under alkaline conditions amounts to 45–60 % and partial polymerisation to dimethyl ethers to 10–20 % (*i.e.*, –NH–CH_2OH 45–60 % and –$N(CH_2OH)_2$ 10–15 %).[35] In addition, 10–15 % of the formaldehyde remained unreacted. The formation of methylol groups mostly depended on the F/U molar ratio, with higher molar ratios increasing the tendency to form highly methylolated species.[36,37]

The significant intensive signal of MMU can be seen at *m*/*z* 91 in the MALDI-TOF mass spectra of samples I–IV shown in Fig. 3. Some examples of polymer chains of ether homologues are demonstrated in Figs. 4 and 5, from which, it is possible to determine the representative type of molecular structure originating in the branching process and growth of the polymer chains. This might reveal if the method of synthesis favours the creation of ether or methyl bonds and, furthermore, allow an estimation of the preferred number of hydroxyl groups per number of carbons in the chain. As expected, the highest MMU intensity of 68,000 was registered for sample I, in comparison to sample IV, with an MMU intensity of 22000. Contrary to sample IV, which had an increased ratio of higher homologues, sample I had increased amounts of simple MMU structures, 3.1 times higher when compared to sample IV, suggesting poor branching in sample I and a high degree of polymerisation of sample IV. The relations between samples II and III were similar to those of samples I and IV. Thus, sample III had a higher ratio of higher polymer structures in comparison to sample II, while sample II had a 2.7 times more intensive MMU signal when compared to sample III.

Structures **A**, **B** and **C** shown in Fig. 5 may also belong to structures with hydroxymethyl groups with secondary and tertiary amines in different positions. Thus, the molecular formulas of structures **A** $C_8H_{18}N_4O_5$, **B** $C_9H_{20}N_4O_6$ and **C** $C_{10}H_{22}N_4O_7$ would have to be preserved. Mass spectra showing the intensity of the structures **A**, **B** and **C** are shown in Fig. 6.

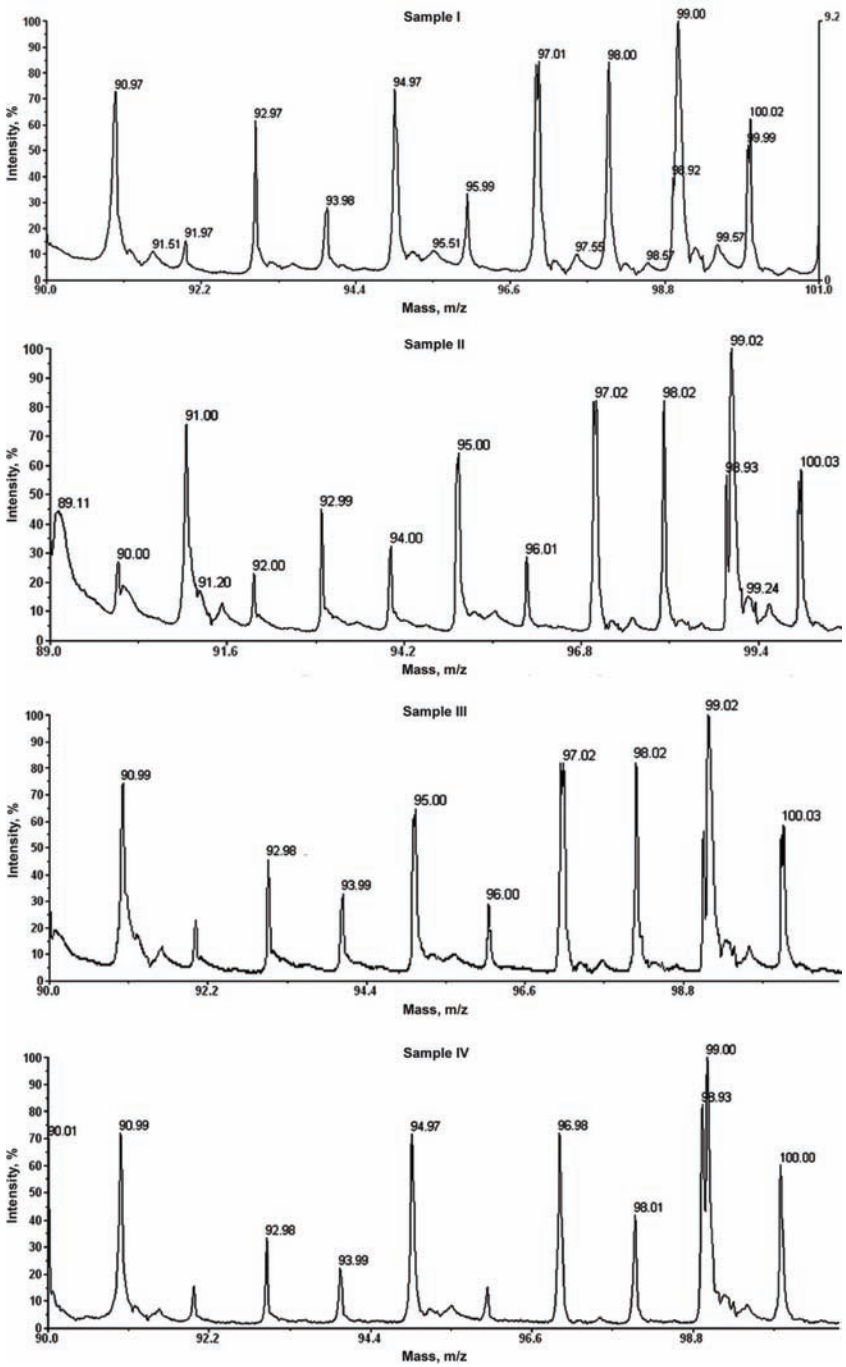

Fig. 3. MALDI-TOF Mass spectra of samples I–IV, with a significant intense signal of monohydroxymethylurea (MMU) at *m*/*z* 91.

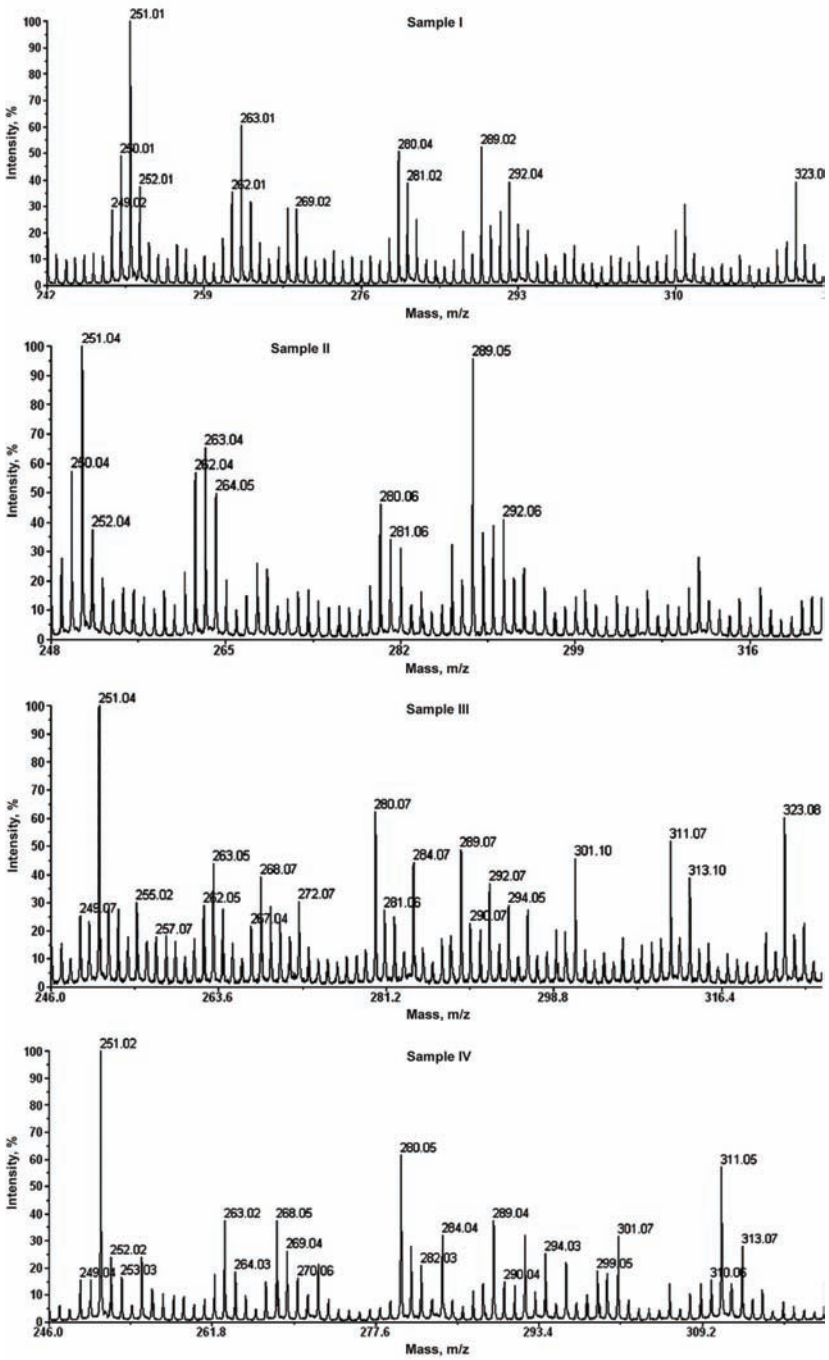

Fig. 4. Molecules formed through reaction of urea and formaldehyde under alkaline conditions, registered in the *m*/*z* range of 250–312.

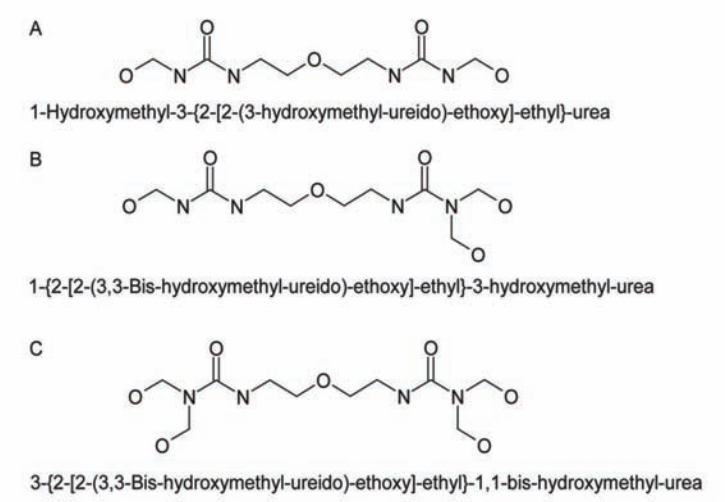

Fig. 5. Molecules formed through reaction of urea and formaldehyde under alkaline conditions, registered in the *m*/*z* range of 250–312. The associated theoretical *m*/*z* values for structures **A**, **B** and **C** are 251.14, 281.14 and 311.16, respectively.

The mass spectrum of sample IV for the selected region is shown in Fig. 6. Identical mass spectra were obtained for samples I–III. According to the signal intensity of the ion structures **A**, **B** and **C**, it may be concluded that the homologues containing ether bonds are more abundant than those of homologues with methylene bonds are. It may also be concluded that the most intensive signals in the spectra belong to structures with terminal di- and tetrahydroxymethylene groups (structures **A** and **C**). The calculation of molecular formulas in regards to the

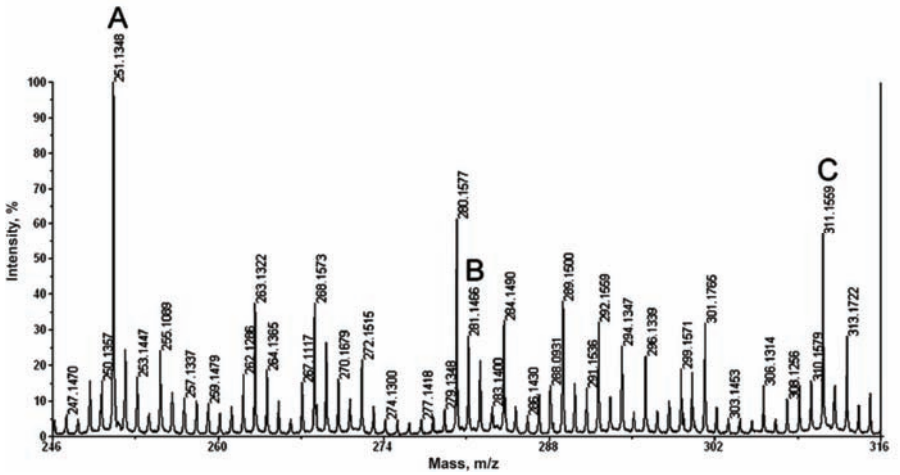

Fig. 6. MALDI-TOF Mass spectra of sample IV with the **A**, **B** and **C** structures designated.

measured molecular masses for structures **A**–**C** were possible because a maximum measurement error of 5 ppm was achieved.

Methylene bridges, branching polymer structures, are present over the whole spectrum and signify the difference between peaks of 12 g mol^{-1} or 12.0072 g mol^{-1} as measured and shown in Fig. 7.

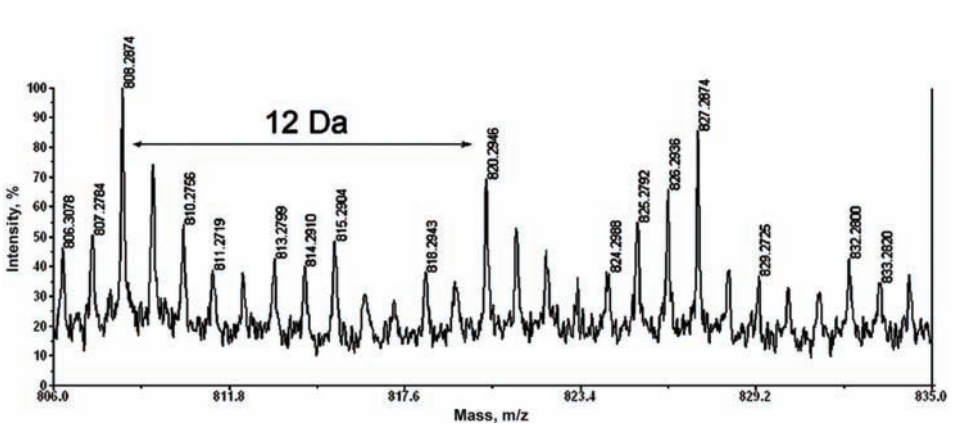

Fig. 7. MALDI-TOF Mass spectrum of sample IV with noticeably constant differences of 12 g mol^{-1} between the most intensive signals in the spectrum.

CONCLUSIONS

This paper describes some results obtained in an investigation of urea–formaldehyde (UF) resins of different degrees of polymerisation by MALDI-TOF mass spectrometry. Each of the four samples gave a contribution to the elucidation of the establishment of the molar masses of the resins. The interpretation and combination of the results led to following conclusions:

1) The average *MW* of the examined samples I–IV of UF resin was between 936 and 1324 g mol^{-1}, with a maximal deviation of 20 %, depending on the ratios of the reactants.

2) The signal intensities and their positions regarding samples I–IV showed no differences. The only noticeable difference concerned the signal intensities in the higher mass ranges (up to 1400 g mol^{-1}), which corresponds to more branched and longer homologues of the polymers.

3) Sample IV had, by far, the highest degree of branching and polymerisation when compared to samples I–III, which was evidenced as it was the polymer giving the highest recorded mass of 1324 g mol^{-1} and multiple higher signal intensities in the *m*/*z* range of 250–1000.

4) MALDI-TOF proved to be an appropriate technique for analyzing these types of polymers, bearing in mind that the results of analysis corresponded with the results of physical and chemical measurements (dry matter content, viscosity,

gel time, *etc*.). For routine polymer analysis, this technique enables a relatively swift and simple determination of the degree of polymerisation, through the monitoring of key changes in the polymer structure. It may be possible to monitor a decrease in the intensity of the MMU signal, which corresponds to an increase of the mass spectra values in the mass range of higher homologues, above 1000 g mol^{-1}.

Acknowledgements. The research work presented in this paper was financed by the Ministry of Science and Technological Development of the Republic of Serbia, Project "Wood biomass as a resource of sustainable development of Serbia", 20070-TP.

И З В О Д

РАСПОДЕЛА МОЛАРНЕ МАСЕ УРЕА–ФОРМАЛДЕХИДНИХ СМОЛА РАЗЛИЧИТОГ СТЕПЕНА ПОЛИМЕРИЗАЦИЈЕ ОДРЕЂЕНА МАСЕНОМ СПЕКТРОМЕТРИЈОМ MALDI-TOF

ИВАНА ГАВРИЛОВИЋ-ГРМУША[1], ОЛИВЕРА НЕШКОВИЋ[2], МИЛАНКА ЂИПОРОВИЋ-МОМЧИЛОВИЋ[1] И МЛАЂАН ПОПОВИЋ[1]

[1]Шумарски факултет, Универзитет у Београду, Кнеза Вишеслава 1, 11030 Београд и [2]Лабораторија за физичку хемију, Институт "Винча", Мике Петровића-Аласа 12–14, 11351 Београд

У циљу карактеризације четири узорака уреа–формалдехидне (УФ) смоле, коришћена је метода масене спектроскопије MALDI-TOF (матрицом потпомогнута ласерска десорпција/јонизација-време прелета). Као један од видова анализе полимера, поменута техника омогућује релативно брзо одређивање степена пилоконденсације путем праћења кључних промена у структури полимера. При анализи узорака УФ смоле утврђено је да смањење интензитета ММУ сигнала одговара повећању вредности масеног спектра у опсегу виших хомолога изнад 1000 g mol^{-1}. Значајна разлика односи се на интензитет сигнала при вишем масеном опсегу (до 1400 g mol^{-1}), што одговара разгранатијим и дужим полимерним хомолозима. Средња *Mw* испитиваних узорака налази се у опсегу од 936 до 1324 g mol^{-1}, са максималном девијацијом од 20 % у зависности од компоненти.

(Примљено 30. октобра 2009, ревидирано 25. јануара 2010)

REFERENCES

1. M. Dunky, A. Pizzi, *Wood adhesives, in Adhesion Science and Engineering – 2. Surfaces, Chemistry and Applications*, Amsterdam, 2002, p. 1039
2. A. Pizzy, *Wood Adhesives, Chemistry and Technology*, Marcel Decker Inc., New York, 1983
3. M. Dunky, In *Proceedings of 5th Pacific Rim Bio-Based Composites Symposium*, Cambera, Australia, 2000, p. 205
4. M. Dunky, *Int. J. Adhes. Adhes.* **18** (1998) 95
5. P. Christjanson, T. Pehkb, K. Siimera, *Proc. Estonian Acad. Sci. Chem.* **55** (2006) 212
6. J. Billiani, K. Lederer, M. Dunky, *Angew. Makromol. Chem.* **180** (1990) 199
7. M. Dunky, K. Lederer, *Angew. Makromol. Chem.* **102** (1982) 199
8. C. Huber, K. Lederer, *J. Polym. Sci. Polym. Lett. Edn.* **18** (1980) 535
9. M. Scheikl, M. Dunky, *Holz. Roh Werkst.* **54** (1996) 113
10. M. Scheikl, M. Dunky, *Holzforschung* **52** (1998) 89

11. M. Scheikl, M. Dunky, *Holzforsch. Holzverwert*. **48** (1996) 55
12. M. Dunky, K. Lederer, E. Zimmer, *Holzforsch. Holzverwert*. **33** (1981) 61
13. S. Katuscak, M. Tomaz, O. J. Schiessel, *Appl. Polym. Sci*. **26** (1981) 381
14. S. Ye, Q. Ran, W. Wu, X. Mao, *Thermochim. Acta* **253** (1995) 307
15. D. Braun, F. Bayersdorf, *Angew. Makromol. Chem*. **81** (1979) 147
16. D. Braun, P. Gunther, *Kunststoffe* **72** (1982) 785
17. D. Braun, P. Gunther, *Angew. Makromol. Chem*. **128** (1984) 1
18. S. Chow, P. R. Steiner, *Holzforschung* **29** (1975) 4
19. G. E. Myers, *J. Appl. Polym. Sci*. **26** (1981) 747
20. B. Tomita, Y. J. Hirose, *J. Polym. Sci. Polym. Chem. Edn*. **14** (1976) 387
21. B. Tomita, S. J. Hatono, *J. Polym. Sci. Polym. Chem. Edn*. **16** (1975) 151
22. M. Chiavarini, N. Del Fanti, R. Bigatto, *Angew. Makromol. Chem*. **46** (1975) 151
23. S. Giraud, L. Lefevre, P. Stracke, H. Francois, A. Merlin, A. Pizzi, X. Deglise, *Holzforsch. Holzverwert*. **49** (1997) 50
24. M. G. Kim, L. W. Amos, *Ind. Chem. Res*. **29** (1990) 208
25. R M. Rammon, W. E. Johns, J. Magnuson, A. K. Dunker, *J. Adhes*. **19** (1986) 115
26. M. Szesztay, Z. Laszlo-Hedving, C. Takacs, E. Gasc-Baitz, P. Nagy, F. Tudos, *Angew. Makromol. Chem*. **215** (1974) 79
27. I. S. Chuang, G. E. Maciel, *Macromolecules* **25** (1992) 3204
28. I. S. Chuang, G. E. Maciel, *Polymer* **35** (1994) 1621
29. I. S. Chuang, B. L. Hawkins, G. E. Maciel, G. E. Myers, *Macromolecules* **14** (1985) 1482
30. R. Ebdon, P. E. Heaton, T. N. Huckerby, W. T. S. O'Rourke, J. Parkin, *Polymer* **25** (1984) 821
31. C. G. Hill, A. M. Hedren, G. E. Myers, J. A. Koutsky, *J. Appl. Polym. Sci*. **29** (1984) 2749
32. M. Zanetti, A. Pizzi, M. Beaujean, H. Pasch, K. Rode, P. J. Dalet, *J. Appl. Polym. Sci*. **86** (2002) 1855
33. A. Pizzi, H. Pasch, C. Simon, K. J. Rode, *J. Appl. Polym. Sci*. **92** (2004) 2665
34. A. Despres, A. Pizzi, C. Vu, H. J. Pasch, *Appl. Polym. Sci*. **110** (2008) 3908
35. P. Christjanson, K. Siimer, T. Pehk, I. Lasn, *Holz Roh- Werkstoff* **60** (2002) 379
36. I. de Jong, J. de Jonge, *Rec. Trav. Chim. Pays-Bas* **71** (1952) 643
37. I. de Jong, J. de Jonge, E. A. K. Eden, *Rec. Trav. Chim. Pays-Bas* **72** (1953) 88.

Journal of the Serbian Chemical Society
JSCS@tmf.bg.ac.rs • www.shd.org.rs/JSCS

J. Serb. Chem. Soc. 75 (5) 703–715 (2010)
JSCS–4000

UDC 546.224–31+66–914:542.08+
519.233(497.11Obrenovac)
Original scientific paper

Impacts of some meteorological parameters on the SO_2 concentrations in the City of Obrenovac, Serbia

SNEŽANA S. NENADOVIĆ[1], LJILJANA LJ. MATOVIĆ[1], MIŠKO M. MILANOVIĆ[2], SAVA V. JANIĆEVIĆ[3], JASMINA D. GRBOVIĆ NOVAKOVIĆ[1]* and MILUTIN A. LJEŠEVIĆ[2]

[1]Vinča Institute, Laboratory of Materials Sciences, P.O. Box 522, 11000 Belgrade, [2]Institute for Environmental Research and Geographic Information Systems, Studentski trg 3/III, 11000 Belgrade and [3]Institute for Geography, Faculty of Natural Sciences and Mathematics, University of Novi Sad, Trg Dositeja Obradovića, 21000 Novi Sad, Serbia

(Received 21 October 2008, revised 12 November 2009)

Abstract: In this paper, the impacts of some meteorological parameters on the SO_2 concentrations in the City of Obrenovac are presented. The City of Obrenovac is located in the north-west part of Serbia on the banks of the River Sava. The observed source emission, the power plants TENT A and B are situated on the bank of the Sava River in the vicinity of Obrenovac. During the period from January to November 2006, the concentrations of sulfur dioxide in the air at 4 monitoring sites in Obrenovac were measured. It was noticed that the maximal measured daily concentrations of sulfur dioxide ranged from 1 μg m^{-3} (16th November, 2006) to 98 μg m^{-3} (29th January 2006) and lie under the maximal allowed concentration value according to the Serbian Law on Environmental Protection. The measured sulfur dioxide concentrations mostly showed characteristics usual for a daily acidification sulfur dioxide cycle, excluding the specificities influenced by the measuring site itself. Sulfur dioxide transport was recorded at increased wind speeds, primarily from the southeast direction. Based on the impact of meteorological parameters on the sulfur dioxide concentration, a validation of the monitoring sites was also performed from the aspect of their representivity.

Keywords: sulfur dioxide; correlation; meteorological data; thermal power plant; environment.

INTRODUCTION

Sulfur dioxide (SO_2) is an important trace species in the atmosphere, both under background conditions and in polluted areas.[1] The present concern on the

* Corresponding author. E-mail: jasnag@vinca.rs
doi: 10.2298/JSC081026030N

increasing level of SO_2 in the troposphere is essentially due to its role in causing environmental issues and posing detrimental effects on human health.[2–8] For instance, sulfate aerosols, through processes of scavenging and acid rain, lead to serious degradation of terrestrial and aquatic ecosystems.[5–10] It can be released into the troposphere as a result of anthropogenic and natural phenomena. The emitted SO_2 is chemically converted to sulfuric acid in the atmosphere, both in the gaseous and aqueous phase.[1] Thus, SO_2 is a major acid rain precursor, and its oxidation product, sulfate, plays an important role in radiative forcing of the climate.[5–10] When these acid rains precipitate, damage is caused to both ecosystems and the environment. The related formation of sulfuric acid aerosols can cause human respiratory morbidity and mortality. Sulfate aerosols have a cooling effect on the Earth's surface (Intergovernmental Panel on Climate Change (IPCC), 2001). These sulfate particles reflect energy coming from the sun, thereby decreasing the amount of sunlight reaching and heating the Earth's surface. The contribution of SO_2 to acidic deposition on terrestrial ecosystems by dry deposition and by precipitation in dissolved forms, such as fogs and clouds, is also clear. When converted into aerosols, it also has an impact on visibility.[9]

Natural sources of air pollution include gaseous emissions, animals and lightning, and gaseous and particulate emissions from volcanic eruptions, soil erosion, wind-blown dust and forest fires.[11]. Anthropogenic sources of air pollution involve combustion of fossil fuels (thermoelectric power plants, motor vehicles, communal and household heating installations), mining operations (sources of fugitive dust emissions), manufacturing processes (metallurgical plants, chemical plants, oil refineries), agricultural activities (crop spraying, burning of crop-residue), *etc*. Anthropogenic emissions of SO_2 occur predominantly at the continental surface and chemical conversion and loss processes occur during transport. Air pollutants are transported in the atmosphere *via* advection and turbulent diffusion processes.

According to Serbian Law on Environmental Protection (Official Gazette of the Republic of Serbia No. 135/04), the emission limit value of the SO_2 concentration into the air is 150 μg m^{-3}.

EXPERIMENTAL

Topological data of the City of Obrenovac and the monitoring sites

The City of Obrenovac is located in the north-west part of Serbia on the banks of the River Sava. The observed sources of pollution, power plants TENT A and B are situated on the bank of the Sava River, 42 km upstream from the Serbian capital Belgrade. They were built in 1970 and produce between 2.2 and 2.5×10^9 kg of coal ash per annum.[1] Approximately 70 % of the total energy production in Serbia is obtained from seven power plants situated near Obrenovac, in the vicinity of coal mines, having a combined installed power of 5766 MW.[1] The coal ash is transported to the dump after being suspended in the water taken from the Sava River, in an approximate ratio 1:10. Hitherto, TENT A has shown itself to be one of the most reliable parts of the Serbian power system, as it provided over 6000 h of work with

the full power connected to the power grid. This activity produces air contamination, so a constant control of the pollutants is required.

The daily average values of SO_2 in Obrenovac were calculated using arithmetic averages of the data obtained from four monitoring points. The meteorological data was provided by the Republic Hydro-Meteorological Service of Serbia. Eighty percent of the measured values were used in this study. A map of the monitoring points near TENT A and B is given in Fig. 1.

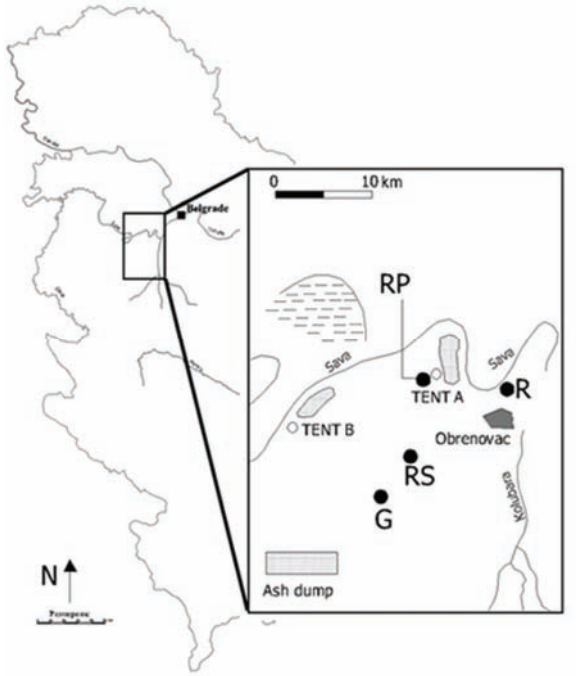

Fig. 1. Monitoring points of sulfur dioxide concentration: R, RS, RP and G located in the vicinity of the power plants TENT A and B. The exact distances are given in Table I. As can be seen, the monitoring points RS and G are located south from TENT A and southeast from TENT B; RP and R are situated east from TENT B while RP is located west from TENT A, R is located east from TENT A.

TABLE I. Distances of the monitoring sites from the SO_2 sources, monitoring method and equipment

Monitoring site	Method of monitoring	Equipment	Distance, km	
			TENT A	TENT B
R	JUS ISO 6767	Ultramat 23-Simens	3.0	–
RS		Biolafite SF8	3.6	–
RP		Ultramat 23-Simens	1.0	–
G		Biolafite SF8	–	9.5

The main factor which defines the weather and climate in Obrenovac is its geographic location. Obrenovac is located near the confluence of the Rivers Kolubara and Sava, 80 m above sea level, 20° 11' 40" east of Greenwich Time at latitude of 44° 39' 34" north. As mentioned before, Obrenovac is situated in the northwest part of Serbia where two regions, Srpska Posavina and Podrinje with Podgorina emerge. Srpska Posavina has a moderate continental climate with appreciable micro-climate differences, mostly arising from the junction between

a Mediterranean Climate (a climate of the bank of the Adriatic Sea) and a Carpathian climate. The primary characteristics of a moderate continental climate are warm summers and cold winters. Obrenovac is open in the north and northwest directions as there are no orographic barriers; hence the cold air current has an easy breakthrough to the south. It can be said that Obrenovac is under the influence of a Pannonian-continental climate. In any case, the Fruška Gora Mountain, which is located around 60 km northwest of Obrenovac (538 m height above sea level), is the only orographic barricade from the north. The mountains Cer (689 m), Povlen (1347 m), Maljen (1104 m), Rudnik (1132 m) are located west and south of the City, while Kosmaj (696 m) and Avala (506 m) are located east of Obrenovac. From both the orographic viewpoint and the atmospheric dynamics process, these mountains play an important role in the development of the weather.

Used equipment

The equipment employed during the experiments and the precise positions of the monitoring sites are presented in detail in Table I. The JUS ISO 6767 method, which is approved by the "Regulations on the boundary levels of emission, the criteria for establishing of monitoring points and the records data" and published in the Official Gazette of RS, No. 54/92, 30/99 and 19/06, was applied to monitored the daily concentration of SO_2 in the vicinity of TENT A and B at the four monitored points. The employed method is a manual spectrophotometric method equivalent to the West Geake method.

Meteorological data for the City of Obrenovac during 2006

The meteorological data were obtained from the local meteorological station (H_s = 71 m, φ = 44°39'34" N and λ = 20°11"40" E), which is located in the city center of Obrenovac. Two seasons: summer (May–mid October) and winter (December–February), with a very short spring (March and April) and autumn (October and November) were observed during 2006. The average summer temperature was 32.8 °C, while the winter one was 8 °C, with an average temperature difference between day and night of 12 °C. This great temperature difference promotes the formation of dew as the relative humidly of the air generally becomes high, especially during the winter season. The relative humidity in the region fluctuated between 86 % in August and 39 % in January, with a visibility of about 5 km (see Fig. 2). This restricted visibility is the result of the presence of solid particles in the atmosphere.

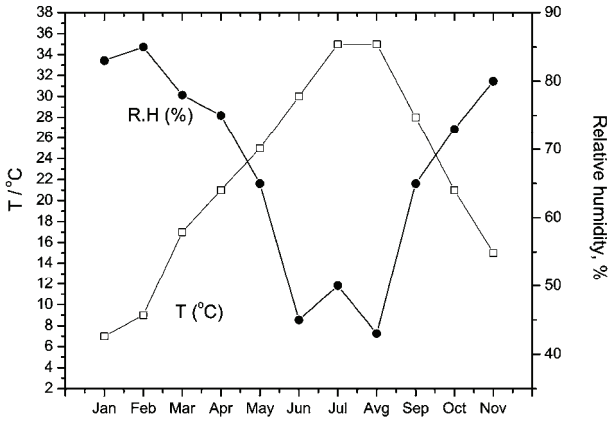

Fig. 2. Meteorological parameters in the City of Obrenovac during 2006.

As mentioned before, Obrenovac is influenced by both cold and warm air because of its geographic location. In the winter time, the penetration of cold air from north and the Carpathian region cause a significant drop in the air temperature, and windy and dry weather. During the spring, the southwestern flows are dominate, leading to an increase in air temperature, while east, northeast and southeast penetrations appear in the cold part of the year. When cold air from the northeast and southeast travels west, it encounters the serious orographic barricade of the Carpathian mountains; hence, direct northeast penetrations are very unusual. This cold air mass, called Koshava Wind, more or less also appears in Obrenovac. During the summer, the penetrations of cold air from the north onto the warm Balkans provoke phenomenon of weather disasters. The cold air warms up quickly from the ground, transforms and obtains the characteristics of continental tropical air. There are no basic differences between the cold north and cold northwest penetrations with respect to the weather development. It is very interesting to analysis the penetration of cold air from the northwest during the winter when in there is a huge accumulation of cold air in the Panonnian basin. In this case, instead of a drop in temperature, the temperature increases. Few days before the cold air incursion, the air pressure becomes reduced, and then during penetration suddenly increases. The air pressure starts to decrease on the day after the incursion and continues for several days. Then, precipitation can often be noticed (see Table II). After a precipitation period, the weather is usually clear and cold. As meteorological parameters (air pressure, air temperature, air humidity, rainfalls, cloudy conditions and wind) have a high influence on the emission of pollution materials and on the air quality in general, these parameters will be discussed individually.

TABLE II. Rainfall amount, mm, for period January–December 2006 in the City of Obrenovac

Month	Rainfall amount
January	111.9
February	133.4
March	141.2
April	112.8
May	221.6
June	108.6
July	28.6
August	222.4
September	109.6
October	97.3
November	102.5
December	98.6

Air pressure: In the City of Obrenovac and its surroundings, the average air pressure was around 1006 mbar. From January, when the average pressure attained its highest value (1010 mbar), the air pressure decreased and had the lowest value (1003 mbar) in April. Just for comparison, in October the value reached 1008 mbar.

Air temperature. The year average temperature in Obrenovac was 11 °C. The highest average value of 21 °C was in July, while the lowest (–2.1 °C) was in January. The average fluctuation during the year was 25 °C, which it is one of the most important indicators of a continental climate in the Obrenovac area.

Cloudiness. The average number of clear days during the year in Obrenovac was 66 (one in December and 11 in August, for comparison). During the year, over 50 days were cloudy, while 115 (17 in December and 3.5 in August) were partially gray with a fog tendency.

Wind. In Obrenovac, northwesterly and westerly winds have the greatest influence on the air quality in the city. There is also a considerable effect of southeasterly winds, as mentioned before; hence, the positions of the measuring points were chosen taking into account the wind rose.

RESULTS AND DISCUSSION

As explained before, the emissions from power plants are mainly due to the type of fossil fuels burnt, which results in the discharge of various pollutants into the atmosphere. Sulfur is prevalent in most types of fossil fuels which are used for power generation, resulting in the release of large quantities of sulfur dioxide into the atmosphere. As stated already, SO_2 and NO_x are further oxidized and either deposited through wet or dry processes, resulting in sulfuric and nitric acid, respectively, or sulfate and nitrate particulates.[2–10] According to İçağa *et al.*, correlations exist between SO_2 and humidity, temperature, and inversion at the 1 % significance level but no significant relationship exists between wind velocity and precipitation variables and pollutants. Based on these findings, the present measurements were divided into two periods: cold and hot and the relationships between the meteorological data and the SO_2 concentration were examined.

Monitoring of SO_2 during the cold season

The average temperature in January 2006 was lower than usual in Obrenovac and the surroundings. From the 23rd to the 28th, the temperature fell to –10 °C. Consequently, the emission of sulfur dioxide was pronounced at the monitoring point R, which is located 3 km from TENT A, as show in Fig. 3. As the monitoring point RP is located at a distance of only 1 km from TENT A, the highest emissions were at this monitoring point. The same situation was found in February, as is shown in Fig. 3b.

Due to the frequent occurrence of snow during February 2006, wet deposition of pollutants on land and the Sava River occurred. During March 2006 (see Table II), the amount of rainfalls were extremely high, two to three times greater than usual. Snow was visible on the mountains during the entire month. This metrological situation cause pronounced wet deposition on the soil and River Sava, and high emissions of SO_2 at the monitoring points located 3 and 9.5 km from the source of pollution, TENT B. At the beginning of October 2006, maximum daily temperatures were 6 to 8 °C higher than the average for this time of the year. The period of hot weather lasted for 2 weeks until the 16th October. Again, from the 21st to the 26th October, a new period with summer temperatures over the whole country arrived, with daily maximum temperatures higher than 25 °C. During October, but also during September, unusual and very small rainfalls were

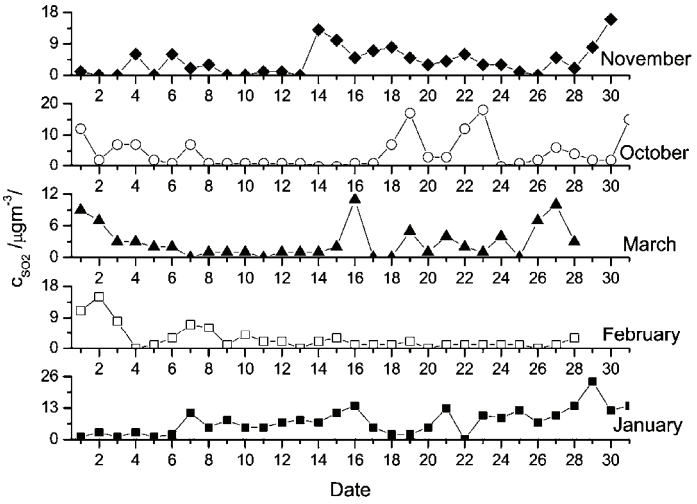

(a)

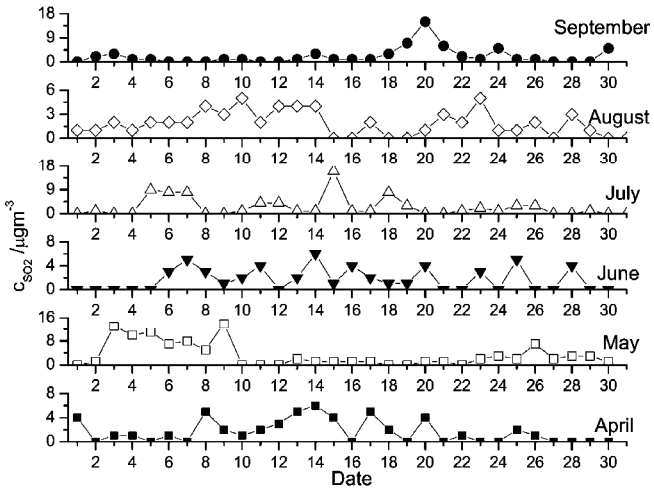

(b)

Fig. 3. Emission of SO_2 (μg m^{-3}) in the atmosphere at the monitoring point R during a) the cold season and b) the hot season. The exact distance from TENT A and B are given in Table I.

registered over the entire country. As can be seen from Figs. 3a–6a, which represent the cold (winter) period, the occurrence of the "warm wave" phenolmena had a great influence on the migration in environment of the emitted SO_2. The temperature curve in November 2006 showed unusual behavior: at the beginning of the month, the average temperature was lower than normal, while in the second and third decades, the temperature was unusually high (see Table II). The

maximum emission of SO_2 (26 μg m^{-3} monitoring point R) was observed in November when the "warm wave" phenomenon was registered in two periods: from the 14th to the 21st and the 24th to the 29th. As in the previous months, there was a lack of rainfall and the autumn in 2006 was warmer than average. The observation of a high peak (24 μg m^{-3}) in the SO_2 concentrations between January and February, as show in Figure 4b, at the RP monitoring point, however, was not consistent with the occurrence of the observed health impact (the sensation of an unusual smell and the onset of symptoms generally occurred between October and November at the RS measuring point). Nevertheless, the lag of several hours between the first onset of symptoms and a peak in the SO_2 readings may not violate the relationship between symptoms and air pollution. The maximum SO_2 concentrations at the monitoring sites G and RS were 11 and 15 μg m^{-3}, respectively, which was expected since these monitoring sites are distant form TENT A and B.

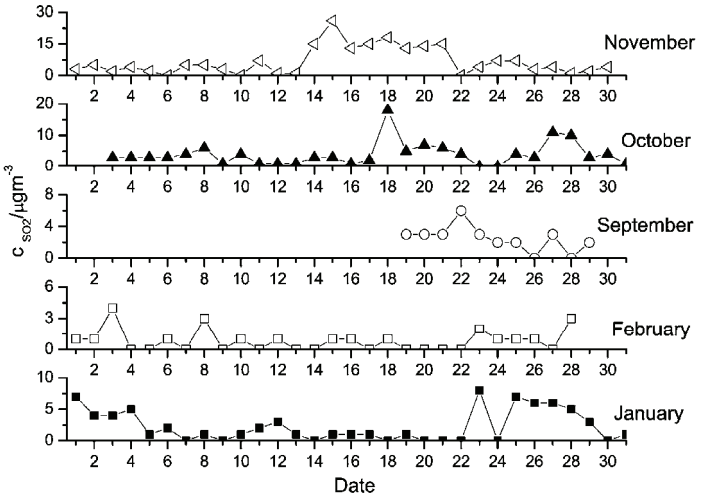

Fig. 4. Emission of SO_2 (μg m^{-3}) in the atmosphere at the monitoring point RP during the cold season. The exact distance from TENT A and B are given in Table I.

Monitoring of SO_2 during the hot season

During April, the average temperature values deviated from the normal ones by 0.5 to 1.9 °C. In the second half of the month, summer temperatures were registered, often accompanied by raining, hence, the monthly rain quantities were higher than usual. The higher temperatures caused marked changes in the sulfur dioxide concentrations. As can be seen in Fig. 3b, the emission from the sources TENT A and B attained maximum values at the monitoring point R.

A completely different weather situation was found throughout May. It was very cold during the first half of the month, with frost phenomena in the moun-

tains, and in the second half, the temperatures reached tropical ones. As the weather conditions were changing, the emission of SO_2 changed. This trend is shown in Fig. 3b. The highest values were measured 3 km from the source TENT A at the monitoring point R.

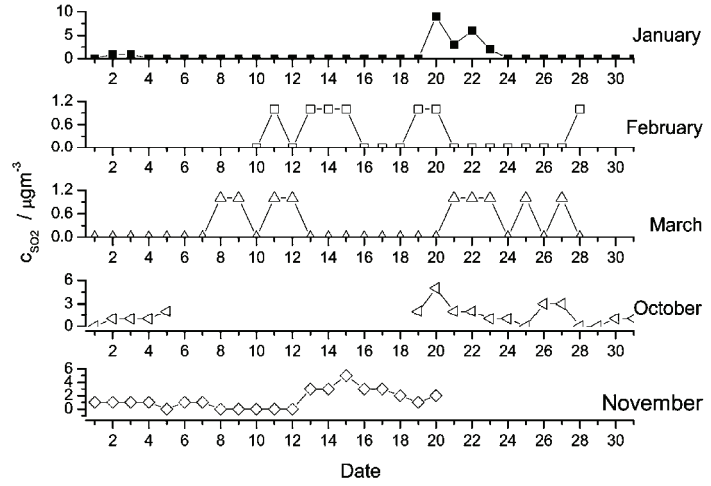

(a)

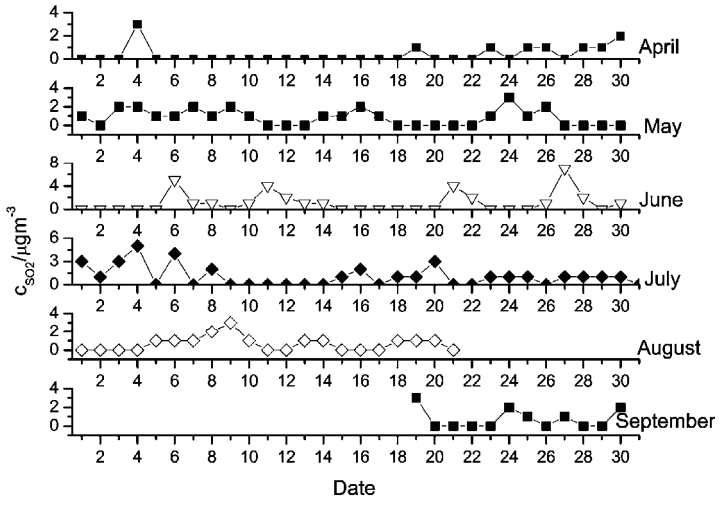

(b)

Fig. 5. Emission of SO_2 (μg m^{-3}) in the atmosphere at the monitoring point RS during a) the cold season and b) the hot season. The exact distance from TENT A and B are given in Table I.

Taking into account the previous results, it can be concluded that the wind rise played an important role in SO_2 migration in the City of Obrenovac.

At the beginning of June, penetration of very wet air with constant precipitations occurred. The maximum temperatures in the first several days were extremely low and in the last 60 years, such low temperatures in June were not evi-

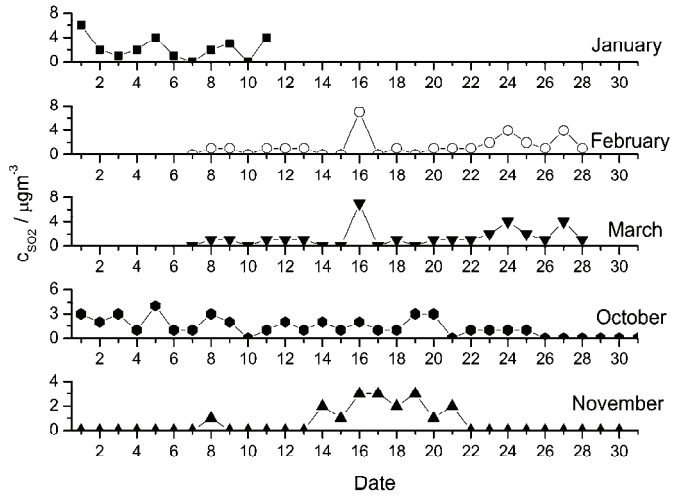

(a)

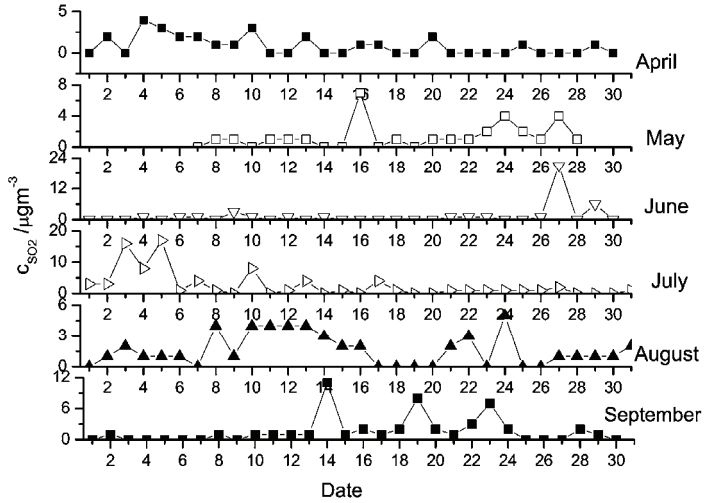

(b)

Fig. 6. Emission of SO_2 (µg m^{-3}) in the atmosphere at the monitoring point of G during a) the cold season and b) the hot season. The exact distance from TENT A and B are given in Table I.

denced. The second and third decades of June were characterized by very high temperatures (over 30 °C). In the second half of June, the phenomenon of tropical nights was evidenced. As can be seen in Fig. 6b, the SO_2 emission was domi-

nant in the period of tropical days at the monitoring site located 9.5 km away from TENT B (this can be explained by the fact that the wind was pronounced). The main climate characteristic in July was a „warm wave" phenomenon in the second half of the mouth (from the 20th to the 29th) in many places on the territory of Serbia. Even though it rained frequently in July, the average value was at the normal level. As can be seen in Fig. 6b, the monitoring point G, which is furthermost of all measuring sites, had the most pronounced emission. As is shown in Fig. 6b, the movement of sulfur dioxide was chaotic. This unusual behavior can be explained taking into account the fact that low temperatures and the large rainfalls were observed during June. In this period, both wet and dry deposition of SO_2 was noticed. During the summer period, the minimal temperatures were higher than the average values for Serbia. There were lot of rainfalls, double the usual; the summer of 2006 was warmer than the norm, and the rainfall regime had a very marked feature. A similar situation was noticed in September, which was a relatively warm mouth. As can be seen from Table III, there was a strong correlation between the amount of rainfall and SO_2 emission since the maximum emission was observed when the rainfall amount was around 100 mm. An exception was found in July when the average amount of rainfall was 28.6 μg m^{-3} at the monitoring site R but the emission of SO_2 was pronounced. A possible reason for the summer maximum is the intense flow of south-east winds. According to information presented in the scientific literature,[11–15], the seasonal variation of the sulfur dioxide concentrations in urban and semi-urban areas is characterized by a maximum during the cold period and a minimum during the warm period of the year. However, the present findings show that the main parameter that affects the concentration of SO_2 is the amount of rainfall, since the maximum was observed during both periods when the amount of precipitation was marked.

TABLE III. Correlation between maximum SO_2 emission and the rainfall amount

Monitoring site	Cold season		Hot season	
	Maximum SO_2 emission, mg m^{-3}	Rainfall amount mm	Maximum SO_2 emission, mg m^{-3}	Rainfall amount mm
R	24 (January)	112	15 (July)	28.6
RP	26 (November)	102	–	108
RS	15(November)	102	7(June)	–
G	11(November)	102	27(June)	108

CONCLUSIONS

This paper presents the impact of some meteorological parameters on SO_2 concentration in the City of Obrenovac. The maximum SO_2 concentrations occurred in the period from December to February. The results show that there is a strong relationship between the meteorological parameters and SO_2 migration in

city center of Obrenovac, within the terms statistically analyzed. The obtained results indicated that the amount of rainfall and the concentration of SO_2 emission are positively correlated. However, all the measured values of SO_2 emission were under the limits allowed by the Serbian Law of Environmental Protection. 95 % of the measured values were less then 10 μg m^{-3}, while the other 5 % ranged between 10 and 49 μg m^{-3}. Moreover, the positions of the monitoring points were well chosen, as they represent the real situation of air pollution in the Obrenovac City and the surroundings.

Acknowledgment. This work was supported by the Ministry of Science and Technological Development of the Republic of Serbia under projects 142016 and 142027. The authors are grateful to the Electric Power Industry of Serbia.

ИЗВОД

УТИЦАЈ МЕТЕОРОЛОШКИХ ПАРАМЕТАРА НА КОНЦЕНТРАЦИЈУ SO_2 У ОБРЕНОВЦУ, СРБИЈА

СНЕЖАНА С. НЕНАДОВИЋ[1], ЉИЉАНА Љ. МАТОВИЋ[1], МИШКО М. МИЛАНОВИЋ[2], САВА В. ЈАНИЋЕВИЋ[3], ЈАСМИНА Д. ГРБОВИЋ НОВАКОВИЋ[1] и МИЛУТИН В. ЉЕШЕВИЋ[2]

[1]Институт за нуклеарне науке Винча, Лабораторија за материјале, п.пр. 522,11000 Београд [2]Институт за заштиту животне средине и ГИС, Студентски трг 3/III, 11000 Београд и [3]Географски институт, Природно–математички факултет, Универзитет у Новом Саду, Трг Доситеја Обрадовића 3, 21000 Нови Сад

У раду су представљени резултати мониторинга концентрације SO_2 у ваздуху у Обреновцу који се налази на северозападу Србије на обалама реке Саве. Посматран је утицај метеоролошких параметара на концентрацију SO_2 емитованог из термоелектрана ТЕНТ А и Б који се сматрају највећим изворима емисије. У периоду од јануара до новембра 2006. године праћене су концентрације сумпор-диоксида у ваздуху на 4 мерна места локализована на различитим удаљеностима од извора емисије. Максималне измерене дневне концентрације сумпор-диоксида су се кретале од 1 μg m^{-3} (16. новембра, 2006) до 24 μg m^{-3} (29. јануара, 2006). Измерене промене концентрација сумпор-диоксида углавном показују уобичајне карактеристике дневне ацидификације циклуса уз разлике које потичу од особености мерних места. Транспорт сумпор-диоксида забележен је при појачаном ветру првенствено из југоисточног правца. На основу корелационих односа између концентрације сумпор-диоксида и одговарајућих метеролошких параметара извршена је карактеризација мерних места у погледу њихове репрезентативности за мерење сумпор-диоксида.

(Примљено 21. октобра 2008, ревидирано 12. новембра 2009)

REFERENCES

1. A. Canak-Nedic, M. Gavrilovic, N. Pavlovic, J. Nozinic, M. Stankovic, U. Kuzmanovic, M. Nedic, *Energy Econ. Ecol.* **2** (1997) 63
2. B. H. Chen, C. J. Hong, H. D. Kan, *Toxicology* **198** (2004) 291
3. N. A. H Janssen. P. H. N van Vliet, F. Aarts, H. Harssema, B. Brunekreef, *Atmos. Environ.* **35** (2001) 3875
4. T. Okita, H. Hara, N. Fukuzaki, *Atmos. Environ.* **30** (1996) 3733
5. J. S. Pandey, R. Kumar, S. Devotta, *Atmos. Environ.* **39** (2005) 6868
6. J. S. Pandey, S. Khan, V. Joseph, R. Kumar, *Environ. Monit. Assess.* **74** (2002) 105

7. A. Srivastava, *Atmos. Environ.* **38** (2004) 6829
8. A. Srivastava, A. E. Joseph, S. Patil, A. More, R. C. Dixit, M. Prakash, *Atmos. Environ.* **39** (2005) 59
9. M. C. Roger, *Environ. Pollut.* **126** (2003) 301
10. V. T. Wang, V. T. F. Cheung, K. S. Lam, G. L. Kok, J. M. Harris, *Atmos. Environ.* **35** (2001) 2735
11. J. An, H. Ueda, K. Matsuda, H. Hasome, M. Iwata, *Atmos. Environ.* **37** (2003) 3039
12. H. D. Kambezidis, N. S. Papanikolaou, *Atmos. Environ.* **22** (1988) 2557
13. H. D. Kambezidis, R. Tulleken, G. T. Amanatidis, A. G. Paliatsos, D. N. Asimakopoulos, *Environmetrics* **6** (1995) 349
14. A. G. Kelessis, *Fresenius Environ. Bull.* **10** (2001) 624
15. A. G. Paliatsos, *Fresenius Environ. Bull.* **6** (1997) 655
16. A. G. Paliatsos, *Fresenius Environ. Bull.* **7** (1998) 539.

Journal of the Serbian Chemical Society
JSCS@tmf.bg.ac.rs • www.shd.org.rs/JSCS

J. Serb. Chem. Soc. 75 (5) 717–732 (2010)
JSCS–4001

UDC 556.551+614.777/.778:
504.45.058(497.11Palić)
Original scientific paper

The evolution of the trophic state of the Palić Lake (Serbia)

IVAN GRŽETIĆ[1*#] and NATAŠA ČAMPRAG[2]

[1]*University of Belgrade, Faculty of Chemistry, Studentski trg 12–16, 11 000 Belgrade and*
[2]*Public Health Institute of Subotica, Zmaj Jovina 30, 24 000 Subotica, Serbia*

(Received 16 October 2009, revised 12 November 2009)

Abstract: The Palić Lake is a shallow lake typical for the Pannonian Plain. Due inadequate water quality, it was dried out in 1971 and re-established in 1977 and since than its trophicity has been worsening. Investigation of the long-term changes in the trophic state of this lake were tracked over the total phosphorous (*TP*), total nitrogen (*TN*), chlorophyll-a and Secchi disk transparency (*SDT*), expressed as the Carlson trophic state index (*TSI*). Regarding the *TSI* values, the water of the Palić Lake has been constantly evolving from eutrophic to hypereutrophic. *TN*/*TP* values < 10 indicate that nitrogen is the limiting factor for algal growth.

Keywords: shallow lake; lake trophicity; eco-chemical status; trophic state index; eutrophication.

INTRODUCTION

The Palić Lake is a natural lake located in the northern part of Serbia near Subotica, next to the Serbian–Hungarian border. It is a shallow lake typical for the Pannonian Plain, where the entire water column is frequently mixed. The Lake has recreational purposes but it is also a collector for treated municipal waste waters coming from the lagoons for active sludge water treatment. The Lake itself was in a very bad condition during late sixties of the last century, polluted and hypertrophic. Due to the inadequate quality of the water, a lot of mud in an anaerobic state, the mortification of aquatic plants and animals and, finally, the impossibility of using the Lake for recreational purposes, it was dried out in 1971 and re-established in 1977.

The sewage discharges from rapidly developing towns in the watershed and the growing use of fertilizers in agriculture have increased the nutrient loading to the Lake in the last decades. Again, a rapid eutrophication became apparent through the increased production of biomass and phytoplankton growth. In spite of clean-

* Corresponding author. E-mail: grzetic@chem.bg.ac.rs
# Serbian Chemical Society member.
doi: 10.2298/JSC091016043G

ing and remediation, which lasted for six years, today the Lake is again in a problematic condition; hence, it was necessary to define the current eco-chemical status and to investigate the evolving changes of the trophic state of the Lake from 1977 up till now. There is a range of factors that can influence the dynamics of eutrophication of a lake. They are useful only over a range of time scales, therefore, eutrophication dynamics may only be fully investigated when long--term, time-series data are available.[1] Eutrophication dynamics could serve to predict the Lake condition in the near future and to confirm whether immediate actions are needed or not. The most appropriate parameter for that purpose is the trophic state index or the Carlson *TSI*,[2] which has recently been adopted by the US EPA nutrient criteria recommendations for lakes and reservoirs.[3]

The aim of this work was to reconstruct the changes in the trophic state in the Palić Lake by application of the effects of the concentrations of nutrients on the changes in the trophic state and the increase of the eutrophication process in the Lake.

EXPERIMENTAL

The main sampling material for the measurements was sampled lake water which was analyzed according to APHA (1976–1998)[4] and US EPA standard methods.[5] The measured parameters important for the determination of the eco-chemical status of the Palić Lake were temperature and pH of the water, oxygen saturation, the concentrations of NH_4, NH_3, NO_2, NO_3, *TN*, PO_4-P, *TP* and chlorophyll-a, and Secchi disk transparency (*SDT*) according to US EPA standards. Analysis of blanks and duplicates were the main instruments of quality control of the measurement throughout all the studied years.

Regular monthly measurements were performed every year, from March to October, typical vegetative months, for the period of the last 29 years (1977–2006). The remaining months were more or less winter months when samples were not taken due to low temperatures and ice.

Surface water samples were taken since they were assumed representative for the entire water column, as the water was always well mixed as a result of the shallow water depth. Sampling was performed 40 cm below the lake surface in the waterfront area, in order to prevent contamination of the sample by mud from the bottom or particles from the water surface. Samples were collected into 5-L plastic jerry cans.

The *SDT*, temperature and pH value of the water samples were determined on site. Samples for the determination of dissolved oxygen concentrations were collected and treated separately. All samples were stored at 4 °C and normally analyzed within a day. The maximum storage time was less than 3 days after sampling.

Unfiltered samples were used for dissolved oxygen determination, Kjeldahl nitrogen and total phosphorous. For chlorophyll-a analysis, homogeneous samples of water were filtered through Sartorius filter-paper.

The total phosphorous (*TP*) incorporated the total of all filterable and particulate phosphorus forms. It is probably the most often analyzed fraction of phosphorus because it is used in a wide variety of empirical models relating phosphorus to a wide variety of limnological variables.[6]

The total nitrogen (*TN*) is an operational value and represents the sum of nitrite, nitrate and Kjeldahl nitrogen, which were determined in unfiltered samples.

Sampling locations

The Palić Lake is divided into four sectors (Fig. 1). Sector I, adjacent to the main collector, serves as the collector for treated municipal waste waters from lagoons for active sludge water treatment. Sector IV, some 387 ha large, is mainly for recreation purposes. Between the first and the fourth sector, there are two additional sectors – the second of about 92 ha and the third of 80 ha. The sampling positions were selected to be at the end of the first accumulation (named sector II), at the end of the second accumulation (named sector III) and at the end of the recreation accumulation (named sector IV) right beside the outflow channel that connects the lake to the Tisa River.[7] Throughout this paper, only sector IV was considered since it is the largest segment of the Lake and because of its recreational purposes.

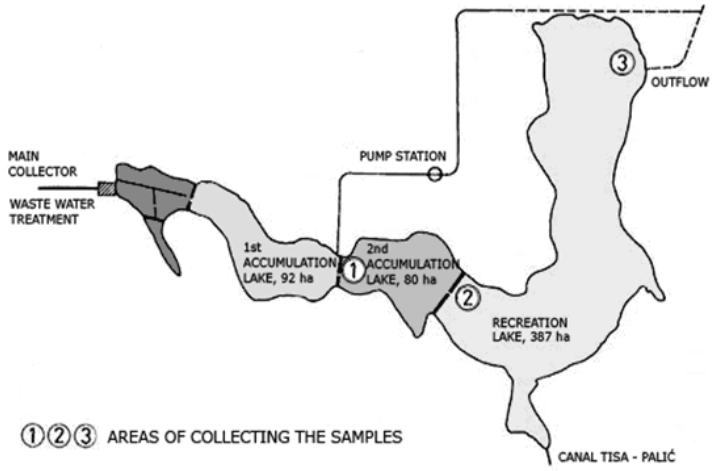

Fig. 1. The Palić Lake is divided into four sectors. Sampling locations are denoted as 1 (sector II), 2 (sector III) and 3 (sector IV). The weirs are presented with bold lines which trisect the lake.

Characteristics of the Palić Lake

The Palić Lake is a natural lake, located in the northern part of Serbia near Subotica, the second largest city of the Vojvodina Province, with a population of 150,000 inhabitants, next to the Serbian–Hungarian border on 46°16' north geographic latitude and 19°43' east geographic longitude (Fig. 2). It is a shallow lake typical for the Pannonian Plain, with an average depth of 2.4 m. As such, it is characterized by the variability of the water level, where the entire water column is frequently mixed – there is no stratification because the lake is shallow.

The Lake is 8 km long from the northern bank to the end of the western arm, and the width varies from 350 to 950 m. In the near vicinity of the Palić Lake lies the Ludaš Lake. The excess water in the Palić Lake is cadged from the east part of sector II, across a pump station, toward the lower Ludaš Lake.

Hydrographical characteristics of the Palić Lake are determined and depend on the geological, geomorphologic and climate characteristics. Urban development of the surrounding settlements (the city of Subotica and the settlement of Palić), development of close lake en-

vironment and activities in the surrounding areas have lead to an enhancement of the negative human influence on the water regime. Significant oscillations in the surface level cause constant problems in the water supply to the lake. According to the project of lake sanitation, the expected annual water wastage reached 411 mm of water column, that in relation to the surface of the lake in total means 2,500,000 m^3 water wastage by evaporation.[8] There are no significant confluents to the Palić Lake; therefore, the level of the surface is supported only by rainfall, refined waste water and underground water infiltration.

Fig. 2. Site maps showing the European and regional location of the Palić Lake.

The average inflow of water at sector I is about 11,440,000 m^3 (from 9.5×10^6 to 12.5×10^6 m^3) and the outflow at sector IV is almost the same. Under exceptional situations, when the inflow is too large, the water is led away through a channel by the end of sector II, or in cases when the water level is low, due to drought or extreme evaporation, water is brought into lake by a special cannel from the nearby Tisa River (some 20 km far-away from the Lake) at the very beginning of sector IV. The water volume in the Palić Lake is approximately 13,440,000 m^3 (total surface 560 ha and average depth 2.4 m). The average precipitation for the period 1977 to 2005 (Fig. 3) was 549 mm $year^{-1}$ (L m^{-2}), which means that the direct yearly rainfall into the lake was around 3,043,000 m^3 of water.

At a temperature of 15 °C, the level of the lake water decreases by 3 mm day^{-1}, due to evaporation; at 35 °C by 12mm day^{-1}.[9] As the average yearly temperature at Palić is some 14.7 °C, it is assumed that approximate yearly loss of water due to evaporation, is 3 mm day^{-1} or 1068 mm $year^{-1}$, almost double the amount of water that the Lake receives per year by precipitation. The exact water balance of the lake has never been properly determined. Nevertheless, the Lake looses water through evaporation (2.5×10^6 m^3) and outflow (11×10^6 m^3) and gains water from inflow (11×10^6 m^3), precipitation (3×10^6 m^3) and from the Tisa River and groundwater (3×10^6 m^3). A rough estimate says that the lake water exchange rate, the time required for a total exchange of water in the lake basin with fresh water is about one year.

In addition to wastewater and water from agricultural areas, wind deposit is a significant parameter for variations in the quality of the surface water in the Vojvodina Province. The prevailing winds from the north and north-west are characterized by erosive and accumulative

effects that decrease the depth of the Lake Basin and also expedite negative transformations and cause extinction of the lake ecosystem.

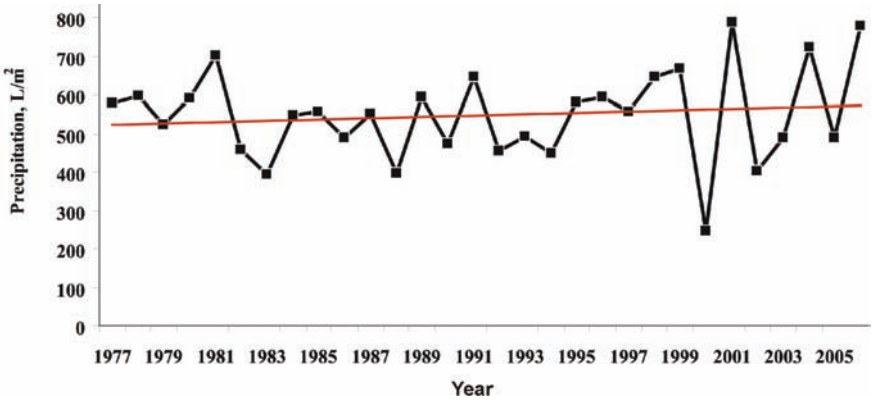

Fig. 3. Yearly precipitation in the region of the Palić Lake with trend line.

The Palić Lake can be rated among lakes that were formed by wind erosion, which caused displacement of material that uncovered underground water and created dunes elsewhere by sedimentation process. This kind of erosion is characteristic for plain areas with a dry climate and a fine-structured, incoherent terrain, without protective vegetation. It is rated among "diffused" pollutants that depose alluvium permanently into natural and artificial water flows and lakes. Being part of the great Pannonian Plain, the territory of the Province of Vojvodina was not an exception in this process, especially in its northern and central Bačka subregion.

Until 1971, the Palić Lake was the recipient of unrefined wastewater from Subotica, which caused its degradation and massive loss of quality in the tourist area. The greatest contamination was produced by waste water from industry, especially from a meat processing factory and chemical industry. The revitalization of the lake that started during the same year lasted until 1977, when all sectors of the lake were refilled by underground water and refined wastewater from the central waste water cleaning unit.

RESULTS AND DISCUSSION

The results obtained for the Palić Lake are discussed from three different aspects: trends of the measured parameters with time – investigation of long term changes, seasonal changes of the measured parameters for the period 1977–2006 and trophic state.

Trends of the measured parameters during years

The source data sets contain hundreds of measurements with some of them having skewed distributions, therefore median, minimum and maximum values are the only remaining statistical parameters that give meaningful averaged data appropriate for discussion. The results obtained for the Palić Lake, sector IV, for the period 1977–2006 are given in Table I. Each presented number corresponds to a yearly median value which covers the measuring months, March to October.

TABLE I. Processed parameters for water qual ity (minimum – Min, maximum – Max, median value - Med); Palić Lake - Sector IV, ob - tained for the period 1977–2006 (for the years 1996, 1999 and 2000, there was no data for total *P*)

Parameter	Level	Year												
		1977	1978	1979	1980	1981	1982	1983	1984	1985	1986	1987	1988	1989
Temperature, °C	Min	–	–	–	5.0	11.5	4.0	10.5	5.0	10.0	9.0	0.3	6.0	9.0
	Max	–	–	–	25.0	26.0	27.0	22.0	20.5	23.0	24.0	22.0	24.0	23.0
	Med	–	–	–	18.0	19.1	20.5	17.5	17.8	18.8	16.3	14.0	19.5	19.5
SD Transparency, cm	Min	20.0	15.0	15	16.0	10.0	20.0	20.0	18.0	20.0	10.0	20.0	20.0	15.0
	Max	180.0	35.0	45	30.0	35.0	180.0	70.0	40.0	25.0	45.0	45.0	130.0	60.0
	Med	55	25	20.5	23.5	17.5	52.5	36.0	25.0	20.0	32.5	35.0	45.0	40.0
pH	Min	8.6	8.8	9.1	8.7	8.5	8.4	8.2	8.6	8.3	8.0	7.8	8.2	8.3
	Max	8.9	9.2	9.5	9.5	9.3	9.5	8.7	9.2	9.3	10.0	9.1	8.9	9.4
	Med	8.8	9.1	9.2	9.1	8.9	8.5	8.5	8.8	8.8	8.6	8.3	8.7	8.7
Oxygen saturation, %	Min	66	83	96	33	51	42	32	85	47	43	42	76	73
	Max	128	140	209	137	191	187	105	138	126	110	209	134	157
	Med	97	119	126	113	121	67	88	98	98	89	88	98	126
Total N, mg/L	Min	0.88	1.25	2.15	1.6	10.0	0.8	1.6	5.0	3.1	3.7	1.8	0.5	5.6
	Max	3.60	5.58	13.337	28.8	31.9	16.3	8.3	10.1	14.2	7.4	57.7	25.9	27.5
	Med	2.06	4.17	8.37	12.2	15.2	7.9	4.0	5.9	7.2	5.4	4.8	10.9	16.2
Total *P*, mg/L	Min	0.37	0.45	0.37	0.7	0.7	0.2	0.3	1.1	0.6	0.5	0.3	0.2	1.0
	Max	2.00	2.08	1.6	2.5	3.7	2.6	0.6	10.6	1.2	1.5	3.3	1.3	3.2
	Med	0.825	0.66	0.93	1.9	1.2	0.4	0.4	2.3	0.8	0.8	0.6	1.1	1.8
Chlorophyll-a, mg/m^3	Min	3.0	26.6	46	88.0	1.8	1.7	2.2	27.5	10.6	25.1	8.5	5.9	7.4
	Max	54.0	189	215	423	425	112.4	29.6	607	115.4	167	3777	245.8	151.5
	Med	9	100	143	255	153.5	12.2	4.2	79.4	67.7	75.9	37.2	94.1	23.6

TABLE I. Continued

Parameter	Level	Year													
		1990	1992	1995	1996	1997	1998	1999	2000	2001	2002	2003	2004	2005	2006
Temperature, °C	Min	10.0	6.0	8.2	7.5	6.0	5.0	7.8	6.5	11.0	10.0	3.3	5.8	8.0	5.2
	Max	24.0	24.0	24.0	28.0	24.7	25.0	25.5	26.0	26.0	27.0	26.0	22.0	22.8	26.4
	Med	22.0	18.8	17.4	15.0	19.1	17.6	19.0	20.0	17.3	18.0	20.0	17.8	17.2	19.1
SD Transparency, cm	Min	20.0	20.0	20.0	15.0	10.0	10.0	–	15.0	5.0	5.0	10.0	10.0	10.0	5.0
	Max	30.0	60.0	100.0	70.0	80.0	80.0	–	80.0	30.0	15.0	50.0	50.0	30.0	10.0
	Med	25.0	30.0	60.0	20.0	35.0	65.0	–	30.0	30.0	15.0	17.5	10.0	15.0	10.0
pH	Min	8.1	8.1	7.6	8.2	8.1	7.6	9.0	9.1	9.3	8.4	8.9	9.0	9.2	9.17
	Max	9.5	9.0	9.3	9.2	9.1	8.7	10.5	10.0	10.1	9.8	10.3	10.4	10.13	10.30
	Med	9.4	8.9	8.9	8.9	8.7	8.2	9.6	9.5	9.6	9.4	9.8	9.8	9.91	9.71
Oxygen saturation, %	Min	81	77	66	62	37	53	95	82	77	87	71	39	81	71
	Max	117	165	108	147	107	222	244	226	194	129	236	151	191	240
	Med	98	116	95	106	83	78	126	121	122	106	94	91	138	122
Total N, mg/L	Min	3.0	1.8	9.1	2.3	0.5	4.1	3.7	3.6	1.9	3.4	1.3	13.6	10.97	9.83
	Max	20.7	53.5	20.1	37.3	13.6	35.7	12.5	16.9	14.0	20.3	33.0	33.1	29.19	22.84
	Med	17.1	7.6	15.7	6.7	3.4	12.8	6.4	7.9	9.7	7.9	12.1	19.8	20.55	12.81
Total *P*, mg/L	Min	1.1	1.1	1.3	–	1.5	2.5	–	–	0.3	0.4	0.3	0.7	0.52	0.53
	Max	7.5	1.9	1.8	–	2.6	4.9	–	–	0.6	1.4	1.1	4.7	1.84	2.44
	Med	2.6	1.6	1.7	–	1.7	3.5	–	–	0.4	0.9	0.5	0.9	0.86	1.22
Chlorophyll-a, mg/m^3	Min	9.0	0.2	3.2	0.9	0.1	0.2	18.7	13.0	15.3	109.0	107.8	147.0	62.0	252
	Max	188.4	41.1	166	104	129.3	107.2	436	585	351	1289	1841	1188	918	1260
	Med	80.1	24.7	15.3	55.0	37.8	7.4	116	128.5	187.8	577.5	315	347.5	296	536.5

Medians were assumed sufficient and very useful for the purposes of the present work, but they are values that do not reflect individual outliers sometimes present in the large data sets.

Linear regression analysis was used for determining the trends in the average values over time.

Selected parameters, oxygen saturation, chlorophyll-a, *TP*, *TN* and *SDT* were taken into account as the most indicative parameters that can directly show the evolution of the trophic state of the Palić Lake since 1977.

The oxygen in lake water is a very important parameter because it gives a general image of the quality of the lake environment. The regression slope for dissolved oxygen was positive (0.361) and the concentrations of oxygen were almost or above 100 %. Values greater than 100 % occur in eutrophic or hypertrophic environmental waters because of pure oxygen production by photosynthetically active organisms.[10]

Chlorophyll-a is the most appropriate parameter to follow the growth of both algae and C*yanobacteria* present in Palić Lake. Its load is a good indicator of the number of algae present in waters.[11] The most likely explanation for the increase in the chlorophyll abundance (fairly positive regression slope of 0.011) is an increase in nutrients, the food for algae, and the alkaline environment (pH around 8.9) is very favorable for algal growth.

Transparency was recorded using a Secchi disk. The readings can be affected by algae and by suspended solids in the water. Plankton scatters light, hence a lake which is less transparent tends to have more plankton and be more productive. The Palić Lake has a low transparency with a positive regression slope (0.361) and, therefore, is generally regarded as very productive. The higher the amounts of algae present in the waters, the lower is the water transparency.

The main nutrients for phytoplankton are phosphorus and nitrogen. The more nutrients there are in the water, the greater is the potential for growth. The nutrients have to be present in the right amounts and if one nutrient is lacking then growth can be retarded. Nutrients (nitrogen and phosphorous) are usually the limiting factors in algal growth. To compare the availability of these nutrients, the ratio *TN*/*TP* is used. Ratios smaller than 10 indicate that nitrogen is limiting.[12] Ratios greater than 30 indicate that phosphorus is limiting; whereas ratios greater than 10 and smaller than 30 indicate that there are enough of both nutrients for excessive algal growth.[12] Throughout all years, the *TN*/*TP* ratio was smaller than 10 (Table II), which indicates that nitrogen could be the limiting factor for algal growth in the Palić Lake.

If lake water oxygen saturation increases, the content of chlorophyll and nutrients (N and P) also gradually increase with time. An increase in the content chlorophyll-a is dependent on both water temperature and nutrient availability[13] and this was true for the present case as well. The oxygen saturation was positi-

vely correlated with the chlorophyll content (r = 0.34) and *TN* (r = 0.26), while it was negatively correlated with the *SDT* (r = –0.51). The *TN* was positively correlated with chlorophyll (r = 0.35) and with the *TP* (r = 0.29), while it was negatively correlated with the *SDT* (r = –0.21). This means with more nutrients, there are more algae and chlorophyll, which produce more oxygen and as a result the transparency of the lake decreases. This indicates very clearly that the trophic state of the Palić Lake has deteriorated with time.

TABLE II. Trends of the yearly medians with time (1977–2006); ⇗↗, increasing trend ⇘↘, decreasing trend and ⇔■, no trend – horizontal trend; median of yearly medians is given in paratheses

Parameter	Palić Lake, Sector IV	Linear regression slope
Temperature of water, °C	⇔■ (18.3)	0.003
SDT/ cm	⇘↘ (27.5)	–0.551
P	⇗↗ (8.89)	0.037
Oxygen saturation, %	⇗↗ (98.5)	0.361
TN/ mg L^{-1}	⇗↗ (7.95)	0.285
TP/ mg L^{-1}	⇔■ (0.91)	0.006
Chlorophyll-a, mg m^{-3}	⇗↗ (80.1)	0.011
TN/*TP*	9.07	–

Seasonal changes of the measured parameters for the period 1977–2006

Trends of the measured parameters and seasonal changes are presented in Fig. 4. Each month corresponds to yearly medians of all measurements of a certain parameter obtained for the same month throughout the years from 1977 to 2006. The available results encompass data from March to October while the remaining months were more or less winter months when measurements were not performed due to low temperatures and ice.

In the vegetative period (from March to October), the dominant nutrient removal process was that of plankton uptake. The application of fertilizers in the spring time for the agricultural land nearby Palić Lake generated slightly higher concentrations of nitrogen and phosphorous in the Lake water, but these concentrations gradually decreased with time going to autumn. There are two explanations for this. First, during summer time, atmospheric precipitation is seldom, hence transfer of nitrogen and phosphorous compounds with rainwater from agricultural land into the lake is prevented, and second, due to algal activity, the consumption of the nutrients is much higher. In addition, the increase of temperature during the summer time favors algal growth resulting in increases in the chlorophyll-a concentration and decreases in transparency.

As found by researchers from the petrochemical industry NIS[14], the sediment of the lake – its muddy bottom layer – contains relatively high concentrations of nitrogen and phosphorus. These can be released into the water, particu-

larly under conditions of low oxygen concentrations. The nutrients in the sediment come from the past settling of algae and dead organic matter. The nutrients released from the sediments are referred to as the internal loading of a lake. Chemical and biological processes for N and P uptake are different. After sedimentation, most of the N load is removed by denitrification, whereas a major fraction of P is reversibly bound to sediments and may become available again after its concentration has decreased in water.[15] Therefore, N is accumulated in the sediments less than P and the time lag for N is expected to be shorter than for P.

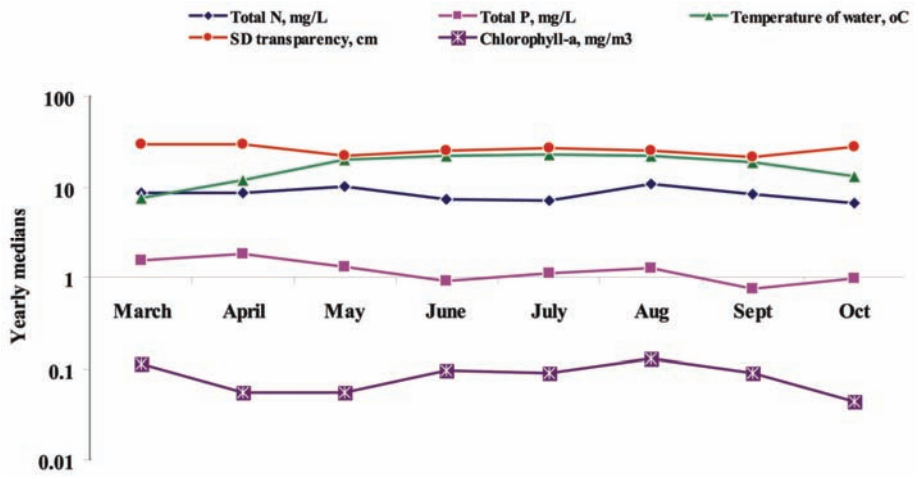

Fig. 4. Yearly medians of the *TN*, *TP*, chlorophyll-a, temperature of the water and *SDT* for Sector IV of the Palić Lake during the months March to October for the period 1977–2006.

The ratio *TN*/*TP* may be a useful method to establish the N and P reduction targets in the environment.[16] This ratio is one of the important components for the calculation of the trophic state index of lakes. Several studies showed that a *TN* to *TP* ratio ≤10:1 appears to favor algal blooms, especially of blue-green algae.[16]

The Palić Lake with a *TN*/*TP* ratio of 9/1 was classified as a N-limited lake and may have a higher probability for algal bloom because of its higher P levels. The *TN*/*TP* ratio increases from March to October for all three lake sectors (Fig. 5). Assuming that algal growth consumes nitrogen and in a constant ratio (the Redfield ratio) and that the concentrations of nitrogen and phosphorous decrease from spring to winter (Fig. 4), then the increasing trend of the *TN*/*TP* ratio indicates that during this time the input of nitrogen into Palić Lake increased slightly. This means that the retention of soluble nitrogen compounds in the lake water increases, or that phosphorus disappears from the water. There are many possible explanations for this; nitrogen compounds are soluble in water at any pH value,

while phosphorus compounds tend to slowly precipitate under slightly alkaline conditions (pH > 8) and the pH of the Palić Lake water was around 8.9. The Lake water has such high pH values because photosynthetic organisms, such as algae, remove carbonic acid from the water causing the pH to rise. High pH values are not very favorable for lakes; at a pH of 9.3, the ratio between ammonia and ammonium ions is 1:1 and at these pH values, or even higher, the production of toxic free ammonia commences.[17]

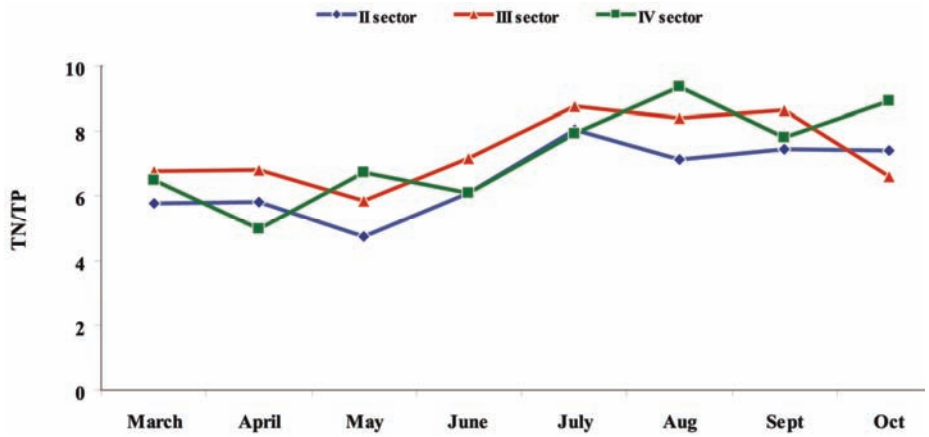

Fig. 5. Yearly medians of ratio *TN*/*TP* for Sectors II–IV of the Palić Lake during the months March to October for the period 1977–2006.

Schindler[18] indicated that a reduced N input into lakes increasingly favors the N_2-fixing activity of *Cyanobacteria* as a response by the phytoplankton community to seasonal N limitations. N_2 fixation is sufficient to allow continuation of biomass production in proportion to the P present in the water. This process contributes to lake eutrophication, despite extreme N seasonal limitations. These results indicate that for eutrophication reduction, lake management must focus on decreasing the P input.

Seasonal pH changes can give a good indication of how productive a lake is as increased algal activity raises the pH value. The increase of the pH of the Palić lake water was positively correlated with algal productivity (r = 0.29), temperature (r = 0.26) and *TN* (r = 0.15), but it was negatively correlated with the *TP* (r = –0.65). This negative correlation between pH and *TP* is explained with the fact that phosphorus becomes less available since fixation as calcium phosphate begins (Yamada *et al.*)[19] and the concentrations of phosphate in the water slightly decreased with increasing pH. This is a typical abiotic process of the settling of inorganic particulate P and the adsorption of dissolved inorganic P, which is responsible for P retention in the reservoir. In addition, the high pH values of the Lake water control the phosphorous concentration very well over time.

It seems that it is at about its maximum and it is rather equalized, fluctuating over a narrow interval around 0.9 mg L^{-1}.

Trophic state

An excellent indicator of the eco-chemical status of any lake would be its trophicity, described by the trophic state index (the Carlson *TSI*).[2] It is usually calculated based on data for the total phosphorus, chlorophyll-a and the Secchi disk transparency, according to the recommendations of the US EPA nutrient criteria for lakes and reservoirs.[3]

The graphs for the trophic state indexes, for phosphorous, *TSI* (P), chlorophyll-a, *TSI* (Ch), and *SDT*, *TSI* (*SDT*) were obtained applying the following formulas:[2]

$$TSI\,(\mathrm{P}) = 4.15 + 14.42 \ln c_1 \quad (1)$$

$$TSI\,(\mathrm{Ch}) = 30.6 + 9.81 \ln c_2 \quad (2)$$

$$TSI\,(SDT) = 60.0 - 14.41 \ln SDT \quad (3)$$

where c_1 is concentration of *TP*, μg L^{-1}, c_2 is concentration of chlorophyll-a, μg L^{-1}, and *SDT* is the value of the *SDT*, m.

According to the US EPA standards, several categories of *TSI* values are possible (Table III). The obtained results for *TSI* (Fig. 6) show constant rising trends for all three parameters. The first parameter, *TSI* for *SDT* had a minimum of 66 and a maximum value of 93, indicating to constant change from a eutrophic to a hypereutrophic state, since the transparency of the Palić Lake was less than 1 m. For example, oligotrophic lakes tend to have water clarity greater than 3.9 m due to the low amounts of free-floating algae in the water column. The second parameter, *TSI* for *TP* had a minimum value of 90 and a maximum one of 122, indicating to a constant hypereutrophic status of the lake. The third parameter, the *TSI* for chlorophyll-a had a minimum value of 45 and a maximum of 93, indicating a rise from mesotrophic to hypereutrophic.

The method used for determining the trends in the average for *TSI* with time was linear regression analysis as well.

It is obvious from Fig. 6 and from the corresponding *TSI* trends and categories that the trophic state of the Palić Lake is worsening with time. The slopes of the regression (*SR*) for all three parameters are positive (*SR* (*SDT*) = 0.164; *SR* (*TP*) = 0.046 and *SR* (Ch) = 0.198). The great majority of all the trophic state indexes belong to eutrophic or even hypereutrophic lake conditions. Generally speaking the lake is showing constant tendency of a worsening of all parameters.

Comparison with another shallow lake in the region

The most significant shallow lake in Central and Western Europe is Lake Balaton, which is the greatest shallow lake in this region located in the western part of Hungary. Due to its low depth (3.3 m), the water temperature follows

quickly the air temperature and reacts sensitively to hydro-meteorological changes. The average temperature of the water is 12.4 °C. The water is soft and rich in oxygen. The main use of the lake water is for recreational purposes and as a supply for the communal water demands. Selesi[20] compared water quality studies of the Palić Lake and the Balaton Lake. These systems show many similarities and differences:

– the Lakes are situated within the same climate zone but the Balaton Lake is about 100 times larger than the Palić Lake and is located some 160 km to the north-west in relation to the Palić Lake. The average water temperature of the Balaton is 12.4 °C and of Palić 14.7 °C;

TABLE III. Categories of *TSI* values (US EPA, 2000)[3]

TSI	Chlorophyll-a, μg L^{-1}	*SDT*/ cm	*TP*/ μg L^{-1}	Attributes
<30	<0.95	>800	<6	Oligotrophic
30–40	0.95–2.6	800–400	6–12	Oligotrophic
40–50	2.6–7.3	400–200	12–24	Mesotrophic
50–60	7.3–20	200–100	24–48	Mildly eutrophic
60–70	20–56	50–100	48–96	Eutrophic
70–80	56–155	25–50	96–192	Hypereutrophic
>80	>155	<25	192–384	Hypereutrophic

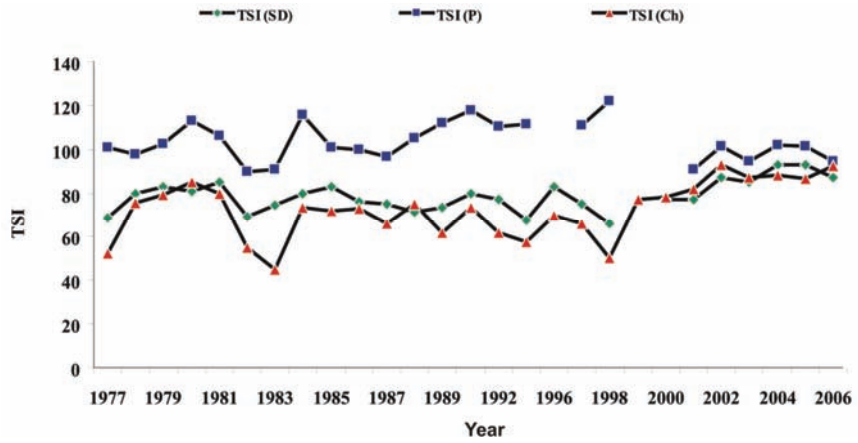

Fig. 6. Trophic state index (*TSI*) for *SDT*, *TP* and chlorophyll-a (Ch) for Sector IV of the Palić Lake for the period 1977–2006 (there was no data for *TP* for the years 1996, 1999 and 2000).

– regarding the water quality, the Balaton Lake was classified as mesotrophic to eutrophic,[21] while the Palić Lake is classified as eutrophic to hypereutrophic. The *SDT* for the Balaton ranges from 47 to 68 cm, while for the Palić, Sector IV, it is around 27.5 cm. The *TP* for the Balaton ranges from 0.1 to 0.03 mg L^{-1}, while for Palić, Sector IV, it is around 0.91 mg L^{-1}. Finally, the chlo-

rophyll-a content for the Balaton ranges from 9.9 to 29.2 mg m^{-3}, while for the Palić, Sector IV, it is around 80.1 mg m^{-3};

– both lakes receive water from sewage purification plants, but the Kis-Balaton reservoir system, located near the Zala River, established for the protection of the Balaton Lake against high nutrient loads is more efficient in comparison to the Palić system. The aim of Balaton system was that nutrients (primarily P) should be removed by macrophytes before entering the lake. In contrast to predictions, the system became an open lake dominated by algae. The retention efficiency has decreased considerably after reduction of the external load because of phosphorus removal at the wastewater treatment plant of the largest town, Zalaegerszeg, of the Zala catchment.[22] This observation can be explained by the increased contribution of the internal loading. Abiotic processes, such as settling of inorganic particulate P and the adsorption of dissolved inorganic P, responsible for the P retention in the reservoirs, are characteristic for both the Balaton and Palić Lakes;

– due to the vegetal nutritive materials available in the water, frequent over multiplication of algae, called "water flowering", during hot summer periods is characteristic for both lakes;

– nutrients discharged into Balaton Lake were utilized by the reeds and by various organisms living in the reeds, mainly fixed algae, and were nearly completely removed. In the autumn, the reeds die down and the materials they filtered out are mixed with lake water by wave action, with the exception of food materials.[23] In the case of the Palić Lake, the reed population declined, the reason for which has yet to be identified.

CONCLUSIONS

Generally speaking, there are several negative factors that threaten the Palić Lake; short term factors, such as municipal waste waters inflow and high concentrations of nutrients which generate constant hypertrophic conditions in the lake and relatively low lake water exchange rate, and long term factor, such as global warming.

Taking into account the fact that 29 years of measurements demonstrate a constant trend of the worsening of the trophic state, it is not difficult to conclude that, with high confidence, the whole situation in the lake under current conditions will tend to worsen.

Positive factors that prevent complete and fast eutrophication of the lake are: there is an exchange of lake water with the nearby river, regardless of how slow it is, and there is still life in the lake, predominantly C*yprinidae*, which prefer weakly alkaline waters, pH 7.8–8.5.[24]

It is possible, but very expensive, to remove the upper nutrient-rich layer of sediment. Covering sediments with clay to seal them and thereby reduce internal loading has also been tried. Even when nutrients are removed in large amounts

from wastewater, it often takes a long time before the nutrient concentrations fall in the upper sediment layer because they are still present in the water environment. Early reduction or elimination of nutrient sources is therefore very important.

Since the main reasons for reed decline are unknown, future research should also focus on involving reed-periphyton studies, which may provide a good basis to find the most appropriate ways to protect and restore the reed communities of shallow standing waters.

It is recommended that the following measures be taken to prevent further eutrophication:

– improvement of sewerage and sewage treatment plants, particularly for P removal;

– increase of the lake water exchange rate with water from the nearby Tisa River;

– enhanced treatment of the municipal waste waters that flow into the first sector of the lake;

– establishment of reservoirs on larger tributaries to retain plant nutrients.

Further and deeper examinations are necessary for a better understanding of the biochemical and biological processes.

Acknowledgements. The authors would like to point out that this study was partly funded by the Ministry of Science of the Republic of Serbia (Project No. 146008) and by the Public Health Institute of Subotica, where all the analytical work was performed.

И З В О Д

ЕВОЛУЦИЈА ТРОФИЧКОГ СТАТУСА ЈЕЗЕРА ПАЛИЋ (СРБИЈА)

ИВАН ГРЖЕТИЋ[1] и НАТАША ЧАМПРАГ[2]

[1]*Универзитет у Београду, Хемијски факултет, Студентски трг 12–16, 11 000 Београд и*
[2]*Завод за јавно здравље Суботица, Змај Јовина 30, 24 000 Суботица*

Језеро Палић је плитко језеро типично за Панонску низију. Због неадекватног квалитета воде исушено је 1971. године и санирано до 1977. године и од тада се његов трофички статус погоршава. Дугорочна испитивања промене трофичког статуса, која обухватају анализе количине укупног фосфора, укупног азота, хлорофила-а и провидности воде преко Secchi-јевог диска, изражена су преко Карлсоновог индекса трофичког статуса. Вредност поменутог индекса указује да је вода језера Палић у еутрофичној и хипереутрофичној класи. Однос укупног азота и укупног фосфора, који је мањи од 10 указује на то да је азот лимитирајући фактор за раст алги.

(Примљено 16. октобра, ревидирано 12. новембра 2009)

REFERENCES

1. S. S. S. Lau, S. N. Lane, *Sci. Total Environ.* **288** (2002) 167
2. R. E Carlson, *Limnol. Oceanogr*. **22** (1977) 361

3. *US-EPA, Ambient Water Quality Criteria Recommendations Lakes and Reservoirs in Nutrient Ecoregion*, XI Office of Water, EPA 822-B-00-012, 2000
4. *APHA, Standard Methods for the Examination of Water and Wastewater*, Washington DC, 20005, 14th ed., 1976, and 20th ed., 1998
5. *US EPA, Methods for Chemical Analysis of Water and Wastes*, EPA/600/4-79/020, 1983
6. R. H. Peters, *Limnol. Oceanogr*. **31** (1986) 1143
7. S. Sakan, I. Gržetić, D. Đordjević, *Environ. Sci. Pollut. Res. Int.* **14** (2007) 229
8. R. Đurović, *Hydrogeological conditions of the regeneration of the drained Palić Lake*, Institute for Mining-Geological Examinations and Investigations of Nuclear and Others Mineral Feedstock, Belgrade, 1973, p. 102 (in Serbian)
9. *PHI, Public Health Institute of Subotica*, Annual reports, 1977–2006 (in Serbian)
10. *YSI Incorporated, Environmental Dissolved Oxygen Values Above 100 % Air Saturation*, YSI Environment technical notes 25, 1999
11. A. Raike, O. P. Pietilainen, S. Rekolainen, P. Kauppila, H. Pitkanen, J. Niemi, A. Raateland, J. Vuorenmaa, *Sci. Total Environ.* **310** (2003) 47
12. P. L. Brezonik, *Lake Reservoir Manage*, 1984, p. 441
13. I. Tatrai, K. Mátyás, J. Korponai, G. Paulovits, P. Pomogyi, *Ecol. Eng.* **16** (2000) 73
14. NIS Naftagas, *Report about physico-chemical examinations of peloids and water from the Palić lake*, Novi Sad, 1999 (in Serbian)
15. S. P. Seitzinger, *Limnol. Oceanogr*. **33** (1988) 702
16. G. C. Sigua, J. S. Steward, W. A. Tweedale, *J. Environ. Manag.* **20** (2000) 199
17. J. Vymazal, L. Kropfelova, *Wastewater Treatment in Constructed Wetlands with Horizontal Sub-Surface Flow*, Environ. Pollut., Kluwer Academic Publishers, Dordrecht, 2008
18. D. W. Schindler, R. E. Hecky, D. L. Findlay, M. P. Stainton, B. R. Parker, M. J. Paterson, K. G. Beaty, M. Lyng, S. E. M. Kasian, *Natl. Acad. Sci. USA* **105** (2008) 11254
19. K. Yamada, K. Haraguchi, C. C. Gacho, L. S. Salinas, C. M. Silverio, B. P. Wongsiri, *Removal of Phosphate from Aqueous Solutions by Crystallization Using Coal Fly Ash*, International Ash Utilization Symposium, University of Kentucky, 2001, p. 7
20. D. Selesi, *Water of the Palić Lake from 1781 to 1999*, JP Palić-Ludaš, Subotica, 2000, p. 18 (in Serbian)
21. E. Hajnal, *Ph.D. Thesis*, Doctoral School in Environmental Science, University of Pannonia, Veszprém, 2008
22. A. Clement, L. Somlyody, L. Koncsos, *Water Sci. Technol*. **37** (1998) 113
23. L. Toth, *Water Res*. **6** (1972) 1533
24. I.-S. Chen, *Environ Biol Fish* **86** (2009) 143.